FORMATION AND PROPERTIES OF TRIOL-BASED POLYURETHANE NETWORKS

BY

MOHAMMED ALAM SHAH

A THESIS SUBMITTED TO

THE VICTORIA UNIVERSITY OF MANCHESTER

(FACULTY OF TECHNOLOGY)

FOR THE DEGREE OF

DOCTOR OF PHILOSOPHY

DEPARTMENT OF POLYMER SCIENCE & TECHNOLOGY

OCTOBER 1984

ACKNOWLEDGEMENTS

I acknowledge my indebtedness to Dr. J.L. Stanford and Dr. R.F.T. Stepto for their kind supervision, help, invaluable suggestions and encouragement throughout the course of the work.

I also gratefully acknowledge:

Prof. R.H. Peters for providing laboratory facilities

Mrs. P. Briggs and Mrs. M. Morgan for typing this thesis

and

Commonwealth Scholarship Commission for financial support.

DECLARATION

No portion of the work referred to in the thesis has been submitted in support of an application for another degree or qualification of this or any other university or institution of learning.

C U R R I C U L U M V I T A E

I have graduated with a first class Honours Degree in Chemistry from the University of Chittagong, Bangladesh followed by a first class Masters Degree in Chemistry from the same University in 1977. Thereafter, I joined the Department of Chemistry in the University of Chittagong as a Lecturer.

After teaching for two years, I did an M.Sc. (by course and dissertation) at UMIST in 1980 and then started full-time research in the Department of Polymer Science and Technology. This research project was completed in May, 1983, and the results are the subject of the present thesis.
Since July, 1983, I have been working as a Research Fellow in the Department of Materials Science and Engineering at the University of Surrey.

ABSTRACT

The formation and properties of polyurethane networks synthesised from a poly(oxypropylene) triol (LG-56) and hexamethylene diisocyanate (HDI) have been studied. Kinetics studies of the reaction in equimolar proportions of polyol and diisocyanate (i.e. $r = 1$) in nitrobenzene and toluene solution at $80^{o}C$ showed that only catalysed reactions in bulk followed second order kinetics. Positive deviations from second order kinetics were observed in uncatalysed reactions, especially at higher extents of reaction due to the autocatalytic effect of the product urethane. Very slight positive deviations were also observed in catalysed reactions in solutions. Catalytic reaction rate constants have been evaluated from kinetics studies of the reaction at different catalyst concentrations and also at different dilutions. The results have been explained in terms of the dielectric constants of the reaction media.

Studies on the effect of catalyst and dilution (especially in toluene) on gel point showed that pre-gel intramolecular reaction increases with increase in catalyst concentration and dilution. Gel point data have been interpreted in terms of different gelation theories and the polyfunctional rate theory (PFRT) and values of b (the effective bond length) evaluated and compared with those from previously studied polyurethane systems.

Stress-strain data obtained from uniaxial compression experiments on fully reacted, dried and equilibrium-swollen (in toluene) networks at $27^{o}C$ have been analysed in terms of Gaussian theory and the Mooney-Rivlin equation. Deviations from Gaussian theory and Mooney-Rivlin equation were observed, which decrease with increase in M_c, i.e. dilution of reaction. M_c/AM_c^{o} (obtained from the slope of the Gaussian stress-strain plots) versus α_c (and/or $p_{r,c}$) showed that in the limit of the ideal gel point (i.e. $\alpha_c = 0.50$) affine, perfect networks are expected to be formed. M_c/AM_c^{o} values

from the present work and from previous investigations have been compared and the effects of pre-gel intramolecular reaction on modulus have been discussed.

Torsion pendulum experiments on fully reacted and dried networks showed two transitions - an α-transition (primary transition or glass transition) and a β-transition (secondary transition). Glass transition temperatures decreased with increase in dilution of reaction and are discussed in terms of pre-gel intramolecular reactions or loop formation. A similar trend in glass transition temperatures was also observed from differential scanning calorimetry (D.S.C.) on dried and fully reacted networks.

CONTENTS

CHAPTER - 1

GENERAL INTRODUCTION

Carothers[1] classified polymerisations on the basis of chemical reactions into two types, condensation and addition polymerisations. Condensation polymerisations are reactions involving loss of a small molecule at each reaction-step whereas in the latter no such loss occurs. A number of polymerisations have been found which formally resemble the condensation type but proceed without the evolution of a byproduct. For example - the formation of polyurethane from diisocyanate and glycol. So a fundamentally sounder classification of polymerisations should be based on the mechanism of the reaction rather than on the identity of polymer composition with the initial monomers. Using kinetics as a basis, Flory[2] classified polymerisations into stepgrowth and chain-growth polymerisations. Stepgrowth polymerisation proceeds by stepwise intermolecular reaction of functional groups of monomers and includes not only condensation polymerisation but also stepwise addition polymerisation such as occurs in polyurethane forming reactions. Chaingrowth polymerisations, on the other hand, proceed by a chain mechanism involving an active centre.

However, the importance of statistics in polymerisation theory has long been recognised, and neither of the preceding classification is wholly satisfactory on statistical grounds. Stanford and Stepto[3] have suggested classification of polymerisations, using statistics as a basis, into (a) random polymerisation which proceeds by the random intermolecular reaction of pairs of groups and (b) sequential polymerisation which proceeds by the sequential addition of monomer units to growing chains.

Random polymerisation is closely related to stepgrowth polymerisation in which like functional groups have equal reactivity. However, some stepgrowth addition polymerisations, as occur in polyurethane formation, are included.

The primary requisite for random polymerisation is that the monomer should have a functionality equal to or greater than two. Monomers having two functional groups can be self-polymerised or can react with another bifunctional monomer. Two molecules react with each other to form a dimer with the disappearance of two reactive sites. The resultant dimers may react with one another or with monomers. Each single step involves the participation and subsequent disappearance of two reactive sites. As the reaction continues, the low molar mass polymer formed reacts further and the average molar mass increases continually. To attain a high molar mass the polymerisation must be continued until reaction is nearly complete. The reactions of bifunctional monomers generally result in a distribution of molecular species. If, however, one of the monomers is polyfunctional, a polymer molecule with junction points results, which at a certain critical point during the polymerisation, becomes of infinite size. Then the reaction mixture loses its fluidity and suddenly exhibits semisolid behaviour, becoming insoluble in good solvents. This sudden transformation is known as gelation. Gelation is an important physical manifestation of a critical stage in the reaction and is susceptible to theoretical analyses of varying complexity and success.

The process of random growth in random polymerisation is, however, restricted to a certain extent by the possibility that a growing molecule may fail to react with other molecules and instead combine with an unreacted group already present on the same molecule. This intramolecular

reaction, generally described as cyclisation or ring formation, competes with intermolecular reaction. In a linear polymerisation cyclisation has the effect of terminating the growth of a polymer chain, giving a ring molecule as shown in fig. 1.1(a), whilst in the case of a non-linear polymerisation cyclisation impedes the branching growth and leads to the formation of molecules of finite size, giving ring structures on branched molecules as shown in fig. 1.1(b), and possibly results in no gelation.

(a) Ring molecule (b) Ring structure on branched molecule

Fig. 1.1. Schematic Representation of Intramolecular Reaction

(a) in Linear Polymerisation

and

(b) in Non-linear Polymerisation

In a linear polymerisation a molecule can react only through its terminal groups and the opportunity for intramolecular reaction depends only on the configurational properties of the chain. In a non-linear polymerisation, however, the amount of intramolecular reaction depends also on the complexity of the molecule as numerous possibilities of intramolecular reaction can arise, as shown in fig. 1.2. For example, the reaction between a trifunctional alcohol and a diisocyanate can be represented as

$$OCN - R - NCO + HO - \underset{\displaystyle OH}{\underset{|}{R'}} - OH \rightarrow OCN - R \left\{ \underset{\displaystyle H}{\underset{|}{N}} - \overset{\displaystyle O}{\overset{\|}{C}} - O \right\} \underset{\displaystyle OH}{\underset{|}{R'}} - OH$$

This can be represented schematically as

$$RA_2 + R'B_3 \rightarrow A - R\{AB\}\overset{B}{\underset{|}{R}}\!\!\diagup\!\!-B$$

where -AB- represents the urethane group.

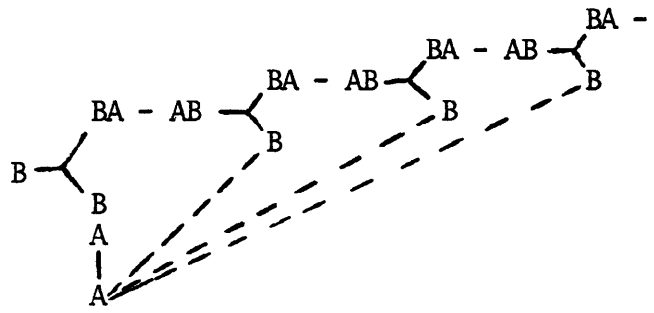

Fig. 1.2. Schematic Representation of a Polymer Chain

Formed by A - A and B(B)(B) units.

— → Intermolecular links

--- → Intramolecular links

Fig. 1.2 shows that there are a number of configurations and hence possibilities for intramolecular reaction. Only some of the configurations, in which the reactive groups are within short mutual distance (of the order of a bond length) and suitably oriented to each other, can lead to intramolecular reaction.

The commercial importance of the polymer networks led to early attempts to explain theoretically the phenomenon of gelation. Carothers[4] believed (incorrectly) that it was necessary for all the molecules to combine in order for gel conditions to be satisfied in RA_f type polymerisations and this reasoning led to the result

$$p = 2/f \qquad \ldots.(1.1)$$

where p is the extent of reaction at gel and f is the functionality of polyol. Others went on to derive molecular weight distributions and gel points in more precise terms. These theories are discussed in more detail in Chapter 2. The first theory for the distribution was due to Flory[5]. This theory did not take into account the possibility of ring formation. Subsequent theories attempted to account for cyclisation or ring formation. The probability of ring formation will depend upon several features, namely the flexibility of the reactant molecules, the dilution of the reaction mixture and the relative concentrations of A and B groups, internal and external to the growing chain which is evident from fig. 1.2. Jacobson and Stockmayer[6] considered ring-chain competition in linear systems and derived for the probability, P, of the two ends of a chain being in the small volume V_s required to form a ring (assuming a Gaussian distribution of chain conformations):

$$P = \left(\frac{3}{2\pi\nu\, n}\right)^{3/2} \cdot \frac{V_s}{b^3} \qquad \ldots.(1.2)$$

where n is the number of monomer units (each containing ν links) and b is the effective bond length. The influence of molecular structure on ring formation which then affects the gel point under otherwise identical conditions thus enters through the parameters ν and b. The distribution of molecular species in a non-linear random polymerisation, neglecting intramolecular reaction, was derived by Flory[7] and by Stockmayer[8]. The observed gel point was always found to occur at a later stage in the reaction than predicted by theory. This delay could be due to the unequal reactivity[9,10] of like functional groups which was assumed to be the same in Flory's and Stockmayer's theory. However, even when the equal reactivity of like functional groups was assured, this delay of gelation

was found to occur[11-14]. The occurrence of intramolecular reaction along with intermolecular reaction was found to be an important factor responsible for this delay. Since then, various theories have been put forward to account for this effect as described briefly below.

Case[15] developed an expression for gel points in the absence of intramolecular reaction which accounted for the intrinsic unequal reactivities of the like functional groups.

Frisch[16] and Kilb[17] derived expressions which account for ring formation and can be applied to gelation data from non-linear random polymerisations, provided equal reactivity of like functional groups is assured. Stepto[18] has modified their expressions to define more explicitly the dependence of the gel point on molecular structures and reaction conditions.

The Polyfunctional Rate Theory[19] and the Cascade Theory[20] are also used in describing non-linear random polymerisations with ring formation. However, some of the treatments developed for irreversible non-linear random polymerisations are accurate only at lower extents of reactions[21].

Basic Chemistry of the Polyurethane Reactions

Isocyanates are compounds containing the unsaturated - N = C = O group, and are generally produced by phosgenation of the corresponding amine. They react readily with any compound containing active hydrogen, and are sufficiently reactive to dimerise (aromatics only), trimerise and may indeed form high polymers such as N-substituted Nylon-1's[22]. However, from the point of view of polyurethane formation, the most important isocyanate reactions are:

	Reagent	Reaction	Product
1.	Alcohol	$RNCO + R'OH \rightarrow R - \underset{H}{N} - \underset{O}{C} - OR'$ (I)	(Urethane)
2.	Water	$RNCO + H_2O \rightarrow RNHC(=O)OH \rightarrow RNH_2 + CO_2$	(Amine)
3.	Amine	$RNCO + R'NH_2 \rightarrow RNH \cdot CO \cdot NH - R'$ (II)	(Urea)
4.	Urea	$RNCO + II \rightarrow RNH \cdot CO \cdot NR \cdot CO \cdot NHR'$	(Biuret)
5.	Urethane	$RNCO + I \rightarrow RNH \cdot CO \cdot NR \cdot CO \cdot OR'$	(Allophanate)

Reactions (2) and (3) are responsible for the enormous proliferation of the polyurethane foams. For the production of solid elastomers, therefore, reaction (2) should be avoided. Reaction (4) is slower than (3) but may be catalysed by strong bases as can (1). Reaction (5) is generally a slower reaction than (4) and requires higher temperatures and excess isocyanate for a significant rate[23,24,25].

The polyols used in polyurethane formation are generally hydroxyl-terminated polyethers or polyesters. The polyols are produced by the stepwise addition of alkylene oxide, primarily propylene oxide (ethylene oxide is sometimes used), to a compound containing active hydrogen[26] using mostly base catalysis. The active-hydrogen compound is usually an alcohol, polyalcohol, or an amine. Propylene glycol, glycerol, trimethylol propane and 1, 2, 6 - hexane triol are most widely used, although products for rigid urethane foams may be formed with a variety of higher functionality compounds, eg, sucrose (f = 8), sorbitol (f = 6), pentaerythritol (f = 5) and aliphatic or aromatic polyamines[23,27] such as ethylene diamine, diethylene triamine and toluene diamine. Potassium

hydroxide is the most widely used catalyst[28]. The molar mass of polyols range from 250 to 7000 g mol $^{-1}$ [26]. As mentioned previously, polyols may be oxypropylene or oxyethylene adducts of polyols, but combinations of both oxypropylene and oxyethylene adducts have also been employed, specially with sucrose as reactant[29-31].

Nowadays, a mixture of high molar mass and low molar mass polyols are also used, specially in Reinforced Reaction Injection Moulding (RRIM) technology[32]. Sometimes low molar mass alcohols such as ethylene glycol and butane diol are used with high molar mass polyols, to modify the properties of the polyurethanes. Generally polyols form the soft block and the diisocyanate and low molar mass diols form the hard block in polyurethanes. When the low molar mass polyols are used with high molar mass polyols then the low molar mass polyols are called chain extenders. Their function is to increase the hard block fraction and to develop crystallinity in polyurethanes. Poly (oxypropylene) polyols have secondary hydroxyl groups, whereas poly (oxyethylene) polyols have primary hydroxyl groups. Primary hydroxyl groups are generally more reactive than the secondary ones in the reaction with isocyanate groups. The greater reactivity of the primary hydroxyl group is an advantage in the preparation of certain polyurethane products[33]. However, in certain uses a greater reactivity is undesirable[34].

When terminal primary hydroxyl groups are desired, ethylene oxide may be used either as the sole alkylene oxide with the polyol reactant, or it may be employed to "cap" or "tip" the oxypropylated polyol[32] with ethylene oxide as shown in the following scheme:

$$R - (CH_2 - \underset{\displaystyle CH_3}{\underset{|}{CH}} - O)_n - CH_2 - \underset{\displaystyle CH_3}{\underset{|}{CHOH}} \xrightarrow{CH_2 \overset{O}{\diagup\diagdown} CH_2} R - (CH_2 - \underset{\displaystyle CH_3}{\underset{|}{\underset{\displaystyle H}{\underset{|}{C}}}} - O)_{n+1} CH_2 - CH_2 - OH.$$

Different diisocyanates are used in the formation of polyurethanes. The most widely used diisocyanates are toluene diisocyanate (TDI) and diphenyl methane diisocyanate (MDI). Other diisocyanates used are 1,6-hexamethylene diisocyanate (HDI), 1,5-naphthalene diisocyanate (NDI), chlorophenyl diisocyanate (CDI), xylene diisocyanate and 4,4-dicyclohexyl methane diisocyanate. These pure diisocyanates are mostly used for flexible as well as rigid foams (TDI), elastomers, thermoplastic materials, shoe-soling compositions and elastomeric fibres of the "spandex" type (MDI). HDI is used for soft rubbery polyurethanes.

The isocyanates used for rigid foams consist primarily of polymeric diisocyanates ie. isocyanates having an -NCO functionality of greater than 2 (mostly in the range 2.6 - 2.8). Polymeric MDI (also known as liquid MDI) has a functionality of 2.8[35]. Similarly, polymeric TDI is employed in the manufacture of rigid foams, specially for use as insulating materials in refrigerators and freezers.

Having prepared the polyurethane networks, a number of physical tests, such as static (or equilibrium) and dynamic mechanical tests, are available to determine the structure-related mechanical properties.

From static experiments (eg. uniaxial compression stress/strain measurements) the entropic nature of rubbery networks can be studied. From the Gaussian network theory of rubber elasticity, the approximate expression for the applied force (σ) and the deformation ratio (λ), with respect to the reference state at which the chains are unstrained, for Gaussian networks is given by

$$\sigma = G \left(\lambda - \lambda^{-2} \right) \qquad \ldots.(1.3)$$

where G is the shear modulus of the network and is related to M_c, the molar mass between junction points (or cross-links) as follows

$$G = \frac{\rho RT}{M_c} \qquad \ldots.(1.4)$$

where ρ is the density of the network, R is the gas constant and T is the absolute temperature. According to equation (1.3), σ (force per unit unstrained area) versus $(\lambda - \lambda^{-2})$ plot should be linear. But in case of real networks this linearity is not always observed due to the presence of structural defects such as chain entanglements and short chainlength which gives a low M_c value. In terms of elasticity, ring-structures contribute nothing to the overall network elasticity since in simple terms they are only attached through one junction point to the network.

Dynamic experiments (eg. torsion pendulum) are also important for the characterisation of polymer properties in which a sinusoidally varying force is applied to the specimen. The strain will lag the stress at any given time, and the modulus will at some part of the cycle be infinite, and a complex modulus, G*, is defined such that

$$G^* = G' + i\,G'' \qquad \ldots.(1.5)$$

where G' and G'' are the storage and loss components, corresponding to elastically stored energy and energy lost as dissipated heat, respectively. G' and G'' may also be defined as

$$G' = G^* \cos\delta \quad \text{and} \quad G'' = G^* \sin\delta \qquad \ldots.(1.6)$$

(where δ is the phase angle) respectively and the loss tangent, tan δ, as

$$\tan\delta = G'' / G' \qquad \ldots.(1.7)$$

which is an important structure-dependent parameter. This loss tangent describes the damping relaxation of the polymers, from which α-, β- and γ- transitions can be observed and thus information regarding polymer structure can be obtained.

The introduction of junction points (or cross links) into a linear polymer should modify the physical properties such as modulus, glass transition temperature (Tg), flexibility, strength and other structure-related properties. For example, the accompanying reduction in chain flexibility due to crosslinking will tend to raise the Tg, but if in addition there are unreacted functionalities or loose ends, these will tend to depress the Tg by virtue of the added freedom of movement imparted to the network chains. The presence of a stiff aromatic ring in the backbone would increase Tg and, in fact, can result in materials which are glassy[24] at room temperature. Tg of rubbers can also be increased by addition of reinforcing fillers such as carbon black, glass fibre, silica, etc.

The various aspects of the raw materials, polyurethane network formation and measurement of the network properties, as presented in this brief introduction will be discussed in detail in subsequent chapters.

The main object of this work is to study the kinetic and gelation behaviour of a reaction system $RA_2 + R'B_3$ under different reaction conditions and to prepare polyurethane networks to study their physical properties and, finally to correlate the effect of chemical structure of the networks to the physical properties.

It is most convenient to divide the thesis into two main sections, to enable a clearer treatment of the subject matter, the contents of which are summarised as follows:

SECTION 1: This section describes the different theories of gelation, a brief review of hydroxyl isocyanate reaction kinetics, preparation of networks, their characterisation for a variety of reaction conditions such as dilutions, catalyst concentrations and solvents, and the

interpretation of the results in terms of different gelation theories. The kinetics of the reaction are also discussed in this section.

SECTION II: This section covers the characterisation of the properties of the networks by uniaxial compression (static) and torsion pendulum (dynamic) tests. The results are discussed in terms of the theories of rubber elasticity and also in terms of structure-property relations.

CHAPTER - 2

INTRODUCTION TO THE CHEMISTRY OF NETWORK FORMATION

2.1 KINETICS OF URETHANE-FORMING REACTIONS

The kinetics of urethane formation from monoisocyanates and alcohols have been extensively studied as compared with those from diisocyanates and polyols. The kinetics are significantly affected by the nature of isocyanate, alcohol, catalyst, solvent and temperature. So it is difficult to give a generalised kinetics treatment and hence mechanism applicable to all isocyanate-alcohol reactions.

The kinetics of isocyanate-alcohol reactions were first studied by Davis and Farnum[36]. They observed that the reaction velocity followed the order:

primary alcohol > secondary alcohol > tertiary alcohol.

Baker et al[37] published the first detailed kinetics treatment of the isocyanate-alcohol reactions. They suggested a mechanism involving the formation of an intermediate complex when a nucleophile :B is present.

$$R-N=C=O + :B \underset{k_2}{\overset{k_1}{\rightleftharpoons}} R-N^{\delta-}=C=O^{\delta-} \quad (B^{\delta+}) \xrightarrow[k_3]{R'OH} R\text{-}NH.CO.OR' + :B$$

The slow 'spontaneous' reaction is given by

$$R.NCO + R'OH \xrightarrow{k_o} R\text{-}NH.CO.OR'$$

The complex is attacked by a molecule of alcohol to regenerate the nucleophile, which may be a molecule of added catalyst, urethane product or alcohol itself. If the concentration of the alcohol is assumed to be stationary, the rate of formation of urethane is given by

$$dx/dt = k_o (a-x) (b-x) + \frac{k_1 k_3 (a-x) (b-x) [B]}{k_2 + k_3 (b-x)} \quad \ldots.(2\text{-}1)$$

where x is the concentration of urethane formed at time t, a and b are the initial concentrations of isocyanate and hydroxyl groups respectively, and $[B]$ represents the concentration of nucleophilic catalyst. Equation (2-1) can be rearranged as

$$dx/dt = \left[k_o + \frac{k_1 k_3 [B]}{k_2 + k_3 (b-x)} \right] (a-x) (b-x)$$

which gives

$$k_{obs} = \left[k_o + \frac{k_1 k_3 [B]}{k_2 + k_3 (b-x)} \right] \quad \ldots.(2\text{-}2)$$

and an overall second order reaction

$$dx/dt = k_{obs} (a-x) (b-x) \quad \ldots.(2\text{-}3)$$

Baker et al[37] found second order kinetics for aryl isocyanate-alcohol reactions when (a) catalysed by a nucleophile, (b) the initial molecular ratio of $[NCO]/[OH] = r$ is constant (because k_o depends on initial molecular ratio, $[NCO]/[OH]$) and (c) $[OH]$ does not vary greatly (as in the case of reactions with excess alcohol). They also noted an autocatalytic effect due to the nucleophilic character of the product, urethane. The alcohol itself was also weakly catalytic and the values of k_{obs} obtained were found to agree with the above scheme, in which $[B]$ is replaced by (b-x).

Considering equation (2-2) and the three conditions, mentioned before, Baker et al[37] showed

$$k_{obs} = k_o + k_{cat} [B] \quad \ldots.(2\text{-}4)$$

where $k_{cat} = k_1 k_3/(k_2 + k_3 (b-x))$ ....(2-5)

Baker observed the predicted linearity between k_{obs} and [B] expected from equation (2-4), as did Borkent[38] using triethylenediamine.

Sato[39] has studied the reactions of ethyl and alk-1-enyl isocyanates with methanol in di-n-butyl ether at 25°; autocatalysis was appreciable. The rate of the spontaneous reaction was equal to the sum of two terms, each of the form of the second term of the R.H.S. of equation (2-1), i.e.

$$dx/dt = \frac{k_1 k_3 (a-x) (b-x)^2}{k_2 + k_3 (b-x)} + \frac{k'_1 k'_3 (a-x) (b-x) x}{k'_2 + k'_3 (b-x)} \quad ....(2-6)$$

where k_o, the spontaneous reaction rate constant is neglected. The first term in equation (2-6) resulted from the reaction of the isocyanate-alcohol complex ([B] = (b-x)) and the second term from the reaction of the isocyanate-urethane complex ([B] = x). Sato assumed that the rates of formation and decomposition of these complexes were fast compared with their reactions with the alcohol to give urethane. This assumption led to equation (2-7).

$$dx/dt = \frac{k_1 k_3}{k_2} (a-x) (b-x)^2 + \frac{k'_1 k'_3}{k'_2} (a-x) (b-x) x \quad ....(2-7)$$

The primed constants refer to the auto-catalytic reaction. He observed that alk-1-enyl urethanes were more nucleophilic than the aryl urethanes of Baker, so that the autocatalytic effect could not be ignored. He also observed that the spontaneous reactions between alkyl isocyanates and alcohols were better explained by the second term in equation (2-7) particularly after the reaction had proceeded to some extent. In addition, Sato[39] found that for reactions with added nucleophile catalyst the

deviations from second-order kinetics were slight; the catalysed reaction predominated leading to equation (2-8),

$$dx/dt \simeq (k'_1 \; k'_3/k'_2)\,(a-x)\,(b-x)\,[B] \qquad \ldots.(2\text{-}8)$$

Okada and Iwakura[40] have shown that the spontaneous reactions between phenyl isocyanate and n-butanol also follow equation (2-7), and the catalysed reactions - the combination of equations (2-7) and (2-8). Other workers[24,41-50] have also studied the effect of solvents, substituents on the aromatic ring and catalysts on the kinetics of the reactions between aromatic isocyanates and alcohols.

Greenshield, Peters and Stepto[51] studied the spontaneous reaction of hexamethylene diisocyanate (HDI) with butan-2-ol, trimethylol propane (OPTMP) and a polyethylene glycol in three solvents - toluene, o-dichlorobenzene and nitrobenzene. The kinetics results were analysed according to the complete equation (2-6). However, to facilitate the mathematical analysis, equation (2-6) was simplified using four mechanistic approximations[51]. Only two of those gave reasonable agreement with experiment and they were:

(1) $k_2 \gg k_3\,(b-x)$ and $k'_2 \gg k'_3\,(b-x)$

which is Sato's assumption that the rate of formation and decomposition of the complex is fast compared with its rate of reaction. This results in Sato's simplified equation (2-7).

(2) $k_3\,(b-x) \gg k_2$ and $k'_3\,(b-x) \gg k'_2$

which assumes that the rate of reaction of the complex is fast compared with its rate of formation resulting in equation (2-9)

$$dx/dt = k_1\,(a-x)\,(b-x) + k'_1\,(a-x)\,x \qquad \ldots.(2\text{-}9)$$

The first approximation produced agreement with those experiments conducted in solvents of low dielectric constant, whilst the second gave better agreement with those experiments conducted in solvents of higher dielectric constant.

Hopkins, Peters and Stepto[11] studied the kinetics of the triethylenediamine-catalysed reactions of urethane formation from aliphatic diisocyanates (HDI and DDI) and poly(oxypropylene) triols and observed second order kinetics for the catalysed reactions. However the autocatalytic effect becomes significant at higher dilutions of the reactants.

Waywell[52] has studied the spontaneous reaction of HDI with polyethylene glycols in benzene. The kinetic results were analysed with reference to equation (2-6) and the approximations proposed by Greenshield, Peters and Stepto[51]. It was found that with equivalent proportions of reactants, the reaction followed apparently first order kinetics. Deviations from first order kinetics were appreciable with the non-equivalence of reactants. By rearranging equation (2-9) Waywell obtained

$$dx/dt = (a-x)\left[x\ (k'_1 - k_1) + k_1\ b\right] \qquad \ldots.(2\text{-}10)$$

and assumed that for all reaction $k_1 = k'_1$, so that equation (2-10) simplifies to

$$dx/dt = k_1\ b\ (a-x) \qquad \ldots.(2\text{-}11)$$

This is a first order rate equation with $k_1 b$ the apparent first order rate constant. The true second order rate constant k_1 in equation (2-11) was evaluated from the first order kinetic plots and was found to increase with initial hydroxyl group concentrations. This trend in value of k_1 was attributed to the increase in dielectric constant[51] of the system

with decreasing dilution. Experiments with excess hydroxyl groups showed a positive deviation for the rate predicted by equation (2-11) whilst a negative deviation was observed with an excess of isocyanate groups. Waywell concluded that his experimental system was adequately explained by equation (2-9) if the assumption was made that

$$k_3 (b-x) >> k_2 \text{ and } k'_3 (b-x) >> k'_2.$$

Stanford[19] studied the kinetics of the spontaneous reaction between LG56 and HDI in benzene at 70°. He observed that this spontaneous reaction cannot be satisfactorily explained by simple first or second order kinetics. The reaction appeared to follow an apparent order which is between first and second order kinetics.

Wilson[53] studied the kinetics of the triethylenediamine-catalysed reactions between HDI and a poly(oxypropylene)triol. He observed positive deviations from second order kinetics for systems $r \geq 1$ but second order kinetics for systems $r < 1$ (where $r = (NCO)o/(OH)o$).

In presence of added catalyst, combining the equations (2-7) and (2-8) gives equation (2-12)

$$dx/dt = \frac{k_1 k_3}{k_2} (a-x) (b-x)^2 + \frac{k'_1 k'_3}{k'_2} (a-x) (b-x)x + \frac{k''_1 k''_3}{k''_2} (a-x) (b-x) (B) \quad \ldots.(2\text{-}12)$$

In the present work, the kinetics of the spontaneous and triethylenediamine-catalysed reactions of HDI and poly(oxypropylene)triol in nitrobenzene and toluene have been studied. The results will be discussed in Chapter 4 in the light of the theories discussed in this short review.

2.2 THEORIES OF GELATION

A number of approximate theories have been proposed to describe the behaviour of gelling systems. These are briefly discussed in the following sections.

2.2.1 Flory-Stockmayer Theory of Gelation

Given the equal reactivity of like functional groups and the absence of intramolecular reaction, the gel-point in an $RA_{f_a} + R'B_{f_b}$ polymerisation occurs when

$$p_a\, p_b\, (f_a - 1)\, (f_b - 1) = 1 \qquad \ldots.(2\text{-}13)$$

where p_a and p_b represent the probability that an A or B group, respectively, has reacted and, f_a and f_b are functionalities of the reactants bearing A and B groups. This equation stems from the more general relationship for the case when several reactants, some bearing A groups and some bearing B groups, are involved[8], namely,

$$p_a\, p_b\, (f_{aw} - 1)\, (f_{bw} - 1) = 1 \qquad \ldots.(2\text{-}14)$$

Here f_{aw} and f_{bw} are the weight-average functionalities of the reactants bearing A groups and B groups. Equations (2-13) and (2-14) state that there is a point in the polymerisation (the gel-point) where there is unit probability that the 'repeating structure' of the polymer formed can continue to infinity. From this point onwards, molecules limited in size only by the macroscopic amount of material in the reaction mixture make their appearance, so that sol and gel fractions coexist, consisting of finite and macroscopic or network species, respectively[7].

Equation (2-14) can be simply derived[54], and in a manner which illustrates the usefulness of the concepts of repeating structure and f_w.

Consider a reaction mixture consisting of N_{a1}, N_{a2}, ... moles of reactants bearing f_{a1}, f_{a2},... A groups reacting with N_{b1}, N_{b2},... moles of reactants bearing f_{b1}, f_{b2},.... B groups. Choose an A group at random from the mixture, as illustrated on the left of fig. 2-1. The probability that it belongs to the monomer of functionality f_{ai} is given by the expression

$$N_{ai} \cdot f_{ai} / \Sigma N_{ai} \cdot f_{ai} = f_a(i) \qquad \ldots.(2\text{-}15)$$

the fraction of A groups which are on units of that functionality. The probability that the unit to which the chosen A group is attached is connected to a unit bearing B groups is $(f_{ai} - 1)\ p_a$. There are $(f_{ai} - 1)$

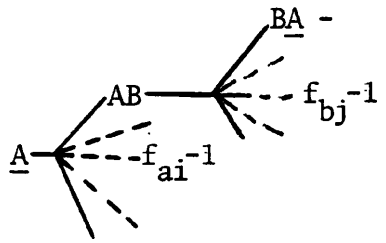

Fig. 2.1 Repeating structure A to A, for RA_{fai} and $\acute{R}B_{fbj}$ units in a general non-linear random polymerisation

possible paths to a unit bearing B groups and each has a probability p_a of continuing. Assume that, as illustrated in fig 2.1, one has continued, then there is a probability $f_b(j)$ (corresponding to $f_a(i)$) that it joins to a unit bearing jB groups. This unit can in turn lead to an A unit with probability $(f_{bj} - 1)\ p_b$, thus spanning the repeating structure defined by RA_{fai} and $\acute{R}B_{fbj}$ units. Hence the probability that this structure is spanned, is

$$f_a(i)\ (f_{ai} - 1)\ p_a \cdot f_b(j)\ (f_{bj} - 1)p_b \cdot$$

The average repeating structure of the whole reaction mixture includes all species i and j and the corresponding probability of continuation is

$$\sum_{i,j} f_a(i)\ (f_{ai} - 1)p_a \cdot f_b(j)\ (f_{bj} - 1)p_b$$

This expression factorises into a product of sums over i and j, giving for gelation

$$p_a\, p_b\ (\sum_i f_{ai}\, f_a(i) - \sum_i f_a(i)) \cdot (\sum_j f_{bj}\, f_b(j) - \sum_j f_b(j)) = 1 \qquad ....(2\text{-}16)$$

However,

$$\sum_i f_{ai} \cdot f_a(i) = \sum_i N_{ai} \cdot f_{ai}^2 / \sum_i N_{ai} \cdot f_{ai} = f_{aw} \qquad ....(2\text{-}17)$$

$$\sum_j f_{bj} \cdot f_b(j) = \sum_j N_{bj} \cdot f_{bj}^2 / \sum_j N_{bj} \cdot f_{bj} = f_{bw} \qquad ....(2\text{-}18)$$

and

$$\sum_i f_a(i) = \sum_j f_b(j) = 1 \qquad ....(2\text{-}19)$$

giving immediately equation (2-14).

A simple application of equation (2-14) is for an $RA_2 + RA_f + \acute{R}B_2$ polymerisation. Flory[8,55] has derived an expression for the gel-point giving

$$p_a\, p_b\ ((2(1 - \rho) + f \cdot \rho) - 1) = 1 \qquad ....(2\text{-}20)$$

where ρ is the fraction of A groups on RA_f units. In fact this equation follows directly from equation (2-14) as $f_{bw} = 2$ and $f_{aw} = 2\ (1 - \rho) + f \cdot \rho$. Application of equation (2-14) for RA_2 and $\acute{R}B_f$ type polymerisation gives, for $\rho = 1$,

$$p_a\, p_b = \frac{1}{f-1} = \alpha_c$$

$$\therefore \alpha_c = p_a\, p_b = \frac{1}{f-1} \qquad \ldots.(2\text{-}21)$$

where α_c is the critical branching coefficient as defined by Flory[7]. Thus, for $RA_2 + R'B_3$ type polymerisation, equation (2-21) reduces to

$$\alpha_c = p_a\, p_b = \tfrac{1}{2} \qquad \ldots.(2\text{-}22)$$

and for such a polymerisation, gelation occurs when $\alpha_c = 0.50$, according to this theory. In practice, gelation occurs at the products of the extents of reaction (ie. $p_a\, p_b = \alpha_c$) higher than the values predicted by this theory. Intramolecular reaction[11-14,18,19,24,25] has been found to be responsible for these discrepancies, although unequal reactivities[61] of functional groups also affect the value of α_c (and hence $p_a\, p_b$).

2.2.2 Modified Kilb's Theory of Gelation (Kilb-Ahmad-Stepto Theory)

Kilb[17] extended Flory's method of calculating the extent of reaction at the gel point by including the possibility of intramolecular reaction and came to the conclusion that gelation occurs when

$$\alpha_c\,(f-1)\,(1-\lambda_\kappa) = 1 \qquad \ldots.(2\text{-}23)$$

where $\lambda_\kappa = k \cdot D \cdot \phi(1,3/2)$, a ring-forming parameter,

with $k = \left(\frac{3}{2\pi\nu}\right)^{3/2} \cdot \frac{V_p}{2b^3}$ and $D = \frac{V}{V_p}$, ν is the number of atoms per repeat unit, b is the effective bond length of the chain comprising the polymer repeat unit, V is the total volume of the system and V_p is the volume of the polymer formed (although it is not possible to determine V_p experimentally in condensation polymerisations and hence D, the dilution of the system);

$$\phi(1,\ 3/2) = \sum_{i=1}^{\infty} (1)^{i} \cdot (i)^{-3/2} = 2.612 \qquad \ldots.(2\text{-}24)$$

as defined by Truesdell[56], for non-equilibrium reactions. For equilibrium reactions the exponent 3/2 will be replaced by 5/2 in the function $\phi(1,3/2)$.

Kilb's theory has been modified[57] to give an alternative approximation to the condition for gelation in $RA_2 + R'B_f$ type polymerisation. The linear sequence, as shown in fig 2.2(a) for $RA_2 + R'B_3$ type polymerisation is modified as shown in fig 2.2(b).

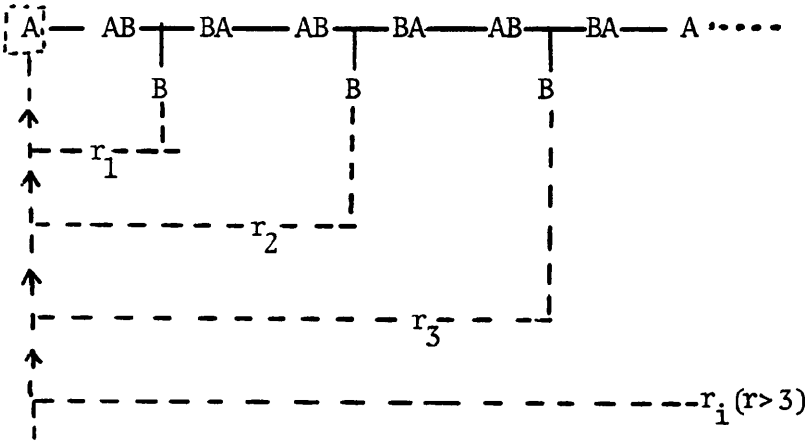

Fig 2.2(a) Kilb's simplification of the molecular structures in an $RA_2 + R'B_3$ type of polymerisation.
r_1, r_2, r_3, ... are probabilities of intramolecular reaction.

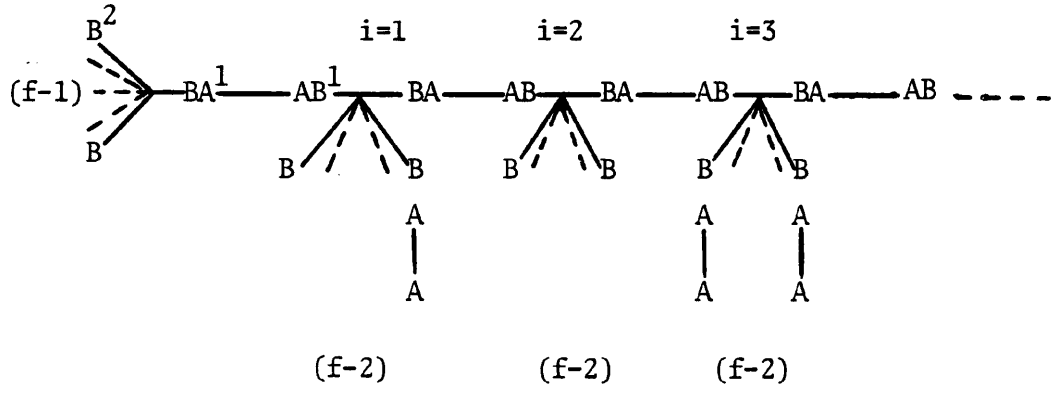

Fig 2.2(b) Development of Kilb's linear sequence to define the condition for gelation in an $RA_2 + R'B_f$ polymerisation[57].

If the sections to the right of B^1 is assumed to exist, each branch unit of the i th generation will have (f-2) unreacted groups, f being the functionality of the molecule. These groups may be either A or B groups. Gelation occurs when the probability that the sequence goes from B^1 to B^2 equals unity. This probability is given by the product of the probabilities of two intermolecular reactions occurring, there also being an opportunity for intramolecular reaction at each step.

B^1 can react intermolecularly with probability $p_b(1-\lambda_a)$ where λ_a is given by

$$\lambda_a = \sum_{i=1}^{\infty} r_{i,a} \qquad \ldots.(2\text{-}25)$$

In this expression $r_{i,a}$ is the probability of intramolecular reaction with one of the unreacted A groups connected to branch unit i, ie.,

$$r_{i,a} = \frac{C_{a,int,i}}{C_{a,int} + C_{a,ext}} \qquad \ldots.(2\text{-}26)$$

$C_{a,ext}$ is the instantaneous concentration of unreacted A groups in the mixture and $C_{a,int,i}$ is the concentration, around B^1, of A groups connected to branch unit i so that

$$C_{a,int} = \sum_{i=1}^{\infty} C_{a,int,i} \qquad \ldots.(2\text{-}27)$$

If the instantaneous external concentrations of unreacted A and B groups are C'_a and C'_b,

$$C_{a,int,i} = \frac{(f-2)}{N} \cdot \frac{P_{ab}}{i^{3/2}} \cdot \frac{C'_a}{C'_a + C'_b} \qquad \ldots.(2\text{-}28)$$

where $P_{ab} = P(\underline{0}, \nu) = \left(\frac{3}{2\pi\nu\, b^2}\right)^{3/2}$ ....(2.29)

ν is the number of bonds in the chain forming the smallest ring, b is the effective bond length, and N is the Avogadro number. Substitution of $r_{i,a}$, as evaluated by equations (2-26) and (2-28) into equation (2-25) gives,

$$\lambda_a = \frac{C_{a,int}}{C_{a,int} + C_{a,ext}} = \frac{(f-2).P_{ab}.\phi(1,3/2) \cdot C'_a/((C'_a+C'_b)N)}{(f-2).P_{ab}.\phi(1,3/2).C'_a/((C'_a+C'_b)N)+C'_a} \quad ..(2.30)$$

Similarly, for A^1 the probability of intermolecular reaction is $p_a(1-\lambda_b)$ with

$$\lambda_b = \frac{C_{b,int}}{C_{b,int}+C_{b,ext}} = \frac{(f-2).P_{ab}.\phi(1,3/2) \cdot C'_b/((C'_a+C'_b)N)}{(f-2).P_{ab}.\phi(1,3/2) \cdot C'_b/((C'_a+C'_b)N)+C'_b} \quad .... (2.31)$$

Reaction of A^1 leads to (f-1) possible paths for continuing the linear sequence to B^2. Thus, gelation occurs when

$$(f-1) \cdot p_b(1-\lambda_a) \cdot p_a(1-\lambda_b) = 1 \quad ....(2.32)$$

giving

$$\alpha_c(f-1)\ (1-\lambda_a)\ (1-\lambda_b) = 1 \quad ....(2.33)$$

Further, comparison of equations (2-30) and (2-31) shows that $\lambda_a = \lambda_b = \lambda_{ab}$ (say), with

$$\lambda_{ab} = \frac{(f-2) \cdot P_{ab} \cdot \phi(1,3/2)/N}{(f-2) \cdot P_{ab} \cdot \phi(1,3/2)/N + (C'_a+C'_b)} \quad ....(2.34)$$

and $$\alpha_c(f-1)\ (1-\lambda_{ab})^2 = 1 \quad ....(2.35)$$

Comparison of equations (2-23) and (2-35) shows that $2\lambda_{ab} = \lambda_{\kappa}$ for small λ_{ab} and f = 3. Equation (2-35) is the simplest analytical result derivable from the correct application of the Kilb model of a linear sequence of branch units. Thus, Kilb's theory may be considered as a special case of the Kilb-Ahmad-Stepto theory.

The two factors $(1-\lambda_{ab})$ arise from the two opportunities for intramolecular reaction in passing from one branch unit to the next. Equations (2-34) and (2-35) lead to the equations

$$\alpha_c^{\frac{1}{2}} (f-1)^{\frac{1}{2}} - 1 = \frac{\lambda_{ab}}{1-\lambda_{ab}} = \lambda'_{ab} \qquad \ldots.(2\text{-}36)$$

and

$$\lambda'_{ab} = \frac{C_{int}}{C_{ext}} = \frac{(f-2) \cdot P_{ab}\, \phi(1,3/2)}{C_{ext}} \qquad \ldots.(2\text{-}37)$$

Now C_{ext} can be put equal to $(C_{ao} + C_{bo})$ and $(C_{ac} + C_{bc})$ as extreme values where $(C_{ao} + C_{bo})$ and $(C_{ac} + C_{bc})$ are total initial and gel concentrations of reactants. Plots of λ'_{ab} versus $(C_{ao} + C_{bo})^{-1}$ and $(C_{ac} + C_{bc})^{-1}$, the initial and gel-point dilutions using the data of Smith and Stepto[14] show approximate linearity[57] when $(C_{ao} + C_{bo})^{-1}$ is used as abscissa and decreasing slopes when $(C_{ac} + C_{bc})^{-1}$ is used. Similar behaviour is observed[58] if other published data (refs. 11,12,18) are also analysed according to equations (2-36) and (2-37).

2.2.3 Frisch's Theory of Gelation

Frisch[16] developed a mathematical theory of gelation representing a growing branched molecule by a "Mathematical Tree". The portion of a molecule between each branch point is represented by a straight line and the centres of each branch unit lie on the circumference of a circle. The distances between each branch point are assumed equal

and the model can, therefore, only be applied to reaction systems of the type $RA_2 + \acute{R}B_f$ where only reaction between A and B groups can occur, and also to the system RB_f where pairs of B groups react together.

On the basis of this model and assuming that only small amounts of rings are formed in the reaction, Frisch obtained an expression for gelation as

$$\alpha_c (f-1) (1 - (1-\alpha_c) \lambda_F) = 1 \qquad \ldots.(2\text{-}38)$$

which can be simplified to (after neglecting higher terms in λ_F)

$$\alpha_c = (f-1)^{-1} (1- \lambda_F)^{-1} \qquad \ldots.(2\text{-}39)$$

where λ_F is defined as an intramolecular branching co-efficient representing the number of vertices (functionalities) lost due to intramolecular reaction. Frisch did not explain λ_F in terms of molecular parameters. However, correlation[18] of Frisch's theory with that of Kilb has enabled λ_F to be interpreted in molecular terms and shown that λ_F and λ_κ become equivalent when both are small.

Gelation data have been used by Ahmad and Stepto[57] in which λ_F and λ_κ are plotted against $(C_{ao} + C_{bo})^{-1}/2$ for $RA_2 + \acute{R}B_3$ type polycondensation. These analyses have shown that if it is assumed that $C_{ext} >> C_{int}$, Frisch's expression is to be preferred, since λ_F gives more linear plot than λ_κ. When gel dilutions are used, both the Frisch and Kilb expressions result in plots of λ versus $(C_{ac} + C_{bc})^{-1}/2$ with decreasing slopes. However, if as in equation (2-36), the assumption $C_{int} \ll C_{ext}$ is not made, λ'_κ gives the more satisfactory plots. Thus, as Kilb's theory is a limiting case of Kilb-Ahmad-Stepto theory, the use of λ'_{ab} is preferred.

2.2.4 Polyfunctional Rate Theory (PFRT)

The rate theory was first developed to describe irreversible random polymerisation of bifunctional monomers[3] and was later extended to cover polyfunctional cases by Cawse, Stanford and Stepto[63]. Cawse, Stanford and Stepto[63] developed a statistical approach to non-linear irreversible polymerisation in terms of rate equations applied to existence states of molecular species. The term 'rate' is used with respect to appearance and disappearance of states as functions of extent of reaction, not time, and so any dependence of the polymerisation process of chemical kinetics is necessarily avoided to a first approximation.

Limited subsets of the A-A and B$\begin{smallmatrix} B \\ \diagup \\ B \end{smallmatrix}$ monomer units in a $RA_2 + R'B_3$ type polymerisation are considered, and the existence probabilities and rates of conversion of each state are thus evaluated. Tables 2.1 and 2.2 show the existence probabilities of A-A and of B$\begin{smallmatrix} B \\ \diagup \\ B \end{smallmatrix}$ units[19].

The existence probabilities, P_{Ai} and P_{Bi}, are obtained by multiplying the various combinations of individual probabilities of an A or B group having reacted (p_a, p_b) or remaining unreacted ($1-p_a$, $1-p_b$) respectively. The coefficients in states A_2-A_4 and A_6-A_8, etc. arise from symmetry considerations necessary to account completely for all possible arrangements of chains adjacent to the reference A—A or B$\begin{smallmatrix} B \\ \diagup \\ B \end{smallmatrix}$ monomer unit.

At the beginning of the reaction ie. (p_a = o, p_b = o) only states A—A and B$\begin{smallmatrix} B \\ \diagup \\ B \end{smallmatrix}$ exist, but as the reaction proceeds, a distribution of molecules represented by the states A_1 to A_{11} and B_1 to B_{13} is generated. The PFRT, in this limiting form, accounts for ring formation of only 1-membered species (see Tables 2.1 and 2.2), but in principle it can be expanded to account for all species. However, it should be noted that the distribution of ring sizes is such that 1-membered rings are the single

TABLE 2.1 A—A Subset in $RA_2 + R'B_3$ type polymerisation.

State	Existence Probability, P_{Ai} (No rings)	No. of continuing branch points
A1 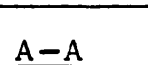	$P_{A1} = (1-p_a)^2$	0
A2 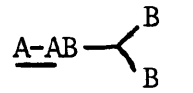	$P_{A2} = 2(1-p_a)\ (1-p_b)^2\ p_a$	0
A3 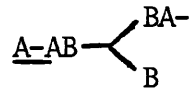	$P_{A3} = 4(1-p_a)\ (1-p_b)\ p_a\ p_b$	1
A4 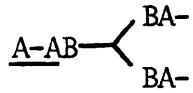	$P_{A4} = 2(1-p_a)\ p_a\ p_b^2$	2
A5 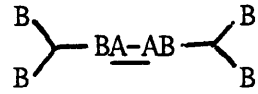	$P_{A5} = (1-p_b)^4\ p_a^2$	0
A6 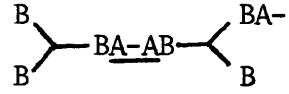	$P_{A6} = 4(1-p_b)^3\ p_a^2\ p_b$	1
A7 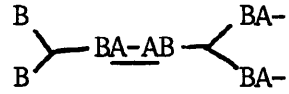	$P_{A7} = 6(1-p_b)^2\ p_a^2\ p_b^2$	2
A8 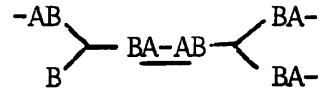	$P_{A8} = 4(1-p_b)\ p_a^2\ p_b^3$	3
A9 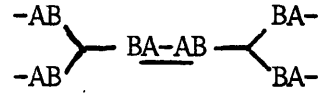	$P_{A9} = p_a^2\ p_b^4$	4
A10 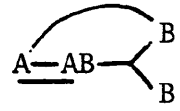	$P_{A10} = 0$	0
A11 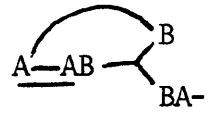	$P_{A11} = 0$	1

$\therefore$ Total probability = $\sum_{i=1}^{i=11} P_{Ai} = 1$

TABLE 2.2 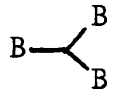 Subset in $RA_2 + R'B_3$ type polymerisation.

State	Existence Probability (no rings), P_{Bi}	No. of continuing branch points
B1 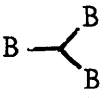	$P_{B1} = (1-p_b)^3$	0
B2 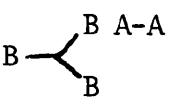	$P_{B2} = 3(1-p_b)^2 (1-p_a) p_b$	0
B3 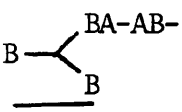	$P_{B3} = 3(1-p_b)^2 p_a p_a$	1
B4 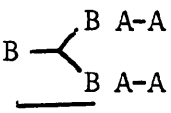	$P_{B4} = 3(1-p_b) (1-p_a)^2 p_b^2$	0
B5 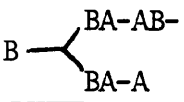	$P_{B5} = 6(1-p_b) (1-p_a) p_b^2 p_a$	1
B6 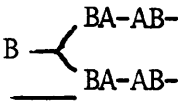	$P_{B6} = 3(1-p_b) p_b^2 p_a^2$	2
B7 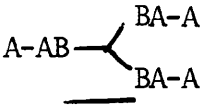	$P_{B7} = p_b^3(1-p_a)^3$	0
B8 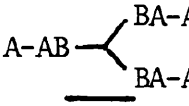	$P_{B8} = 3(1-p_a)^2 p_b^3 p_a$	1
B9 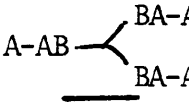	$P_{B9} = 3(1-p_a) p_b^3 p_a^2$	2
B10 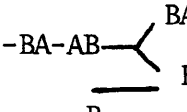	$P_{B10} = p_a^3 p_b^3$	3
B11 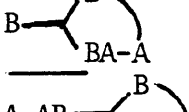	$P_{B11} = 0$	0
B12 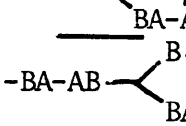	$P_{B12} = 0$	0
B13 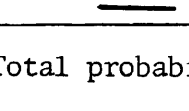	$P_{B13} = 0$	1

$\therefore$ Total probability = $\sum_{i=1}^{i=13} P_{Bi} = 1$

most prominent species, and so even the limiting form of the theory is a useful approximation to the general case.

States 1, 2 and 5 in A-A subset (Table 2.1) are 'discrete' molecules and as such cannot contribute to the gel, whereas the remaining states, possessing A- at the end of a branch unit are 'continuing' molecules and can contribute to the gel. Similarly, 'discrete' and 'continuing' molecules are also present in B 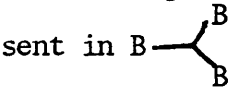 subsets.

The reactions by which interconversion from one subset to another occurs are summarised in Table 2.3, in which $A_{1,2}$ represents conversion of state A_1 to state A_2 (ie. the appearance of state A_2, the dimer,

TABLE 2.3

Route	Reactions	Ringless Reaction Rate
$A_{1,2}$	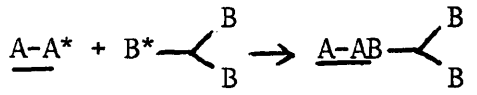	$A'_{A1,2} = 2(1-p_a)(1-p_b)^2$
$A_{2,3}$	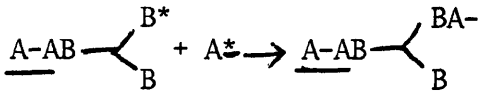	$D'_{A2,3} = 4(1-p_a)(1-p_b).p_b$
$A_{2,5}$	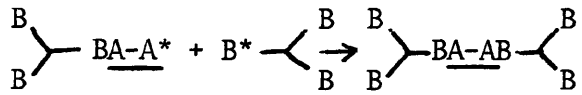	$D'_{A2,5} = 2(1-p_b)^4\ p_a$
$A_{2,6}$	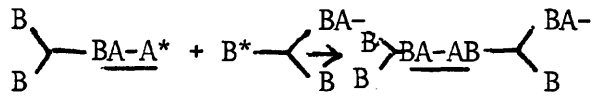	$D'_{A2,6} = 4(1-p_b)^3\ p_a\ p_b$
$A_{2,7}$	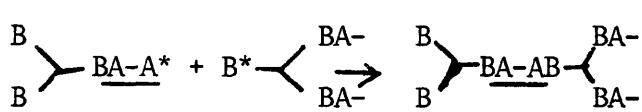	$D''_{A2,7} = 2(1-p_b)^2\ p_a\ p_b^2$
$A_{2,10}$		$R'_{A2,10} = 0$

from monomer A_1) while the other routes represent disappearance reactions. The starred groups, A* and B*, must react[3], and this reaction is, therefore, assigned unit probability. The rate of reaction is then equal to the product of the existence probabilities of the sequence of bonds walking away from either side of A* and B*. When the probability equations are differentiated, a series of positive and negative terms result for each state, and these differential terms can be interpreted as the rates of appearance to and disappearance from each state, corresponding to the reaction routes as shown in Table 2.3 for state 2. The total of the rates of appearance (A´) and disappearance (D´) for each state sum up to the value obtained by differentiating the existence probabilities from Tables 2.1 and 2.2.

Considering A-A subsets, clearly, state 1 will only contain a negative term since A-A monomer can only disappear and similarly state 9 will only contain a positive term since this state cannot disappear further, according to this scheme. Such a differential procedure enables the pattern of continuous reaction to be established in terms of rate equations for each reaction step.

Since the total concentration of A groups external to given state is C_a and of B groups is C_b where

$$C_a = C_{ao}\ (1-p_a) \text{ and } C_b = C_{bo}\ (1-p_b),$$

then the relative concentration of a reactive species is given by multiplying the total concentration of A or B groups (C_a or C_b) by the fractional probability describing chain structure attached to the reacting A or B group of the reactive species: For example, the reactive species for route $A_{2,3}$ ie. A*- the relative concentration will be

$2\,C_a \times 1$, for route $A_{2,5}$ the relative concentration will be $C_b \times (1-p_b)^2$, for route $A_{2,6}$ the relative concentration will be $C_b \times 2(1-p_b)p_b$ and for route $A_{2,7}$ the relative concentration will be $C_b \times p_b^2$. Their total concentration is thus $(A_{2,3} + A_{2,5} + A_{2,6} + A_{2,7}) = 2\,C_a + C_b$, and the rate of disappearance of each species is thus a weighted fraction of the total rate of disappearance of state 2, D'_{A2}, where (in absence of ring formation)

$$D'_{A2} = D'_{A2,3} + D'_{A2,5} + D'_{A2,6} + D'_{A2,7}$$

$$= 4(1-p_a)(1-p_b).p_b + 2(1-p_b)^4 p_a + 4(1-p_b)^3 p_a p_b + 2(1-p_b)^2 p_a p_b^2$$

(from Table 2.3)

$$\therefore\ D'_{A2} = 2(1-p_b)\ (p_a(1-p_b) + 2(1-p_a)\ p_b)$$

With intramolecular reaction, not only the relative concentration of reacting species must be considered, but also the positions of the reactive end groups of state 2 molecules. The latter necessitates the introduction of a ring-forming parameter, P_{ab}, which accounts for the 'internal' concentration of A and B groups belonging to a given branch unit, and is related to the Jacobson-Stockmayer P by the relation

$$P_{ab} = \frac{P}{v_s}$$

where v_s is the small volume occupied by reacting A and B groups on the same molecule.

Thus,

$$P_{ab} = \left(\frac{3}{2\pi\nu}\right)^{3/2} . b^{-3}$$

where b is the effective bond length of a chain of ν bonds, forming the smallest ring.

The routes by which intramolecular reaction can occur have been given in Table 2.3 and the rates of disappearance of each state should now be renormalised to account for this. This is summarised in Table 2.4 for state A_2 in which $C_{A2} = (2C_a + C_b + 2P_{ab})$.

TABLE 2.4

Route	Rate of disappearance (no rings)	Rate of disappearance (rings)
2,3	$D'_{A2} \times 2C_a/(2C_a + C_b) = D'_{A2,3}$	$D'_{A2} \times 2C_a/C_{A2} = D'_{A2,3}$
2,5	$D'_{A2} \times C_b(1-p_b)^2/(2C_a + C_b) = D'_{A2,5}$	$D'_{A2} \times C_b(1-p_b)^2/C_{A2} = D'_{A2,5}$
2,6	$D'_{A2} \times 2C_b(1-p_b)p_b/(2C_a + C_b) = D'_{A2,6}$	$D'_{A2} \times 2C_b(1-p_b)p_b/C_{A2} = D'_{A2,6}$
2,7	$D'_{A2} \times C_b p_b^2/(2C_a + C_b) = D'_{A2,7}$	$D'_{A2} \times C_b p_b^2/C_{A2} = D'_{A2,7}$
2,10		$D'_{A2} \times 2P_{ab}/C_{A2} = D'_{A2,10}$

Integration between o and p_a (or p_b) of these rate equations for each possible route will now give weight (or unit) fractions of molecules reacted by that route, and summing the integrated rate expressions will give fractions of molecules in each state. The total unit fraction of any species, taking into account both subsets, can be found by weighting the fractions from each subset in proportion to the initial unit fractions of RA_2 and $R'B_3$ units, x_A and x_B, where

$$x_A = \frac{N_a}{N_a + N_b} = \frac{3r}{3r + 2}$$

and

$$x_B = \frac{N_b}{N_a + N_b} = \frac{2}{3r + 2}$$

with N_a and N_b as the numbers of A and B units. For example,

$$P_2 = x_A P_{A2} + x_B P_{B2} \qquad (P_{A2} \text{ and } P_{B2} \text{ are defined in Tables 2.1 and 2.2})$$

Flory's gelation theory predicts the critical point to occur when $p_a p_b = 0.5$. Similarly, it is possible to define the critical point in the reaction in presence of intramolecular reaction, using the PFRT. In the PFRT, only those states which have continuing branches, contribute to the gel which for A-A subset are states A_3, A_4, A_6, A_7, A_8, A_9 and A_{11} (see Table 2.1). If there are no rings, the sum of these states, weighted according to the number of continuing chains, is defined as the "Critical Total of the A-A subset" (CTA) and is given as

$$P_{A3} + 2P_{A4} + P_{A6} + 2P_{A7} + 3P_{A8} + 4P_{A9} = CTA$$
$$= 4p_a p_b \qquad \ldots.(2\text{-}40)$$

Similarly, for the B  subset (see Table 2.2),

$$P_{B3} + P_{B5} + 2P_{B6} + P_{B8} + 2P_{B9} + 3P_{B10} = CTB$$
$$= 3p_a p_b \qquad \ldots.(2\text{-}41)$$

In equation (2-40), the product $4p_a p_b$ corresponds to the 4 branches in the molecular species

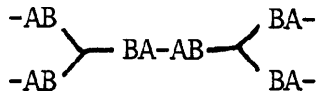

and the product $3p_a p_b$ in equation (2-41) corresponds to the 3 branches in the species

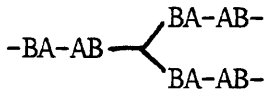

Thus the critical point is given by

$$x_A\left(\frac{CTA}{4}\right) + x_B\left(\frac{CTB}{3}\right) = 0.5 \qquad \ldots.(2\text{-}42)$$

The equations for CTA and CTB are altered in presence of rings by employing unit fractions evaluated as before. For the A-A subset,

$$P^*_{A3} + 2P^*_{A4} + 2P^*_{A7} + 3P^*_{A8} + 4P^*_{A9} + P^*_{A11} = CTA^* \qquad \ldots.(2\text{-}43)$$

and for the B  subset,

$$P^*_{B3} + P^*_{B5} + 2P^*_{B6} + P^*_{B8} + 4P^*_{B9} + 3P^*_{B10} + P^*_{B13} = CTB^* \qquad \ldots.(2\text{-}44)$$

and thus the theoretical condition for gelation is given by

$$\frac{3r}{(3r+2)} \cdot \left(\frac{CTA^*}{4}\right) + \frac{2}{(3r+2)} \cdot \left(\frac{CTB^*}{3}\right) = 0.5 \qquad \ldots.(2\text{-}45)$$

When ring-forming routes are considered, it is found that their respective rates of formation can be rearranged entirely in terms of P_{ab}, C_{ao} and r. For example, for $A_{2,10}$ the rearranged rate of formation becomes (from Table 2.4)

$$\frac{D_{A2} \times 2r\ P_{ab}/C_{ao}}{(1+2r - 3rp_a + 2rP_{ab}/C_{ao})}$$

and similar equations, in terms of the dimensionless quantity P_{ab}/C_{ao} can be derived for the other ring-forming routes. Thus to apply the theory to experimental data, for a given value of r, it is only necessary to feed in the values of P_{ab}/C_{ao} and to compute values of the critical totals and then average according to equations (2-42) and (2-45), at selected increments of p_a. Such a plot is shown in fig 4.23, chapter 4 for r = 1. The values of P_{ab}/C_{ao} at which $p_a p_b$ equals the critical gel condition are read-off and plotted to give a "master curve" and from such a curve, experimental values of $(p_a p_b)_c$ can be identified with values of P_{ab}/C_{ao} which accounts for the amount of intramolecular reaction during the polycondensation. Hence multiplying this value of P_{ab}/C_{ao} by the initial concentration of A groups, the ring-forming parameter P_{ab} can be found and its dependence on the molecular attributes of the system evaluated. The theory also enables ring fraction data to be interpreted in experiments where molar mass have been measured during the reaction[19].
Thus the ability of PFRT to account for the variation in C_{ext} during the polymerisation marks an advance over the approximate theory (Kilb-Ahmad-Stepto) of gelation, which requires some arbitrary, single value of C_{ext} for the pregel reaction to be chosen. Practical use of the theory (PFRT) will be discussed in more detail in chapter 4.

2.3 Determination of Effective Functionalities from Gelation Data

Gelation data from reactions at various dilutions are sometimes used to determine chemical functionalities of reactants[59-62]. Such a procedure should be viewed with caution as it assumes that the functional form of the dependence of ring-forming parameter upon dilution which is predicted by theory is that obtained in practice, and this assumption is not always justified[60]. To estimate functionality from α_c, equations (2-34) and (2-35) may be equated with the equation (2-46)

$$\lambda = \frac{C_{int}}{C_{int} + C_{ext}} \qquad \ldots.(2\text{-}46)$$

which gives

$$\alpha_c^{\frac{1}{2}} = \frac{1}{(f-1)^{\frac{1}{2}}} + \frac{(f-2)}{(f-1)^{\frac{1}{2}}} \cdot \frac{P_{ab} \cdot \phi(1,3/2)}{N \cdot C_{ext}} \qquad \ldots.(2\text{-}47)$$

According to equation (2-47), a plot of $\alpha_c^{\frac{1}{2}}$ versus C_{ext}^{-1} should be linear with intercept equal to $(f-1)^{-\frac{1}{2}}$ or more strictly $(f_w-1)^{-\frac{1}{2}}$. It has been shown[60] that the data should be represented by a curved plot rather than linear plot as the functionality obtained from the curved plot is more consistent with the known functionality of the triol. The curved plot is in fact just an alternative manifestation of the curved λ versus C_{ext}^{-1} plots, which will be discussed in chapter 4.

2.4 PRESENT WORK

The object of the present research is to study the non-equilibrium reaction between a bifunctional monomer of the type A-A and a trifunctional monomer of the type 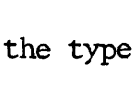 under different reaction conditions in order to study the intramolecular reaction during a polycondensation polymerisation. The reaction between hexamethylene diisocyanate (HDI) and a poly(oxypropylene) triol (LG-56) in nitrobenzene and toluene, with or without added catalyst (DABCO), has been used. The HDI/hydroxyl system has been shown to be suitable for a study of ring formation for several reasons[25]. Extensive kinetics studies proved that the functional groups of HDI[51] and LG-56[11] are of equal reactivities. Among the known Niax triols (supplied by Union Carbide), LG-56 has the maximum molar mass ($\simeq$3000 g mol^{-1}). It has also a narrow molar mass distribution. Considering these factors, it is expected that HDI/LG-56 system may give nearly perfect networks, with few loops in them.

The functional groups of LG-56 molecule are secondary hydroxyl groups and initial experiments showed that uncatalysed reactions proceed at a very slow rate. Thus gelation reactions were carried out with and without catalyst (DABCO) to study the effect of catalyst on gel points and kinetics in bulk, nitrobenzene and toluene. More ring formation is observed in nitrobenzene than in toluene and the amount of ring formation increases with catalyst concentration in nitrobenzene. Some subsidiary experiments with HDI and DABCO in nitrobenzene and toluene (excluding triols) show that HDI concentration decreases more in nitrobenzene. So toluene has been chosen as solvent for the main part of the research work.

Two series of gelation reactions, with 5% (mol DABCO/mol NCO) catalyst

and without catalyst, have been carried out at different dilutions in toluene at 80°C. All the gelation reactions have been performed in equivalent concentrations of isocyanate and triol (ie. r = 1). From these two series of reaction mixtures, samples are moulded for uniaxial compression and torsion pendulum experiments to study the effect of pregel intramolecular reaction on the network properties. Differential Scanning Calorimetry (DSC) experiments have also been done on the networks to supplement the transition data obtained from the torsion pendulum experiments. Uniaxial compression tests have been performed with both dried and equilibrium swollen networks (in toluene); but torsion pendulum and DSC experiments are carried out only with dried networks.

The gelation data have been analysed on the basis of different gelation theories and polyfunctional rate theory. From these theories the effective bond length (b) is calculated and compared with results of the previous works. Gaussian theory and Mooney-Rivlin equation are applied to analyse the uniaxial compression data. Dynamic mechanical properties of the networks are also studied by torsion pendulum experiments.

Thus the experimental data for the effect of dilution and catalyst on the kinetics, gel points and properties of the networks are obtained and discussed.

CHAPTER - 3

NETWORK FORMATION : EXPERIMENTAL

Experiments were planned to study the effect of catalyst and dilution on the amount of intramolecular reaction during the polycondensation reaction between hexamethylene diisocyanate (HDI) and a poly (oxypropylene) triol (LG-56) in toluene at 80°C. Some preliminary experiments were also carried out using nitrobenzene as solvent. The initial ratio of the reactants, ie. $r = (NCO)_o/(OH)_o$, was kept to unity in all the reactions. In the majority of the gelation experiments, samples suitable for subsequent physical characterisation were also required. This chapter describes the purification and analyses of the reagents, the gelation procedure and the treatment of the experimental data.

3.1 Purification and Analyses of Starting Materials

3.1.1 Niax Triol LG-56

LG-56 was supplied by Union Carbide Corporation as a colourless, viscous liquid and is prepared by the addition polymerisation of propylene oxide with glycerol in the presence of catalyst. LG-56 has the structural formula

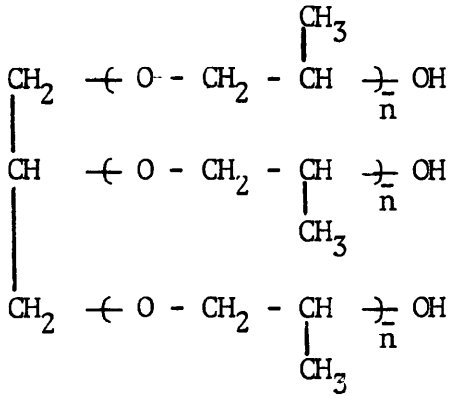

where $\bar{n}$, the number average degree of polymerisation of each branch, is approximately equal to 16.7. Poly (oxypropylene) triols are somewhat hygroscopic and require removal of small quantities of water before use. This was carried out by azeotropic distillation.

About 400 g of the triol and 1600 g of dried n-heptane (described later) were refluxed for about 10 hours and the water-n-heptane azeotrope was removed periodically using a Dean and Stark trap. Most of the heptane was removed whilst ensuring that the temperature of the mixture did not exceed about 102°C. The final traces of heptane were removed by distilling under vacuum at a pressure of about 0.05 mm of mercury, and the temperature of the flask was not allowed to exceed 80°C during the vacuum distillation. To ensure the complete removal of heptane, the triol was left under vacuum for about 20 hours. Infra-Red analysis on the wet triol showed a prominent peak at 1650 cm^{-1} due to the presence of water, but after drying, this peak was almost reduced and the more accurate Karl-Fischer analysis was used to determine the amount of water present. The results showed the water content to be less than 0.04% by weight or 2.22% by equivalent (see Table 3.1).

The equivalent weight of the dry triol was determined by end-group analysis using the well known acetylation method given by Sorensen and Campbell[64] with minor modification. About 5 g of dry triol were weighed directly into each of 3 dry, 250 ml round-bottomed flasks and to each of these was added 25 ml of a solution of acetic anhydride (18 ml) in dried pyridine (200 ml) (described later). The mixture was refluxed for about 5 hours after which time the flask was allowed to cool. About 8 ml of water were added down the condenser to hydrolyse the remaining acetic anhydride and the flask was heated again for a further 5 minutes. After cooling, the condenser and the neck of the flask were washed with 50 ml

of methanol. The mixture was then titrated to a phenolphthalein end point with 1 M potassium hydroxide solution (Titre A). Three blanks were carried out on a mixture of water (8 ml) and acetylating mixture (25 ml) in methanol (50 ml), (Titre B). Poly (oxypropylene) triols are slightly acidic in pyridine solution. A correction titre was carried out to account for this acidity by using a mixture of 10 g triol and 25 ml pure dried pyridine (Titre C). The equivalent weight of the triol is given by

$$\text{Equivalent weight} = \frac{\text{weight of triol} \times 10^3}{\text{Molarity of KOH} \times (B-A+C_2)}$$

where C_2 is the acid correction adjusted for the actual weight of triol used: C_2 was usually less than 0.05 ml.

Table 3.1 summarises the equivalent weights and the water contents of the different batches of dried triols used.

TABLE 3.1 Analysis of Niax Triol LG-56

Batch	Equivalent Weight*	% Water by Weight	% Water by Equivalent
1	998.8 ± 1.3**	0.03	1.66
2	997.2 ± 2.2	0.04	2.22
3	999.1 ± 3.0	0.04	2.22
4	998.6 ± 2.1	0.03	1.66
5	997.1 ± 1.2	0.03	1.66

* All equivalent weights and molar mass quoted in this thesis are expressed in g mol^{-1}

** Each value is the average of 3 determinations

Dry triol was stored in small, sealed bottles over phosphorous pentoxide in a desiccator containing silica gel and was kept in a freezer (-20°C) until required.

3.1.2 Hexamethylene-Diisocyanate (HDI)

Hexamethylene diisocyanate was supplied by Aldrich Chemical Company. The purity of HDI was estimated by titration. About 0.15 g of HDI was directly (accurately) weighed into each of three 250 ml conical flasks containing 25 ml solution of 2.5% di-n-butylamine in methylethyl ketone (MEK). After about half an hour, 50 ml of equivalent mixture of MEK/propan-2-ol were added to each flask. The remaining amine was titrated against 0.1 M hydrochloric acid to the bromocresol green end-point. Similarly, three blank titrations were carried out by titrating a solution of 25 ml di-n-butylamine in MEK added to 50 ml of MEK/propan-2-ol mixture. A value for the purity was determined using the expression

$$\frac{(\text{Blank titre} - \text{Sample titre}) \times M(HCl) \times 84.1}{1000 \times \text{Weight of Sample}} \times 100\%$$

Values between 99 and 101% were obtained and thus the purity of HDI was taken as 100%. HDI was also stored over phosphorous pentoxide in a desiccator, containing silica gel and was also kept in a freezer (-20°C).

3.1.3 Solvents

n-Heptane: Freshly prepared sodium wire was added to Analar grade n-heptane and allowed to react with any water present in the heptane for about 2 days. Then the heptane was decanted and refluxed over calcium hydride for about 8 hours and distilled at 98.5°C. The first and last fractions of the distillate (approximately 10%) were rejected. Immediately after drying, the heptane was used for drying triol as described in section 3.1.1.

Nitrobenzene: Analar grade nitrobenzene was used as a solvent for some preliminary studies. It was freed from any alkaline impurities (eg. amines) by washing with 10% sulphuric acid followed by three washings with distilled water. The nitrobenzene was then dried over calcium chloride, and was decanted before being distilled. The first and last fractions (about 10%) were rejected and the fraction boiling between 210-211^{o}C was collected and stored over a grade 4A molecular sieve.

Toluene: Analar grade toluene was used as a solvent in this work. It was refluxed over calcium hydride for about 8 hours and distilled at 110.5^{o}C. As before, the first and last fractions (10%) were rejected. The purified toluene was stored over a grade 4A molecular sieve, until required for gelation experiments.

Methyl Ethyl Ketone (MEK): MEK was dried over anhydrous potassium carbonate overnight, decanted and then distilled at 78^{o}C. This dried MEK was used as a solvent for the quenching mixture in gelation reactions.

Pyridine: Pyridine used in the determination of equivalent weights of triols was refluxed with sodium hydroxide pellets for about 5 hours and distilled at 115^{o}C.

Propan-2-ol was used without any purification.

3.1.4 1,4-Diazabicyclo (2,2,2-) Octane (DABCO)

This catalyst (DABCO), also known as triethylene diamine (TED), was obtained from BDH. Titration of an aqueous solution of DABCO against 0.1 M HCl to a methyl red end-point gave an equivalent weight of 112.0 $\pm$ 0.5 (theoretical value is 112.2). DABCO was, therefore, assumed pure and used without further purification.

The structure of DABCO may be written as below

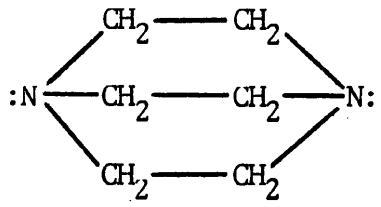

Its catalytic efficiency is due to the lack of steric hindrance in its structure. However, it is effectively mono-functional in its catalysis of isocyanate reactions, because once one of its nitrogen atoms is involved in a reaction, the other one cannot participate in the reaction simultaneously due to (1) the steric effect, on the free nitrogen atom, of the polymer chain attached to the first one, and (2) the decrease in nucleophilic character of the free nitrogen atom by the inductive effect as shown below

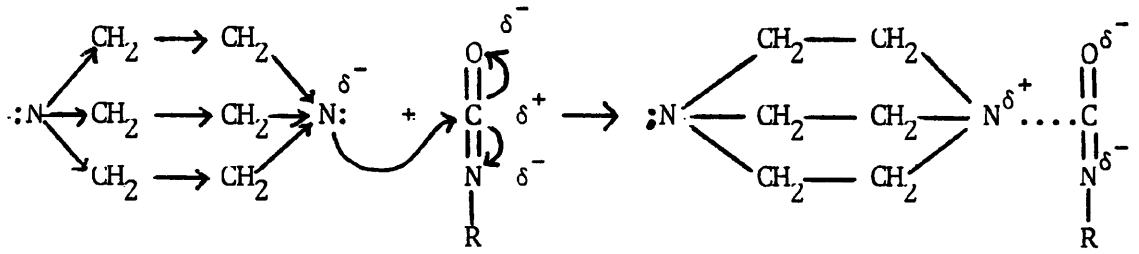

3.2 Polymerisation Procedure

All the reactions were carried out at 80°C ± 0.1 in a thermostatted, glass-sided water bath (Grants Instruments, Cambridge). Triol was directly weighed into the reaction flask (250 ml, 3-neck round-bottomed quickfit) and the calculated amounts of any necessary solvent and/or catalyst were added to the triol. The reaction flask was fitted with

a stirrer gland and a glass stirrer. The flask was immersed in the water bath and allowed to reach the reaction temperature. The amount of HDI required was calculated and weighed in a calibrated syringe and added to the flask directly from the syringe by method of difference.

A stop clock was immediately started within 1 minute of addition of HDI. For kinetics analysis, 2 to 4 g (depending upon the composition) of a reaction mixture were extracted at suitable intervals. Early in the reaction, sample extraction could be accomplished using a wide-bore hypodermic needle and syringe. Later on, the mixture became too viscous and a 5 mm -bore glass tube with close-fitting pipette bulb was used. The samples were ejected into pre-weighed 250 ml conical flasks containing 25 ml of quenching mixture (2.5% di-n-butylamine in MEK). The flasks were reweighed and left for 30 minutes and then 50 ml of MEK/propan-2-ol mixture (50% v/v) were added along with 1 ml of bromocresol green indicator solution. The contents of the flasks were titrated against 0.1 M hydrochloric acid (BDH CVS grade) to a yellow, stable end-point. Two blank titrations of 25 ml di-n-butylamine in MEK plus 50 ml MEK/propan-2-ol mixture were also carried out for every run. The concentration of isocyanate at time t can be calculated from the expression as equiv kg^{-1}.

$$(\text{Blank-Titre}) \times M\ (HCl) / \text{weight of sample}$$

A correction was made to the titrations to account for the basic nature of any added catalyst.

Gelation was observed as the time at which the reaction mixture lost its fluidity, climbing the stirrer irreversibly (so-called Weissenberg effect[65]) and pulling the mixture away from the sides of

the flask. At this stage the infinite network is assumed to have formed. It is possible to estimate the gel point to within 1 to 10 minutes in catalysed reactions, but in uncatalysed reactions gel points become less sharp and so it has been found necessary to place a 30 to 60 minutes error bar on a gel time typically of the order 24,000 to 48,000 minutes.

3.3 Calculation of the Kinetic Data

The extents of reaction of isocyanate and hydroxyl groups are given by $p_a = x/a$ and $p_b = x/b$, respectively, where x is the instantaneous concentration of urethane product, and a and b are the initial isocyanate and hydroxyl group concentrations. The quantity measured by the procedure (section 3.2) is therefore (a-x). Assuming that reaction occurs only between -NCO and -OH groups then the extent of reaction of hydroxyl groups is given as $p_b = r\, p_a$, where r is the initial ratio of -NCO to -OH groups in the reaction mixture.

The integrated form of the rate equation for a second order reaction is either

$$k_2 t = \frac{1}{(a-b)} \ln \frac{b(a-x)}{a(b-x)} \quad \text{for } a \neq b, \qquad \ldots.(3\text{-}1)$$

or

$$k_2 t = x/a(a-x) \quad \text{for } a = b \qquad \ldots.(3\text{-}2)$$

Since all the reactions were carried out at r = 1 (ie. a = b), equation (3-2) was used for the calculation of the kinetic data. The gel-point conversions, $(p_a)_c$ and $(p_b)_c$ were determined by extrapolating the time-conversion plots to the gel time (see section 3.2). Critical extent of reactions were calculated from the value of x_c obtained from the time-conversion plots. Gel points can, therefore, be defined in terms

of the critical product, $(p_a\ p_b)_c = r\ (p_a)_c^2$.

3.4 Formation, Moulding and Drying of Polyurethane Network Samples

The physical properties of the completely reacted polyurethane networks will be discussed in section 2, but it is convenient to describe the preparation and drying of the network samples made concurrently with the relevant gelation experiments.

After a suitable time had elapsed in a polymerisation, a portion of the reaction mixture was poured directly into the moulds. The pouring step had to be carried out very slowly and carefully so that no air-bubbles were formed in the moulds.

Network samples for torsion pendulum experiments were moulded using rectangular moulds (constructed from PTFE sheets) with inner dimensions of 160x 50x 3 mm. The filled moulds were placed in a vacuum oven at the reaction temperature 80°C and evacuated for about one minute until no further air bubbles broke the surface in the mould. The vacuum was then released and the reaction mixture allowed to cure at 80°C under anhydrous conditions.

Network samples for uniaxial compression tests were prepared in closed moulds (also constructed from PTFE sheets) containing three cylindrical cavities each with a diameter and height of about 10 mm. Since the mould was closed (after pouring the reaction mixture into the cavities) evacuation was not necessary during the preparation of samples for uniaxial compression tests.

Toluene (solvent) was removed from the network samples in two stages. In the first stage the samples were placed in a vacuum oven at a temperature of about 80°C to dry the samples slowly at atmospheric pressure (thus preventing cracking of the samples) for about one day.

In the second stage, vacuum was applied to remove the last traces of solvents completely until the weights of the samples became constant. This drying process took about two weeks. The dried network samples were stored prior to testing in sample bottles in a desiccator containing silica gel.

3.5 Equilibrium Swelling of Network Samples

Uniaxial compression tests were carried out with dried and swollen samples. For equilibrium swelling, each dried network sample was placed into a 60 ml sample bottle containing toluene and closed with a screw-lid. All the bottles containing samples in toluene were kept in a room thermostatted at $27.0^{o}C \pm 0.5$, the temperature at which subsequent compression tests were to be conducted. The weights of the swollen samples were taken each day until equilibrium was achieved (care being taken to remove any surface toluene before weighing). After each weighing, the toluene being used to swell a network was changed until constant weight of the swollen samples was achieved. It is worth mentioning that the swollen samples were so soft due to high M_c value (low modulus) and the higher degree of swelling (300 to 400%) that the samples had to be handled very carefully and quickly to prevent sample cracking. The process of equilibrium swelling took about two weeks.

It is possible that even at complete reaction there will be a small amount of residual sol fraction which may affect the physical properties of the dried networks. So some attempts were made to dry the equilibrium swollen samples to give dry networks for uniaxial compression tests. In attempting to dry the swollen samples, most of them began to crack even though they were dried at ambient temperatures in a partial atmosphere of toluene. The few samples which did not crack, when heated

slowly in an oven to complete the drying process became tacky and lost their cylindrical shape because of the high M_c value of the networks and also higher sensitivity to small amounts of degradation, even though the temperature never exceeded 40°C (without any vacuum). As a result of these drying experiments on the swollen samples, it was decided to study only the networks dried directly from partially swollen reaction systems (ie. dried as reacted). So the dried networks may have contained some small amounts of sol fraction, although it has been shown[24] that for gels (LHT 240/MDI system) with r ≈1.0, the sol fraction was almost negligible (for this low molar mass triol/MDI system) which is about 1% w/w at 80% dilution and 0% in bulk reactions.

The next chapter presents the results and discusses the results of kinetics and gelation reactions in the light of different kinetics and gelation theories, and the effects of catalyst and solvents on kinetics and gel points of the reaction system.

CHAPTER - 4

CHEMISTRY: RESULTS AND DISCUSSIONS

4.1 Introduction

This chapter discusses the results of the kinetics and gelation data from reactions between LG56 and HD1 with reactant ratio r = 1, in bulk and in solution. Nitrobenzene and toluene were used as solvents in reactions which were conducted at 80°C with and without added catalyst (DABCO). The experimental details of the various systems 1 to 7 are described in Table 4.1; Tables 4.2.a and 4.2.b summarise the approximate concentrations for each experiment, expressed as weight %, and the exact concentrations expressed in equivalent per kilogram (equiv kg^{-1})* of reactive groups. In addition, the concentrations of experimental systems 6 and 7 are expressed in both equiv kg^{-1} and equivalent per litre (equiv ℓ^{-1}), using the approximate density values given in Appendix A. The ratio r is defined as the ratio of initial reactant concentrations, $(NCO)o/(OH)_o$.

The kinetics data expressed as the experimentally determined amounts of urethane in equiv kg^{-1} formed at time t for all the experimental systems are presented in Appendix B.

* mol of reactive groups kg^{-1} ≡ equiv kg^{-1}

TABLE 4.1 Summary of the Different Experimental Systems with LG56 and HD1

Reaction System	Description
1	Bulk Reactions : with and without catalyst
2	Nitrobenzene Solutions (16.7%w/w)*: with and without catalyst
3	Nitrobenzene Solutions (37.5%w/w): with and without catalyst
4	Toluene Solutions (16.7%w/w): with and without catalyst
5	Toluene Solutions (37.5%w/w): with and without catalyst
6	Dilution Series (Toluene): without catalyst
7	Dilution Series (Toluene): with catalyst

* weight percent of added solvent

4.2 Kinetics of LG56/HD1 Reactions

The various conversion and kinetic plots for the seven reaction systems studied are summarised in Table 4.3, together with the respectively designated figure numbers. Thus each system is described by two figures contained in the last two columns of Table 4.3, the first containing plots of urethane concentration (x) and the extent of reaction (p_a) versus time (t), and the second containing the second order kinetics term, x/a(a-x) from equation (3.2) versus time (t). In the second case, for systems 1 to 5, the figures are split into (a) and (b) with the latter as an insert for the spontaneous reactions (reactions without any added catalyst) for which disproportionately longer time axes are required.

TABLE 4.2.a Solvent and Catalyst Concentrations for Different Experimental Systems

Expt No.	Solvent used	Solv. Conc. (w/w%)	Catalyst Conc. $\frac{(DABCO)}{(NCO)_o}$ %
1.1	-	-	0
1.2	-	-	5
1.3	-	-	10
1.4	-	-	15
1.5	-	-	20
2.1	Nitro-benzene	16.7	0
2.2	"	"	5
2.3	"	"	10
2.4	"	"	20
3.1	Nitro-benzene	37.5	0
3.2	"	"	10
3.3	"	"	15
3.4	"	"	20
4.1	Toluene	16.7	0
4.2	"	"	5
4.3	"	"	10
4.4	"	"	20
5.1	Toluene	37.5	0
5.2	"	"	5
5.3	"	"	10
5.4	"	"	20
6.1	-	-	0
6.2	Toluene	9.1	0
6.3	"	20.0	0
6.4	"	28.6	0
6.5	"	37.5	0
6.6	"	44.4	0
6.7	"	59.6	0
6.8	"	69.5	0
7.1	-	-	5
7.2	Toluene	9.1	5
7.3	"	20.0	5
7.4	"	28.6	5
7.5	"	37.5	5
7.6	"	44.4	5
7.7	"	59.5	5
7.8	"	69.6	5

TABLE 4.2.b Initial Concentrations and Ratios of Reactants

Expt No.	DABCO Conc. $\frac{(DABCO)}{(NCO)_o}$ (%)	Monomer Conc. (w/w%)	HD1 (equiv kg^{-1})	LG56 (equiv kg^{-1})	Reactant Ratio (r)
1.1	0	100(bulk)	0.9248	0.9222	1.0028
1.2	5	"	0.9188	0.9176	1.0013
1.3	10	"	0.9193	0.9170	1.0025
1.4	15	"	0.9334	0.9081	1.0279
1.5	20	"	0.9092	0.9077	1.0016
2.1	0	83.3	0.7734	0.7722	1.0017
2.2	5	"	0.7696	0.7677	1.0024
2.3	10	"	0.7616	0.7622	0.9992
2.4	20	"	0.7562	0.7536	1.0034
3.1	0	62.5	0.5785	0.5789	0.9993
3.2	10	"	0.5745	0.5734	1.0020
3.3	15	"	0.5732	0.5702	1.0052
3.4	20	"	0.5656	0.5671	0.9973
4.1	0	83.3	0.7822	0.7816	1.0008
4.2	5	"	0.7664	0.7680	0.9979
4.3	10	"	0.7678	0.7640	1.0050
4.4	20	"	0.7609	0.7562	1.0062
5.1	0	62.5	0.5768	0.5765	1.0005
5.2	5	"	0.5735	0.5736	0.9998
5.3	10	"	0.5752	0.5730	1.0038
5.4	20	"	0.5709	0.5669	1.0070

TABLE 4.2.b (cont'd) Initial Concentrations and Ratios of Reactants

Expt No.	DABCO Conc. $\frac{(DABCO)}{(NCO)_o}$ (%)	Monomer Conc. (w/w%)	HDI		LG56		Reactant Ratio (r)
			equiv kg^{-1}	equiv ℓ^{-1}	equiv kg^{-1}	equiv ℓ^{-1}	
6.1	0	100(bulk)	0.9248	0.9059	0.9222	0.9035	1.0028
6.2	"	90.9	0.8378	0.8058	0.8387	0.8066	0.9989
6.3	"	80.0	0.7381	0.6946	0.7380	0.6944	1.0001
6.4	"	71.4	0.6586	0.6094	0.6588	0.6097	0.9997
6.5	"	62.5	0.5768	0.5247	0.5765	0.5244	1.0005
6.6	"	55.6	0.5153	0.4627	0.5123	0.4599	1.0058
6.7	"	40.4	0.3717	0.3244	0.3724	0.3250	0.9981
6.8	"	30.5	0.2816	0.2414	0.2810	0.2409	1.0021
7.1	5	100(bulk)	0.9188	0.9002	0.9176	0.8990	1.0013
7.2	"	90.9	0.8335	0.8017	0.8341	0.8022	0.9993
7.3	"	80.0	0.7344	0.6912	0.7341	0.6909	1.0004
7.4	"	71.4	0.6540	0.6053	0.6556	0.6067	0.9975
7.5	"	62.5	0.5735	0.5217	0.5736	0.5218	0.9998
7.6	"	55.5	0.5093	0.4572	0.5098	0.4577	0.9990
7.7	"	40.5	0.3740	0.3266	0.3718	0.3247	1.0059
7.8	"	30.4	0.2796	0.2397	0.2792	0.2394	1.0014

System 1 comprises reactions in bulk with experiment 1.1, a spontaneous reaction and 1.2 to 1.5 catalysed with different concentrations of DABCO (5% to 20% mol DABCO/mol NCO). The kinetics plots for system 1 (bulk) are illustrated in figures 4.1 and 4.2(a) and (b). Second order kinetics are generally observed in catalysed reactions but positive deviations are observed in the spontaneous reactions. The catalytic effect of DABCO is exceptionally high as compared with other tertiary amines[66-68]. For example, for the bulk systems studied here, 5% catalyst concentration reduces the gel time from 4410 minutes to 388 minutes.

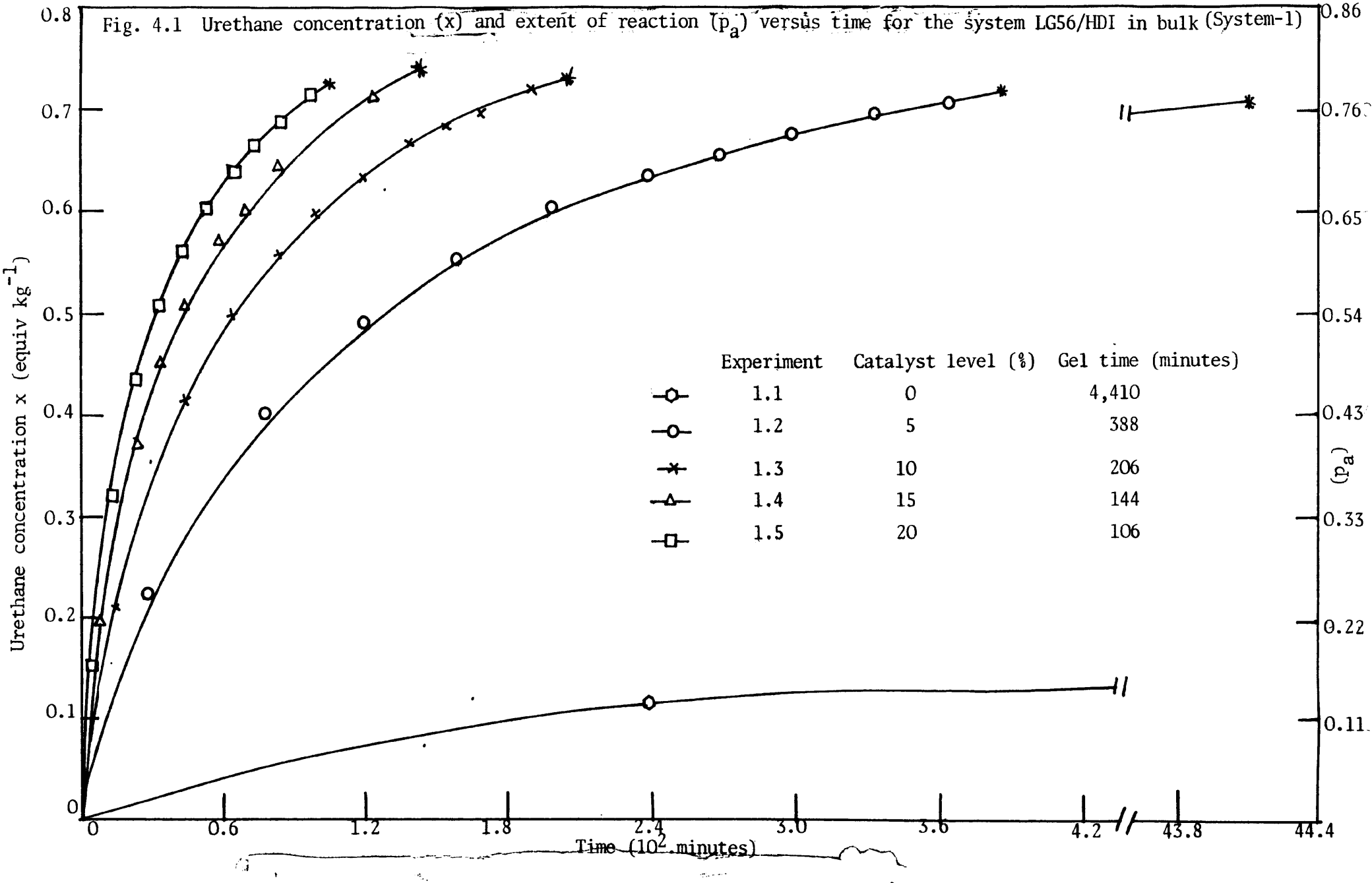
Fig. 4.1 Urethane concentration (x) and extent of reaction (p_a) versus time for the system LG56/HDI in bulk (System-1)
Urethane concentration x (equiv kg^{-1})
(p_a)
Time (10^2 minutes)
0
0.1
0.2
0.3
0.4
0.5
0.6
0.7
0.8
0.11
0.22
0.33
0.43
0.54
0.65
0.76
0.86
0.6
1.2
1.8
2.4
3.0
3.6
4.2
43.8
44.4
Experiment
Catalyst level (%)
Gel time (minutes)
1.1
0
4,410
1.2
5
388
1.3
10
206
1.4
15
144
1.5
20
106

Fig. 4.2(a) Second order kinetic plot: x/a(a-x) versus time (System-1)

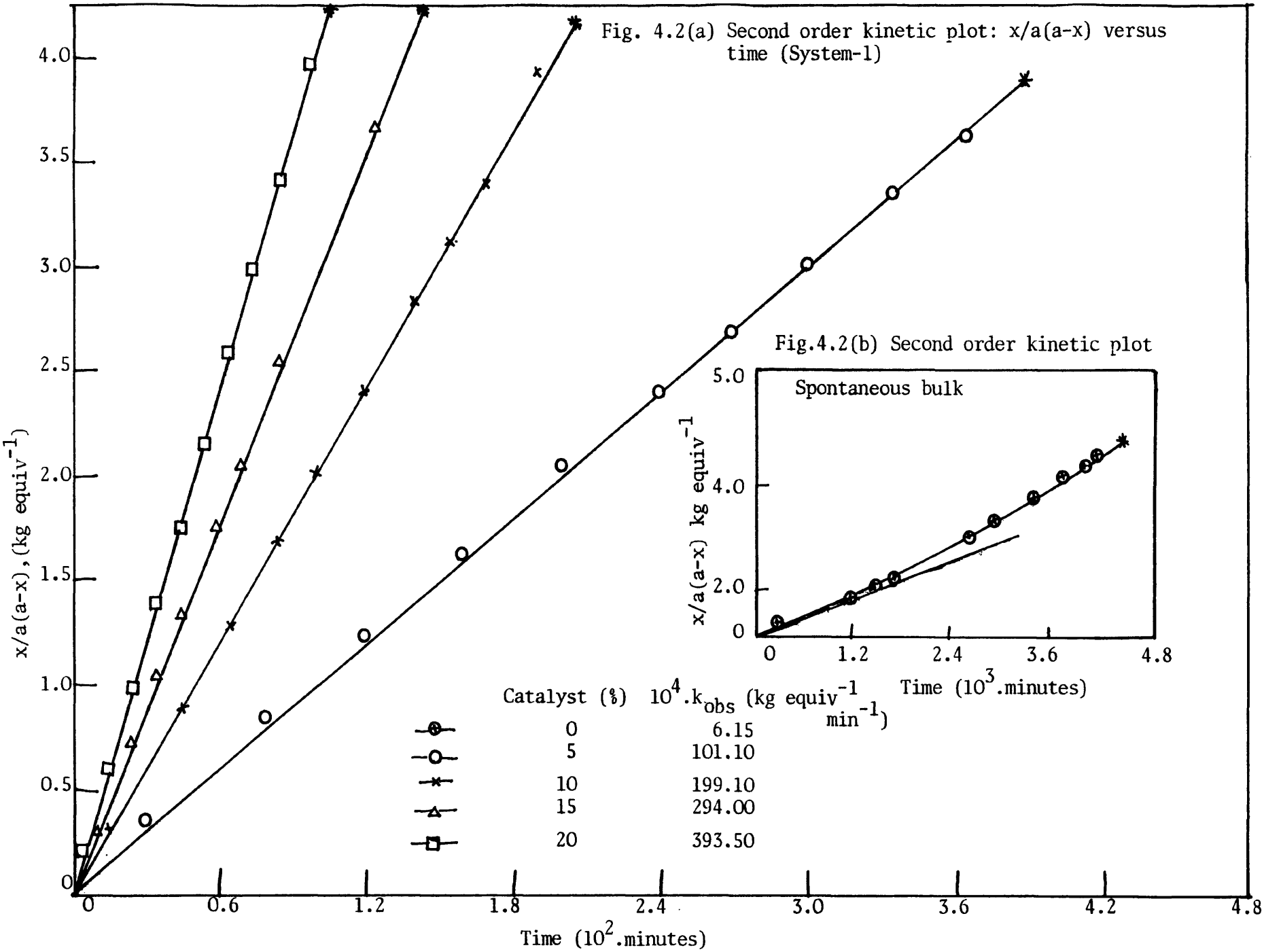

Fig.4.2(b) Second order kinetic plot

Catalyst (%)	$10^4.k_{obs}$ (kg equiv^{-1} min^{-1})
0	6.15
5	101.10
10	199.10
15	294.00
20	393.50

TABLE 4.3 Summary of the Kinetics Plots

Expt System	Description	Conversion Plot: x and p_a versus. t plot	Second Order Plot: x/a(a-x) Vs.t Plot
1	Bulk Reactions: with and without catalyst	Fig. 4.1	Fig.4.2(a) and (b)
2	Nitrobenzene Solutions (16.7%w/w)*: with and without catalyst	Fig. 4.3	Fig.4.4(a) and (b)
3	Nitrobenzene Solutions (37.5%w/w): with and without catalyst	Fig. 4.5	Fig.4.6(a) and (b)
4	Toluene Solutions (16.7%w/w): with and without catalyst	Fig. 4.7	Fig.4.8(a) and (b)
5	Toluene Solutions (37.5%w/w): with and without catalyst	Fig. 4.9	Fig.4.10(a) and (b)
6	Dilution Series (toluene): without catalyst	Fig. 4.11	Fig. 4.12
7	Dilution Series (toluene): with catalyst	Fig. 4.13	Fig. 4.14

* weight percent of added solvent

Kinetics data for systems 2 and 3 in nitrobenzene solutions are shown in figures 4.3 to 4.6 as plots of both x and x/(a-x) versus t. The catalysed reactions show very slight positive deviations from second order kinetics. These deviations in the spontaneous reactions are much more pronounced.

Kinetics data for systems 4 and 5 (at fixed level of toluene solvent and varying catalyst) are shown in figures 4.7 to 4.10 and, the dilution series (in toluene solvent) of systems 6 and 7 are shown in figures 4.11 to 4.14. Almost all the catalysed reactions show possibly very slight positive deviations from second order kinetics. The spontaneous reactions follow the normal trend, showing positive deviations as observed in bulk and nitrobenzene solutions.

From these experimental observations, it is clear that spontaneous reactions (figs 4.2(b), 4.4(b), 4.6(b), 4.8(b), 4.10(b) and 4.12) show positive deviations from second order kinetics in bulk, nitrobenzene and toluene, which are mostly due to the autocatalytic effects of the urethane product as observed by a number of previous workers[11,19,24,37,39,51,53,69,70]. In catalysed, bulk reactions, second order kinetics were generally observed (figs. 4.2(a) and 4.14 (bulk only)), because in the presence of a nucleophilic catalyst, the autocatalytic effect due to the urethane product and also the catalytic effect due to hydroxyl groups is negligible. But in the presence of solvents, slight deviations from second order kinetics in the catalysed reactions show that there is still some autocatalytic effect. This observation (ie. slight positive deviations) indicates that the catalyst is relatively less effective in solvents than in bulk.

Second order rate constants were evaluated from the initial slopes (for spontaneous reactions) and slopes of the second order plots for each of the catalysed reactions and the values are presented in Table 4.4.

Fig. 4.3 Urethane concentration (x) and extent of reaction (p_a) versus time for the system LG56/HDI in nitrobenzene (16.7% w/w) (System-2)

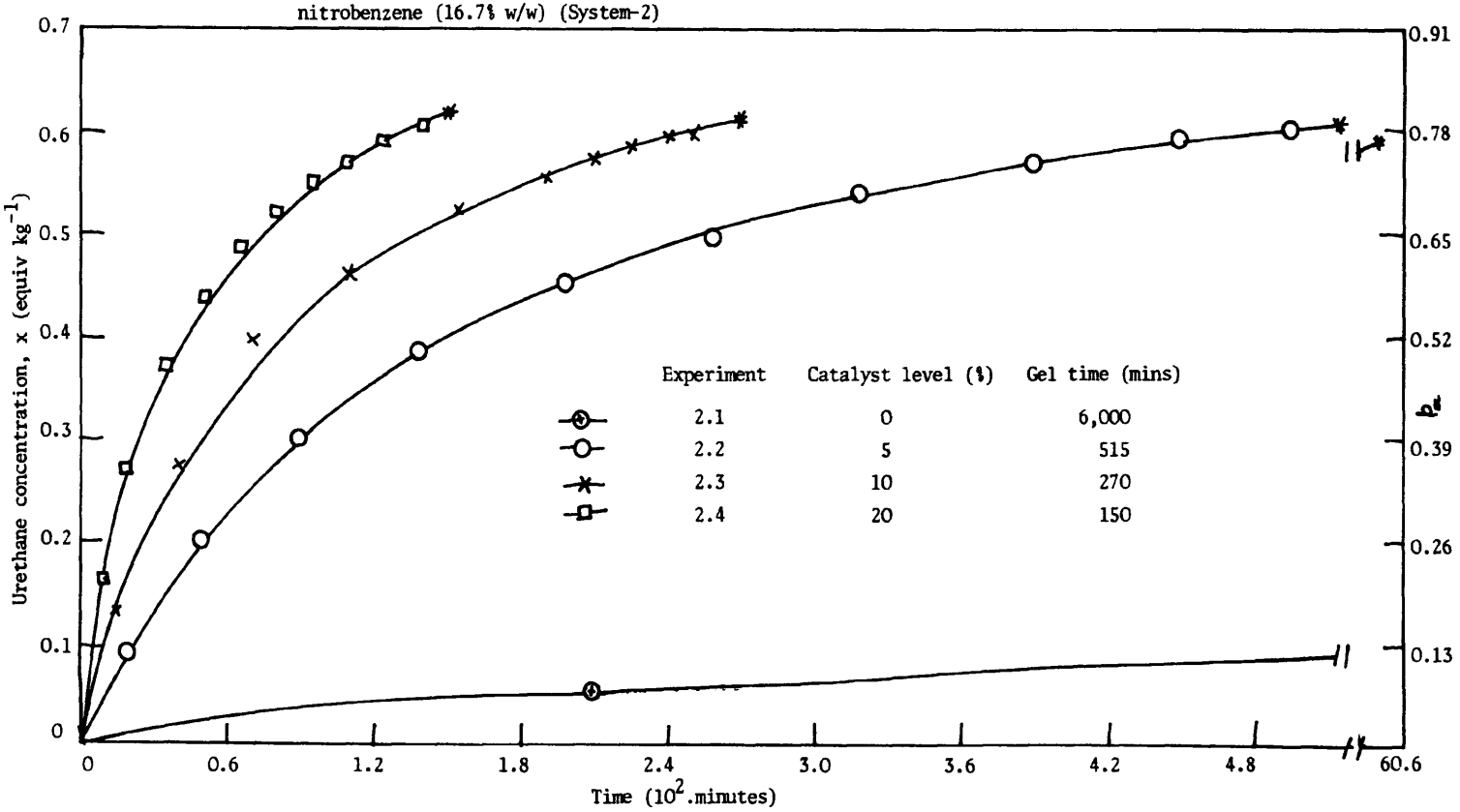

Fig. 4.4(a) Second order kinetic plot: x/x(a-x) versus time for the system LG56/HDI in nitrobenzene (16.7% w/w) (System-2)

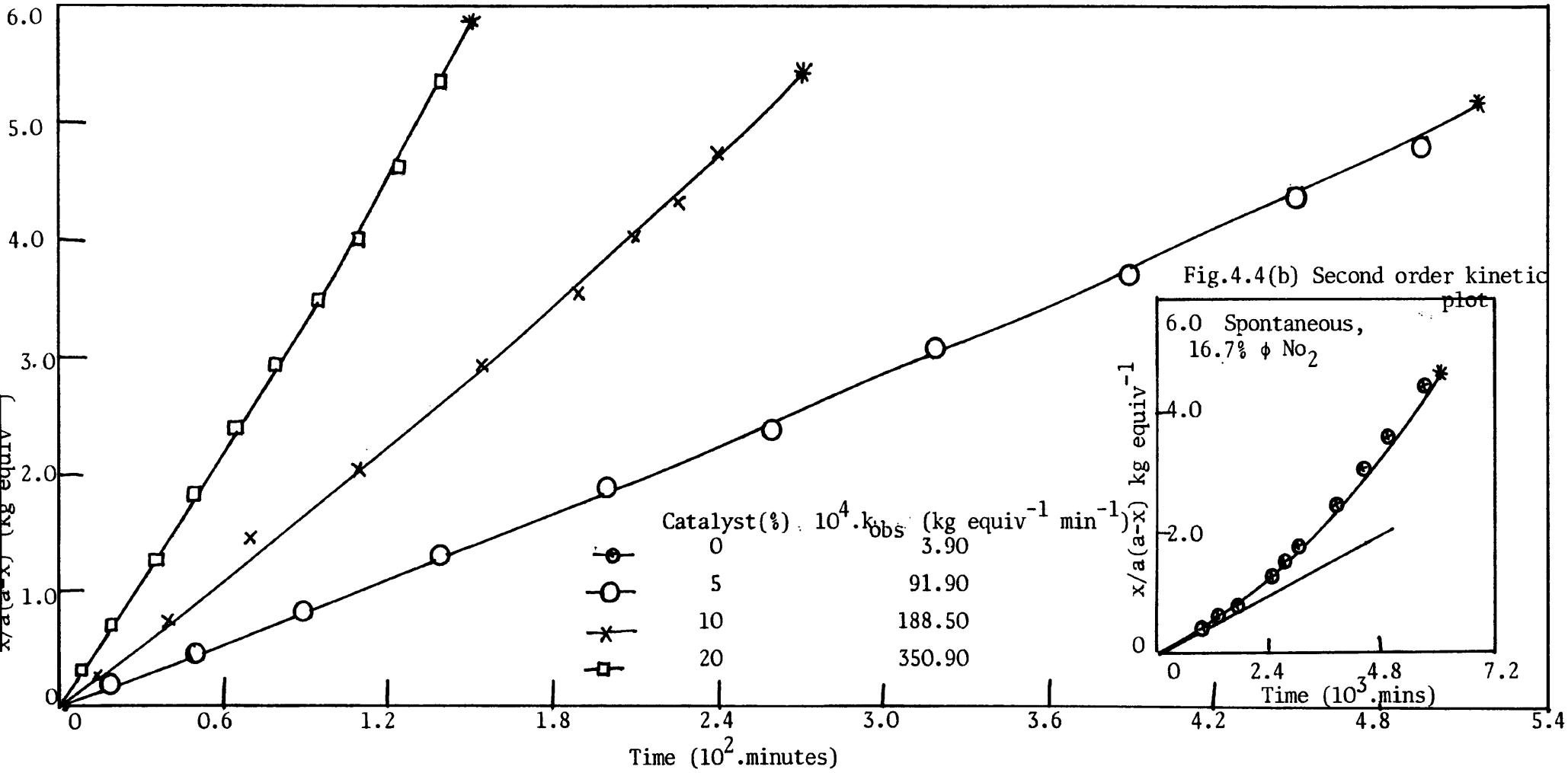

Fig.4.4(b) Second order kinetic plot

Fig. 4.5 Urethane concentration (x) and extent of reaction (p_a) versus time for the system LG56/HDI in nitrobenzene (37.5% w/w) (System -3)

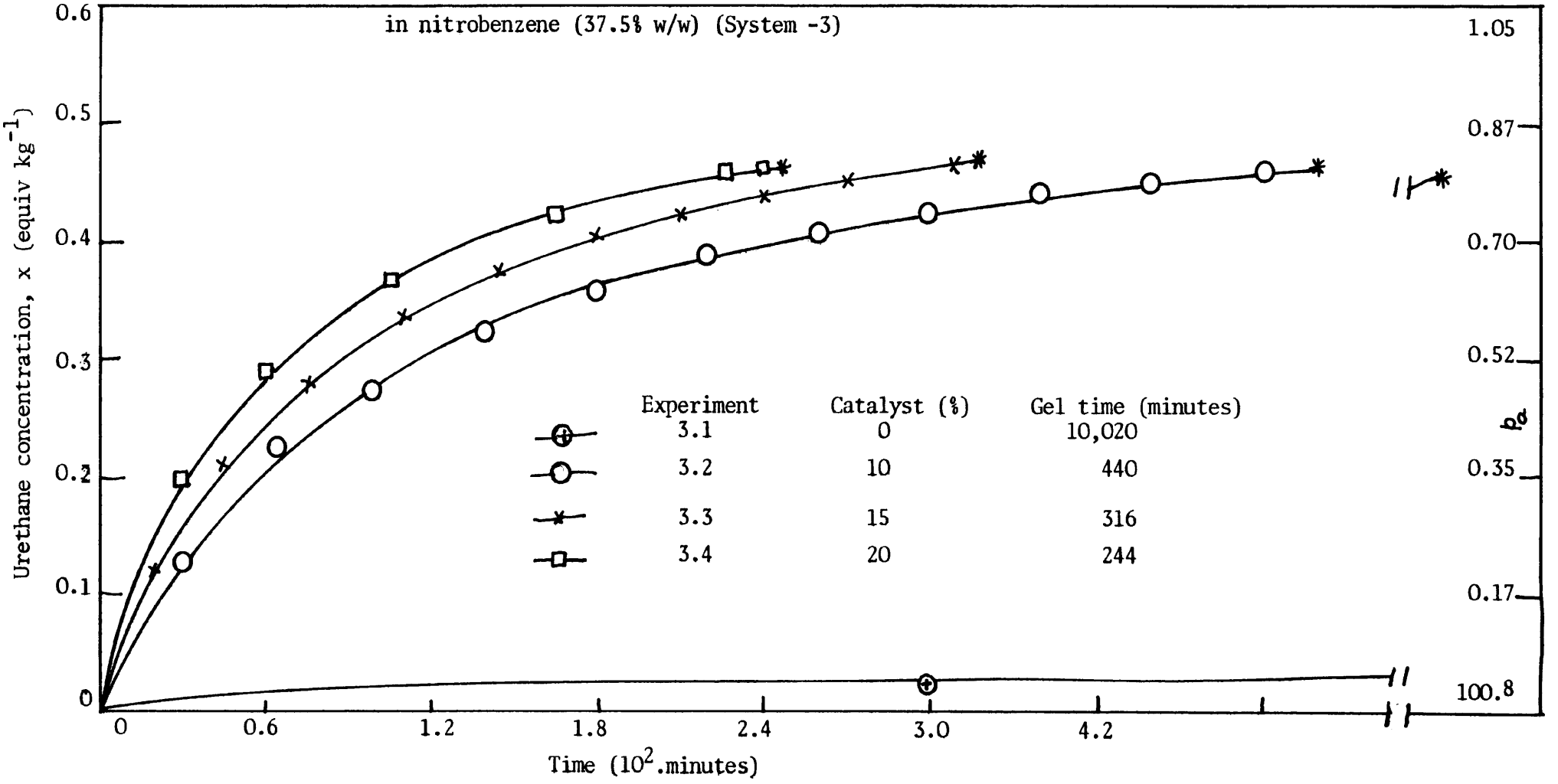

Fig. 4.6(a) Second order kinetic plot: x/a(a-x) versus time for the system LG56/HDI in nitrobenzene (37.5%w/w)(System-3)

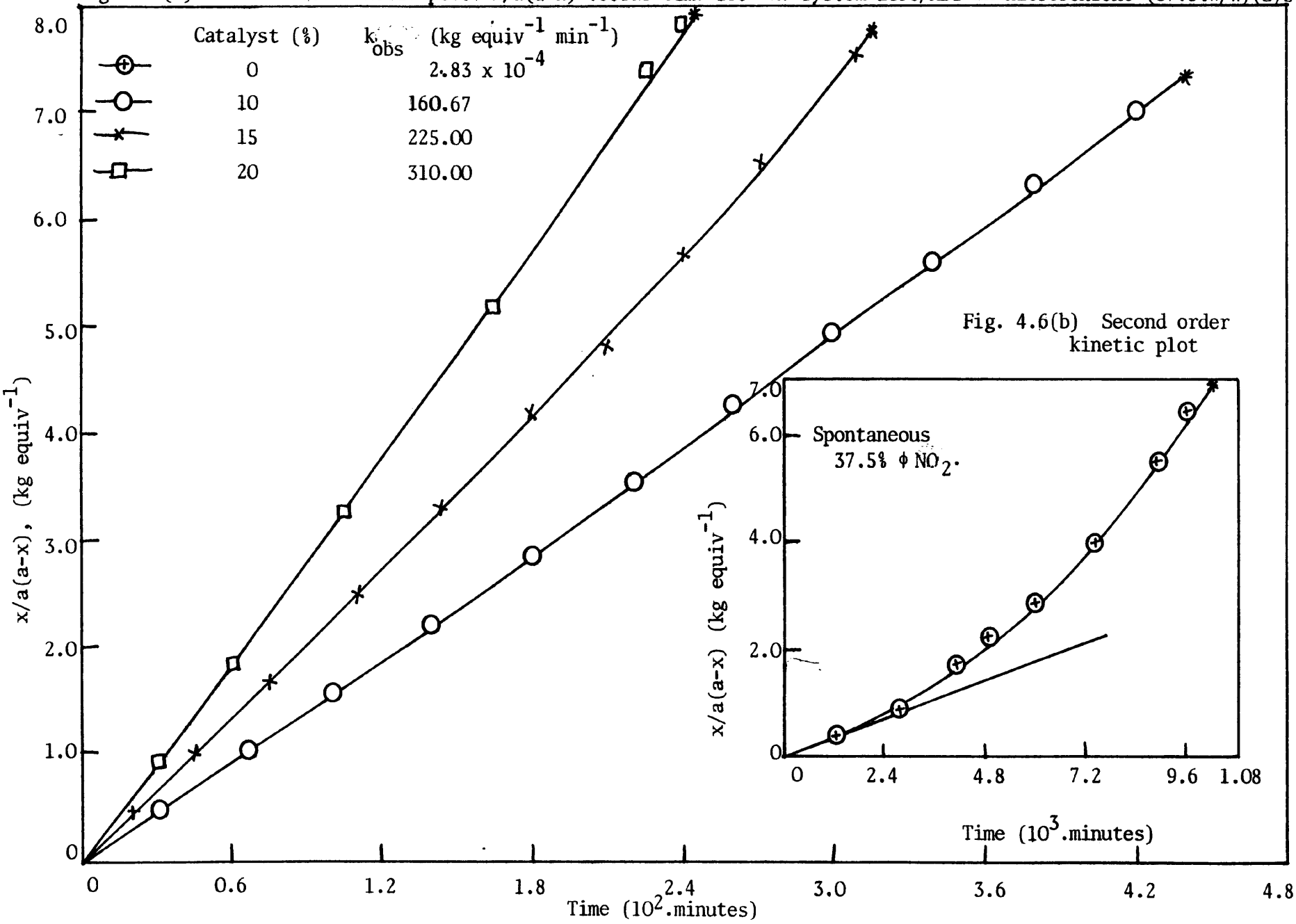

Fig. 4.6(b) Second order kinetic plot

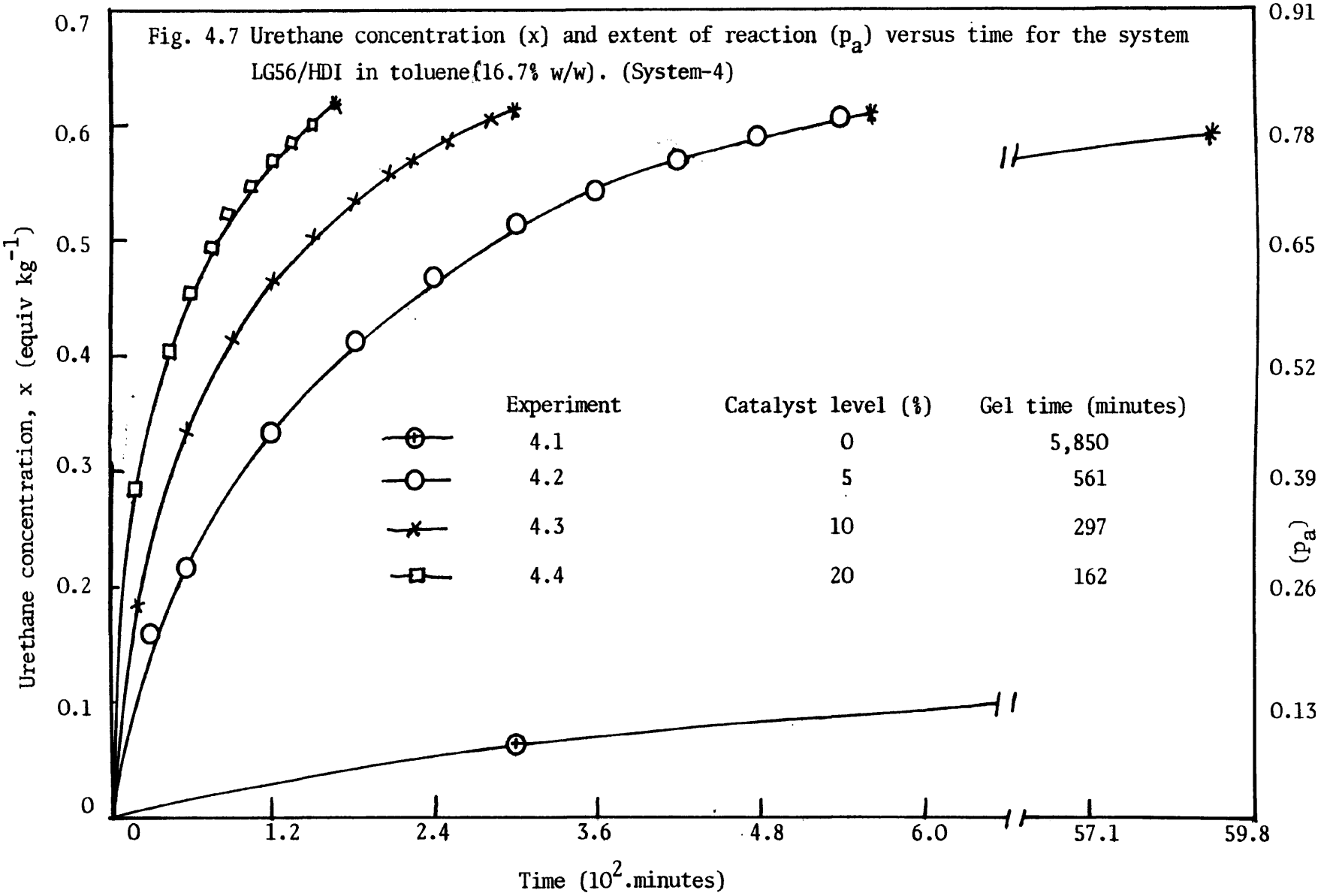

Fig. 4.7 Urethane concentration (x) and extent of reaction (p_a) versus time for the system LG56/HDI in toluene(16.7% w/w). (System-4)

Fig. 4.8(a) Second order kinetic plot: x/a(a-x) versus time for the system LG56/HDI in toluene (16.7%w/w) (System-4)

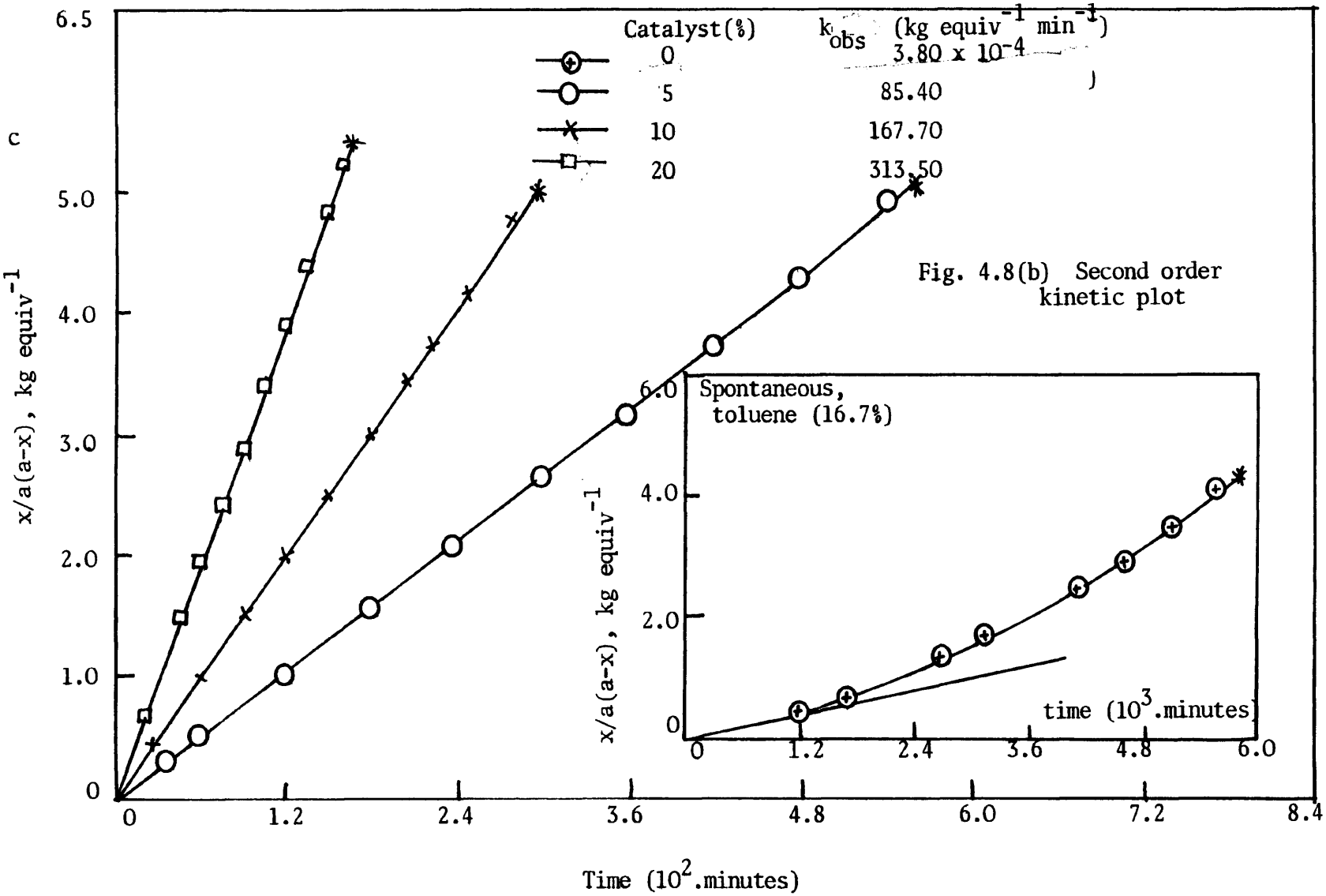

Fig. 4.8(b) Second order kinetic plot

Fig. 4.9 Urethane concentration (x) and extent of reaction (p_a) versus time for the system LG56/HDI in toluene (37.5 w/w) (System 5)

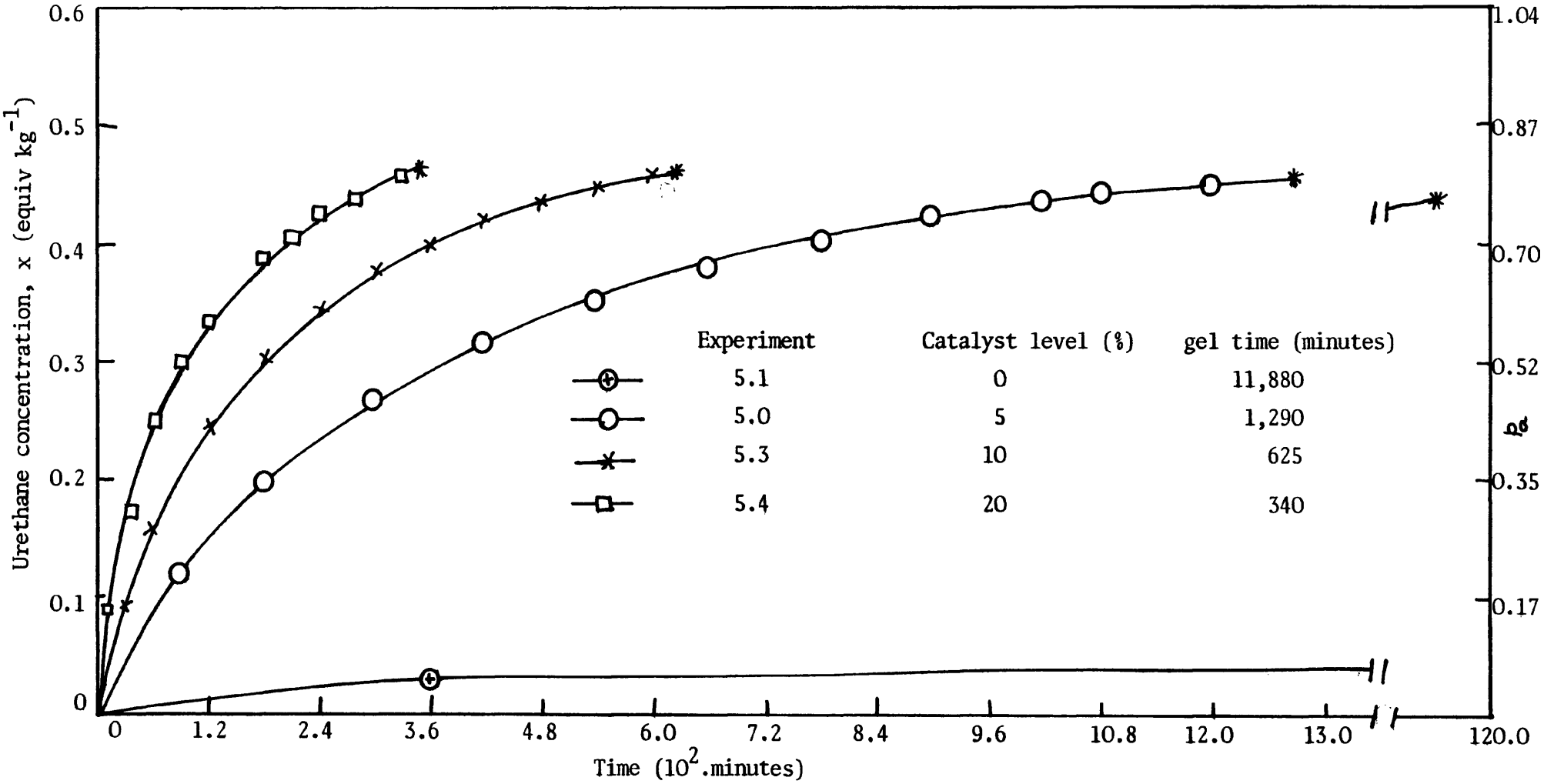

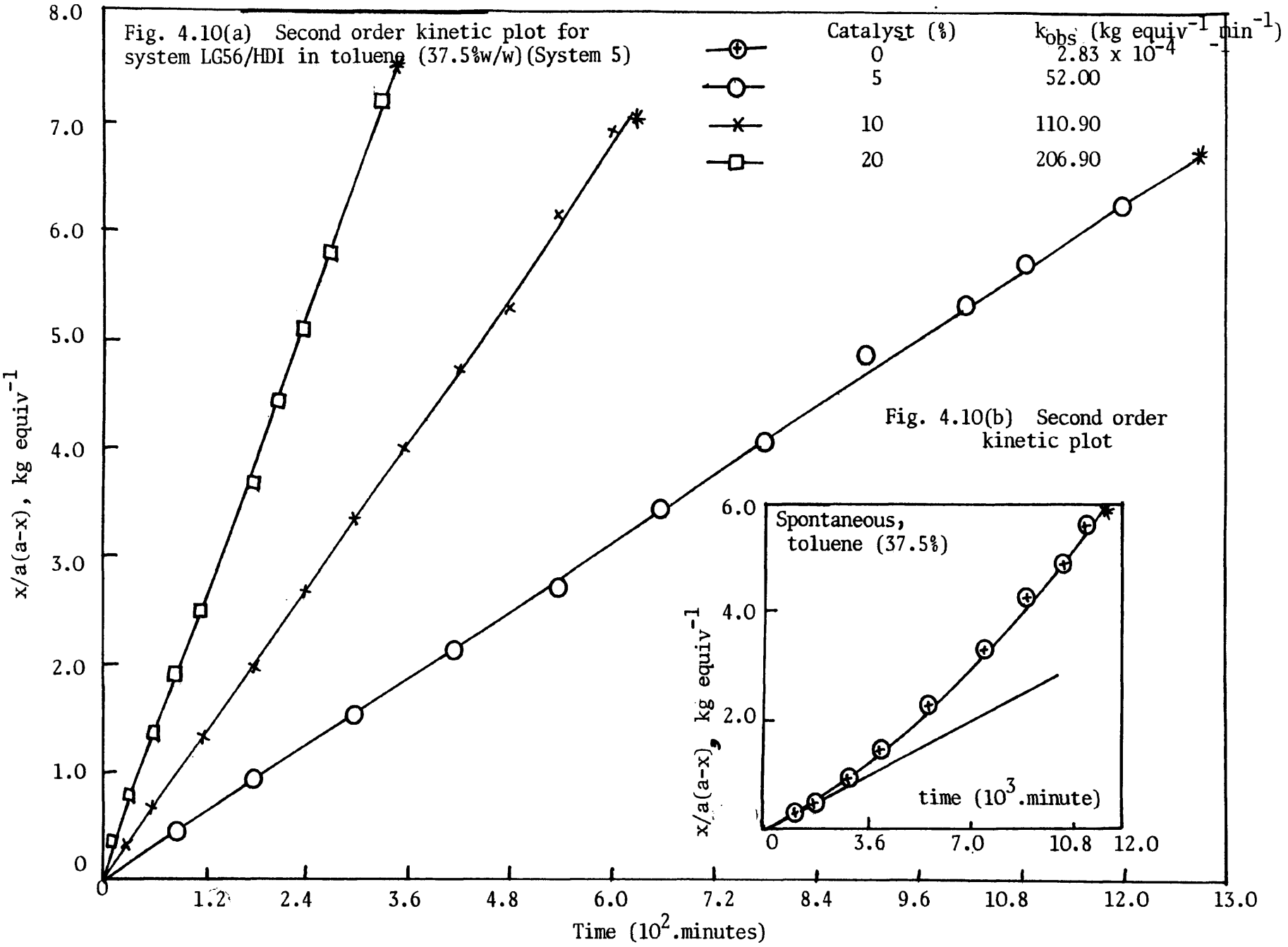

Fig. 4.10(b) Second order kinetic plot

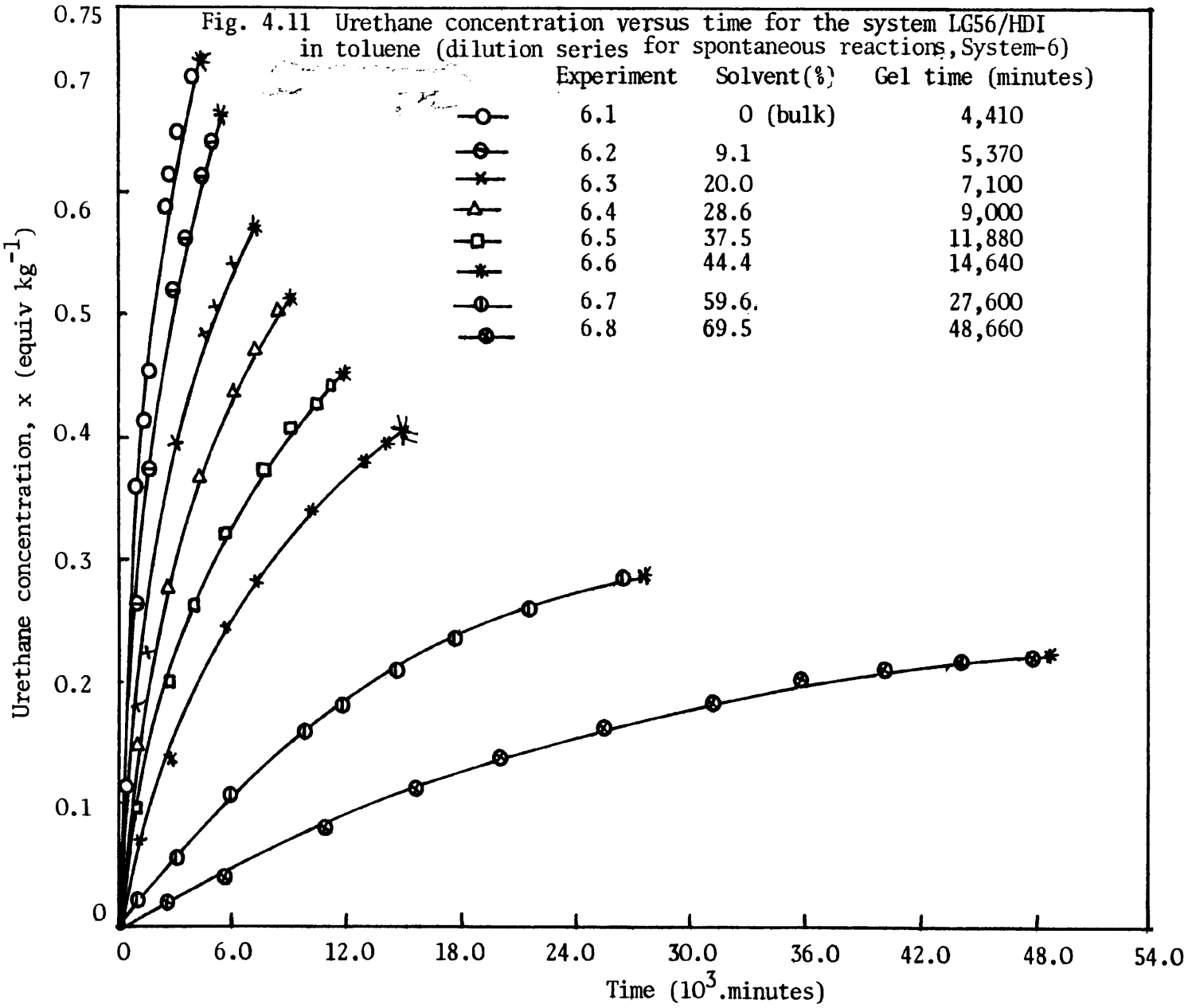

Fig. 4.11 Urethane concentration versus time for the system LG56/HDI in toluene (dilution series for spontaneous reactions, System-6)

Experiment	Solvent(%)	Gel time (minutes)
6.1	0 (bulk)	4,410
6.2	9.1	5,370
6.3	20.0	7,100
6.4	28.6	9,000
6.5	37.5	11,880
6.6	44.4	14,640
6.7	59.6.	27,600
6.8	69.5	48,660

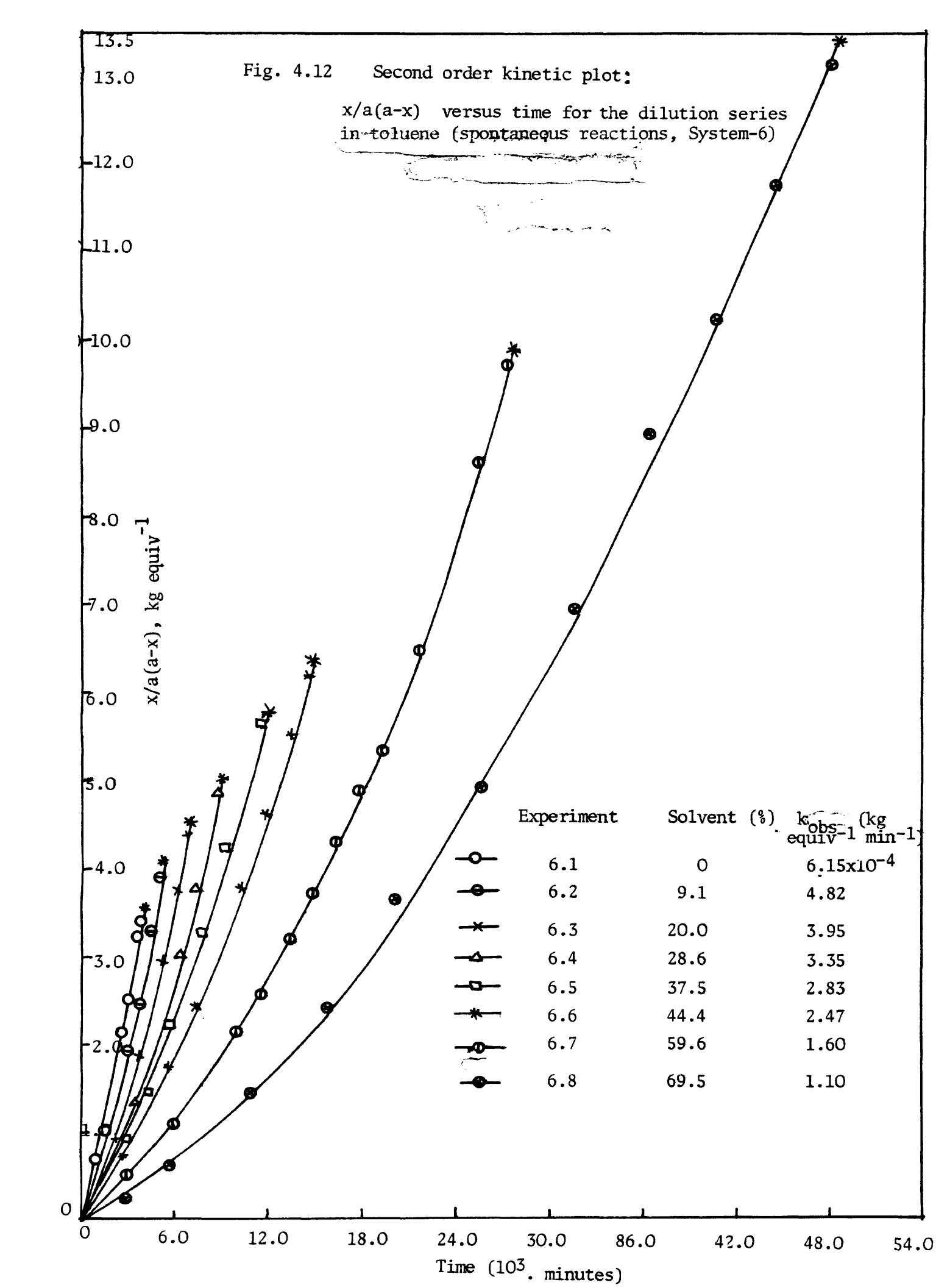
Fig. 4.12 Second order kinetic plot:
x/a(a-x) versus time for the dilution series in toluene (spontaneous reactions, System-6)
x/a(a-x), kg equiv^{-1}
Time (10^3. minutes)
Experiment
Solvent (%)
k_{obs} (kg equiv^{-1} min^{-1})
6.1 0 6.15×10^{-4}
6.2 9.1 4.82
6.3 20.0 3.95
6.4 28.6 3.35
6.5 37.5 2.83
6.6 44.4 2.47
6.7 59.6 1.60
6.8 69.5 1.10

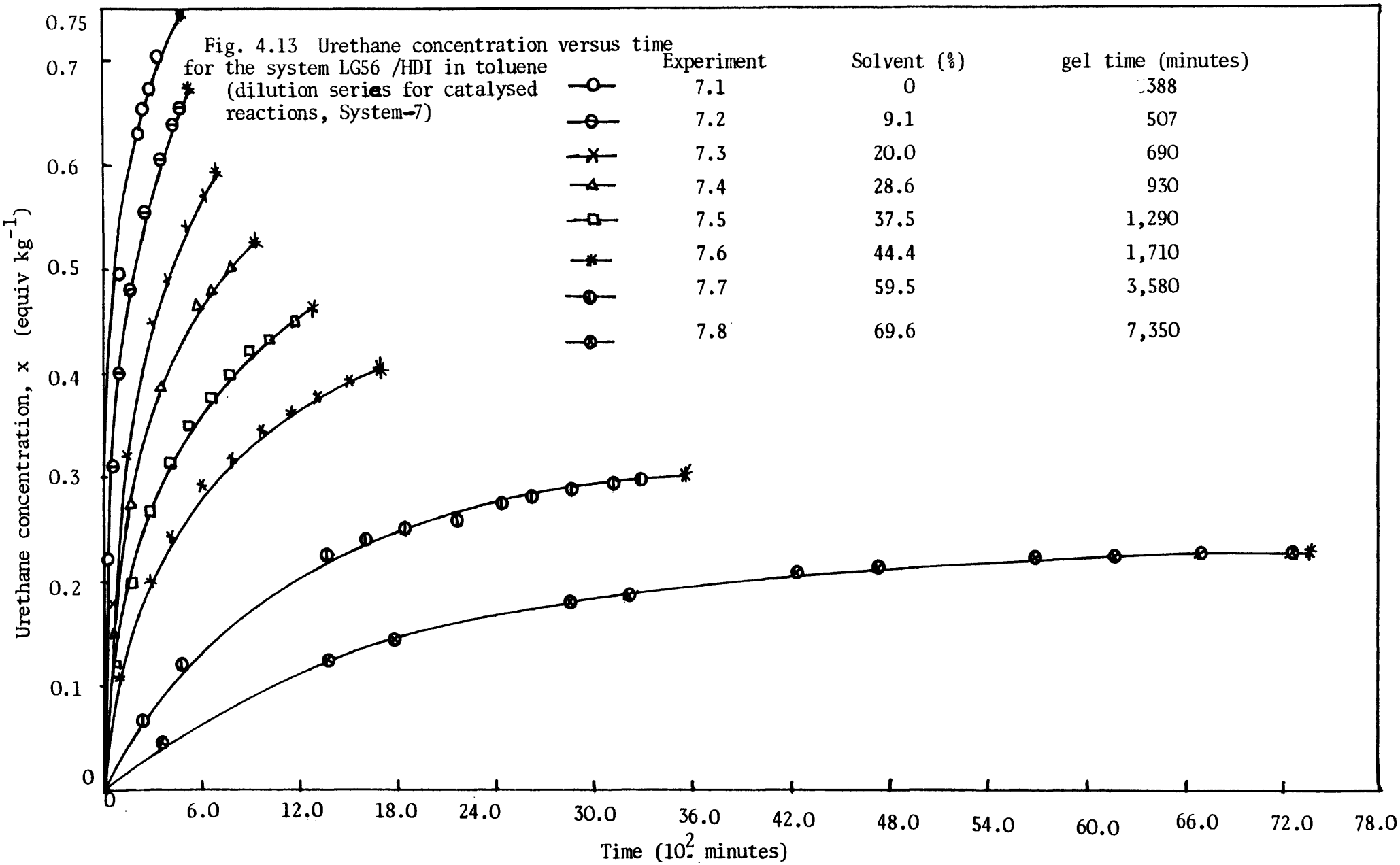

Fig. 4.13 Urethane concentration versus time for the system LG56 /HDI in toluene (dilution series for catalysed reactions, System-7)

Experiment	Solvent (%)	gel time (minutes)
7.1	0	388
7.2	9.1	507
7.3	20.0	690
7.4	28.6	930
7.5	37.5	1,290
7.6	44.4	1,710
7.7	59.5	3,580
7.8	69.6	7,350

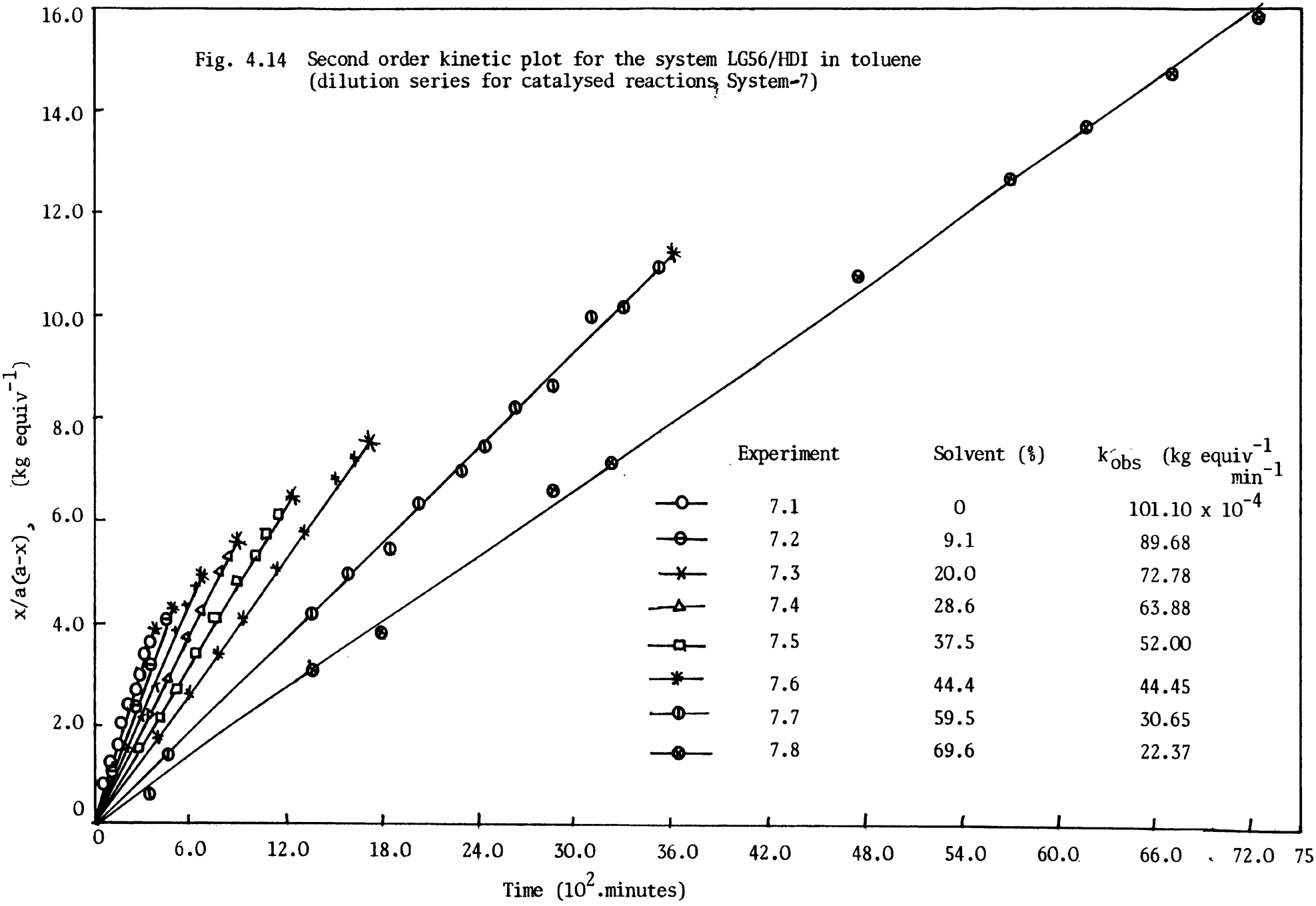
Fig. 4.14 Second order kinetic plot for the system LG56/HDI in toluene (dilution series for catalysed reactions, System-7)
16.0
14.0
12.0
10.0
8.0
6.0
4.0
2.0
0
x/a(a-x), (kg equiv^{-1})
0
6.0
12.0
18.0
24.0
30.0
36.0
42.0
48.0
54.0
60.0
66.0
72.0
75.0
Time (10^2.minutes)
Experiment
Solvent (%)
k'_{obs} (kg equiv^{-1} min^{-1})
7.1 0 101.10 x 10^{-4}
7.2 9.1 89.68
7.3 20.0 72.78
7.4 28.6 63.88
7.5 37.5 52.00
7.6 44.4 44.45
7.7 59.5 30.65
7.8 69.6 22.37

TABLE 4.4 Second order rate constants for the Reaction LG56 + HD1 in bulk, nitrobenzene and toluene (obtained from the slope of second order kinetic plots).

Expt No.	Cao (equiv kg^{-1})	Catalyst Concentration(B) (equiv kg^{-1})	Catalyst Concentration(B) $\frac{\text{mol DABCO}}{\text{mol NCO}}$ (%)	$10^4.k_{obs}$ (kg $equiv^{-1}$ min^{-1})
1.1	0.9248	0	0	6.15
1.2	0.9188	0.0460	5	101.10
1.3	0.9193	0.0916	10	199.10
1.4	0.9334	0.1362	15	294.00
1.5	0.9092	0.1816	20	393.50
2.1	0.7734	0	0	3.90
2.2	0.7696	0.0385	5	91.90
2.3	0.7616	0.0763	10	188.50
2.4	0.7562	0.1508	20	350.90
3.1	0.5785	0	0	2.83
3.2	0.5745	0.0573	10	160.67
3.3	0.5732	0.0856	15	225.00
3.4	0.5656	0.1135	20	310.00
4.1	0.7822	0	0	3.80
4.2	0.7664	0.0384	5	85.40
4.3	0.7678	0.0767	10	167.70
4.4	0.7609	0.1513	20	313.50
5.1	0.5768	0	0	2.83
5.2	0.5735	0.0290	5	52.00
5.3	0.5752	0.0574	10	110.90
5.4	0.5709	0.1135	20	206.90

TABLE 4.4 (cont'd)

Expt No.	Cao (equiv kg^{-1})	Catalyst Contentration(B)		10^4 k_{obs} (kg $equiv^{-1}$ min^{-1})
		(equiv kg^{-1})	$\frac{mol\ DABCO}{mol\ NCO}$ (%)	
6.1	0.9248	0	0	6.15
6.2	0.8378	0	0	4.82
6.3	0.7381	0	0	3.95
6.4	0.6586	0	0	3.95
6.5	0.5768	0	0	2.83
6.6	0.5153	0	0	2.47
6.7	0.3717	0	0	1.60
6.8	0.2816	0	0	1.10
7.1	0.9188	0.0460	5	101.10
7.2	0.8335	0.0417	5	89.68
7.3	0.7344	0.0367	5	72.78
7.4	0.6540	0.0328	5	63.88
7.5	0.5735	0.0287	5	52.00
7.6	0.5093	0.0255	5	44.45
7.7	0.3740	0.0186	5	30.65
7.8	0.2796	0.0139	5	22.37

From the mechanism proposed by Baker and Holdsworth[37], k_{obs} is given by

$$k_{obs} = k_o + k_{cat}(B) \qquad \ldots. \quad (2\text{-}4)$$

where $$k_{cat} = k_1 \, k_3/(k_2 + k_3 \, (b-x)) \qquad \ldots. \quad (2\text{-}5)$$

for the reaction scheme

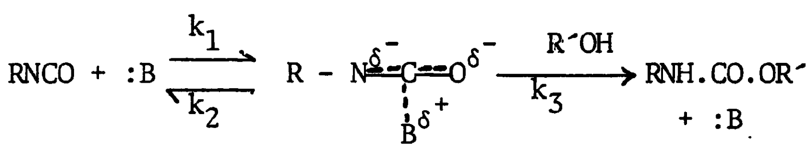

In an externally catalysed reaction, the assumption can be made that (i) $k_{cat} >> k_o$ and (ii) $k_2 >> k_3$ (ie. the complex forming step is fast compared with the rate of formation of urethane from the complex) and thus

$$k_{obs} \simeq k_{cat}[B] \qquad \ldots. \quad (4\text{-}1)$$

and $$k_{cat} \simeq k_1 \, k_3/k_2 \qquad \ldots. \quad (4\text{-}2)$$

A similar relation for k_{cat} can also be obtained from Sato's expression as shown by equation (2-6), chapter 2, for externally catalysed reactions, but not for spontaneous reactions, because the latter reactions are better explained by the autocatalytic term (second term in equation 2-6).

Figure 4.15 shows that k_{obs} is a linear function of catalyst concentration as predicted by equation (2-4) or equation (4-1) in bulk (system - 1), nitrobenzene (systems 2 and 3) and toluene (systems 4 and 5). This observation is in agreement with those of Baker[37] and Borkent[38]. The slopes of the linear plots give k_{cat}, the rate constant for the catalysed reactions. The values of k_{cat} obtained from the linear plots in fig. 4.15 are given in Table 4.5. Table 4.5 shows that the

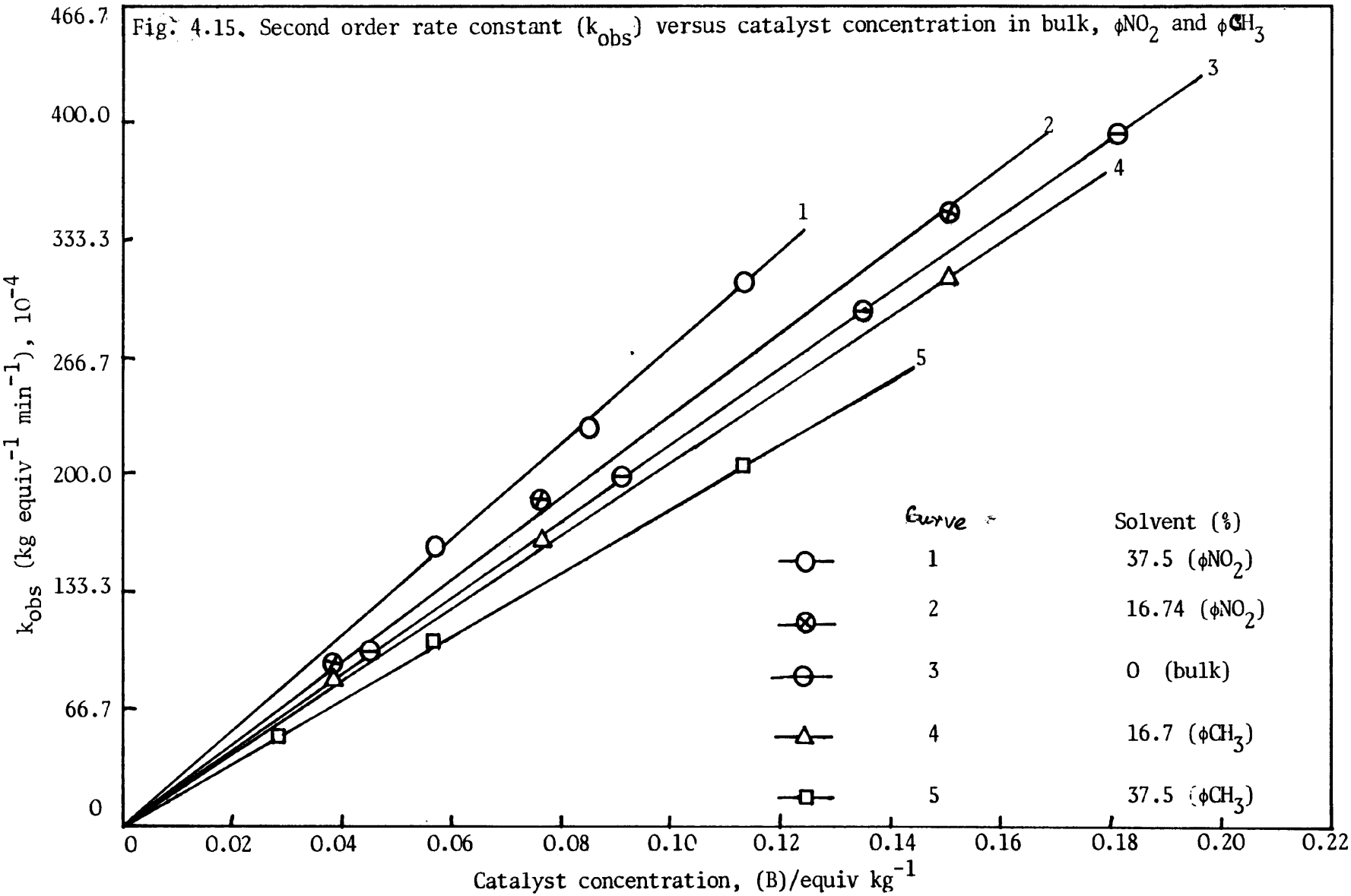
Fig. 4.15. Second order rate constant (k_{obs}) versus catalyst concentration in bulk, ϕNO_2 and ϕCH_3
466.7
400.0
333.3
266.7
200.0
133.3
66.7
0
k_{obs} (kg equiv^{-1} min^{-1}), 10^{-4}
0
0.02
0.04
0.06
0.08
0.10
0.12
0.14
0.16
0.18
0.20
0.22
Catalyst concentration, (B)/equiv kg^{-1}
1
2
3
4
5
Curve
Solvent (%)
1 37.5 (ϕNO_2)
2 16.74 (ϕNO_2)
3 0 (bulk)
4 16.7 (ϕCH_3)
5 37.5 (ϕCH_3)

TABLE 4.5 Third order rate constants, k_{cat}, for the catalysed reactions of LG56/HD1 in bulk, nitrobenzene and toluene (obtained from k_{obs} versus (B) plots).

System	Composition	$10^4.k_{cat}$ (kg^2 $equiv^{-2}$ min^{-1})
1	Bulk	2124
2	16.7% Nitrobenzene	2309
3	37.5% "	2678
4	16.7% Toluene	2046
5	37.5% "	1802

values of k_{cat} are higher in nitrobenzene than in bulk, and increase with increasing dilution. The opposite behaviour is observed in toluene; k_{cat} is lower in toluene than in bulk, and decreases with increasing dilutions. These observations of the present work (Table 4.5) can be explained on the basis of dielectric constants (ε). For this purpose the following dielectric constants are quoted[71]: phenyl isocyanate, $\varepsilon_{20} = 8.8$; ethyl carbamate, $\varepsilon_{90} = 12$; butan-2-ol, $\varepsilon_{25} = 16$; toluene, $\varepsilon_{90} = 2.3$ and nitrobenzene, $\varepsilon_{90} = 25$ (subscripts refer to temperature).

In the present system, k_{cat} increases in nitrobenzene with dilution, because the dielectric constant of the reaction system increases with dilution. There may be association between solvent (nitrobenzene) and polyol-hydroxyl groups, but the stabilization of the activated complex probably predominates (which increases k_1) over the solvent-hydroxyl association (which decreases k_3), thus giving a resultant increase in k_{cat}. But in toluene, k_{cat} decreases with increasing

dilution. With increase in dilution of the reaction mixture in toluene, the dielectric constant of the reaction mixture decreases which decreases the number of free hydroxyl groups and also the stability of the complex, both of which decrease k_3 and hence k_{cat}. A similar trend in k_{cat} was also observed by Hopkins, Peters and Stepto[11] and Greenshield, Peters and Stepto[51] in polyurethane-forming reaction systems and the results were explained on the basis of the dielectric constant of the reaction systems, HDI/alcohols in solvents. A drop in k_{cat} could be caused by association of polyol-hydroxyl groups leading to a decrease in k_3 as observed with the LHT240/HDI system[11] in nitrobenzene. On the other hand, an increase in k_{cat} could be caused[15] by an increase in the number of free hydroxyl groups (which increases k_3) or by the increased stability of the activated complex (which also increases k_3) or both. Thus, k_{cat} is related mainly to the overall dielectric constant of the reaction mixture.

4.3 Calculation of Gel Point Data

4.3.1 Evaluation of the Extent of Reaction at Gel

The extents of reaction at gel, $(p_a)_c$ and $(p_b)_c$, were evaluated by extrapolating the time-conversion plots to the gel time, as shown in fig 4.16. Since, the method of extrapolation is applied to evaluate $(p_a)_c$ and $(p_b)_c$, the critical extents of reaction at gelation, the values of $(p_a)_c$ and $(p_b)_c$ are subject to some error, due to the uncertainty in defining the exact gel point. The percentage of error in $(p_a)_c$ are calculated, as shown in fig 4.16, from the upper and lower limits of the values of x_c or $(p_a)_c$ from the conversion plots. Fig 4.16 shows that the upper limit of the extent of reaction at gel is 0.784, obtained from the line drawn through the last two or three experimental points and the lower limit is 0.762, obtained from the horizontal line drawn

through the last experimental point, as shown in the figure. The value of $(p_a)_c$ obtained from the main conversion plot is 0.773. Thus, the corresponding α_c values ($\alpha_c = p_{ac}\, p_{bc} = r\, p_{ac}^2$) are

$$(\alpha_c)_{max} = 0.616$$

$$(\alpha_c)_{min} = 0.583$$

$$(\alpha_c)_{calculated} = 0.599 \text{ (from the main plot)}$$

This α_c value is presented in the gel point data Tables (Tables 4.7 and 4.9) as 0.599 ± 0.017. The percentage of error (or better uncertainty) in $(p_a)_c$ = 1.4% and the corresponding error (or uncertainty) in α_c = 2.8%. It is worth mentioning that, since the lower limit of the p_{ac} value (and hence α_c value) is taken from the last experimental point of the conversion plot, more error or uncertainty results in those experiments in which the last experimental point is far away from the gel point, as shown by the last two points in bulk reactions in figures 4.17 and 4.18.

In this way the extents of reaction at gelation and the uncertainty (or error) involved are calculated for every gelation reaction and the corresponding α_c values with the uncertainties (or error) are presented in gel point data in Tables 4.7 and 4.9. It has been observed that the uncertainty (or error) in p_{ac} values ranges from 0.1% (the corresponding uncertainty or error in α_c is 0.2%), as in experiment 7.7, to about 2.8% (the corresponding uncertainty or error in α_c is 5.6%), as in experiment 1.4.

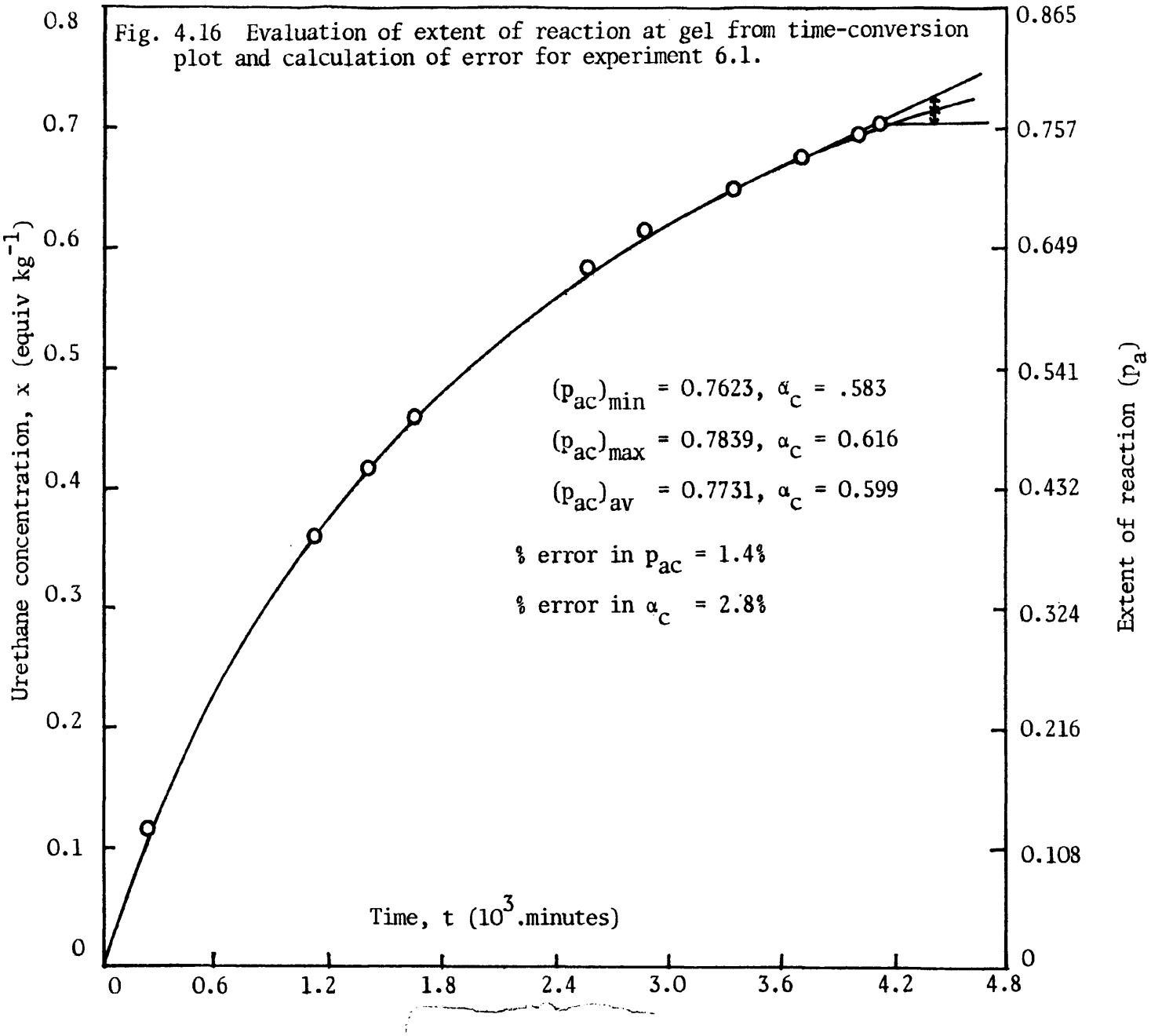
Fig. 4.16 Evaluation of extent of reaction at gel from time-conversion plot and calculation of error for experiment 6.1.
$(p_{ac})_{min}$ = 0.7623, α_c = .583
$(p_{ac})_{max}$ = 0.7839, α_c = 0.616
$(p_{ac})_{av}$ = 0.7731, α_c = 0.599
% error in p_{ac} = 1.4%
% error in α_c = 2.8%
Urethane concentration, x (equiv kg^{-1})
Extent of reaction (p_a)
Time, t (10^3.minutes)
0
0.1
0.2
0.3
0.4
0.5
0.6
0.7
0.8
0.108
0.216
0.324
0.432
0.541
0.649
0.757
0.865
0.6
1.2
1.8
2.4
3.0
3.6
4.2
4.8

4.3.2 Reproducibility in Gel-Point Determination

Two experiments (7.1 and 7.3) were repeated to check the reproducibility of the gelation data and the results are summarised in Table 4.6. On the basis of these data, therefore, the gelation experiments may be considered to be reproducible to within an error of less than 1% in α_c values (which is less than the error or uncertainty in determining the α_c value from the conversion plot as discussed in section 4.3.1) and less than 2% in gel time (t_c). The duplicated values of α_c for experiments 7.1 and 7.3 are plotted (together with α_c values for other dilutions) in figure 4.18(a).

TABLE 4.6 Reproducibility in Gel-Point Determination

Gel-Point	Expt.7.1(0% ϕCH_3,5% TED)		Expt.7.3(20% ϕCH_3,5% TED)	
	(i)*	(ii)*	(i)*	(ii)*
t_c(mins)	388	385	690	680
α_c	0.615	0.615	0.626	0.628

(i)* and (ii)* are two gelation experiments with same reactant composition

4.4 The Effects of Catalyst and Solvents on Gel Points

The gelation data obtained from systems 1 to 5 are presented in Table 4.7. The effect of catalyst on the products of the extents of reaction at gel, $(p_a p_b)_c = \alpha_c$, in bulk and nitrobenzene, and in bulk and toluene, are shown in figures 4.17(a) and 4.17(b), respectively. In the bulk systems, α_c increases almost linearly with increasing catalyst level up to about 10%, above which the change becomes negligible. However, in

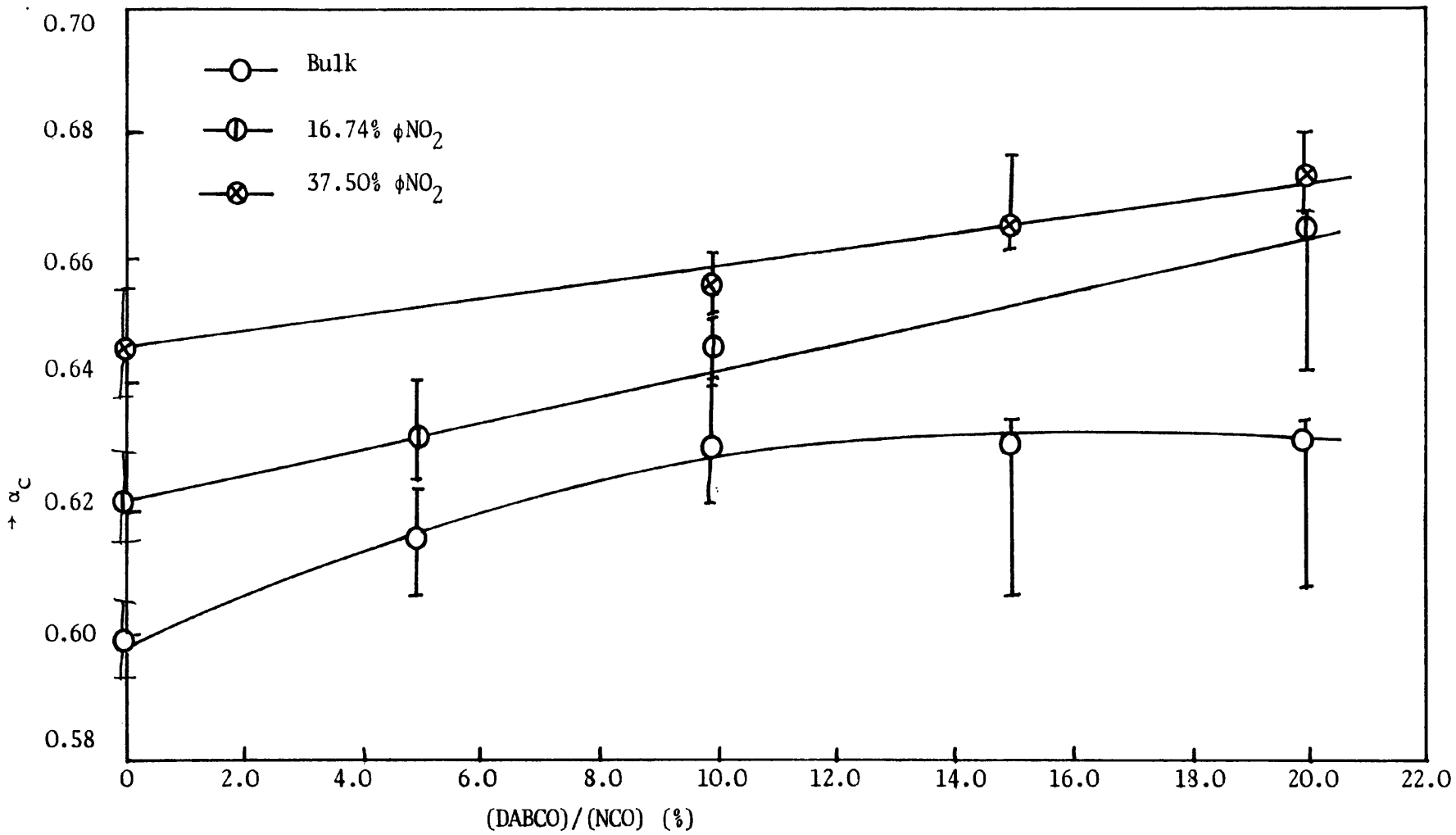

Fig. 4.17(a) Effect of catalyst on gel points in bulk and in nitrobenzene.

(The lower limit corresponds to α_c value obtained from the urethane concentration of last experimental point before gelation and the upper limit from the urethane concentration obtained from a line through the last two or three experimental points.)

Fig. 4.17(b) Effect of catalyst on gel points in bulk and toluene

(The lower limit corresponds to α_c value obtained from the urethane concentration of the last experimental point in conversion plot and the upper limit corresponds to α_c value obtained from the urethane concentration from the line through the last two or three experimental points).

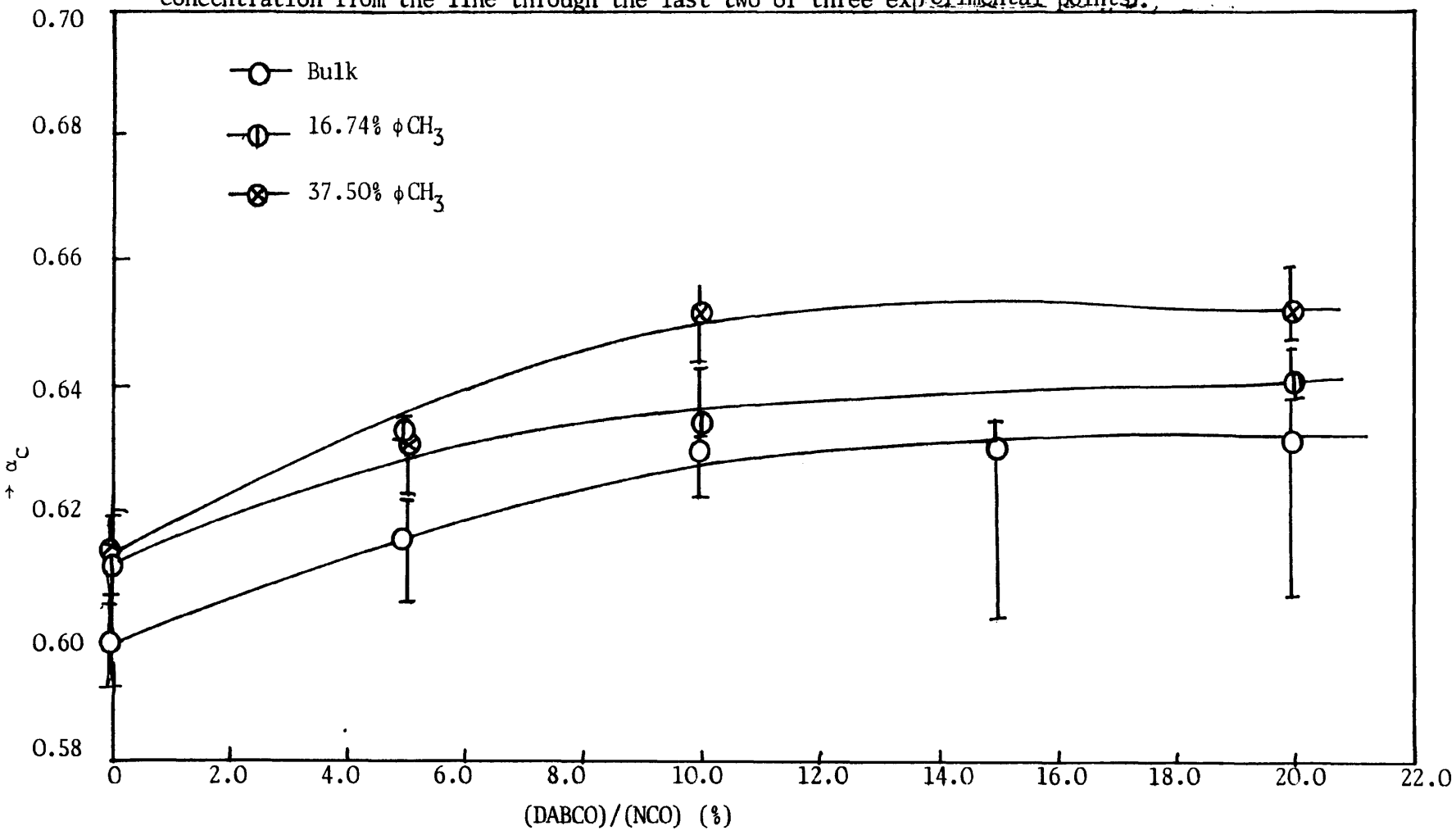

TABLE 4.7 Gelation Data for the Systems LG56 + HD1 in Bulk, Nitrobenzene and Toluene at 80°C.

Expt No.	% Solvent (w/w)	Catalyst Conc (DABCO)/(NCO) (%)	Gel Time (t_c) (10^2.mins)	$(p_a)_c$	$(p_b)_c$	$(p_a p_b)_c$	$(p_a p_b)_c^{-1}$
1.1	0(bulk)	0	44.10	0.7735	0.7756	0.599±.017	1.667
1.2	"	5	3.88	0.7838	0.7848	0.615±.008	1.626
1.3	"	10	2.06	0.7929	0.7949	0.630±.010	1.586
1.4	"	15	1.44	0.7833	0.8051	0.631±.018	1.586
1.5	"	20	1.06	0.7938	0.7951	0.631±.013	1.584
2.1	16.7(ϕNO_2)	0	60.00	0.7879	0.7891	0.622±.010	1.608
2.2	"	5	5.15	0.7935	0.7955	0.631±.010	1.584
2.3	"	10	2.70	0.8046	0.8040	0.647±.010	1.546
2.4	"	20	1.50	0.8141	0.8160	0.665±.009	1.504
3.1	37.5(ϕNO_2)	0	100.20	0.8040	0.8034	0.646±.009	1.548
3.2	"	10	4.40	0.8095	0.8110	0.656±.003	1.524
3.3	"	15	3.16	0.8132	0.8172	0.665±.007	1.504
3.4	"	20	2.44	0.8218	0.8196	0.674±.010	1.484
4.1	16.7(toluene)	0	58.50	0.7810	0.7816	0.610±.018	1.638
4.2	"	5	5.61	0.7964	0.7947	0.633±.005	1.580
4.3	"	10	2.97	0.7939	0.7979	0.633±.010	1.579
4.4	"	20	1.62	0.7984	0.8033	0.641±.003	1.559
5.1	37.5(toluene)	0	118.80	0.7808	0.7812	0.610±.004	1.640
5.2	"	5	12.90	0.7948	0.7946	0.631±.015	1.583
5.3	"	10	6.25	0.8059	0.8090	0.652±.007	1.534
5.4	"	20	3.40	0.8049	0.8106	0.652±.015	1.533

the nitrobenzene systems shown in fig. 4.17(a), an almost linear increase in α_c with catalyst concentration is observed. The effect in toluene systems, shown in fig. 4.17(b), is similar to that in bulk, α_c increasing up to about 10% catalyst concentration and then becoming almost constant. The α_c values show that catalyst affects gel points more in the presence of nitrobenzene (α_c ranges from 0.60 to 0.67) than in toluene (α_c ranges from 0.60 to 0.65). Thus under identical conditions, the amount of excess reaction over that expected from ideal behaviour (α_c = 0.50) is greater in nitrobenzene than in toluene. The reason is not clear. Apart from side reactions, toluene may be a better solvent and the network chains may be expanded more in toluene, possibly resulting in less ring formation.

In addition to the above experiments, some subsidiary experiments were carried out in order to observe whether there is any change in HDI concentration in solutions of toluene and nitrobenzene, with and without catalyst, and in the absence of triol. Thus reactions involving HDI and catalyst at 5%, 10% and 20% concentrations, excluding triol, were carried out in toluene and nitrobenzene at 80°C over a period of about 8 hours. Samples were taken out at one hour intervals and titrated to determine the decrease in HDI concentration using the procedure described in section 3.2, chapter 3. Table 4.8 summarises the results obtained in terms of the decreases in HDI concentrations after 8 hours as percentages of the initial isocyanate concentrations, ie,

$$\% \text{ decrease in (HDI)} = \frac{((NCO)_o - (NCO))}{(NCO)_o} \times 100$$

TABLE 4.8 Results of Subsidiary Experiments carried out with HDI and Solvents with Catalyst at 80°C, excluding Triol.

Solvent	Catalyst Concentration $(DABCO)/NCO)_o$ (%)	Decrease in HDI Concentration (%) after 8 hours
Nitrobenzene	0	0.1
"	5	7.2
"	10	8.4
"	20	14.0
Toluene	0	0.2
"	5	2.9
"	10	4.4
"	20	6.8

Similar reactions were also conducted under identical conditions in nitrobenzene and toluene without catalyst, but no such decrease in HDI concentrations was observed after 8 hours at 80°C, (0.1% in nitrobenzene and 0.2% in toluene) which are within the experimental errors of (NCO) determination).

Table 4.8 shows that HDI concentrations decrease more in nitrobenzene than in toluene. This decrease may be due to the trimerisation[22] of HDI in presence of catalyst and solvents. The decrease in HDI concentration (= 2.9%) in toluene with 5% catalyst (mol DABCO/mol NCO) is minimal as compared with all other subsidiary experimental systems, which is evident from Table 4.8.

Thus from these subsidiary experiments and the results of experimental systems 1 to 5, a catalyst level of 5% and the solvent

toluene was chosen for the more detailed studies of the effects of dilution on gel points and network properties in the polyurethane-forming system LG56/HD1 at 80°C. Thus two series of experimental systems (6 and 7), one without catalyst and the other with 5% catalyst, using 8 different initial dilutions in each, were carried out in order to determine the gel points in terms of experimental values of α_c. In this way, systematic variations in the reaction conditions of network formation can be defined by the values of α_c which can then be used to characterise the structures of fully reacted networks. In these model systems, α_c can be interpreted in terms of the amount of pre-gel intramolecular reaction which results in structural defects (closed-loop structure) in the final networks. Thus the physical properties of fully reacted polyurethane networks formed from the various reaction systems could be investigated with particular reference to the structures of the networks in terms of quantitatively defined amounts of network defects.

4.5 The Effect of Dilution on Gel Points

The gelation data obtained from experimental system 6 (uncatalysed) and system 7 (catalysed with 5% DABCO) are presented in Table 4.9.

For the ranges of dilutions (bulk to 30% monomer by weight) studied in these two systems, and also in systems 1 to 5, gelation was found to occur at higher extents of reaction than those predicted by Flory's theory of gelation[7], as shown in Tables 4.7 and 4.9 and figs. 4.17(a) and (b) and 4.18(a) and (b). Thus the condition for gelation, expressed in terms of equation (2-21) in chapter 2, section 2.2 for $RA_2 + R'B_f$ type polymerisation,

$$\alpha_c = (p_a\, p_b)_c = (f - 1)^{-1} \qquad \ldots\ (2\text{-}21)$$

is not applicable. For the present polymerisation systems LG56/HD1, α_c

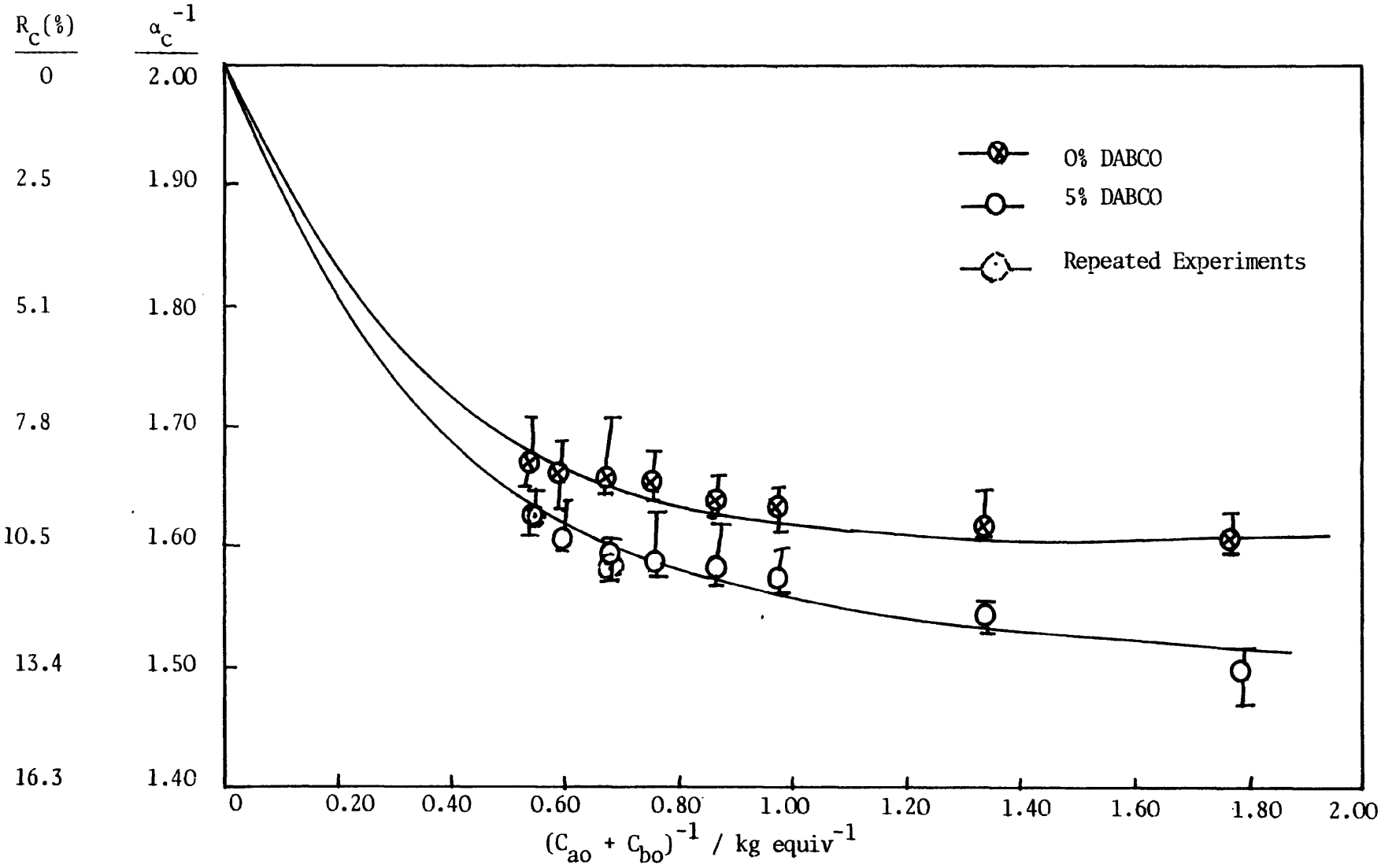

Fig. 4.18(a) Kilb-Stepto plot: effect of dilution on gel points in catalysed and uncatalysed reaction systems

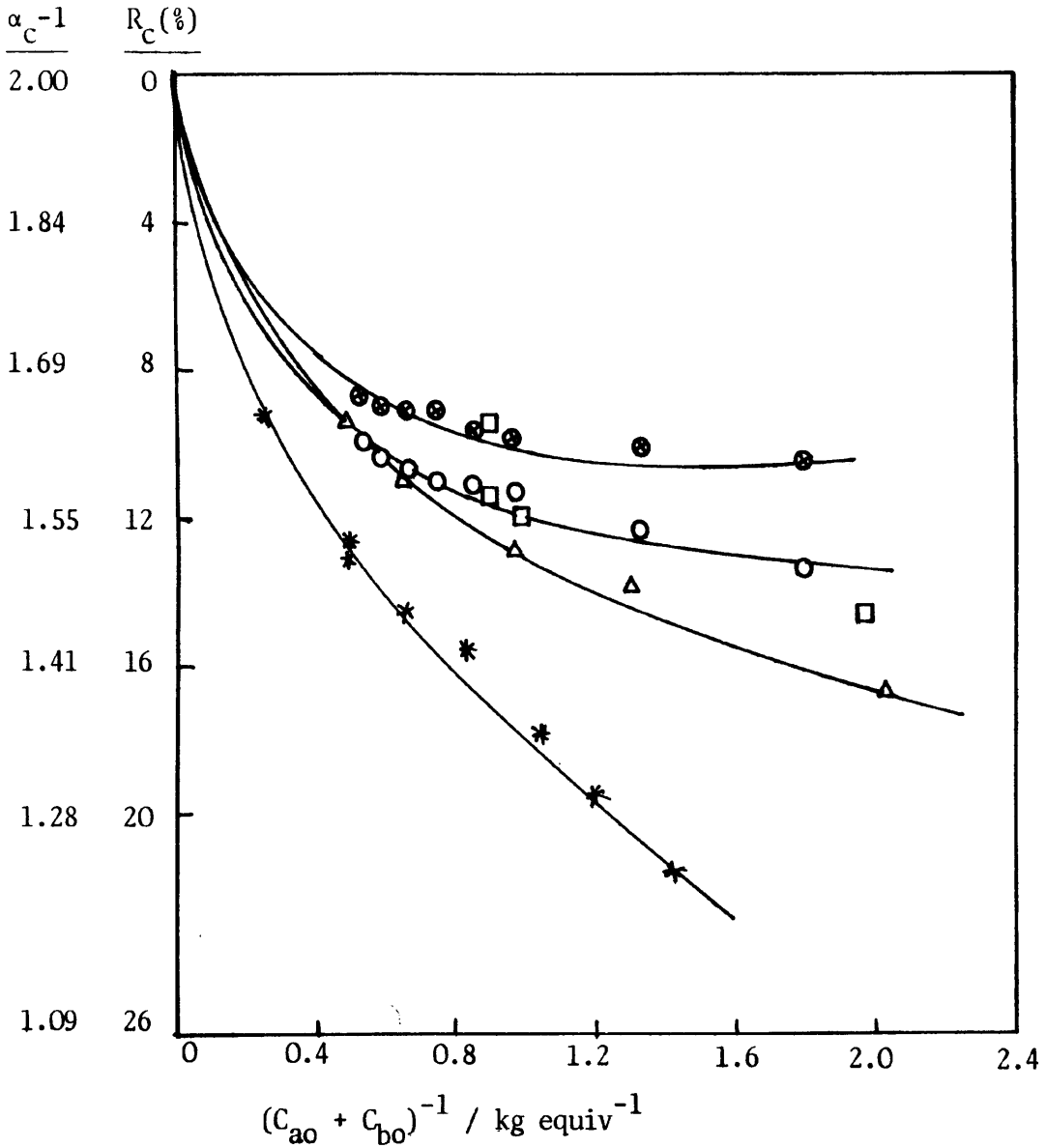

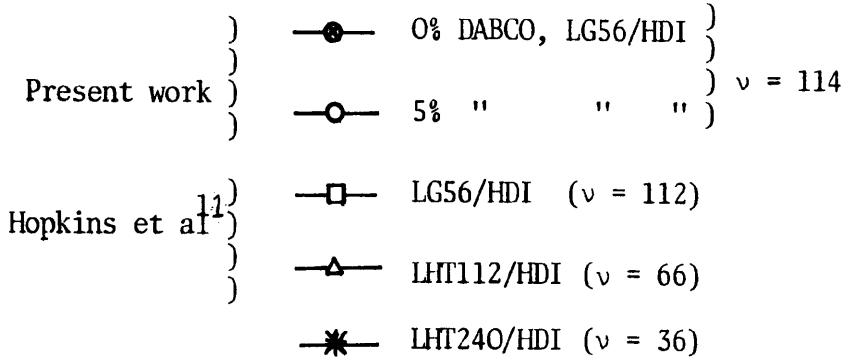

Fig. 4.18(b) Percentages of intramolecular reaction at gelation (R_c) and α_c^{-1} versus initial dilution of the reactant groups in Diisocyanate-Triol Systems.

TABLE 4.9 Gelation Data for the Dilution Series (Catalysed and Uncatalysed) involving LG56 + HD1 in Toluene at 80°C

Expt No.	Solvent Conc (%)	$(C_{ao} + C_{bo})^{-1}$ kg equiv^{-1}	$(C_{ao} + C_{bo})^{-1}$ ℓ equiv^{-1}	$(C_{ac} + C_{bc})^{-1}$ ℓ equiv^{-1}	Gel Time (t_c) 10^2.minutes	$(p_a)_c$	$(p_b)_c$	$(p_a\ p_b)_c$	$(p_a\ p_b)_c^{-1}$
6.1	0	0.5414	0.5527	2.4522	44.10	0.7735	0.7756	0.599±.017	1.667
6.2	9.1	0.5965	0.6202	2.7719	53.70	0.7767	0.7759	0.603±.010	1.659
6.3	20.0	0.6775	0.7199	3.2258	71.00	0.7768	0.7768	0.603±.012	1.657
6.4	28.6	0.7591	0.8203	3.6817	90.00	0.7773	0.7771	0.604±.008	1.655
6.5	37.5	0.8671	0.9532	4.3522	118.80	0.7808	0.7812	0.610±.004	1.640
6.6	44.4	0.9731	1.0839	4.9679	146.40	0.7796	0.7842	0.611±.009	1.636
6.7	59.6	1.3439	1.5399	7.2040	276.00	0.7870	0.7856	0.618±.005	1.617
6.8	69.5	1.7775	2.0734	9.8419	486.60	0.7885	0.7900	0.623±.005	1.605
7.1	0	0.5445	0.5558	2.5768	3.88	0.7838	0.7848	0.615±.008	1.626
7.2	9.1	0.5997	0.6235	2.9593	5.07	0.7896	0.7890	0.623±.009	1.605
7.3	20.0	0.6810	0.7235	3.4661	6.90	0.7911	0.7914	0.626±.011	1.597
7.4	28.6	0.7636	0.8251	3.9914	9.30	0.7943	0.7924	0.629±.008	1.589
7.5	37.5	0.8718	0.9583	4.6683	12.90	0.7948	0.7946	0.631±.015	1.583
7.6	44.4	0.9812	1.0930	5.3740	17.10	0.7970	0.7962	0.634±.009	1.576
7.7	59.5	1.3408	1.5354	7.8846	35.80	0.8029	0.8077	0.648±.002	1.542
7.8	69.6	1.7895	2.0872	11.3985	73.50	0.8163	0.8175	0.667±.007	1.498

values increase with increasing dilution both in catalysed and uncatalysed reactions. In these systems, where equal reactivity of like functional groups is assured, it has been established[11-14,19,24,53,57,58,72] that intramolecular reaction is the most important, single factor responsible for the higher extents of reaction at gelation.

The parameter R_c, defined as

$$R_c = 100(1 - \{(f-1)\ \alpha_c\}^{-\frac{1}{2}}) \qquad \ldots\ (4\text{-}3)$$

for an $RA_2 + R'B_f$ type polymerisation at r = 1, may be used to compare ring formation in a semi-quantitative way. Thus, the effect of dilution on the pre-gel intramolecular reaction can be represented by the parameter R_c, the percentage of intramolecular reaction at gelation. R_c values have been calculated for the present polyurethane system (LG56/HD1 in toluene at 80°C) which are plotted in fig. 4.18(a) along with α_c^{-1} values against initial dilution (Kilb-Stepto plot). For comparison of the present system with Hopkin et al's[11] data, the latter data have also been plotted in fig. 4.18(b) along with the data of the present work. It is evident from both the figures (figs. 4.18(a) and (b)) that pre-gel intramolecular reaction increases with dilution for a particular value of ν. Again, for a particular dilution, R_c increases with decrease in ν (see fig. 4.18(b)). The results of the present work follow this trend. It may be mentioned that R_c values are always higher for the catalysed systems than the uncatalysed ones, indicating more intramolecular reaction in the former, probably due to more side reactions.

Theories giving explanations and interpretations of the effects of intramolecular reaction on the gel points, namely those due to Frisch [16], Kilb[17] and modified Kilb[57], have been discussed in section 2.2, chapter 2. The theories may be summarised as follows:

1. Modified Kilb or Kilb-Stepto:

$$\alpha_c(f-1)\ (1-\lambda_k) = 1 \quad \text{....(2-23)} \quad \text{with } \lambda_k = C_{int}/(C_{int} + C_{ext})$$

2. Modified Frish or Frisch-Stepto:

$$\alpha_c(f-1)\ (1-\ (1-\alpha_c)\ \lambda_F) = 1 \quad \text{....(2-38)} \quad \text{with } \lambda_F = C_{int}/(C_{int} + C_{ext})$$

3. Kilb-Ahmad-Stepto or Ahmad-Stepto:

$$\alpha_c(f-1)\ (1-\ \lambda_{ab})^2 = 1 \quad \text{....(2-35)} \quad \text{with } \lambda_{ab} = C_{int}/\ (C_{int} + C_{ext})$$

It has already been mentioned in section 2.2, chapter 2, that equation (2-23) and (2-35) are identical and, for small values of λ_{ab} and f = 3, $\lambda_k = 2\lambda_{ab}$. So the experimental data of the present work are analysed on the basis of the two theories - Frisch-Stepto (equation 2-38) and Kilb-Ahmad-Stepto (equation 2-35) and correlated with other earlier works. In all cases, the parameter λ' ($\lambda' = \frac{\lambda}{1-\lambda} = \frac{C_{int}}{C_{ext}}$) was used to analyse the results, because the assumption $C_{int} << C_{ext}$ need not be made if λ' is used, as discussed by Ahmad and Stepto[57].

4.5.1 Frisch-Stepto's Theory:

Stepto[18] has used Frisch's[16] approach to describe gelation in polyester and polyurethane forming systems.

According to Frisch's theory, the criterion for gelation is defined by the simplified expression (2-38),

$$\alpha_c(f - 1)\ (1 - (1 - \alpha_c)\ \lambda_F) = 1 \qquad \text{....(2-38)}$$

For experimental systems, as in this study where f = 3, using equation (2-38),

$$\frac{C_{int}}{C_{ext}} = \frac{\lambda_F}{1-\lambda_F} = \lambda'_F = \frac{2\alpha_c - 1}{1 - 2\ \alpha_c^2} \qquad \text{....(4-4)}$$

Frisch did not relate λ_F to any molecular parameter.

Stepto[18] showed that equations (2-39) and (2-23) in chapter 2 are identical for small values of λ. He derived the functional dependence of λ from α_c (equation 2-38) and the molecular interpretation of λ from λ_K (equation 2-23), which is described as Frisch-Stepto's Theory.

The Frisch-Stepto theory was applied to the gelation data of the present polyurethane systems. λ'_F was plotted against both initial and gel dilutions, gel dilutions being calculated using the expression $(C_{ac} + C_{bc})^{-1} = \{C_{ao}\,(1 - 2\,p_{ac} + \frac{1}{r})\}^{-1}$, the derivation of which is given in Appendix C.

For comparison, gel point data of some earlier works[73,74] are also plotted in the same plot in figures 4.19 and 4.20.

According to equation (2-37), chapter 2,

$$\lambda' = \frac{C_{int}}{C_{ext}} = \frac{(f-2)\,.\,p_{ab}\,.\,\phi\,(1,3/2)}{N\,.\,C_{ext}} \qquad \ldots.(2\text{-}37)$$

where N is the Avogadro number. For f=3 and $p_{ab} = (\frac{3}{2\pi\nu\, b^2})^{3/2}$,

$$\lambda'_F = (\frac{3}{2\pi\nu\, b^2})^{3/2}\,.\,\frac{\phi\,(1,3/2)}{N\,.\,C_{ext}} \qquad \ldots.(4\text{-}5)$$

and also,

$$\lambda'_F = \frac{2\,\alpha_c - 1}{1 - 2\alpha_c^2} \qquad \ldots.(4\text{-}4)$$

According to equation (4-5), λ'_F should be a linear function of C_{ext}^{-1}. Non-linear behaviour (figures 4.19 and 4.20) was observed for λ'_F against both initial dilution ($C_{ext}^{-1} = (C_{ao} + C_{bo})^{-1}$) and gel dilution ($C_{ext}^{-1} = (C_{ac} + C_{bc})^{-1}$) for both catalysed and uncatalysed systems of

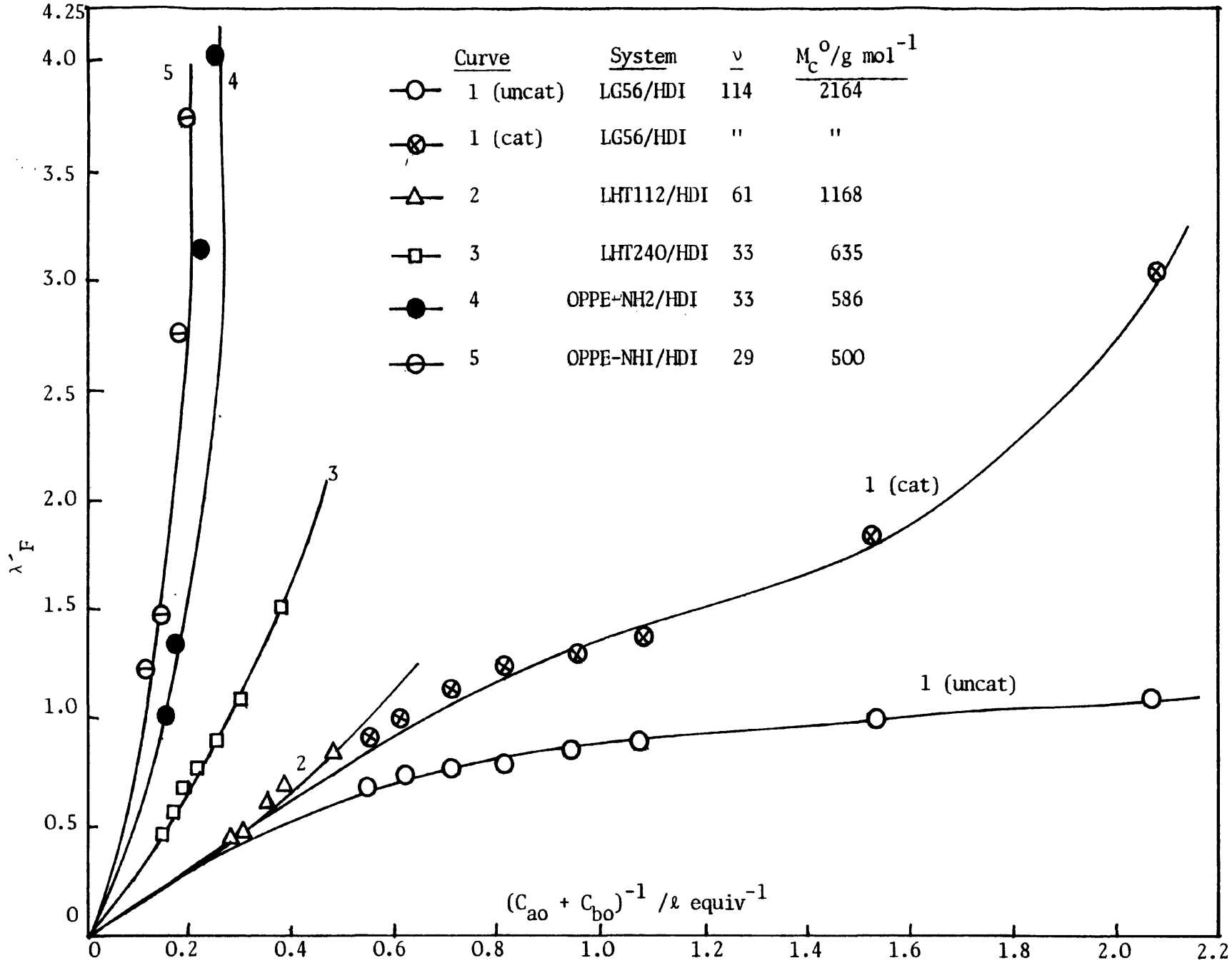

Fig. 4.19 Frisch-Stepto Analysis: λ'_F versus initial dilution

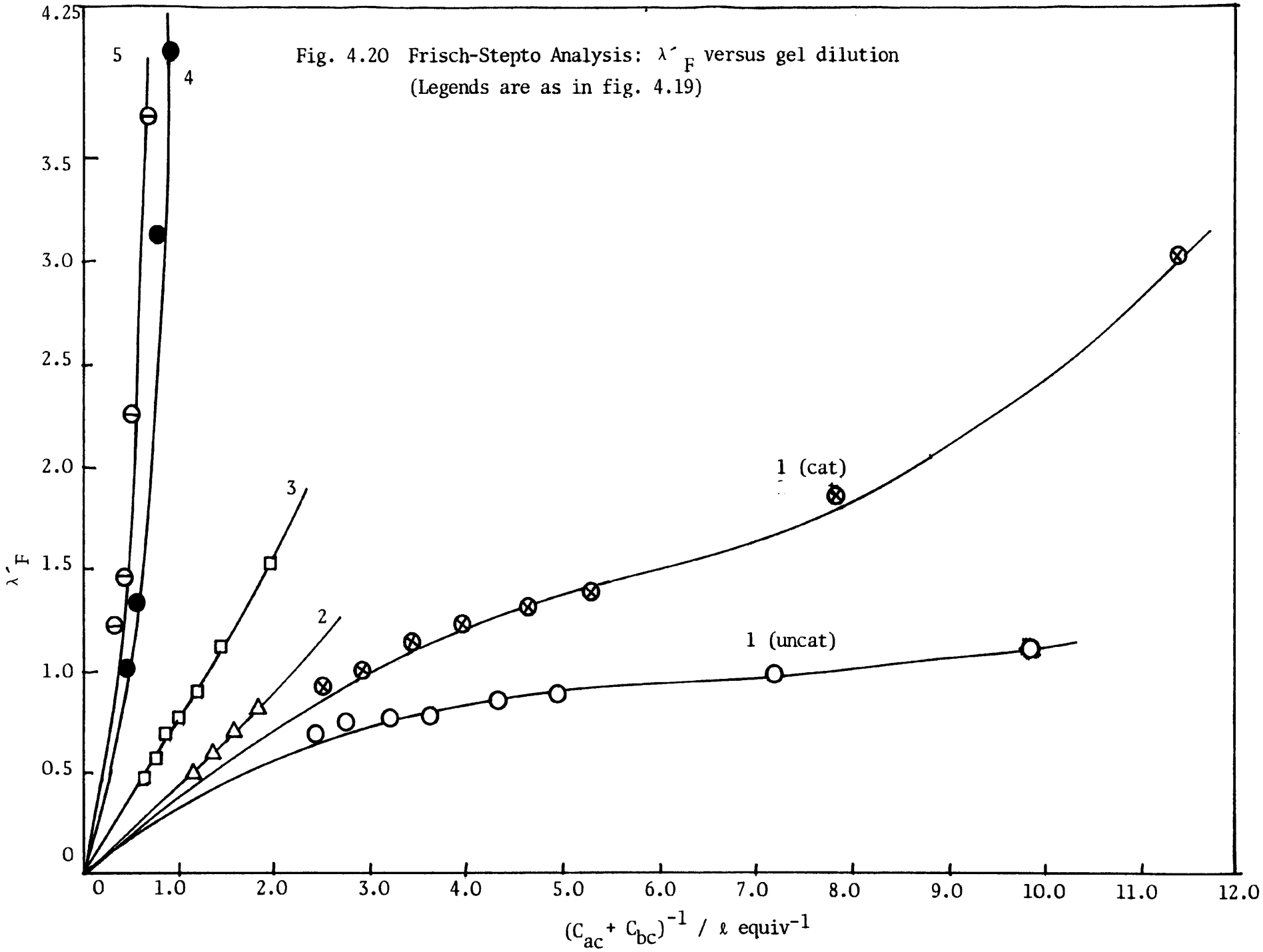

Fig. 4.20 Frisch-Stepto Analysis: λ'_F versus gel dilution
(Legends are as in fig. 4.19)

the present work. Non-linear behaviour was also observed with the earlier gelation data[73,74] of triol and tetrol/HDI systems for both initial and gel dilutions (figs. 4.19 and 4.20). On the other hand, an upward turn was observed in the plots of the figures 4.19 and 4.20 with increase in dilution with all the systems except the uncatalysed system of the present work (ie. system 1 (uncat.)). This general upward curvature is ascribed as being due to the approximations used (eg. higher powers of $(1-\alpha_c)$ were neglected) in deriving equation (2-38) and thus undercounting the rings. Similar non-linear behaviour was also observed by earlier workers[11-14,24,58,72] for other systems.

The values of the effective bond length, b, the characteristic of the chains forming the smallest ring structures, have been calculated from the initial slopes of the plots for both the catalysed and uncatalysed systems of the present system from both initial and gel dilution plots from the expression,

$$b = \left(\frac{3}{2\pi\nu} \left(\frac{N \cdot \text{slope}}{\phi\ (1,3/2)} \right)^{-2/3} \right)^{\frac{1}{2}} \qquad \ldots.(4\text{-}6)$$

which is derived from equation (2-37). The values are presented in Table 4.10. These b values are very small (0.095 and 0.157 nm from the initial and gel dilutions, respectively, for the uncatalysed system and 0.084 and 0.140 from the initial and gel dilutions, respectively, for the catalysed system) compared with those obtained from solution properties[75,76] for these types of polymer chains (0.34 nm to 0.40 nm).

4.5.2 Kilb-Ahmad-Stepto's Theory (or Ahmad-Stepto's Theory)

As stated Ahmad and Stepto[57] have given a more rigorous exposition of the Kilb model which recognises that two opportunities exist for intramolecular reaction per repeat unit. This results in the introduction of an extra factor $(1-\lambda)$ in Kilb's expression (equation 2-23), giving the modified equation (2-35), in chapter 2, namely,

$$\alpha_c \, (1-\lambda_{ab})^2 \, (f - 1) = 1 \qquad \ldots.(2\text{-}35)$$

λ_{ab} can be evaluated using the experimental values of α_c from equation (2-35) and identifying again $\lambda_{ab}/(1-\lambda_{ab}) = \lambda'_{ab} = C_{int}/C_{ext}$, values of the effective bond length, b, can be calculated using equation (4-6).

Figures 4.21 and 4.22 represent the plots of λ'_{ab} versus initial and gel dilutions for both catalysed and uncatalysed systems. For comparison, gelation data of some earlier works[73,74] on triol and tetrol/HDI systems have also been plotted in the same figures. Both the figures (figs. 4.21 and 4.22) show non-linear behaviour. Similar non-linear behaviour has also been observed with other aliphatic polyurethane-forming systems[11,58] and also with aromatic polyurethane-forming systems[24]. However, Ahmad[58] observed linear behaviour in λ'_{ab} versus initial dilution plots but not in λ'_{ab} versus gel dilution plots with polyester-forming systems. In general, compared with the polyester-forming systems, curved plots of λ'_{ab} versus C_{ext}^{-1} are usually obtained[60] and the values of b, from the initial slopes of such plots are smaller, at least for systems based on aliphatic diisocyanates and poly (oxypropylene) triols[11,18,58,74,77]. The b values obtained from the initial slopes of the λ'_{ab} versus initial and gel dilution plots for both the catalysed and uncatalysed systems are presented in Table 4.10 and the results are compared with some other earlier works in Table 4.11.

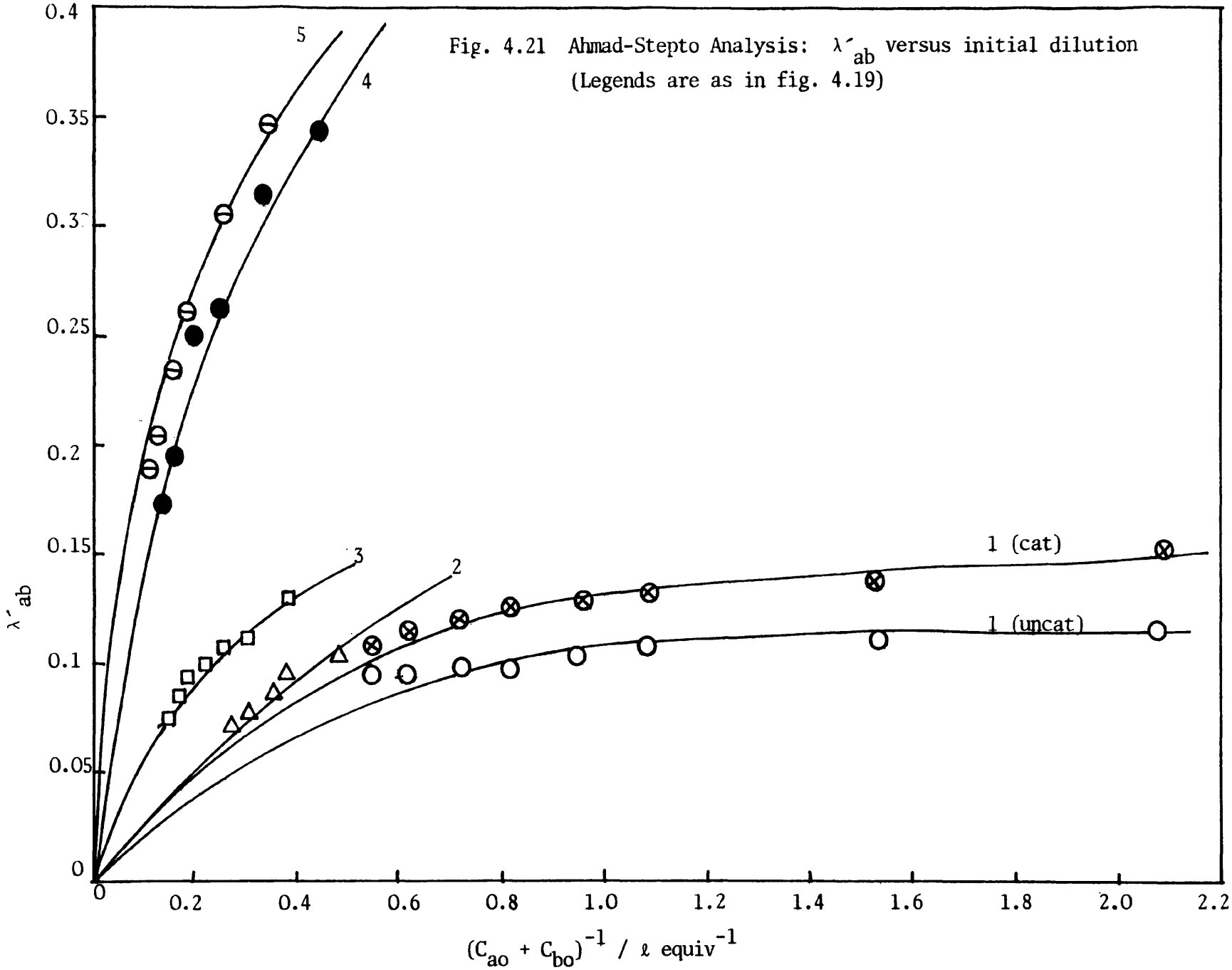

Fig. 4.21 Ahmad-Stepto Analysis: λ'_{ab} versus initial dilution
(Legends are as in fig. 4.19)

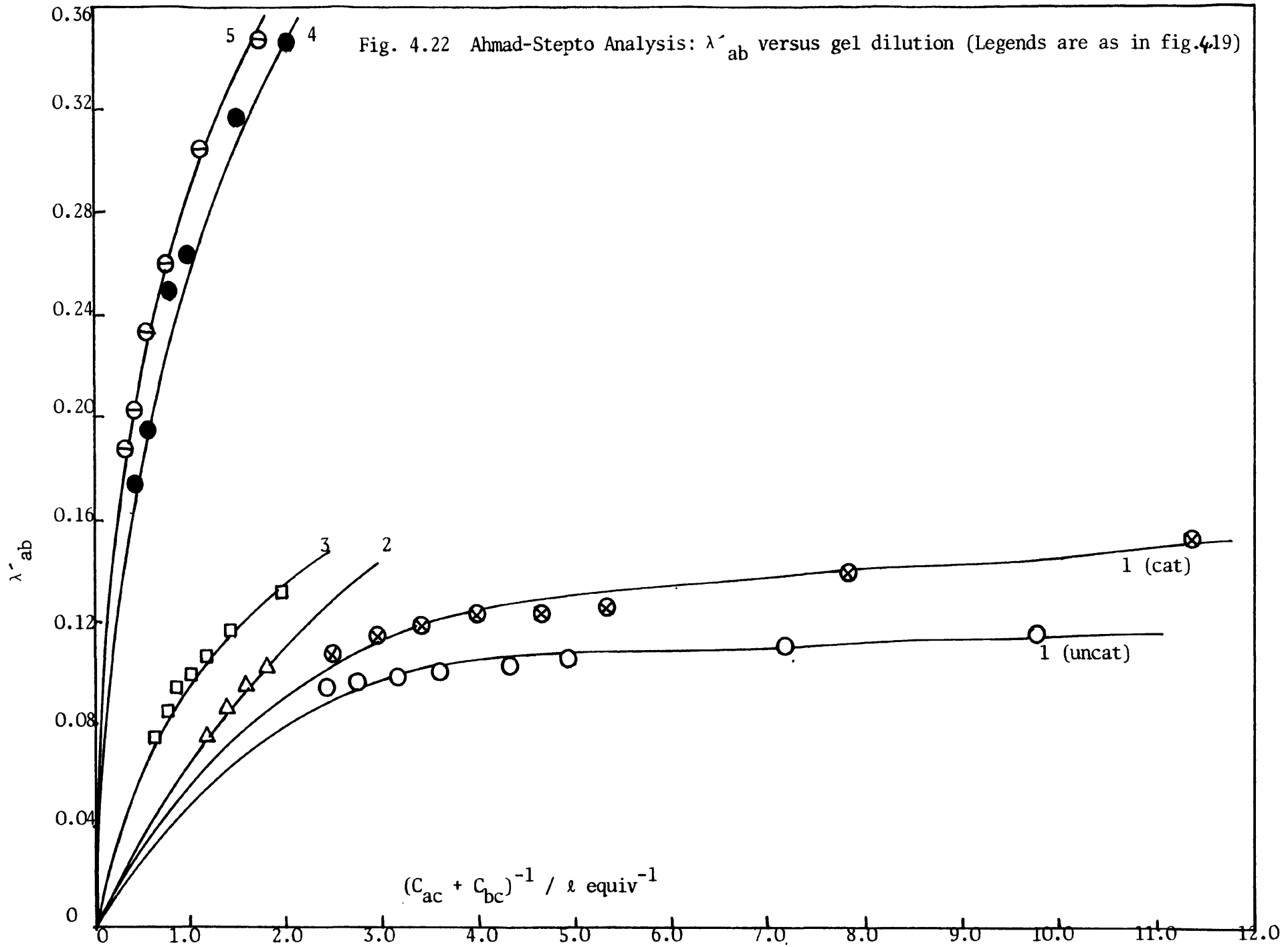

Fig. 4.22 Ahmad-Stepto Analysis: λ'_{ab} versus gel dilution (Legends are as in fig.4.19)

TABLE 4.10 Values of b (nm) for the present polyurethane-forming system LG56/HD1 ($\nu = 114$) in toluene at 80°C obtained from the plots of λ'_F and λ'_{ab} versus initial and gel dilutions. (Comparison of the results of present work and earlier works are given later in Tables 4.11 and 4.13.)

Catalyst Concentration (DABCO)/(NCO)$_o$ (%)	λ'_F Vs. C_{ext}^{-1} plot		λ'_{ab} Vs. C_{ext}^{-1} plot	
	(i)	(ii)	(i)	(ii)
0	0.095	0.157	0.170	0.274
5	0.084	0.140	0.154	0.260

(i) $C_{ext}^{-1} = (C_{ao} + C_{bo})^{-1}$

(ii) $C_{ext}^{-1} = (C_{ac} + C_{bc})^{-1}$

Table 4.10 shows that b values obtained from λ'_{ab} versus initial dilution plots are small (0.170 nm for the uncatalysed and 0.154 nm for the catalysed system) but those obtained from λ'_{ab} versus gel dilution plots are close (0.274 nm for the uncatalysed system and 0.260 nm for the catalysed system) to those obtained from solution properties[75,76].

In figures 4.19 to 4.22, the larger values of λ'_F and λ'_{ab} for systems 4 and 5 compared with other systems illustrate the increased opportunities for intramolecular reaction in tetrafunctional compared with trifunctional systems. The figures (figs. 4.19 to 4.22) also show that the values of λ'_F and λ'_{ab} are higher the lower is the value of ν, the number of bonds in the smallest ring, indicating the increase in opportunity for intramolecular reactions with decrease in ν. It may

TABLE 4.11 Values of b for polyurethane-forming systems derived[79] from the plots of λ'_{ab} versus C_{ext}^{-1} according to equation (2-37). ν_{DI}/ν - fractional length of diisocyanate residue in the chain of ν bonds, (i) $C_{ext}^{-1} = (C_{ao} + C_{bo})^{-1}$, (ii) $C_{ext}^{-1} = (C_{ac} + C_{bc})^{-1}$.

System	f	ν	ν_{DI}/ν	b/nm(i)	b/nm(ii)
1. LG56/HDI (ϕCH_3)*	3	114	0.098	0.170	0.274
2. LHT112/HDI (ϕNO_2)	3	61	0.164	0.222	0.363
3. LHT240/HDI (ϕNO_2)	3	33	0.303	0.247	0.400
4. OPPE-NH2/HDI (ϕNO_2)	4	33	0.303	0.237	0.347
5. OPPE-NH1/HDI (ϕNO_2)	4	29	0.345	0.240	0.356
6. LHT240/MDI (ϕNO_2)**	3	30	0.233	0.307	0.488

* Present work → b values from the uncatalysed system are quoted

** LHT240/MDI → is not plotted in the figures 4.19 to 4.22

Systems 1, 2 and 3, POP triol and HDI; 4 and 5, POP tetrol and HDI;
6, POP triol and MDI.

Key: 1. LG56/HDI, ν = 114; 2. LHT112/HDI, ν = 61;
3. LHT240/HDI, ν = 33; 4. OPPE-NH2/HDI, ν = 33;
5. OPPE-NH1/HDI, ν = 29; 6. LHT240/MDI, ν = 30

HDI - Hexamethylene diisocyanate,

MDI - Diphenyl methane diisocyanate,

LHT112/240 - Oxypropylated adduct of 1,2,6-hexane triol,

LG56 - Oxypropylated adduct of glycerol,

OPPE-NH1/OPPE-NH2 - Oxypropylated penta-erythritol

also be mentioned that in λ'_F and λ'_{ab} versus C_{ext}^{-1} plots (figs. 4.19 to 4.22), the plot for the catalysed system always lies above the uncatalysed one, indicating apparent increased opportunities for ring formation (ie. intramolecular reaction) in the catalysed system.

Table 4.11 shows that the b values of the present work, in terms of the correlation of b values with chain structures as reflected by ν or ν_{DI}/ν, are consistent with those obtained from the earlier works[27,74]. For a given difunctional unit, an increase in the value of ν means a larger proportion of oxypropylene units as compared with methylene units. Polyoxypropylene chains are more flexible than polymethylene chains, so that values of b for the mixed polyurethane chains (ie. polyurethane containing both polyoxypropylene and polymethylene chains) should decrease with increasing values of ν. Thus b values of the present work correlate with this general trend as shown in Table 4.11. Further, the smaller values of b for system 4 compared with those for system 3, with the same value of ν, probably indicates that equation (2-35) relatively undercounts the opportunities for intramolecular reaction for tetrafunctional as compared with trifunctional reactants, so that smaller values are required in compensation. System 6, based on aromatic diisocyanate, gives the largest values of b, characteristic of its stiffer chain structure.

Thus Frisch's theory undercounts the ring formation, giving smaller b values whereas Ahmad-Stepto's theory overcounts it, giving b values closer to those obtained from solution properties[75,76]. Thus Ahmad-Stepto's theory interprets the results of the present work and also earlier works, in general, better than the Frisch's theory.

4.5.3 Polyfunctional Rate Theory (PFRT)

This theory, originally developed by Stanford and Stepto[3,19], has been applied[63] to analyse the data of Ahmad[58] on aliphatic polyesters, Hopkins[11] and Stanford[19] on aliphatic polyurethanes, and Cawse[24] on aromatic polyurethanes. These investigations showed that, at infinite dilution, the limiting value of the ring-forming parameter, $(P_{ab})_o$, defined in section 2.2.4, chapter 2, gave values of effective bond lengths (b) in reasonable agreement with those derived from solution properties[75,76]. So this theory has also been applied in the present work. The main aspects of the theory have been discussed in section 2.2.4 and its application to the present system is now considered in detail.

An existing computer programme[3] was used to calculate the values of the critical total (equation 2-42) at selected increments in extent of reaction, for chosen P_{ab}/C_{ao} values as explained in section 2.2.4, chapter 2). The computed curves are shown in fig. 4.23 using a much reduced scale. When the critical total reaches a value of 0.5 $(=(f-1)^{-1})$ gelation will occur: this is represented by the horizontal datum line drawn in the graph (fig. 4.23). For sufficiently large values of P_{ab}/C_{ao} it is possible that gelation will not occur before complete reaction, an observation confirmed experimentally in some urethane systems[19,78]. It is also clear that gelation occurs at progressively higher critical values of p_a or p_b as P_{ab}/C_{ao} increases.

At the intercept of each P_{ab}/C_{ao} curve with the datum line, the corresponding critical value of p_a was read-off. The latter was then converted to a value of $(p_a p_b)_c$ and plotted against P_{ab}/C_{ao}, as shown in figure 4.24, thus generating the master plot, which is applicable to any $RA_2 + R'B_3$ type polycondensation reaction at r = 1 (given equal

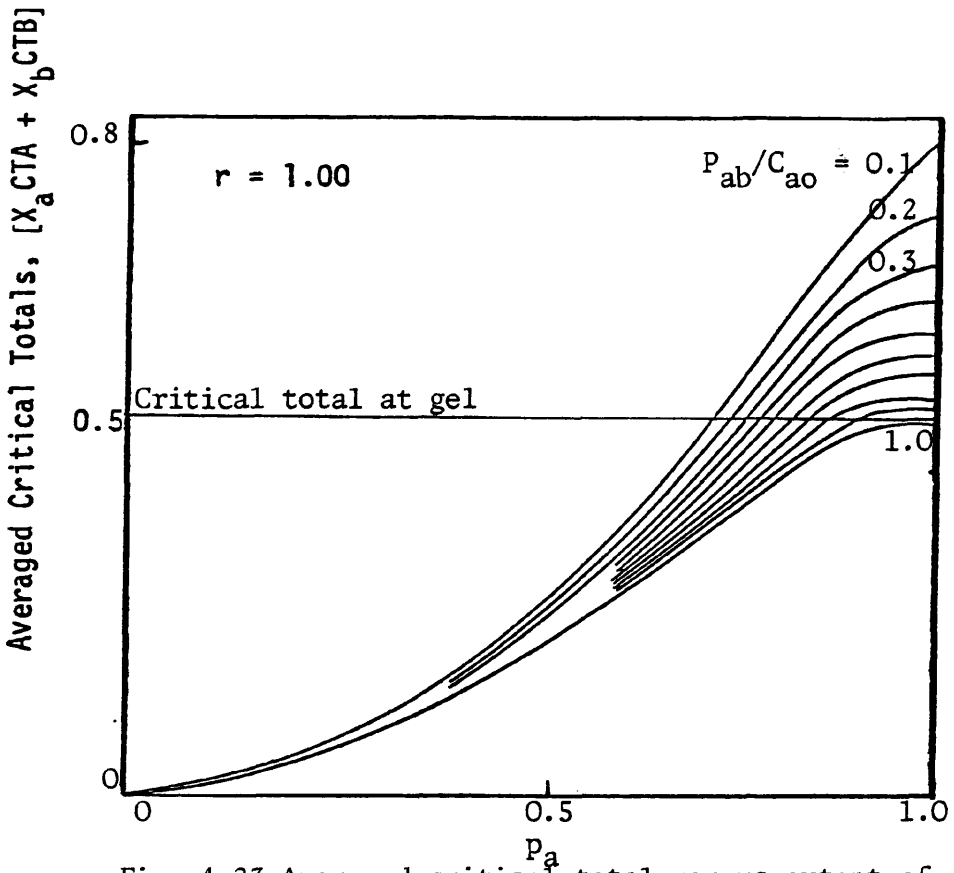

Fig. 4.23 Averaged critical total versus extent of reaction in PFRT for RA_2 + $R'B_3$ type polymerisation with r = 1.00 (reproduced from ref.19)

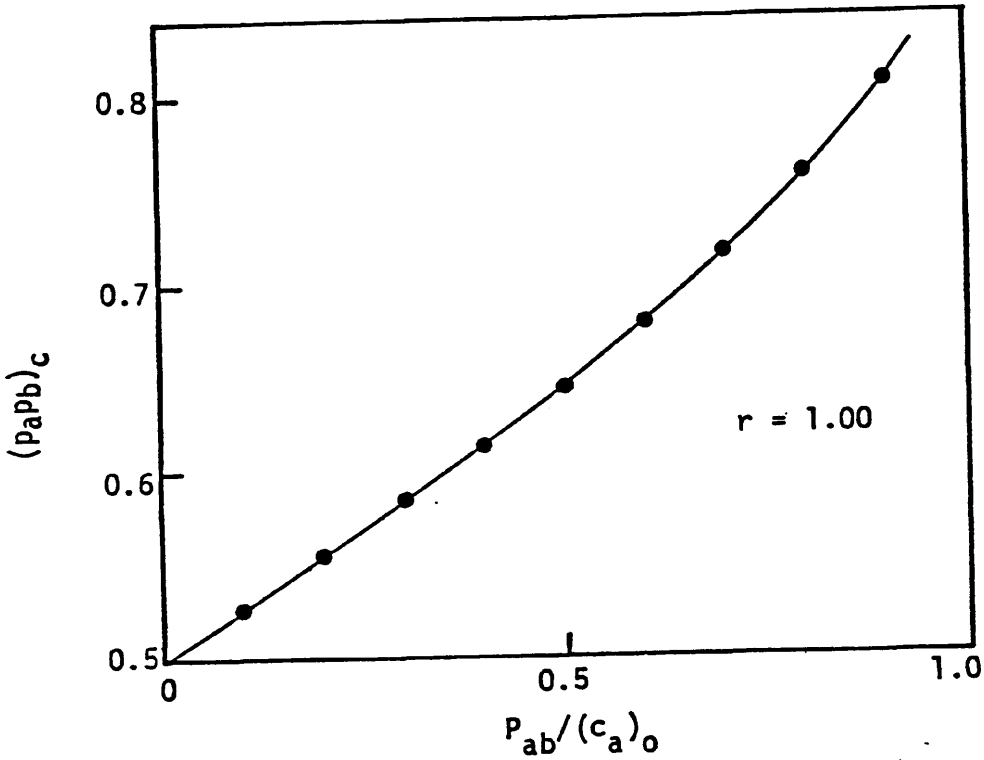

Fig. 4.24 Universal plot of $(p_a\ p_b)_c$ versus P_{ab}/C_{ao} for PFRT, in RA_2 + $R'B_3$ polymerisation r = 1.00 (reproduced from ref. 19)

reactivity of the functional groups). The experimental values of $(p_a p_b)_c$ were next used to interpolate values of the reduced ring-forming parameter (P_{ab}/C_{ao}) for each gelation experiment. Finally, each P_{ab}/C_{ao} value thus determined for each experiment was multiplied by the corresponding initial isocyanate concentration (C_{ao}) to give a particular P_{ab} value. Thus, the values of P_{ab} are ring-forming parameters necessary to give agreement with the experimentally determined gel points for the gelation experiments. The various P_{ab} values are plotted against initial, total concentration, $(C_{ao} + C_{bo})$, as in fig. 4.25. This procedure was carried out for both the catalysed and uncatalysed systems studied and the various data obtained are recorded in Table 4.12.

Fig. 4.25 shows the P_{ab} values to be linear functions of initial total concentration. Both the systems, catalysed and uncatalysed, show similar dependence of P_{ab} on concentration, but on extrapolation to zero concentration, two different intercepts are obtained. The intercepts define the limiting values of P_{ab} for each system and these are designated $(P_{ab})_o$. The catalysed system gives a higher value of $(P_{ab})_o$, 0.051 equiv ℓ^{-1}, than the uncatalysed system for which $(P_{ab})_o$ is 0.029 equiv ℓ^{-1}. If only one-membered rings were being formed, a single value of $(P_{ab})_o$ would suffice for all the data, and the plots (fig. 4.25) would be parallel to the concentration axis. The positive slopes observed in fig. 4.25 imply that higher-membered rings are being formed and their number increases with increasing initial concentration. These plots are, therefore, consistent with the assumption that in the limit of zero concentration, only one-membered rings can form. The slightly higher slope for the catalysed systems indicates that higher-membered rings are formed in greater proportions than in the uncatalysed systems.

Fig. 4.25 P_{ab} versus initial concentration plot in Polyfunctional Rate Theory

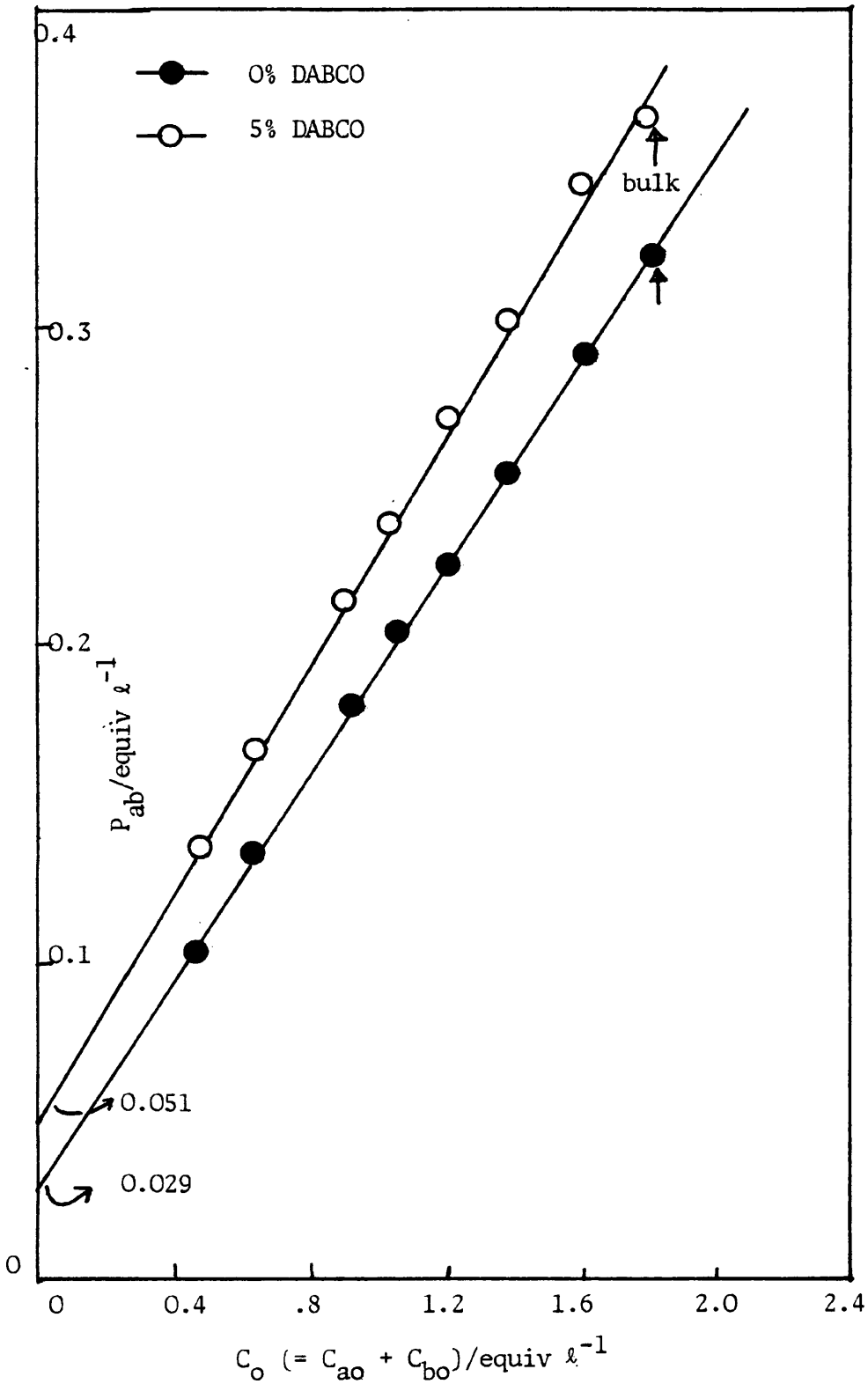

TABLE 4.12 Polyfunctional Rate Theory Data

Expt.No.	α_c(Expt)	Pab/C_{ao}	C_{ao} (equiv ℓ^{-1})	P_{ab} (equiv ℓ^{-1})	(C_{ao} + C_{bo}) (equiv ℓ^{-1})
6.1	0.599	0.356	0.9059	0.3225	1.8093
6.2	0.603	0.362	0.8058	0.2917	1.6124
6.3	0.603	0.366	0.6946	0.2542	1.3891
6.4	0.604	0.370	0.6094	0.2255	1.2191
6.5	0.610	0.390	0.5247	0.2046	1.0491
6.6	0.611	0.394	0.4627	0.1823	0.9226
6.7	0.618	0.416	0.3244	0.1349	0.6494
6.8	0.623	0.430	0.244	0.1038	0.4823
7.1	0.615	0.406	0.9002	0.3655	1.7992
7.2	0.623	0.430	0.8017	0.3447	1.6038
7.3	0.626	0.440	0.6912	0.3041	1.3822
7.4	0.629	0.450	0.6053	0.2724	1.2120
7.5	0.631	0.458	0.5217	0.2389	1.0435
7.6	0.634	0.466	0.4572	0.2130	0.9149
7.7	0.648	0.511	0.3266	0.1669	0.6513
7.8	0.667	0.570	0.2397	0.1366	0.4791

More side reactions in the catalysed system may also be responsible for the slightly higher slope. The higher intercept for the catalysed systems at infinite dilution (ie. zero concentration) over the uncatalysed systems (fig 4.25) may be the result of higher probability of ring formation and/or more side reactions in the former systems. Higher $(P_{ab})_o$ value implies lower b values, which is evident from equation (4.7). This observation (ie. lower b value in the catalysed systems) is consistent with the lower b values obtained from different gelation theories for

the catalysed systems than the uncatalysed ones (see Tables 4.10 for approximate gelation theories and 4.13 for PFRT).

The effective bond length, b, may be obtained from the following equation:

$$(P_{ab})_o = \left(\frac{3}{2\pi\nu b^2}\right)^{3/2} \cdot \frac{1}{N} \qquad \ldots\ (4.7)$$

where ν is the number of bonds in the smallest ring and N is the Avogrado number. Substituting the values of $(P_{ab})_o$ obtained from fig 4.25 (0.051 and 0.029 equiv ℓ^{-1} for catalysed and uncatalysed systems respectively), values of b = 0.206 nm and 0.250 nm respectively, are obtained for ν = 114. These values lie within the range of b values obtained from other approximate theories of gelation (see Table 4.11). Table 4.13 shows that b value obtained for the catalysed system of the present work from PFRT is comparable with the b values obtained from the gelation data of the earlier works[63]. b value obtained from the uncatalysed systems is higher as compared with the b values of the earlier works[63]. Considering the b value obtained from the catalysed system, it may be mentioned that this b value follows the decreasing trend with increasing ν (or ν_{op}/ν) as evident from the b values of reference[63] and b values of the present work. Aromatic polyurethane gives the largest b value, characteristic of its stiffer chain structure, as observed also from approximate gelation theories (see Table 4.11).

Table 4.13 b(nm) values obtained from PFRT

Experimental System	ν	ν_{op}/ν	$(P_{ab})_o$/equivℓ^{-1}	b(nm)
(i)Present work 0% DABCO (Aliphatic Polyurethane) LG-56/HDI, toluene, 80°C, 5%DABCO	114	0.902	0.029 0.051	0.250 0.206
(ii)Aliphatic Polyurethane[63] LHT240/HDI, nitrobenzene, 80°C, catalysed	36	0.694	0.200	0.233
LHT112/HDI, " "	66	0.833	0.105	0.213
LG56/HDI " "	112	0.902	0.063	0.194
(iii)Aromatic Polyurethane[63] LHT 240/MDI, 80°C, catalysed	(a)26*	0.962	0.262	0.251
	(b)27*	0.926	0.262	0.246

* 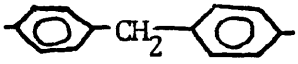 counted as (a) 1 bond and (b) 2 bonds

4.5.4 Comparison of the Effective Bond length, b:

It is now possible to summarise the b values for the aliphatic polyurethane systems, studied in the present work, calculated from the different gelation theories, in order to make comparisons with those obtained from other aliphatic and aromatic polyurethane systems studied previously. The values are tabulated in Tables 4.10, 4.11 and 4.13.

Table 4.10 shows that b values obtained from Frisch-Stepto's analysis are low for both initial and gel dilution plots for the present systems when compared with values for C-C and C-O bond lengths, namely 0.154 and 0.143 nm. Cawse[24], using similar analysis, also obtained a low value of b for aromatic polyurethane systems based on LHT 240/MDI in nitrobenzene, when initial dilution is used. Application of the modified Kilb theory (Kilb-Ahmad-Stepto's theory) also give low b values for the present polyurethane systems which again is a similar observation to that

obtained in the previously studied systems[11,19], when initial dilutions are used. On this basis, it appears more reasonable to use the values of b obtained from plots using gel dilutions as abscissae from which b values are obtained in closer agreement with those derived from solution properties (0.34 and 0.40 nm for poly(oxypropylene) and polyethylene chains). The PFRT also gives similar b values (Table 4.13) but are determined with a greater degree of accuracy. This is because, generally, b is calculated from plots of ring-forming parameter versus dilution and only in the case of PFRT are all the experimental gel points taken into account, whereas in the case of the other gelation theories only the limiting (initial) slope is used, which results in significant uncertainty. It is noteworthy that, in the present systems, the values of b are always lower for the catalysed system than for the uncatalysed one (Table 4.10).

The general trend in all the systems presented in Tables 4.11 and 4.13 is towards a decrease[18] in b as the total number of bonds in the smallest ring, ν, increases or ν_{op}/ν increases or ν_{D1}/ν decreases.

As mentioned earlier, in the present system, the values of b are always lower for the catalysed systems than the uncatalysed one, probably due to more side reactions in the former. Aromatic polyurethane gives higher b values from both approximate gelation theories (see Table 4.11) and PFRT (see Table 4.13) due to its stiffer chain structures.

4.6 Effective Functionality from Gelation Data

From modified Kilb theory of Gelation, equation (2-47)

$$\alpha_c^{\frac{1}{2}} = \frac{1}{(f_w - 1)^{\frac{1}{2}}} + \frac{(f_w - 2)}{(f_w - 1)^{\frac{1}{2}}} \cdot \frac{P_{ab} \cdot \phi(1,3/2)}{N \cdot C_{ext}} \qquad \ldots. (2\text{-}47)$$

can be used to determine the effective functionality of the polyols. A plot of $\alpha_c^{\frac{1}{2}}$ versus C_{ext}^{-1} should be linear with an intercept equal to $1/(f_w - 1)^{\frac{1}{2}}$ and a slope equal to $\frac{(f_w - 2)}{(f_w - 1)^{\frac{1}{2}}} \cdot \frac{P_{ab} \cdot \phi(1,3/2)}{N}$.

Fig. 4.26 Gelation data plotted according to equation (2-47) to determine the effective functionality of polyol (LG56) in LG56/HDI (in toluene at 80°C) system.

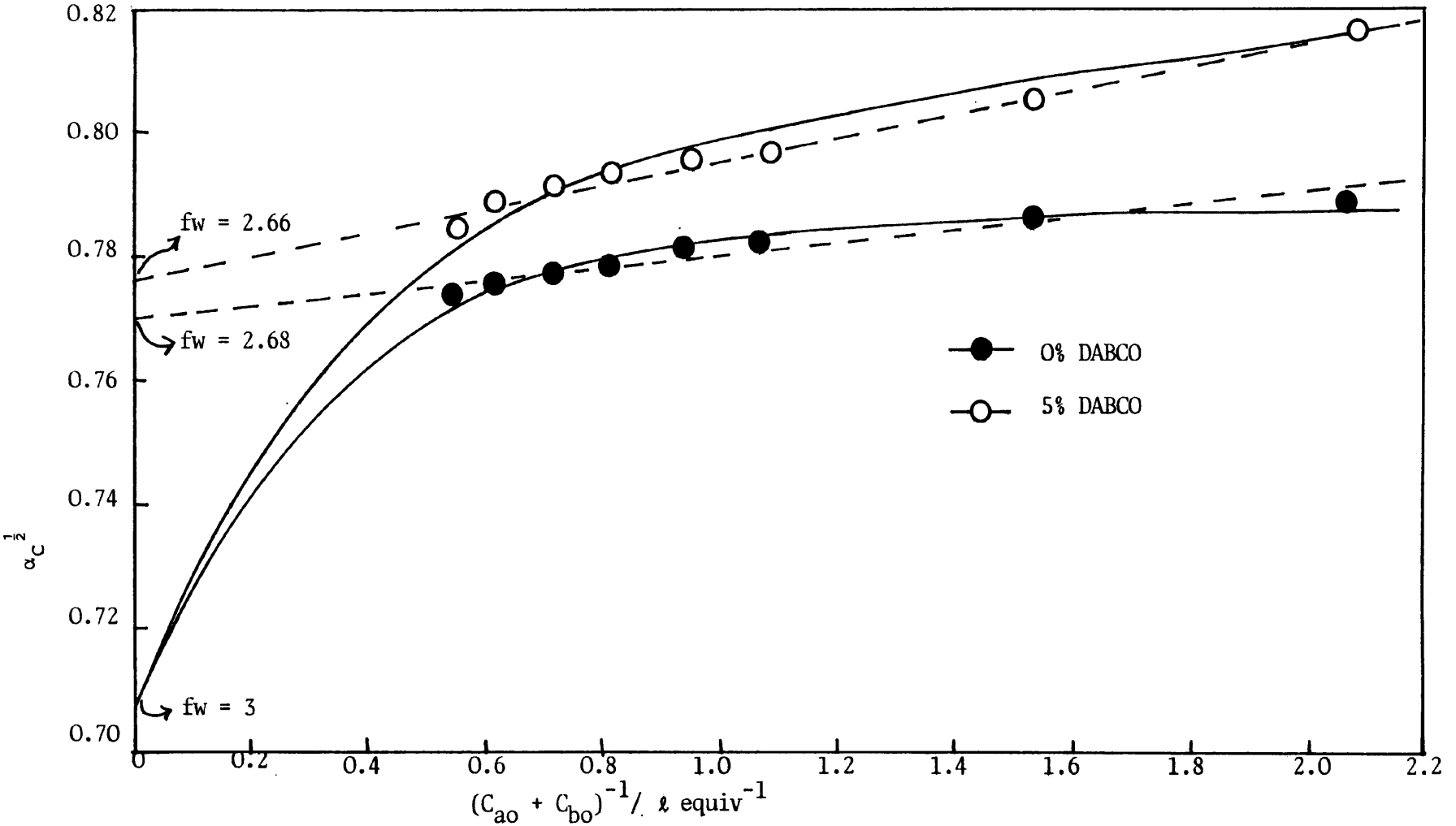

Such a plot is shown in figure 4.26 for the present work and analysed to give the effective functionality of the polyol (LG-56). Least squares analyses of the gelation data of the present work gives f_w = 2.68 (for the uncatalysed system) and 2.66 (for the catalysed system) for LG-56 in LG-56/HDI (in toluene at 80°C) system. f_n (the number average functionality) was calculated for LG-56 from the number average molar mass ($\bar{M}_n$) of the polyol determined by Gel Permeation Chromatography (GPC) and the equivalent weight (E.W.) of the same by the end group analyses (using acetylation method), from the expression:

$$f_n = \frac{\bar{M}_n}{E.W.}$$

For LG-56 in the present work, $\bar{M}_n$ = 2842 g mol^{-1} and the average equivalent weight = 998.2 g mol^{-1}, giving f_n = 2.85. Thus, this analysis shows that $f_n > f_w$, which is impossible. Hence, this procedure cannot be used to determine f_w. The procedure can only be applied when λ'_{ab} versus dilution plot is linear. λ'_{ab} versus dilution plots of the present systems show a lot of curvature. So $\alpha_c^{\frac{1}{2}}$ versus dilution plots will also be highly curved. A similar inconsistent f_w value, with the known functionality of the triol, has also been observed by Stanford and Stepto[60] from the linear plot of $\alpha_c^{\frac{1}{2}}$ versus dilution plot for LG-56 in LG-56/HDI (benzene at 70°C) system. They obtained f_w = 2.90 and f_n = 2.95 - 2.99 from equivalent weight and cryoscopic data. So f_w value should lie above 2.95-2.99. They have shown that a curved plot gives a more consistent functionality (f_w) value than a linear plot.

Thus, the curved plot in figure 4.26 and also in their system[60] is in fact just an alternative manifestation of the curved λ'_{ab} versus dilution plots for these systems.

SECTION 2 : NETWORK PROPERTIES

CHAPTER - 5

THE STRUCTURE AND PHYSICAL PROPERTIES OF POLYMER NETWORKS

5.1 Molecular Structure and Physical Properties

The molecular structure and physical properties of a polymer network and indeed of any other polymer depends on the method of synthesis and the condition of its formation. Although the morphology and the chemical structure of polymer networks may differ, different polymer networks may possess some common physical properties. In general, polymer networks exhibit complete insolubility in all solvents, are infusible, and exhibit some degree of elasticity which varies between that of a highly viscous fluid and a viscoelastic solid. These characteristics have been attributed to the restraining effects of the three-dimensional molecular structure of the polymer[2,80].

As discussed in section 2.2, chapter 2, real networks are not ideal: they do not in general fulfil the requirements of f-functional junction points in which all functionalities have reacted with different molecules, and the network chains themselves may not obey Gaussian statistics. In other words, real networks can be considered to deviate from ideality due to the presence of network defects, including chain interactions possibly leading to so-called entanglements, inelastic loops, loose ends, and non-Gaussian chain effects such as finite extensibility.

Loops may be elastically active if they are connected at two or more junction points to the rest of the network. An elastically inactive loop is connected to the network at only one junction point and has the effect on the network structure of making the value of M_c, the number average molar mass of a real network chain, greater than that of an ideal network chain, M_c^o.

M_c^o is the molar mass of network chains of an ideal network, formed in the absence of pre-gel intramolecular reaction and having no inelastic loops formed post-gel, while M_c is the effective number average molar mass of elastically active network chains (EANC) in a real network.

In a trifunctional network, a free-end increases M_c in a similar manner to an elastically inactive loop, as shown schematically in Fig. 5.1.

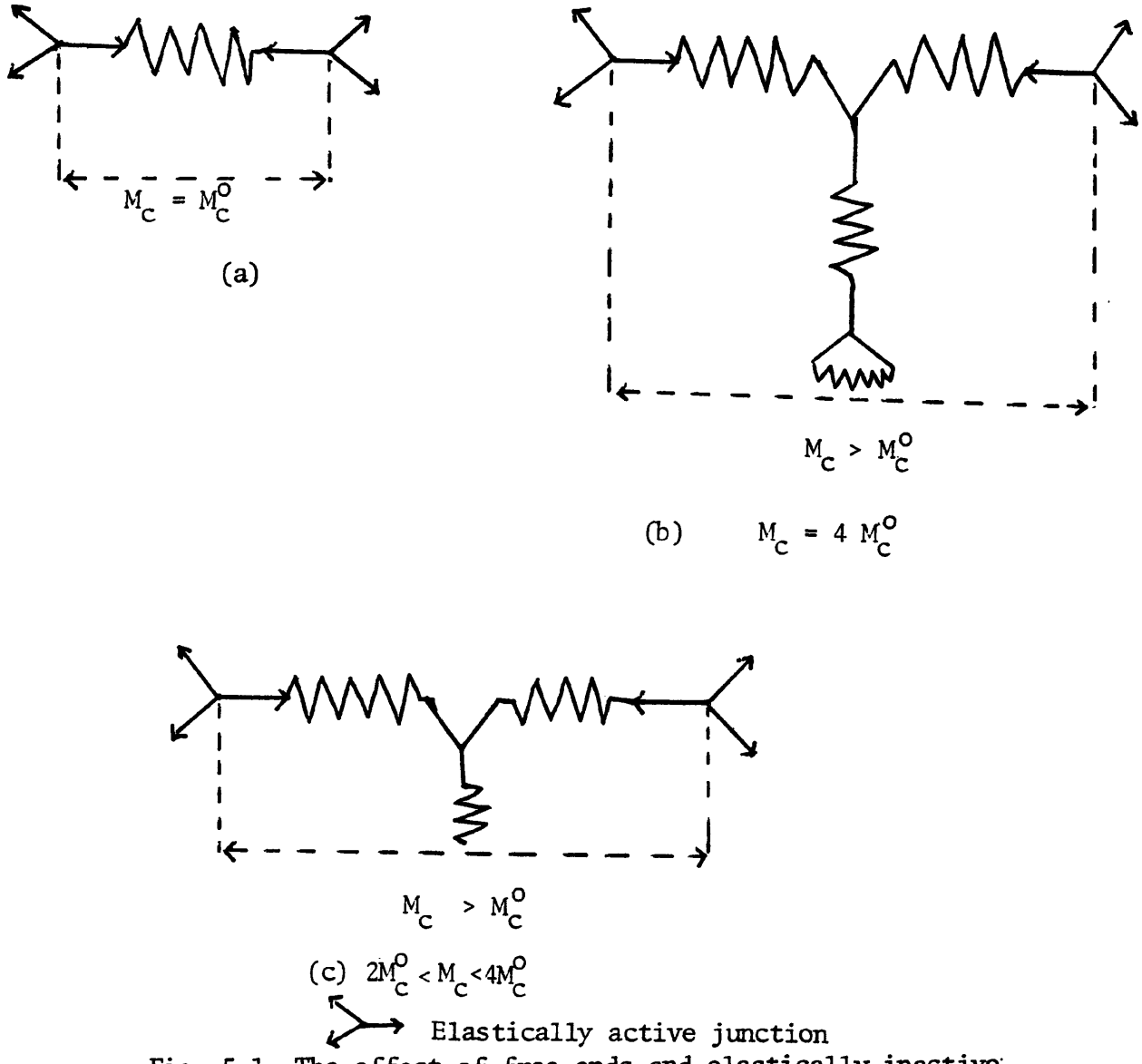

Fig. 5.1 The effect of free-ends and elastically inactive loops on M_c of a trifunctional network

(a) Ideal
(b) Network chain with simplest elastically inactive loop
(c) Network chain with pendant unreacted end group

Considering the simple example of intramolecular reaction, fig. 5.2 shows that a one-membered intramolecular loop or ring structure removes two potential network junction points and causes M_c to exceed M_c^o by a factor of 4. Higher membered rings which are elastically inactive also cause M_c to increase.

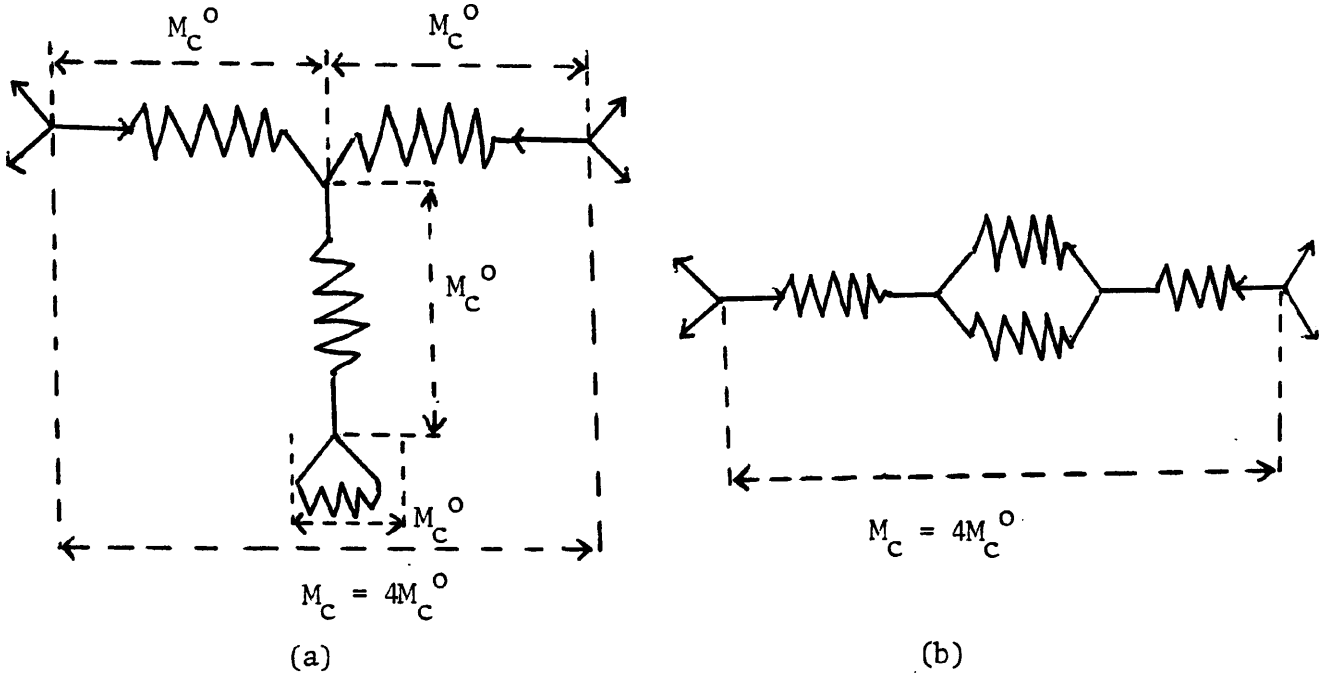

Fig. 5.2 Effect of intramolecular reaction on average molar mass of a network chain

(a) One-membered ring

(b) Two-membered ring

In Fig. 5.2 (b), the two-membered ring shown has resulted from one intramolecular reaction only as $M_c = 4\ M_c^o$ as in the case of one-membered ring.

5.2 Elastic Properties of Rubbery Polymer Networks

5.2.1 General Review

The statistical mechanics and thermodynamics underlying rubber elasticity, applicable to polymer networks, have been frequently reviewed[81-84]. The contribution to the development of the statistical theory of rubber elasticity are those of Flory and Wall[85-88], James and Guth[89-91], Herman[92-93], Treloar[94], Graessley[95], Mark and Flory[96-98], Valles and Macosko[99] and Mark and co-workers[100-104]. Each of the contributions quantifies a stored (or free) energy function, ΔF_{el}, related to the configurational entropy of the network chains (a network chain is the portion of the network that lies between two elastically active junction points) and network chain density (the number of network chains per unit volume). Each contribution is based on the consideration of the network as an assembly of chains interconnected with one another in such a way that the distribution of vector lengths of the network chains conforms to Gaussian statistics.

5.2.2 Gaussian Theory of Rubber Elasticity[89,105,106]

Elasticity of single chain

The density distribution $P(\underline{r})$ of chain vectors $\underline{r}$ for the free chain is essential for the treatment of rubber elasticity. The Gaussian approximation usually provides a satisfactory basis for the density distribution of chain vectors in real rubber networks. Accordingly, for a single chain,

$$P(\underline{r}) = \left(\frac{3}{2\pi\langle r_o^2\rangle}\right)^{3/2} \exp\left(-3r^2/2\langle r_o^2\rangle\right) \qquad \ldots (5.1)$$

From statistical mechanics, $P(\underline{r})$ may be defined as the ratio of two configuration integrals[107] as follows:

$$P(\underline{r})\, d\underline{r} = Z\underline{r}/Z \qquad \ldots (5.2)$$

where Z is the chain configuration partition function over all $\underline{r}$ for the

free chain, and $Z_{\underline{r}}$ is the corresponding value at $\underline{r}$ where $d\underline{r}$ is the volume around $\underline{r}$ where $P(\underline{r})$ is constant. Assuming the elasticity of a chain due to its numerous configurations, the elastic free energy of the chain at $\underline{r}$ is

$$F_{el,\underline{r}} = - kT \ln Z_{\underline{r}} \quad \ldots. (5.3)$$

Using equation (5.2),

$$F_{el,\underline{r}} = -kT \ln Z - kT \ln P(\underline{r})d\underline{r} \quad \ldots. (5.4)$$

$$\ln P(\underline{r}) = \ln \left(\frac{3}{2\pi \langle r_o^2 \rangle}\right)^{3/2} - \frac{3 \quad r^2}{2 \langle r_o^2 \rangle} \quad \ldots. (5.5)$$

$$\therefore \quad F_{el,\underline{r}} = F^*_{el}(T) + \frac{3\ kT\ r^2}{2 \langle r_o^2 \rangle} - kT \ln d\underline{r} \quad \ldots. (5.6)$$

For the undeformed chain, equation (5.6) may be written as

$$F_{el,\underline{r}_o} = F^*_{el}(T) + \frac{3\ kT\ r_o^2}{2 \langle r_o^2 \rangle} - kT \ln d\underline{r}_o \quad \ldots. (5.7)$$

Affine chain deformation

Let $\underline{\underline{\lambda}}$ be the deformation ratio tensor for the sample and $\underline{\underline{\lambda}} = (\lambda_x \ \lambda_y \ \lambda_z)$ in terms of principal ratios.

Also $\det(\underline{\underline{\lambda}}) = \lambda_x \lambda_y \lambda_z = V/V_o \quad \ldots. (5.8)$

with change in volume from the undeformed state V_o to volume V. Assuming a chain in the sample is also deformed by $\underline{\underline{\lambda}}$, then

$$\underline{r} = \underline{\underline{\lambda}}\, \underline{r}_o \quad \ldots (5.9)$$

and $d\underline{r} = \underline{\underline{\lambda}}\, d\underline{r}_o$ i.e. $d\underline{r}/d\underline{r}_o = \lambda_x\lambda_y\lambda_x = V/V_o \quad \ldots. (5.10)$

The free energy change per chain from $\underline{r}_o$ to $\underline{r}$ is

$$\Delta F_{el} = \frac{3\ kT}{2 \langle r_o^2 \rangle} (r^2 - r_o^2) - kT \ln (V/V_o) \quad \ldots. (5.11)$$

Affine deformation of a collection of independent chains

For a collection of ν independent chains, the free energy change is

$$\Delta F_{el,\nu} = \sum_{i=1}^{\nu} \Delta F_{el,i} = \frac{3\ kT}{2 \langle r_o^2 \rangle} (\Sigma r_i^2 - \Sigma r_{o,i}^2) - \nu kT \ln (V/V_o)$$

$\ldots. (5.12)$

Now $\sum_{i=1}^{\nu} r_i^2 = \nu \langle r^2 \rangle$ and $\sum_{i=1}^{\nu} r_{o,i}^2 = \nu \langle r_o^2 \rangle$ .... (5.13)

Hence, $\Delta F_{el,\nu} = \frac{3\ kT\ \nu}{2\ \langle r_o^2 \rangle} (\langle r^2 \rangle - \langle r_o^2 \rangle) - \nu\ kT\ \ln (V/V_o)$ .. (5.14)

$$\Delta F_{el,\nu} = \frac{3\ kT\ \nu}{2} \left(\frac{\langle r^2 \rangle}{\langle r_o^2 \rangle} - 1 \right) - \nu kT \ln (V/V_o) \quad \ldots. \quad (5.15)$$

Affine deformation of network of chains

For a network of ν chains between junction points there are only $2\ \nu/f$ junction points or $(2\ \nu/f - 1) \simeq 2\ \nu/f$ distinct chain ends which can occupy independent positions in the network. The difference $\nu - 2\nu/f = \xi$ is the cycle rank[105] of the network, namely, the number of chains to be cut to reduce the network to a tree-like molecule.

Thus, a network is a collection of ν chains with only $2\nu/f$ independent chain-end positions and hence the term $\nu kT \ln (V/V_o)$ in equation (5.15) for $\Delta F_{el,\nu}$ becomes $\frac{2\nu}{f}\ kT \ln (V/V_o)$, i.e.

$$\Delta F_{el,net} = \frac{3\ kT\ \nu}{2} \left(\frac{\langle r^2 \rangle}{\langle r_o^2 \rangle} - 1 \right) - \frac{2\nu}{f} kT \ln (V/V_o) \quad \ldots. \quad (5.16)$$

Considering r^2

$$r^2 = \underline{r} \cdot \underline{r} = \underline{\Delta}\ \underline{r}_o \cdot \underline{\Delta}\ \underline{r}_o$$

In terms of components along the principal axes

$$r^2 = r_x^2 + r_y^2 + r_z^2 = \lambda_x^2 r_{ox}^2 + \lambda_y^2 r_{oy}^2 + \lambda_z^2 r_{oz}^2 \quad \ldots \quad (5.17)$$

However, in the undeformed state the chains have random orientations within the sample, hence

$$r_{ox}^2 = r_{oy}^2 = r_{oz}^2 = \frac{1}{3} r_o^2$$

Thus, $r^2 = (\lambda_x^2 + \lambda_y^2 + \lambda_z^2)\ r_o^2/3$ .... (5.18)

Averaging over ν chains,

$$\langle r^2 \rangle = (\lambda_x^2 + \lambda_y^2 + \lambda_z^2) \langle r_o^2 \rangle / 3 \quad \ldots. \quad (5.19)$$

Thus, for a network of ν Gaussian chains all of which deform affinely

$$\Delta F_{el,net} = \frac{kT\,\nu}{2}\,(\lambda_x^{\,2} + \lambda_y^{\,2} + \lambda_z^{\,2} - 3) - \frac{2\nu}{f}kT \ln (V/V_o) \quad \ldots (5.20)$$

The affine deformation assumes that each chain has the same configuration available to it as in the free state. The network structure is reflected only in the number of chain ends. The configurations of the ν chains are assumed independent. This gives an overestimation of the configurations accessible to the network.

Small strain - Large strain behaviour

At small strains the configurational probabilities available to the network chains are essentially those available to free chains i.e. at $\langle r^2 \rangle$ near $\langle r_o^{\,2} \rangle$. Thus independent affine behaviour of all chains may be assumed.

At large strains the connectivity of junction points reduces the number of their possible relative positions relative to the free-chain behaviour, assuming chains have deformed affinely. In the limit of infinite strain they are fixed relative to each other. The deviations from free-chain statistics may be properly accounted for by considering the co-operative statistics of ν connected chains under different macroscopic deformations. A reduction in $\Delta F_{el,net}$ follows if each chain on average deforms less than would be expected from independent affine behaviour.

Affine deformation of Mean-chain-vectors (in the Phantom Network)

One way to account for a reduced chain deformation on strain is to assume that the mean-chain-vectors rather than the chain vectors themselves deform affinely and fluctuations of the mean vectors are unaffected by strain.

Assuming constant fluctuations $d\underline{r} = d\underline{r}_o$ and equation (5.12) becomes:

$$\Delta F_{el,\nu} = \sum_{i=1}^{\nu} \Delta F_{el,i} = \frac{3\,kT}{2\langle r_o^2\rangle} \left(\sum_{\nu} r_i^2 - \sum_{\nu} r_{o,i}^2\right) \quad \ldots. (5.21)$$

and averaging over ν chains (as in equation 5.14) gives

$$\Delta F_{el,\nu} = \frac{3\,kT\,\nu}{2\langle r_o^2\rangle} \left(\langle r^2\rangle - \langle r_o^2\rangle\right) \quad \ldots. (5.22)$$

Mean-square fluctuations are defined as the variance of the distribution of end-to-end separations:

i.e. $$\langle(\Delta r)^2\rangle = \langle r^2\rangle - \langle r\rangle^2 \quad \ldots. (5.23)$$

and

$$\langle(\Delta r_o)^2\rangle = \langle r_o^2\rangle - \langle r_o\rangle^2 \quad \ldots. (5.24)$$

Assuming $\langle(\Delta r)^2\rangle = \langle(\Delta\, r_o)^2\rangle$

$$\Delta F_{el,\nu} = \frac{3\,kT\,\nu}{2\langle r_o^2\rangle} \left(\langle r\rangle^2 - \langle r_o\rangle^2\right) \quad \ldots. (5.25)$$

$\langle r\rangle^2$ and $\langle r_o\rangle^2$ are related by invoking an affine change of $\langle\underline{r}\rangle$, the mean end-to-end vector.

Let $\langle\underline{r}_o\rangle$ deform affinely to $\langle\underline{r}\rangle$, then

$$\langle\underline{r}\rangle = \underline{\underline{\lambda}}\,\langle\underline{r}_o\rangle$$

$$\langle r\rangle^2 = \langle r\rangle.\langle r\rangle = \underline{\underline{\lambda}}.\langle\underline{r}_o\rangle.\,\underline{\underline{\lambda}}\langle\underline{r}_o\rangle$$

i.e. $$\langle r\rangle^2 = \lambda_x^2\langle r_{ox}\rangle^2 + \lambda_y^2\langle r_{oy}\rangle^2 + \lambda_z^2\langle r_{oz}\rangle^2 \quad \ldots. (5.26)$$

For random orientations of chains in undeformed sample

$$\langle r\rangle^2 = (\lambda_x^2 + \lambda_y^2 + \lambda_z^2)\langle r_o\rangle^2/3 \quad \ldots. (5.27)$$

Thus from equation (5.25)

$$\Delta F_{el,net} = \frac{3\,kT\,\nu}{2\langle r_o^2\rangle} \left((\lambda_x^2 + \lambda_y^2 + \lambda_z^2)\frac{\langle r_o\rangle^2}{3} - \langle r_o\rangle^2\right)$$

$$= \frac{kT\,\nu}{2}\frac{\langle r_o\rangle^2}{\langle r_o^2\rangle}(\lambda_x^2 + \lambda_y^2 + \lambda_z^2 - 3) \quad \ldots. (5.28)$$

The ratio of the square of the mean $\langle r_o\rangle^2$ to the mean-square $\langle r_o^2\rangle$ has been shown[95,105,108] to be (1-2/f)

i.e. $$\frac{\langle r_o\rangle^2}{\langle r_o^2\rangle} = 1 - \frac{2}{f} \quad \ldots. (5.29)$$

Thus,

$$\Delta F_{el,net} = \frac{kT\ \nu}{2} (1 - 2/f) (\lambda_x^2 + \lambda_y^2 + \lambda_z^2 - 3) \quad .... (5.30)$$

The derivation and model[106] giving equation (5.30) corresponds to Flory's[105] derivation for the deformation of a phantom network.

Uniaxial deformation of networks (affine)

For affine deformation,

$$\Delta F_{el,net} = \frac{kT\ \nu}{2} (\lambda_x^2 + \lambda_y^2 + \lambda_z^2 - 3) - \frac{2\nu}{f} \ln (V/V_o) \quad .... (5.20)$$

$$\lambda_x \lambda_y \lambda_z = V/V_o \quad .... (5.8)$$

Let $\lambda_x = \ell/\ell_o = \lambda$ .... (5.31)

and $\lambda_y = \lambda_z$

i.e. $\lambda_z = \lambda_y = (\frac{V}{V_o})^{\frac{1}{2}} \frac{1}{\lambda^{\frac{1}{2}}}$ .... (5.32)

Equation (5.32) holds for uniaxial deformation along X-axis with corresponding changes occurring along the other axes. It includes isotropic deformation as on swelling when

$$\lambda^3 = (V/V_o) \text{ with } \lambda_x = \lambda_y = \lambda_z = \lambda$$

Thus,

$$\Delta F_{el,net} = \frac{kT\ \nu}{2} (\lambda^2 + \frac{2}{\lambda} (\frac{V}{V_o}) - 3) - \frac{2\ \nu}{f} kT \ln (V/V_o) \quad .... (5.33)$$

At constant volume, the retractive force

$$f = (\delta\ \Delta F/\delta\ \ell)_{T,V} = (\delta\ \Delta F/\delta\lambda)_{T,V}/\ell_o \quad .... (5.34)$$

$$\frac{\delta\ \Delta F}{\delta\ \lambda} = \nu\ kT\ (\lambda - \frac{V}{V_o} \cdot \frac{1}{\lambda^2})$$

and $$f = \frac{\nu\ kT}{\ell_o} (\lambda - \frac{V}{V_o} \cdot \frac{1}{\lambda^2}) \quad .... (5.35)$$

The experimental deformation is measured relative to $\ell_{i,V}$, the initial length at volume V. It is assumed that the change from V_o to V is isotropic (e.g. by swelling or drying). The experimental deformation ratio

$$\Lambda = \ell/\ell_{i,V} = \ell/\ell_o \cdot \frac{\ell_o}{\ell_{i,V}} = \lambda \cdot (V/V_o)^{-1/3} \quad \ldots. (5.36)$$

using equations (5.8) and (5.31).

Thus,

$$f = \frac{\nu kT}{\ell_o} \left(\Lambda \left(\frac{V}{V_o}\right)^{1/3} - \left(\frac{V}{V_o}\right) \cdot \frac{1}{\Lambda^2} \left(\frac{V}{V_o}\right)^{-2/3}\right)$$

ie $$f = \frac{\nu kT}{\ell_o} \left(\frac{V}{V_o}\right)^{1/3} \left(\Lambda - \frac{1}{\Lambda^2}\right)$$

or $$f = \frac{\nu kT}{\ell_{i,V}} \left(\frac{V}{V_o}\right)^{2/3} \left(\Lambda - \frac{1}{\Lambda^2}\right) \quad \ldots. (5.37)$$

Thus, the stress per unit undeformed area at volume V is given by

$$\sigma = \frac{\nu kT}{a_V \ell_{i,v}} \left(\frac{V}{V_o}\right)^{2/3} \left(\Lambda - \frac{1}{\Lambda^2}\right)$$

where $a_V \cdot \ell_{i,V} = V$. Let $\nu/V = \nu^*$, the number of chains per unit volume, then

$$\sigma = \nu^* kT \left(\frac{V}{V_o}\right)^{2/3} \left(\Lambda - \frac{1}{\Lambda^2}\right) \quad \ldots. (5.38)$$

Equation (5.38) may be used for swollen (S) or dry (D) states,

with $$\nu = \nu_S^* V_S = \nu_D^* V_D \quad \ldots. (5.39)$$

$$\sigma_S = \nu_S^* kT \left(\frac{V_S}{V_o}\right)^{2/3} \left(\Lambda - \frac{1}{\Lambda^2}\right) \quad \ldots. (5.40)$$

and

$$\sigma_D = \nu_D^* kT \left(\frac{V_D}{V_o}\right)^{2/3} \left(\Lambda - \frac{1}{\Lambda^2}\right) \quad \ldots. (5.41)$$

It is convenient to refer σ_S to the chain density in the dry state linked with swelling ratio. From equation (5.39), equation (5.40) can be written as

$$\sigma_S = \nu_D^* kT \frac{V_D}{V_S} \left(\frac{V_S}{V_o}\right)^{2/3} \left(\Lambda - \frac{1}{\Lambda^2}\right)$$

i.e. $$\sigma_S = \nu_D^* kT \left(\frac{V_D}{V_S}\right)^{1/3} \cdot \left(\frac{V_D}{V_o}\right)^{2/3} \left(\Lambda - \Lambda^{-2}\right) \quad \ldots. (5.42)$$

where $V_D/V_s = \phi_2$, the volume fraction of polymer in the swollen network. Hence

$$\sigma_s = \nu_D^* \, kT \, \phi_2^{1/3} \left(\frac{V_D}{V_o}\right)^{2/3} (\Lambda - \Lambda^{-2}) \qquad \ldots. \quad (5.43)$$

To include phantom or affine-chain vector behaviour,

$$\sigma_s = A\nu_D^* \, kT \, \phi_2^{1/3} \left(\frac{V_D}{V_o}\right)^{2/3} (\Lambda - \Lambda^{-2}) \qquad \ldots. \quad (5.44)$$

where $A = 1$ for affine chain-vector behaviour[105,121], and

$A = 1 - 2/f$ for affine mean-chain-vector behaviour (phantom)[105,121].

Further

$$\frac{\nu_D^*}{N_A} = \rho/M_c \text{ moles chains per unit volume}$$

where ρ is the density of the dried network.

Thus,

$$\sigma_s = \frac{A\rho RT}{M_c} \cdot \phi_2^{1/3} \left(\frac{V_D}{V_o}\right)^{2/3} (\Lambda - \Lambda^{2}) \qquad \ldots. \quad (5.45)$$

when $\phi_2 = 1$, $\sigma_s = \sigma_D$, and equation (5.45) applies to both dry and swollen states, i.e.

$$\sigma = \frac{A\rho RT}{M_c} \phi_2^{1/3} \left(\frac{V_D}{V_o}\right)^{2/3} (\Lambda - \Lambda^{-2}) \qquad \ldots. \quad (5.46)$$

σ is always measured per unit initial area of the actual network. V_o is the volume with the chains in their natural strain free reference state i.e. ($\underline{r} = \underline{r}_o$) and is taken as the volume at formation (V_f) and V_D is the dry volume, after removal of solvent and any sol fraction.

Experimentally, equation (5.46) may be interpreted as

$$\sigma = G (\Lambda - \Lambda^{-2}) \qquad \ldots. \quad (5.47)$$

where

$$G = \frac{A\rho RT}{M_c} \phi_2^{1/3} \left(\frac{V_D}{V_f}\right)^{2/3} \qquad \ldots. \quad (5.48)$$

G is the shear modulus of the network.

Equation (5.46) has been used to analyse the stress-strain data of both dried and equilibrium swollen networks obtained from uniaxial compression tests in the present work. Stress (σ) is plotted against ($\Lambda - \Lambda^{-2}$) for the networks and the modulus calculated from the slope (discussed in section 6.1.5 chapter 6), and M_c/A values evaluated using equation (5.48).

5.2.3 Mooney-Rivlin Equation

Stress-strain measurements at constant temperature almost invariably show departure from the simple equation[60,73,74,81,109-118]

$$\sigma = \frac{A \rho RT}{M_c} \cdot \phi_2^{1/3} \left(\frac{V_D}{V_f}\right)^{2/3} (\Lambda - \Lambda^{-2}) \quad \ldots\ (5.46)$$

The function $\sigma/\{\phi_2^{1/3} (\Lambda - \Lambda^{-2})\}$ decreases as Λ increases. For this reason, an empirical equation[110,119] of the approximate form

$$\sigma = (2C_1 + 2C_2/\Lambda) (\Lambda - \Lambda^{-2}) \quad \ldots\ (5.49)$$

where C_1 and C_2 are constants (independent of Λ[80,110,120]), is frequently used to represent the observed stress-strain data. This approximate equation is known as Mooney-Rivlin equation. Comparison of equations (5.46) and (5.49) shows that $2C_1$ represents the modulus in the limit at large deformation ($\Lambda \to \infty$), and $(2C_1 + 2C_2)$ its modulus in the limit at small deformation ($\Lambda \to 1$).

According to equation (5.49) the plot of $\sigma/(\Lambda - \Lambda^{-2})$ versus Λ^{-1} should be linear with a slope of $2C_2$ and an intercept of $2C_1$ on the $\sigma/(\Lambda - \Lambda^{+2})$ axis at $\Lambda^{-1} = 0$ and $(2C_1 + 2C_2)$ at $\Lambda^{-1} = 1$

Thus,

when $\Lambda^{-1} = 1$, $2C_1 + 2C_2 = \frac{A' \rho RT}{M_c} \cdot \phi_2^{1/3} \left(\frac{V_D}{V_f}\right)^{2/3}$ .... (5.50)

and $\Lambda^{-1} = 0, \quad 2C_1 = \frac{A\rho RT}{M_c} \cdot \phi_2^{1/3} \left(\frac{V_D}{V_f}\right)^{2/3}$ .... (5.51)

From equations (5.50) and (5.51)

$$2C_2 = (A' - A) \frac{\rho RT}{M_c} \cdot \phi_2^{1/3} \left(\frac{V_D}{V_f}\right)^{2/3}$$

Assuming $A' = 1$ at $\Lambda = 1$ for affine networks[105,121] and

$A = (1 - 2/f)$ at $\Lambda = \infty$ for phantom networks[105,121],

$$2C_2 = \left(1 - 1 + \frac{2}{f}\right) \frac{\rho RT}{M_c} \cdot \phi_2^{1/3} \left(\frac{V_D}{V_f}\right)^{2/3}$$

$$2C_2 = \frac{2}{f} \cdot \frac{\rho RT}{M_c} \cdot \phi_2^{1/3} \cdot (V_D/V_f)^{2/3} \quad \text{.... (5.52)}$$

Comparing equations (5.50) and (5.52)

$$\frac{2C_2}{2C_1 + 2C_2} = \frac{\text{Slope}}{\text{Intercept}} = 2/f \quad \text{.... (5.53)}$$

Thus a Mooney-Rivlin plot should give a slope and an intercept, so that the ratio of slope to intercept is equal to 2/f which is 2/3 in the present trifunctional networks.

The Mooney-Rivlin equation has also been used to analyse the uniaxial compression data of the present work.

5.3 Glass-Transitions in Networks:

The transition from the glassy to the rubber-like state is an important feature of polymer behaviour, representing a region where dramatic changes in the physical properties, such as hardness and elasticity, are observed. The changes are usually reversible. The glass transition (T_g) is often defined experimentally in terms of the discontinuity in a plot of specific volume against temperature and associated with the concept that there exists, on a molecular scale, spatial packing irregularities or "free volume"[122,123]. Free volume (V_f) is the volume within a polymer structure not occupied by any atom belonging to the polymer chains. If V_o is the occupied volume including that due to the

molecules and their vibrations[124], the total volume (V) of the polymer is:

$$V = V_o + V_f \quad \ldots\ (5.54)$$

It has been argued[125] that the occupied volume increases uniformly with temperature, the discontinuity in the expansion co-efficients at T_g then corresponds to a sudden change in the free volume. Hence, it has been suggested that T_g is an iso-free-volume transition.

The effect of junction point density on T_g can be significant. Shibayama[126] has reviewed the effect of crosslinking on T_g. T_g has been observed to increase with crosslink density (i.e. T_g increases with decrease in M_c). Such a dependence has been observed in aromatic polyurethanes[24,60,127,128], unsaturated polyesters[129,130] and polydimethyl siloxane (PDMS)[131]. Such effects are also considered in the present aliphatic polyurethane systems.

5.4 Dynamic Properties of Networks

Dynamic-mechanical tests measure the response of a material subjected to deformation varying periodically with time. Generally, the applied force and the resulting deformation both vary sinusoidally with time. From such tests, it is possible to obtain simultaneously an elastic modulus and a mechanical damping factor at a particular temperature and frequency. The mechanical damping gives the amount of energy dissipated as heat during the deformation of the material.

Dynamic tests are especially important for investigating the properties of polymeric materials to be used in structural applications, as the variation of properties is easily determined as a function of temperature and frequency. The variation of modulus or stiffness of a material with variables is obviously important for strucutral applications. Tests may be done over wide temperature and frequency ranges in a short time, and

from the results the overall performance of a material can be predicted. If only a single frequency is to be used rather than a range of frequencies, it is generally better to choose a low frequency such as 1 Hz since secondary transitions and other structural features may more easily be detected.

The techniques used for dynamic tests have been reviewed by Ferry[124], McCrum[132] and Nielsen[133]. The most widely used apparatus is the "torsion pendulum" which is a free-vibration device giving storage and loss moduli and mechanical damping factor for a range of temperatures as described in section 6.2, chapter 6.

The shear modulus (G') of nearly all polymers in the glassy state is about 10^9 Nm^{-2} and the modulus decreases very slowly as temperature increases. Near T_g the modulus decreases by a factor of about 10^3. In this transition state a polymer is semi-rigid. Above T_g the polymer becomes rubbery and the shear modulus again changes relatively slowly with the temperature. In case of a linear polymer, the modulus decreases as higher temperatures are reached due to the increasing role of viscous flow.

A polymer generally has low damping (tan δ) in the glassy state. The damping goes through a maximum in the glass transition region. That is damping decreases in the rubbery and viscoelastic region at temperatures above T_g.

The loss modulus (G'') goes through a peak at a slightly lower temperature than does the dissipation factor (tan δ) where tan $\delta = G''/G'$. The maximum heat dissipation per unit of deformation occurs at the temperature where G'' is maximum.

In addition to the main transition (T_g) many polymers show some secondary transitions at lower temperatures due to the motion of smaller

groups on the polymer chains. These secondary transitions may be due to the motions of side-groups, or of a very localised number of segments in the main polymer chain. Although such secondary transitions are generally difficult to detect by certain experimental techniques, they are easily measured by mechanical damping tests. Secondary transitions are sometimes related to the toughness of a polymer. Brittle polymers generally have no low temperature transitions or only very weak ones. The tougher polymers always have large secondary damping peaks, well below room temperature.

5.5 Summary

This chapter has given a brief discussion of some of the properties of polymer networks with particular emphasis on static and dynamic elastic properties in relation to network structures as defined by the related parameters-junction point density and molar mass between junction points (M_c). The next chapter will describe the experimental details of the techniques used for measuring network properties, in particular, uniaxial (static) compressive stress-strain and temperature-dependent dynamic properties under shear deformation.

CHAPTER - 6

DETERMINATION OF PHYSICAL PROPERTIES : EXPERIMENTAL

The static and dynamic mechanical properties of the polyurethane networks discussed in previous chapters were investigated by using the apparatuses, namely (i) a uniaxial compression apparatus, (ii) a torsion pendulum and (iii) a differential scanning calorimeter.

In the uniaxial compression apparatus a sample is compressed by applying a stress and the resulting compression is measured in terms of voltage changes by means of a calibrated linear voltage displacement transducer (LVDT). Since it was found[109] that equilibrium was reached within a few seconds when the stress is applied and the deformation rate is very low in the uniaxial compression, this method is an equilibrium-static method. The stress-strain properties of both the dry and swollen networks were investigated at 27°C.

Experiments conducted on the torsion pendulum apparatus gave information on modulus/temperature and relaxation behaviour such as glass transition (primary transition) and secondary transitions of the networks.

A third method, Differential Scanning Calorimetry (DSC) was used to complement the transition data from the torsion pendulum experiments.

6.1 Uniaxial Compression Apparatus

6.1.1 Description

This apparatus was a development by Fasina and Stepto[72,109], of that used previously by Bates[134]. The apparatus consists of four parts, namely, a stressor (a counterbalanced piston device for applying stress), a cathetometer (not shown), a linear voltage displacement transducer (LVDT) with a digital multimeter and a rigid metal frame, shown in Figure 6.1[72].

The key parts of the apparatus used are shown in Figure 6.2[109]. The network sample (A) could be placed on a PTFE surface (B) on a metal block. The load could be applied through a rod (C) fitted with a PTFE end-plate (D). The rod could move smoothly through a close-fitting sleeve (E). Calibrated weights (F) could be attached to the top of the rod which was connected,

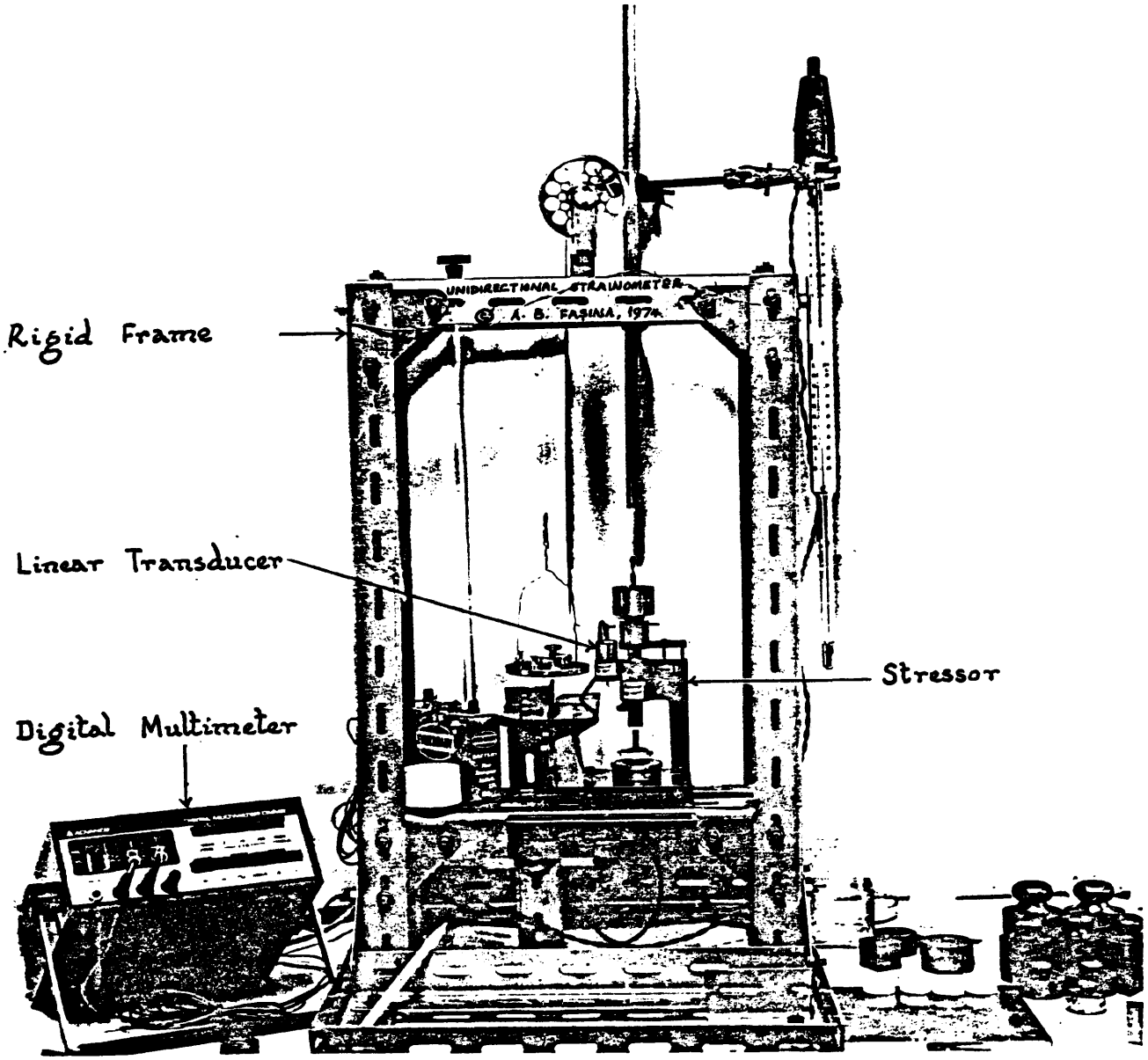

Fig. 6.1 Unidirectional Compression Apparatus, Principal Parts

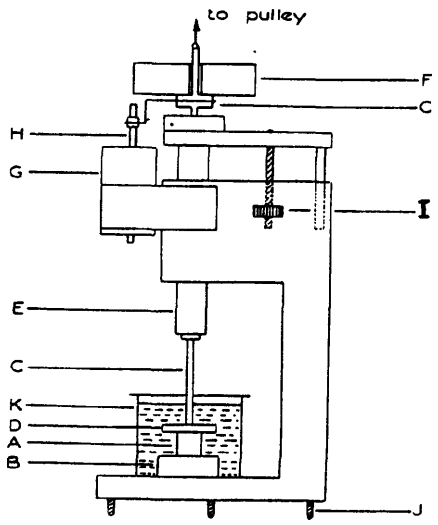

Fig. 6.2 Part of uniaxial compression apparatus.
For details see text.

by a line over a pulley, to a scale pan (Fig. 6.1) which could contain weights to partially counter-balance the weight of the rod C and the weights F. In this way, forces in the range 0-22 N could be applied to the sample. The linear compression of a sample was measured by means of the linear displacement transducer (G) connected to a digital voltmeter. The moving rod of the transducer (H) moved with the rod C. The total range of movement of C and H relative to the body of the transducer (G) and the sample (A) could be adjusted by means of the screw I. To ensure that forces were applied vertically, the whole apparatus could be levelled by means of the screws J. For measurements on swollen networks, the sample was immersed in a solvent reservoir (K).

Initial experiments were carried out to calibrate the voltmeter in terms of linear displacement of the LVDT, and to evaluate the frictional forces arising from the moving parts of the apparatus (rod C and sleeve E, and the pully and line).

6.1.2 Calibration of the Linear Voltage Displacement Transducer (LVDT)

To calibrate the LVDT, the PTFE end-plate D (shown in Fig. 6.2) was screwed down to the bottom PTFE plate B by means of adjustment screw I. The distance between plates B and D was increased by small increments using the adjustment screw I and the distance at each adjustment was measured by means of a cathetometer (accuracy 10^{-2} mm) and the corresponding changes in voltage produced by the LVDT were recorded. The distance between the plates B and D was measured. In this way, approximately 50 readings of distance and corresponding voltages were recorded over a total distance of about 17 mm. The experimental data are presented in Table 6.1 and plotted in Figure 6.3 as voltage (v) against height or displacement (mm). An s-shaped curve was obtained. From this plot, the linear response region of the transducer was determined. The slope of the linear portion of the plot was found to be 0.8426 volt mm^{-1}. Thus, the sensitivity of the LVDT used was 0.8426 volt mm^{-1} in the linear region of the LVDT response.

In all subsequent experiments conducted on network samples, the stress-strain measurements were carried out within the linear response region of the transducer.

6.1.3 Evaluation of the Frictional Forces arising from the moving parts of the apparatus

Experiments were conducted to check the frictional forces arising from the moving parts of the apparatus on dried network samples (made from a reaction in bulk and 5% DABCO) at different applied loads. Forces from 0 to 500 g were applied to samples at levels of (i) 0-500 g, (ii) 500-1000 g and

TABLE 6.1 CALIBRATION OF THE TRANSDUCER

Arbitrary Voltage/volt	Height/mm
-6.180	0
-5.920	0.47
-5.646	0.93
-5.199	1.62
-4.790	2.15
-4.492	2.56
-4.216	2.86
-3.984	3.16
-3.743	3.38
-3.510	3.64
-3.212	4.05
-2.901	4.38
-2.603	4.76
-2.307	5.09
-2.008	5.42
-1.708	5.77
-1.455	6.09
-1.255	6.34
-1.030	6.62
-0.898	6.79
-0.680	7.04
-0.475	7.26
-0.252	7.53
-0.001	7.85
+0.206	8.05
+0.420	8.37
+0.601	8.50
+0.802	8.76
1.001	9.03
1.201	9.50
1.602	9.77
1.801	9.96
2.000	10.20
2.201	10.42
2.404	10.70
2.602	10.93
2.802	11.14
3.002	11.42
3.308	11.82
3.803	12.33
4.327	12.94
4.907	13.73
5.400	14.36
5.848	15.13
6.299	16.08
6.563	17.29

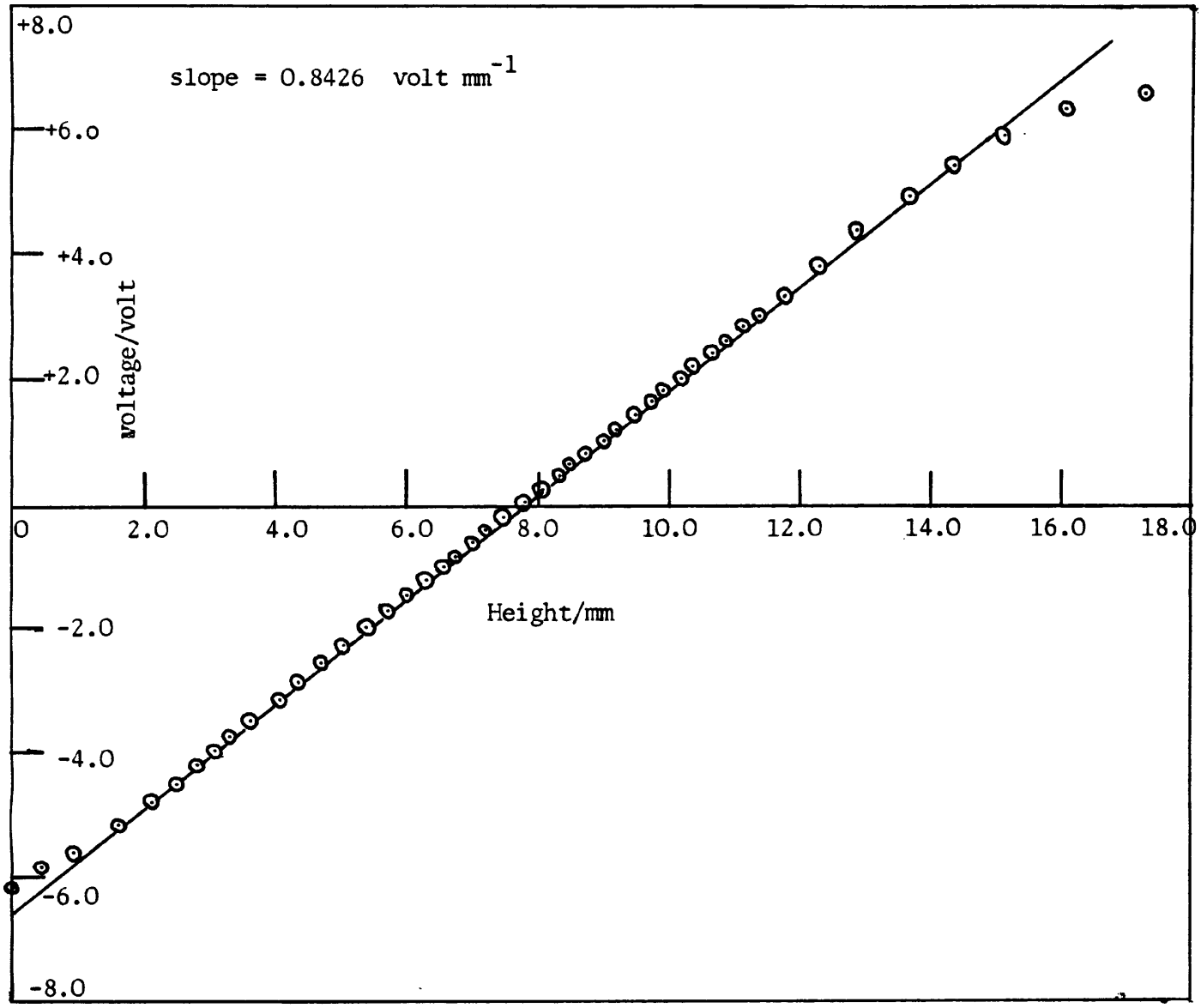

Fig. 6.3 Calibration of the Transducer

(iii) 1000-1500 g loads, thus giving a net load range of 500 g at each level. The results are presented in Table 6.2 and figure 6.4, and show that the difference in the values of $(\Lambda - \Lambda^{-2})$ for the same force applied at different counterbalanced levels of load are less than that of $(\Lambda - \Lambda^{-2})$ for different samples made from the same reaction composition. Thus the effect of friction of the moving parts of the strainometer at different applied stresses in the uniaxial compression tests may be neglected.

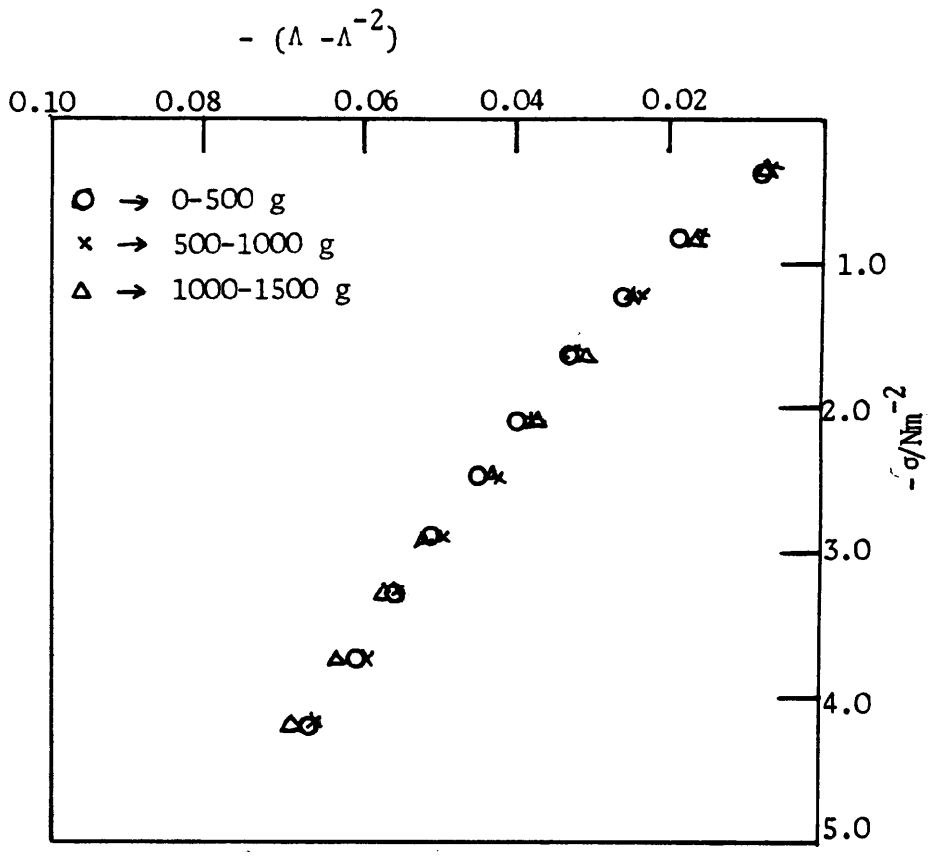

Fig. 6.4 (a) σ versus (Λ-Λ^{-2}) plots for frictional force experiments for a sample at different levels of load

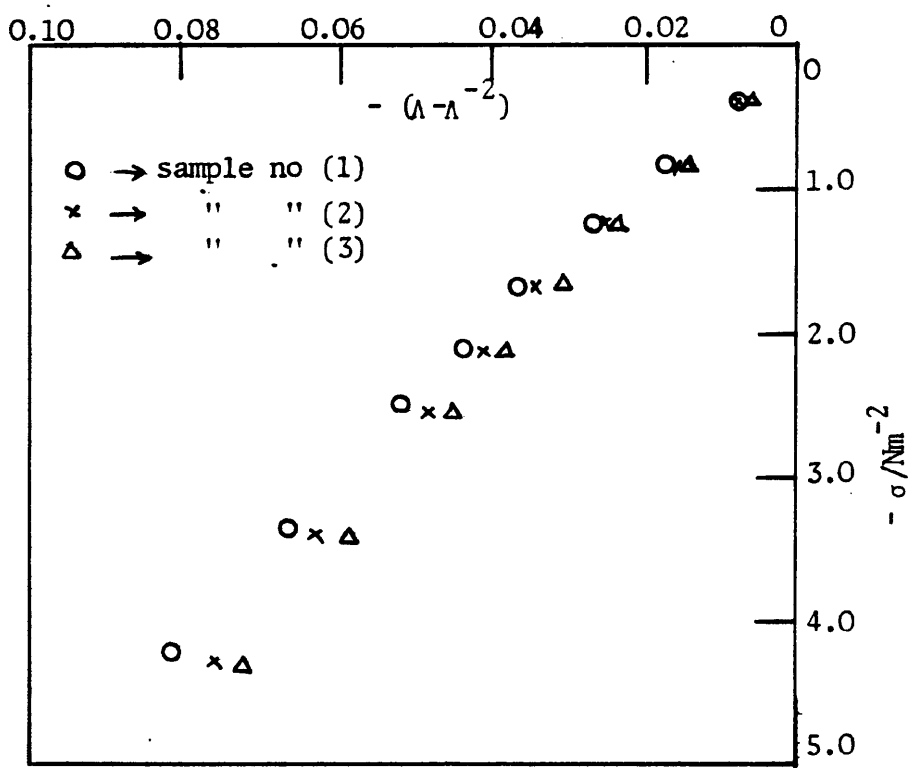

Fig. 6.4 (b) σ versus (Λ-Λ^{-2}) plots for different samples made from same reaction mixture

Table 6.2 Data from frictional experiments on dried network (from expt. 7.1, i.e. 0% ϕCH_3 and 5% DABCO (1)**) using the uniaxial compression apparatus

h_o = 10.00 mm r = 6.11 mm	h^*_c = 9.9735 mm 0 - 500 g	h_c = 9.9825 mm 500 - 1000 g	h_c = 9.9880 mm 1000 - 1500 g
$10^{-4}.\sigma/Nm^{-2}$	$-(\Lambda - \Lambda^{-2})$	$-(\Lambda - \Lambda^{-2})$	$-(\Lambda - \Lambda^{-2})$
0.42	0.0072	0.0069	0.0071
0.84	0.0178	0.0159	0.0157
1.25	0.0251	0.0231	0.0237
1.67	0.0320	0.0307	0.0313
2.09	0.0386	0.0369	0.0371
2.51	0.437	0.0420	0.0434
2.93	0.0503	0.0490	0.0507
3.34	0.0555	0.0553	0.0574
3.76	0.0603	0.0594	0.0626
4.18	0.0663	0.0657	0.0693

r - Radius of the sample

h_o - Measured height (or initial height)

h^*_c - Corrected height (discussed in section 6.1.5)

**(1) - Number within bracket represents the sample identification number

6.1.4 Unidirectional Stress-Strain Measurements

The measurements were carried out in a room thermostatted at 27.0 $\pm$0.5°C. Test samples were generally kept in the thermostatted room for at least 24 hours prior to the beginning of experiments. The initial height h_o and the diameter of the sample were measured by a cathetometer. The dimensions of the swollen samples were measured carefully and quickly using a cathetometer so that the samples did not crack when removed temporarily from the solvent. It should also be possible to measure the dimensions of the samples in the solvent. For each dimension, the average value of two readings was taken.

Dry samples were simply placed on the PTFE plate (B) on a metal block (shown in fig. 6.2). However, to conduct experiments with equilibrium swollen samples, the sample was immersed in a solvent reservoir (K). The effect of buoyancy of the solvent on the force applied to the sample was shown to be negligible[72].

The stress was calculated from the applied force and the cross-sectional area of the unstrained sample. The change in height, Δh, of the sample due to the applied force was calculated from the recorded voltage changes on the voltmeter using the calibration gradient from figure 6.3. Strain values could then be calculated using the values of Δh with the initial height, h_o, of the sample. The applied stress was increased in suitable steps ranging from 50 g in the initial stages of an experiment to 200 g at the end.

Generally an equilibrium state at each level of stress was attained apparently instantaneously. The voltmeter reading was very stable, the worst variation observed was of the order $\pm$ 2 mV (or $\pm$ 2.37 x 10^{-3} mm) after a few hours.

6.1.5 Calculation of stress (σ), compression ratio (Λ) and Correction of initial height (h_o)

A computer programme developed by Fasina and Stepto[72] was used to evaluate the results from uniaxial compression tests.

Compressive stress (σ) in Nm^{-2} is given by the simple expression

$$\sigma = \frac{W \times 9.81}{A}$$

where W is the applied mass in kg and A is the cross-sectional area of the specimen in m^2. The mean percentage of error per experimental point from the least-squares line through the origin of a σ versus $(\Lambda - \Lambda^{-2})$ plot was determined by the programme and was minimised using a series of values

for the initial (measured) height, h_o, of the sample used. The value which gave minimum error was taken as the corrected height (h_c) which was then used for calculations of the values of compression ratio, Λ, corresponding to various compressive stresses, σ.

The computer programme calculates Λ from the following expression:

$$\Lambda = \frac{h_c - \left| \frac{Vo - Vx}{F} \right|}{h_c}$$

where h_c is the corrected height, Vo is the voltage at zero displacement, Vx is the voltage at displacement x (mm) and F (volt/mm) is the slope of the LVDT calibration plot.

After choosing the initial height which gives minimum error (and this height is referred to as corrected height, h_c), the programme calculates Λ using h_c and hence $(\Lambda - \Lambda^{-2})$ for the corresponding stresses. Finally, the programme plots σ versus $(\Lambda - \Lambda^{-2})$ and calculates the shear modulus, G, from the slope of the least-squares fit of the plot. All the uniaxial compression data were analysed and the shear moduli were calculated for both dry and swollen network samples using the programme.

6.2 The Torsion Pendulum

6.2.1 Theory

When a viscoelastic rectangular specimen of known dimensions is subjected to free torsional sinusoidal oscillation, the general equation of motion for free decay is given by[135]

$$I\ddot{\theta} + \eta\dot{\theta} + \frac{K G_1 \theta}{\ell} + \frac{K G_2 \dot{\theta}}{\ell} = 0 \qquad \ldots\ (6.1)$$

where ℓ is the sample length, I is the moment of inertia of the oscillating system, $\ddot{\theta}$ is the angular acceleration, θ is the angle of torsion, η is the coefficient of frictions (e.g. air damping), K is a shape factor and

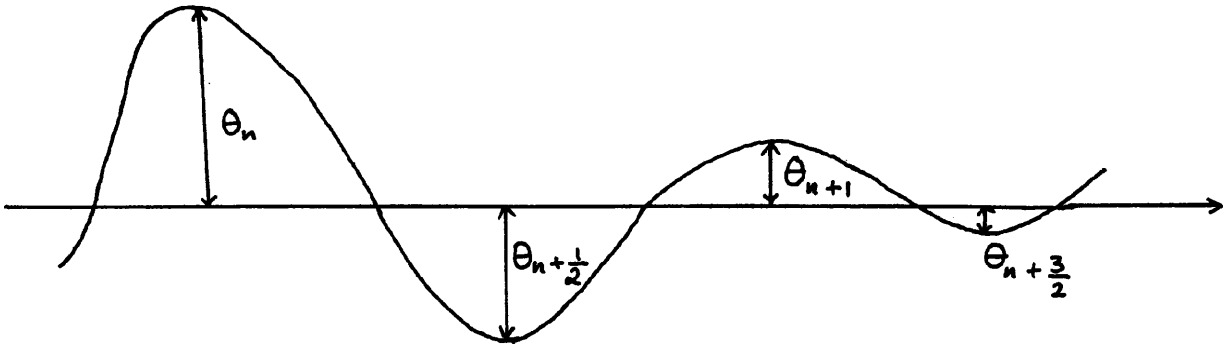

Fig. 6.5 Notation for the decay of oscillation amplitude

G_1 and G_2 are components of the complex modulus G* which are related as

$$G^* = G_1 + i\,\omega\, G_2 \qquad \ldots\ (6.2)$$

where $G_1 = G'$ and $\omega G_2 = G''$ with G' and G'' as the real and imaginary part of the complex shear modulus.

Rearrangement of equation (6.1) gives

$$I\ddot{\theta} + (\eta + \frac{K\,G_2}{\ell})\dot{\theta} + \frac{K\,G_1}{\ell}\theta = 0 \qquad \ldots\ (6.3)$$

Putting $Z_2 = \eta + \frac{K\,G_2}{\ell}$ and $Z_1 = \frac{K\,G_1}{\ell}$,

$$I\ddot{\theta} + Z_2\dot{\theta} + Z_1\theta = 0 \qquad \ldots\ (6.4)$$

Solution for damped oscillation is given by[135]

$$\theta = A \exp\left((-Z_2 + i\sqrt{4IZ_1 - Z_2^2})\, t/2I\right) + B \exp\left((-Z_2 - i\sqrt{4IZ_1 - Z_2^2})\, t/2I\right)$$

(with the condition that $Z_2 < 4IZ_1$)

or $$\theta = \exp(-Z_2\, t/2I)\left(C \cos\left((\sqrt{4IZ_1 - Z_2^2})\, t/2I\right) + D \sin\left((\sqrt{4IZ_1 - Z_2^2})\, t/2I\right)\right)$$

where $C = A + B$ and $D = i\,(A - B)$

or $$\theta = E \exp(-Z_2\, t/2I)\left(\cos\left((\sqrt{4IZ_1 - Z_2^2})\, t/2I\right) - F\right) \qquad \ldots(6.5)$$

where $E = (C^2 + D^2)^{\frac{1}{2}}$ and $F = \tan^{-1}(D/C)$

or $\theta = E \exp(-Z_2 t/2I) \cdot \cos((\sqrt{4IZ_1 - Z_2^2})(t - t_o/2I))$ .... (6.6)

with E = amplitude at t = 0

F = phase at t = 0 and $F = \omega t_o$

and $\omega = (\sqrt{4IZ_1 - Z_2^2}) / 2I$ = Angular frequency.

Then the measured or derived quantities are:

$$\text{Period} = \frac{2\pi}{\omega} = \frac{4\pi I}{\sqrt{4IZ_1 - Z_2^2}} = P \qquad \ldots. (6.7)$$

and

$$\text{log decrement} = \Lambda = \ln \theta(t) - \ln \theta(t + P)$$

$$= \ln E - Z_2 t/2I + \ln(\cos(\omega t + F))$$

$$- (\ln E - Z_2 t/2I - Z_2 P/2I) + \ln(\cos(\omega t + F + 2\pi))$$

$$\Lambda = Z_2 P/2I \qquad \ldots. (6.8)$$

Using equation (6.8),

$$Z_2 = 2 I \Lambda/P \qquad \ldots. (6.9)$$

From equation (6.7)

$$16 \pi^2 I^2 = P^2 (4 I Z_1 - Z_2^2),$$

Using equation (6.9)

$$16 \pi^2 I^2 = P^2 \cdot 4 I Z_1 - P^2 \cdot \frac{4 I^2 \Lambda^2}{P^2}$$

$$\therefore \quad Z_1 = \frac{16 \pi^2 I^2 + 4 I^2 \Lambda^2}{4 P^2 I}$$

$$\therefore \quad Z_1 = \frac{4 \pi^2 I}{P^2} \left(1 + \frac{\Lambda^2}{4 \pi^2}\right)$$

i.e.

$$G_1 = \frac{4 \pi^2 I \ell}{K P^2} \left(1 + \frac{\Lambda^2}{4 \pi^2}\right) = G' \qquad \ldots. (6.10)$$

From equation (6.9)

$$\eta + \frac{K G_2}{\ell} = \frac{2 I \Lambda}{P}$$

Since separation of η and G_2 is not possible, neglecting air-damping i.e. accounting for damping due solely to material

$$\eta \cong 0$$

$$G_2 = \frac{2\ I\ \Lambda\ \ell}{K\ P}$$

$$\omega\ G_2 = G'' = \frac{2\ I\ \Lambda\ \ell}{K\ P} \cdot \frac{2\ \pi}{P} = \frac{4\ \pi\ I\ \Lambda\ \ell}{K\ P^2} \qquad \ldots\ (6.11)$$

Thus equations (6.10) and (6.11) represent the expressions for real and imaginary part of the complex modulus respectively.

For a rectangular specimen of width b and thickness h, the shape factor K is given by

$$K = \mu\ b\ h^3 \qquad \ldots\ (6.12)$$

for $h/b < \frac{1}{2}$,

where $$\mu = \frac{1}{3}\left(1 - \frac{0.63\ h}{b}\right) \qquad \ldots\ (6.13)$$

Substitution of the values of K in expressions for G' and G'' gives

$$G' = \frac{4\pi^2\ I\ \ell}{\mu\ b\ P^2\ h^3}\left(1 + \frac{\Lambda^2}{4\ \pi^2}\right) \qquad \ldots\ (6.10a)$$

and

$$G'' = \frac{4\ \pi\ I\ \ell\ \Lambda}{\mu\ b\ P^2\ h^3} \qquad \ldots\ (6.11a)$$

G' and G'' are related by the damping parameter, tan δ, as

$$\tan\delta = \frac{G''}{G'} = \frac{4\ \pi\ \Lambda}{4\pi^2 + \Lambda^2} \qquad \ldots\ (6.14)$$

These equations (6.10a), (6.11a) and (6.14) have been used to analyse the torsion pendulum experimental data of the present work.

6.2.2 Description

The torsion pendulum used in this work is of an inverted design basically similar to that developed by Heijboer et al[136], shown in figure 6.5. In this apparatus, the specimen, A, is firmly clamped to a rigid support at its base and the top is firmly clamped to a freely

oscillating inertia bar, B. The inertia bar (B) is centrally suspended by a steel wire, C, which passes over two pulleys, D, to a counterbalanced weight, E. A PTFE bush, F, helps to reduce parasitic oscillations. The oscillation of the test piece is initiated by displacing the inertia bar from its rest position to a predetermined amplitude (between 1 and 3° radial) using the lever, G. G is then rapidly returned and locked in its

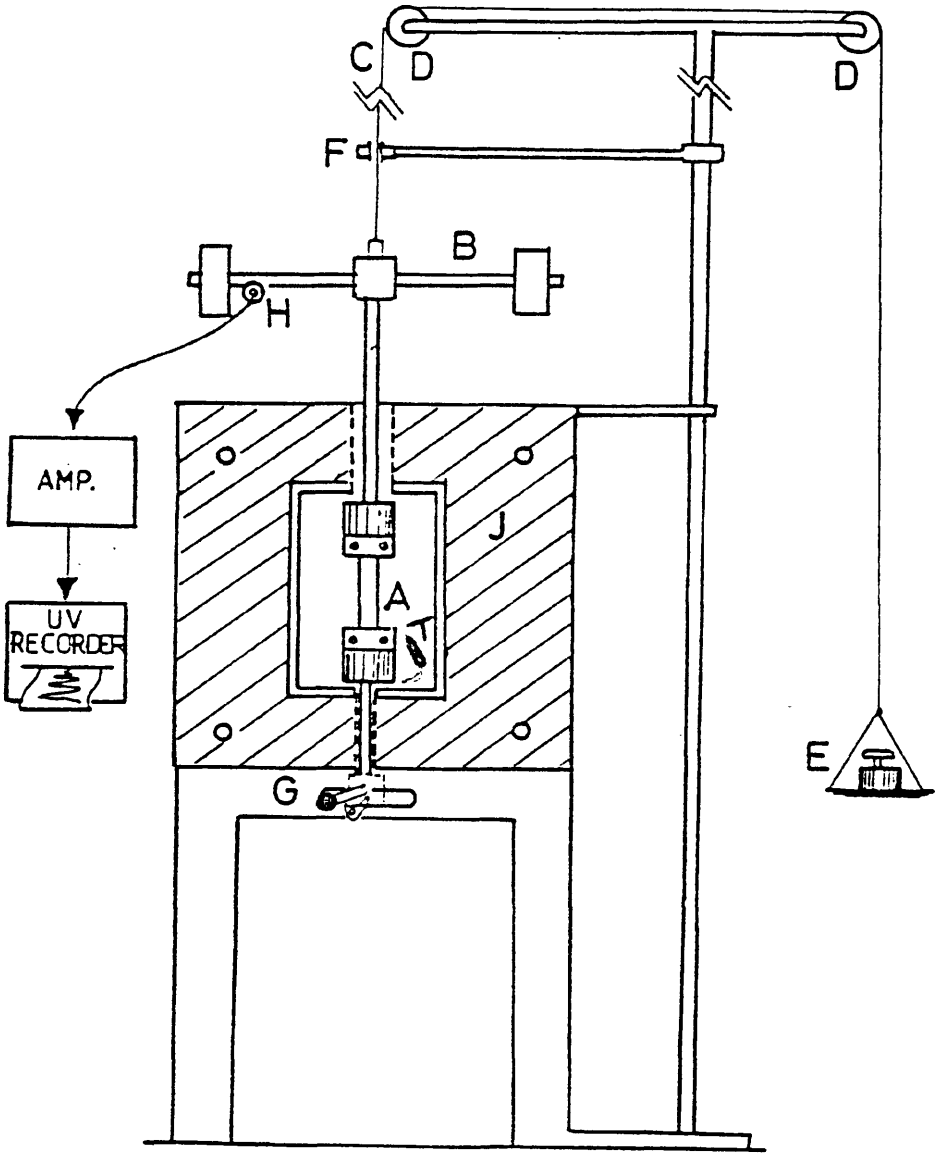

Fig. 6.5 Schematic Diagram of Torsion Pendulum

original central position, thereby setting the system into free oscillation. The sample vibrations are allowed to decay while being monitored continuously by the capacitive proximator probe, H. The output from the probe is amplified (type B731A, Wayne Kerr) and then recorded by a flat-bed recorder (type PL4, J.J. Instruments). Typical sample dimensions used were: length 25 to 30 mm, width 10 to 12 mm and thickness 1.7 to 3.0 mm. It is essential to ensure that the clamped sample is placed centrally and vertically in the apparatus.

An environmental chamber, J, surrounds the specimen, which is used to cool or heat the specimen at controlled rates. A thermocouple, T, is placed close to the sample in the environmental chamber. Heating is achieved with heaters controlled by a Variac transformer cartridge. Cooling is achieved by charging the chamber with liquid nitrogen enabling temperatures down to -195^{o}C to be attained.

External disturbances from air currents were avoided by enclosing the inertia system in a Perspex cabinet (not shown).

6.2.3 Calibration and Operation of the Torsion Pendulum

In section 6.2.1, equations (6.10a) and (6.11a) giving expressions for G' and G'', show that a value for the moment of inertia (I) of the oscillating system is required to calculate the values of G' and G''. A schematic representation of the oscillating system is shown in figure 6.6. The oscillating system includes the horizontal bar, hb, the top specimen clamp, tc, and the rigid, vertical bar, vb, connecting them, together with the added masses, m_1 and m_2 (in this particular apparatus $m_1 = m_2 = 0.318$ kg). The value of Io (when $m_1 = m_2 = 0$, I = Io) was determined by measuring the period of oscillation for a thin steel plate at room temperature using different displacements of the masses (m_1 and m_2)

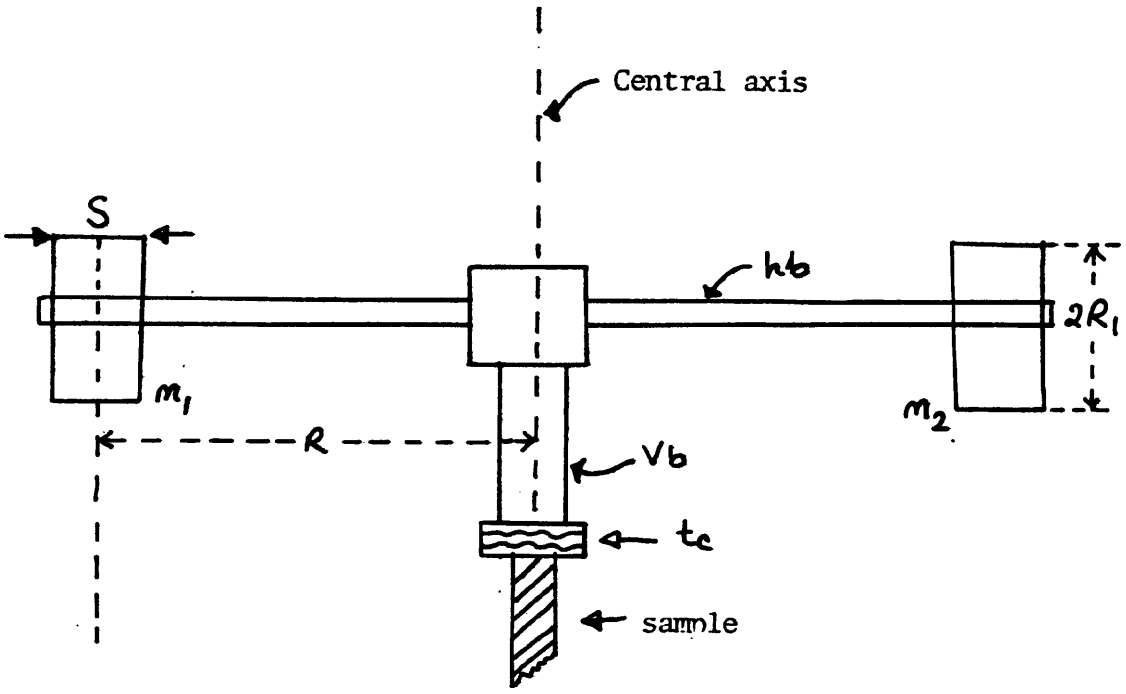

Fig. 6.6 Schematic representation of the oscillating system.

on the bar, hb (i.e. changing the value of R). From equation (6.10a),

$$P^2 = \frac{4\pi^2 I \ell}{\mu b h^3 G'}\left(1 + \frac{\Lambda^2}{4\pi^2}\right) = K I \quad \ldots\ (6.15)$$

where $K = \frac{4\pi^2 \ell}{\mu b h^3 G'}\left(1 + \frac{\Lambda^2}{4\pi^2}\right)$

Thus $P^2 \propto I$

since $$I = I_o + (m_1 + m_2)(R^2 + S^2/12 + R_1^2/4) \quad \ldots\ (6.16)$$

where R is the distance of each weight from the centre of the inertia bar, S is the thickness of the weight, R_1 is the radius of the weight .

Substituting for I in equation (6.15) gives

$$P^2 = I_o K + K(m_1 + m_2)(R^2 + S^2/12 + R_1^2/4) \quad \ldots\ (6.17)$$

A plot of P^2 against $(R^2 + S^2/12 + R_1^2/4)$ is therefore linear with slope = $K(m_1 + m_2)$ and intercept = $I_o K$. Such a plot, obtained using the experimental data in Table 6.3, is shown in figure 6.7 from which a value of I_o was calculated as 1.42×10^{-3} kg m^2. Analysis of the traces was carried out by measuring the amplitudes θ_o and θ_n and the distance between the amplitudes as shown in figure 6.8

Table 6.3 Calibration Data of the Inertia Bar

$10^2 . P^2/s^2$	$10^3 . (R^2 + S^2/12 + R_1^2/4)/m^2$
9.18	3.79
11.07	5.08
13.58	6.60
16.34	8.29
19.40	10.18
22.76	12.29
25.50	14.58
29.99	17.09
33.74	19.79

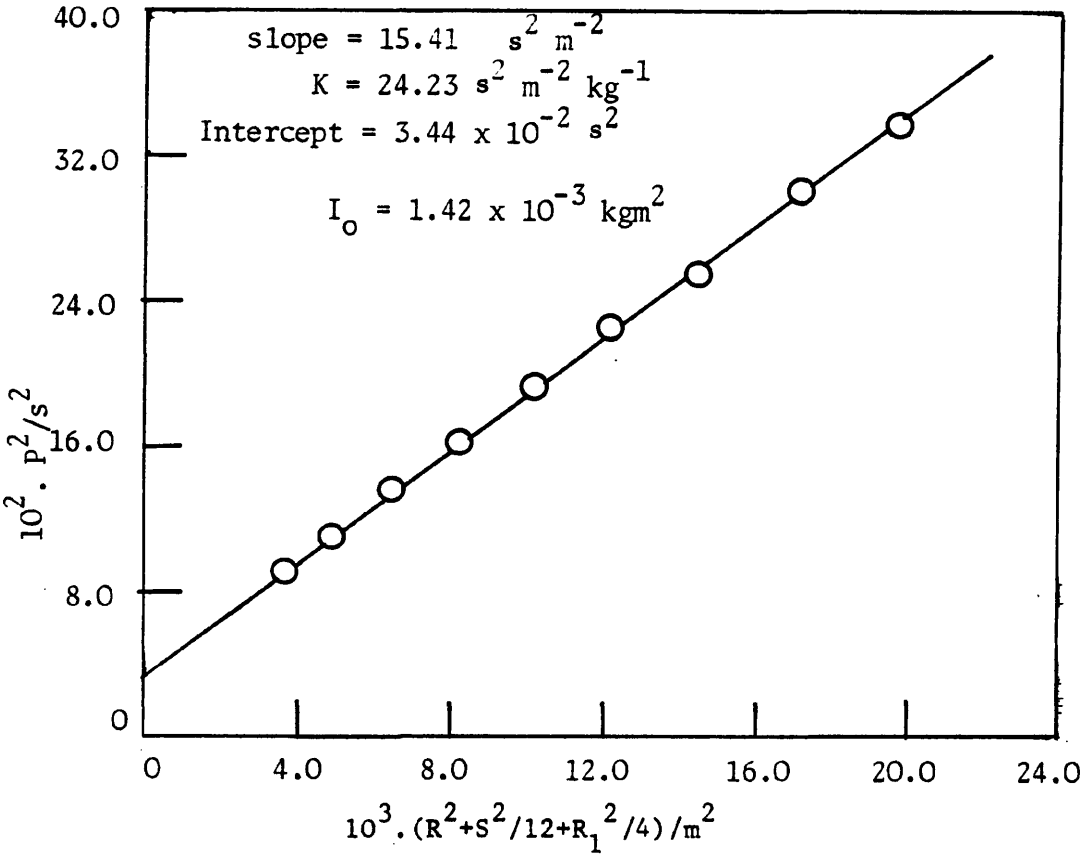

Fig. 6.7 Calibration of the Inertia Bar of Torsion Pendulum

In the present work, for polymer samples, experiments were conducted from -190 to +100°C at intervals of 5° (near glass transition) or 10°C, with a heating rate of about 1° per minute. At each temperature a sufficient number of oscillations (between 10 and 20) were recorded to enable accurate determinations of damping and period, except near the main transition where due to the very high damping of samples, only one or two cycles could be recorded.

The uncertainty in period (P) was found to be within the range of 0.5 to 1.5% but more with highly damped specimens (2 to 5%).

The main source of error in the experiment arises from the measured values of the dimensions of the sample, particularly of the thickness h which occurs in equations (6.10a) and 6.11a) as h^3. Specimen thickness

h and width, b, were measured to within ($\pm$ 0.01 mm) using a micrometer and the specimen length, ℓ, using a cathetometer. The specimens used in torsion pendulum experiments, generally, had regular cross-sectional areas and were void-free after removal of the solvent from completely reacted polyurethane network samples.

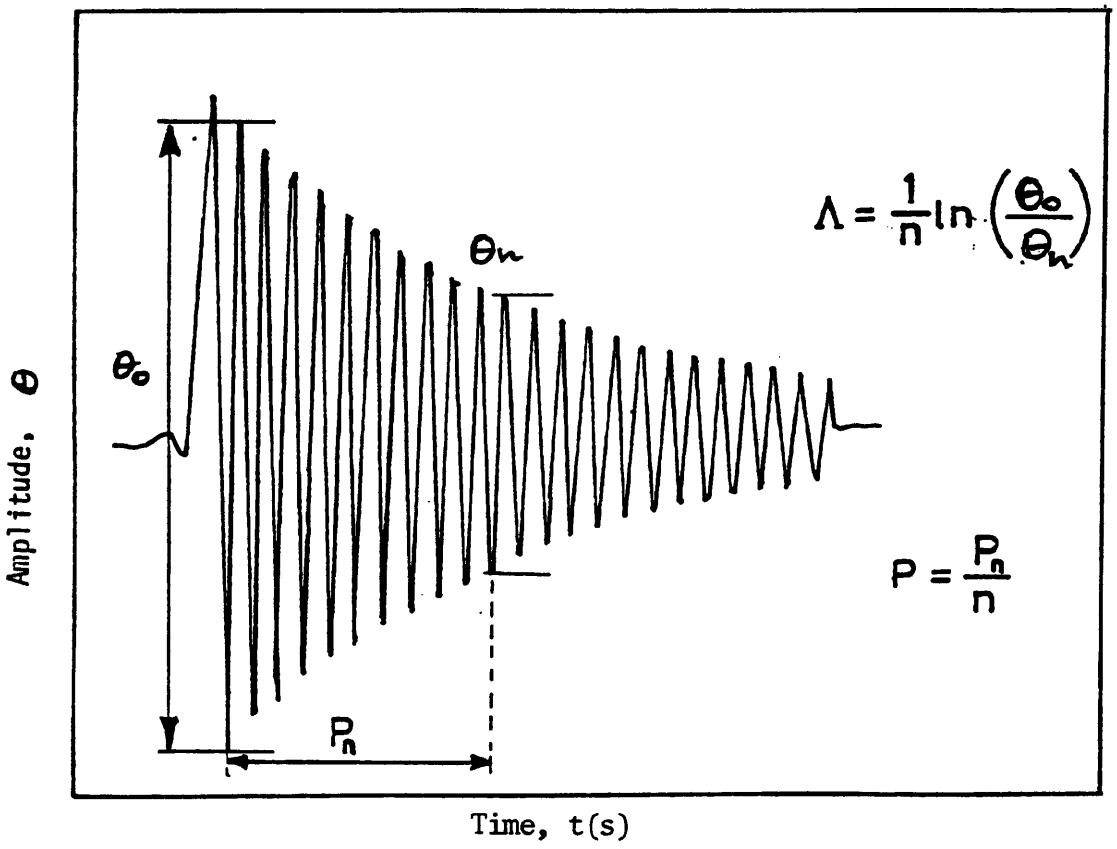

Fig. 6.8 Analysis of Torsion Pendulum Traces. Damped, sinusoidal oscillations (~1 Hz) obtained from a polymer sample using the Torsion Pendulum, and including expressions for logarithmic decrement, Λ, and period, P.

It has been shown that[137] the specimen length between clamps (ℓ_m) differs from the effective specimen length over which shear deformations are actually occurring during torsion. The difference arises for two reasons.

Firstly, there will be a zone at each end of the sample over which the shear deformations sustained by the sample fall to zero. This zone will extend into that part of the sample within the jaws of the clamps, so that the clamp separation underestimates the effective sample length. The second contribution to a length correction arises through warping restraint by the clamps. This restraint increases the effective torsional rigidity of the sample above its true value. A correction $\Delta\ell$ should therefore be applied to ℓ in equation (6.10a) where

$\ell = \ell_m + \Delta\ell$ (ℓ_m = clamp separation)

i.e.

$$P^2 = \frac{4\pi^2 I}{G'_\mu bh^3}\left(1 + \frac{\Lambda^2}{4\pi^2}\right)\left(\ell_m + \Delta\ell\right) \qquad \ldots. \quad (6.18)$$

If measurements of the vibration period are recorded with the variation of clamp separation, then a plot of P^2 against ℓ_m will be linear if all other quantities in equation (6.18) are kept constant. Extrapolation to P = 0 then allows $\Delta\ell$ to be recorded from the intercept on the ℓ_m axis.

The resultant correction ($\Delta\ell$) may be positive or negative depending upon which effect predominates. It has been reported that[137] for polyurethane elastomer samples ($G' = 4.92\ M\ Nm^{-2}$) of length ℓ = 118 mm, width b = 9.7 mm and thickness h = 2.76 mm, that the length correction was -10 mm. Similar experiments for length correction were carried out with polyurethane elastomer samples (bulk, dried) of the present work with sample dimensions ℓ = 35 mm, b = 10 mm and h = 2.8 mm, at 20°C. The correction was observed to be 1 mm from least-squares analysis (see fig. 6.9). The results are shown in Table 6.4 and as a plot of P^2 versus ℓ_m in figure 6.9. More scatter was observed at higher sample lengths (22 to 35 mm) as shown in figure 6.9 from three repeated experiments with three samples of same composition (bulk, dried, uncatalysed) and almost the same dimensions. This scatter may arise from the parasitic oscillations of the samples under deformation or very soft nature of the networks.

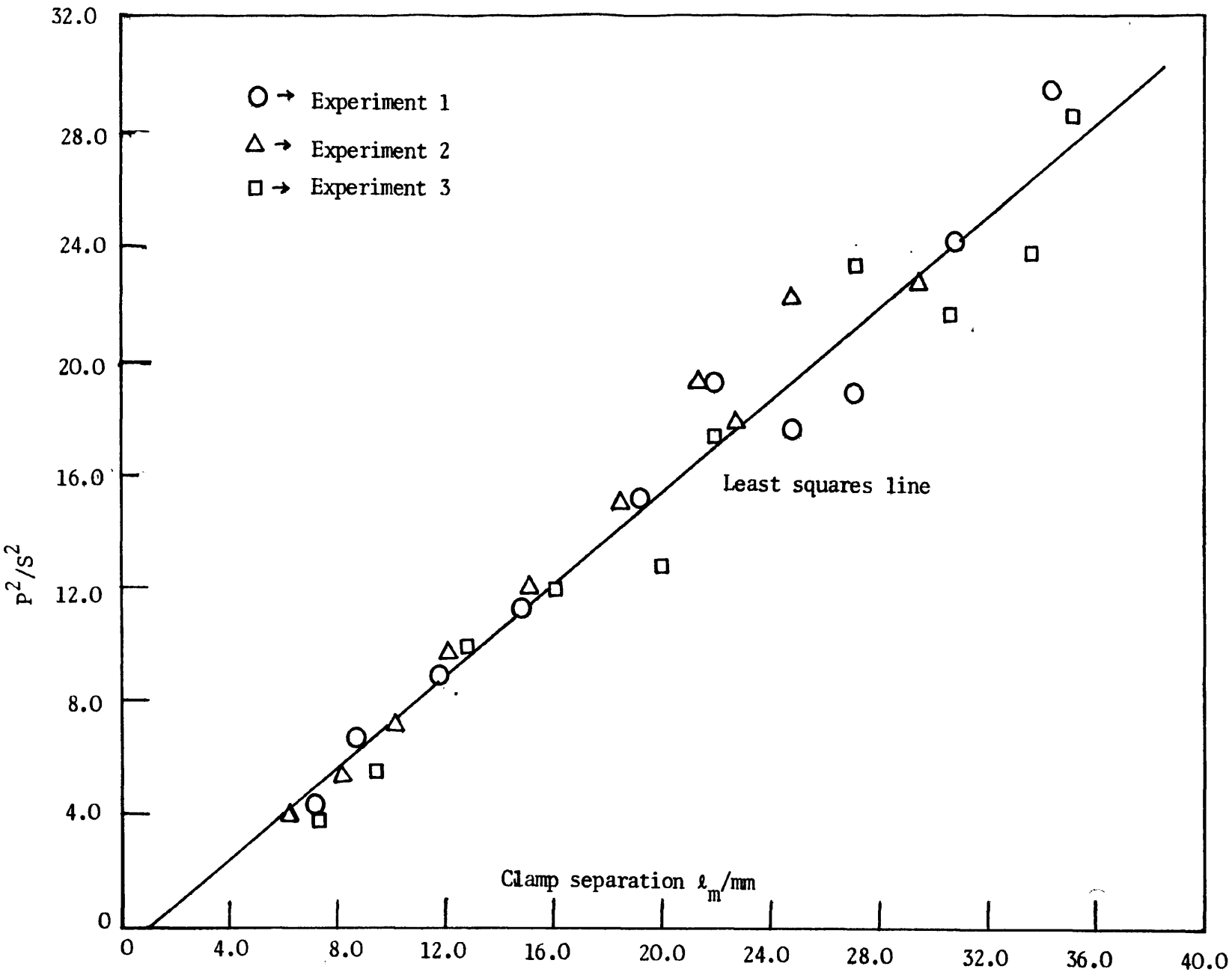

Fig. 6.9 Plots of P^2 against clamp separation for length correction according to equation (6.18) for 3 polyurethane networks (bulk, dried) at 20°C.

Table 6.4 Data for Length Correction in Torsion Pendulum from Repeated Experiments with three different samples but same Composition and almost same Dimensions at 20°C

Experiment 1		Experiment 2		Experiment 3	
P^2/s^2	ℓ_m^*/mm	P^2/s^2	ℓ_m/mm	P^2/s^2	ℓ_m/mm
29.57	34.40	22.67	29.58	28.53	35.17
24.10	30.89	22.16	24.75	23.66	33.70
18.95	27.26	17.81	22.78	21.59	30.71
17.59	24.81	19.35	21.45	23.34	27.22
19.18	21.98	14.99	18.62	17.33	21.96
15.08	19.26	11.97	15.24	12.77	20.03
11.31	14.93	9.69	12.14	11.96	16.24
8.99	11.91	7.24	10.25	9.92	12.94
6.73	8.80	5.37	8.22	5.56	9.49
4.30	7.37	4.02	6.36	3.78	7.40

ℓ_m^* → clamp separation (also called measured length)

From length correction, the calculated error in G' and G'' was about 3-4%. Unfortunately, the design of the torsion pendulum used for the dynamic mechanical properties of the polyurethane networks of the present work was such that only samples in 25-30 mm range could in general be conveniently used. This is in the region of high scatter which produces uncertainties of about 3-4% in P^2.

Scatter in G' versus T, G'' versus T and tan δ versus T plots was also observed (discussed in section 7.2, chapter-7) which was greater than that due to $\Delta\ell$ particularly at temperatures above T_g in experiments carried out for different polyurethane network samples. In these circumstances, it was thought that application of $\Delta\ell$ was not meaningful.

CHAPTER - 7

PHYSICAL PROPERTIES OF NETWORKS: RESULTS AND DISCUSSIONS

The experimental details of the uniaxial compression and torsion pendulum experiments have been discussed in the previous chapter. The results of the uniaxial stress-strain measurements (static experiments) and torsion pendulum measurements (dynamic experiments) conducted on the completely reacted polyurethane networks of the present work are discussed in this chapter. Attempts have been made to investigate structure-property relationships with particular reference to the effects of pre-gel intramolecular reaction on the mechanical properties of the networks. Results of Differential Scanning Calorimetry (D.S.C.) have also been included to complement the transition data from torsion pendulum experiments.

7.1 RESULTS OF THE UNIAXIAL COMPRESSION EXPERIMENTS

7.1.1 Interpretation of stress-strain data in terms of Gaussian Theory:

According to the Gaussian theory of rubber elasticity, the stress-strain behaviour of a polymer network is governed by the relationship between compressive stress (σ) and compression ratio (Λ) given by equation (5-46), section 5.2, chapter 5, namely,

$$\sigma = \frac{A \rho RT \ \phi_2^{1/3} \ (V_{D/V_f})^{2/3}}{M_c} \cdot (\Lambda - \Lambda^{-2}) \qquad .... \quad (5\text{-}46)$$

where all the symbols have already been defined. The constant of proportionality between σ and $(\Lambda - \Lambda^{-2})$ according to Gaussian theory, is equated with the shear modulus, G, of the network, so that

$$G = \frac{A \rho R T \phi_2^{1/3} (V_{D/V_f})^{2/3}}{M_c} \quad \ldots\ldots (5\text{-}48)$$

Values of G can be determined from the slopes of σ versus $(\Lambda - \Lambda^{-2})$ plots for the various networks studied.

Figures 7.1 to 7.4 show typical plots of σ versus $(\Lambda - \Lambda^{-2})$ for completely reacted polyurethane networks prepared from reaction mixtures of experimental series 6 (uncatalysed) and 7 (catalysed) at different solvent (toluene) concentrations (see chapter 4, Tables 4.2(a) 2(b)). For clarity, in each figure, experimental data from only five dilutions are plotted. The error bars on three dilution-plots due to different samples (three samples made from same reaction mixture) are also shown in each figure. All the data from uniaxial stress-strain measurements are presented in Appendix D.

Figures 7.1 and 7.2 show the behaviour of dried networks while figures 7.3 and 7.4 show that of networks swollen to equilibrium in toluene (the reaction solvent) at 27°C. Each plot proceeding from the origin is curved towards the σ-axis. The swollen networks are curved slightly more than the dried networks towards the σ-axis. Thus deviations from Gaussian behaviour are apparent with the present polyurethane networks in figures 7.1 to 7.4. It may be mentioned that the results plotted in figures 7.1 to 7.4 are based on corrected height, h_c (see section 6.1.5, chapter 6). A measure of these deviations from Gaussian behaviour observed is the mean |% error| per data point with respect to the least-squares line through the origin. The |% error|

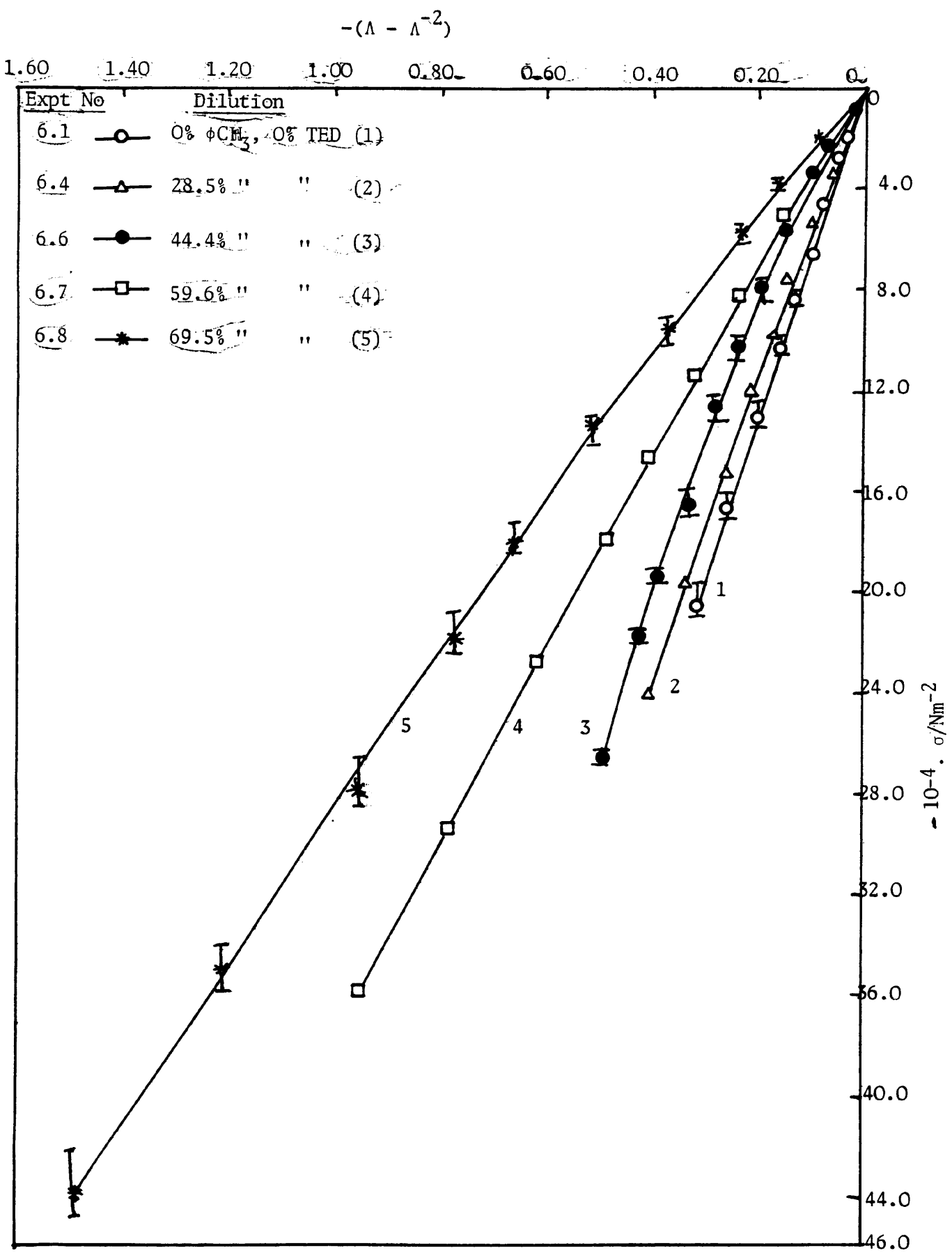

Fig. 7.1 Gaussian stress-strain plots of uncatalysed, dried networks (experimental system -6)

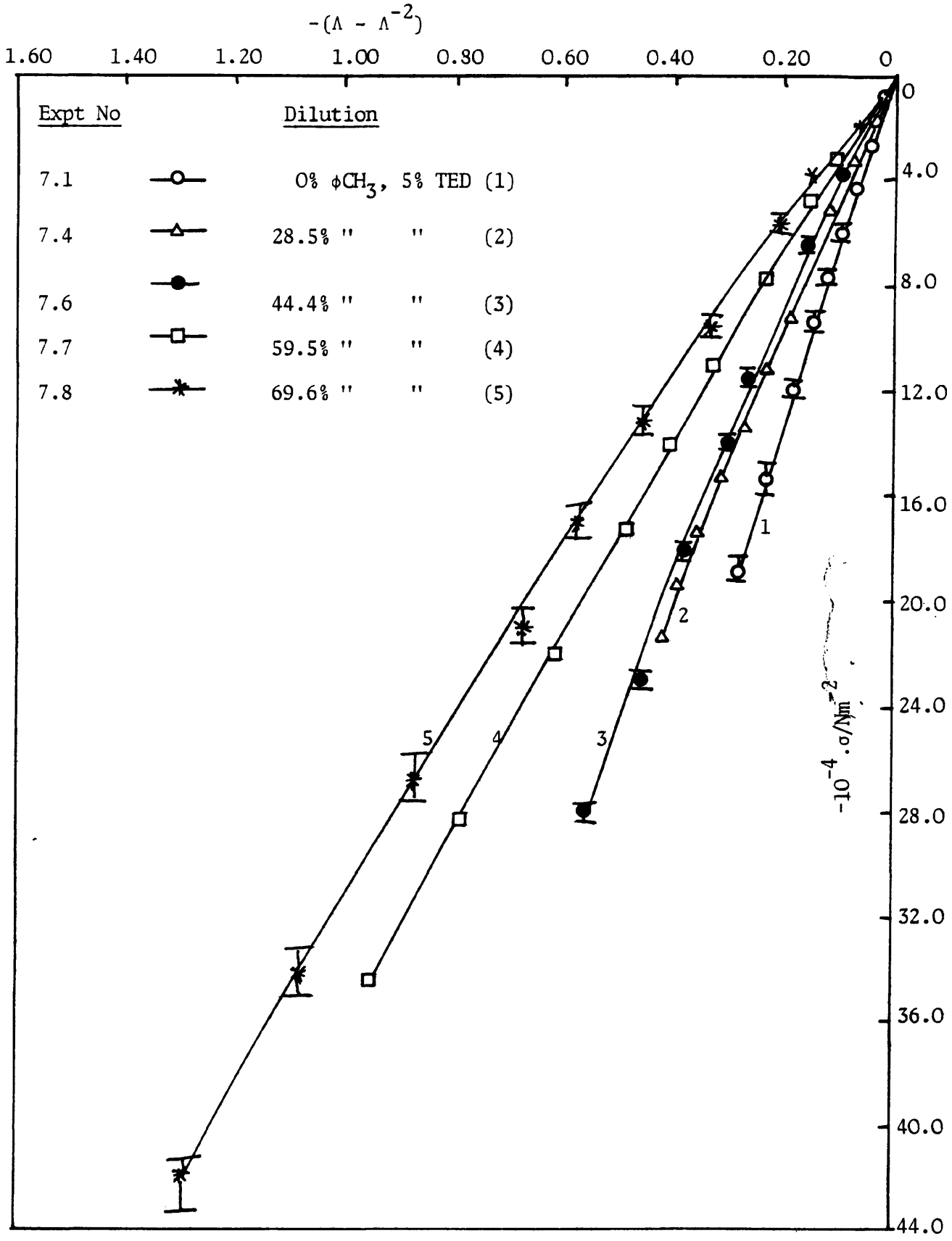

Fig. 7.2 Gaussian stress-strain plots of catalysed, dried networks (Experimental system -7)

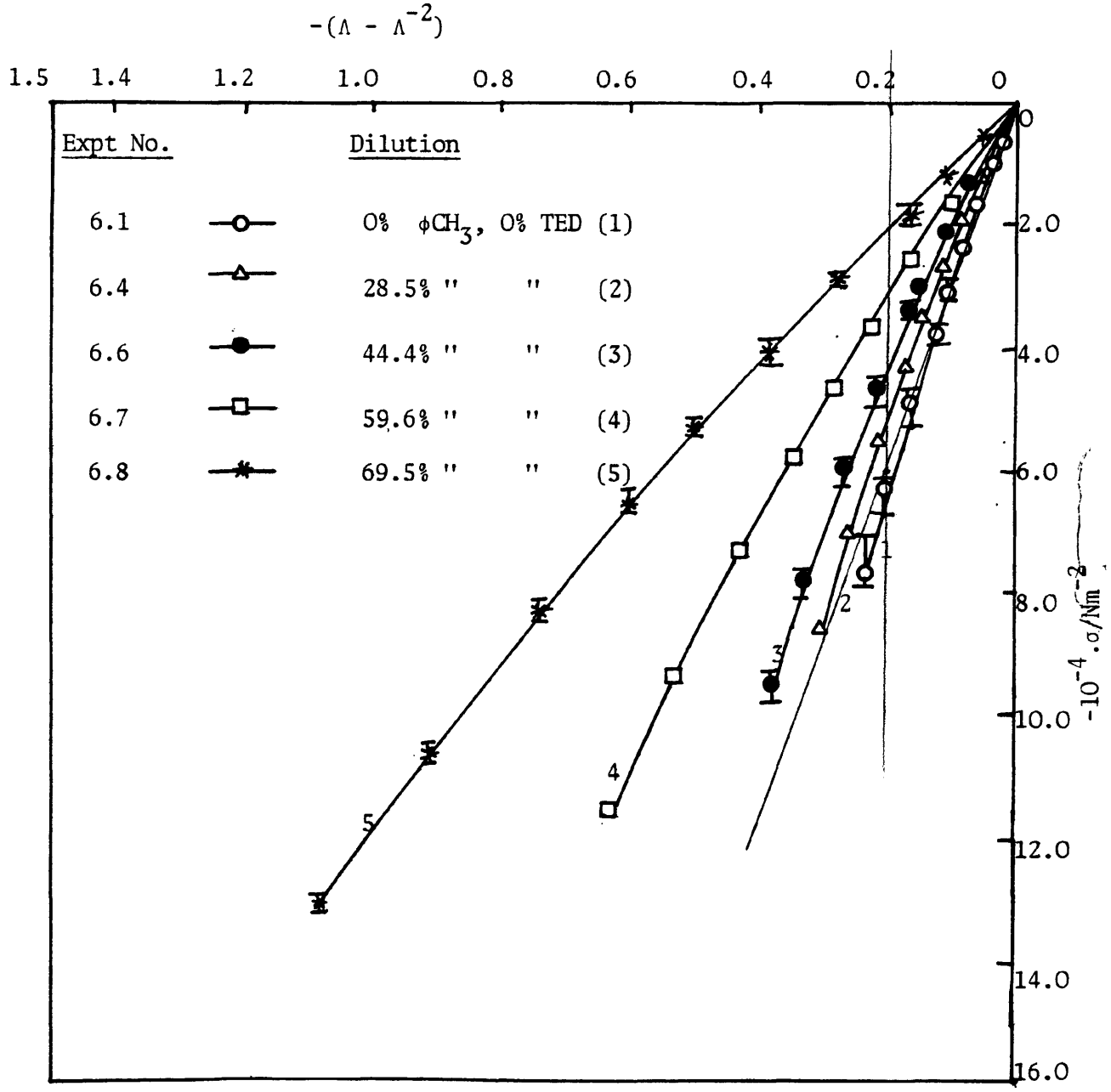

Fig. 7.3 Gaussian stress-strain plots of uncatalysed, swollen networks (Experimental system - 6)

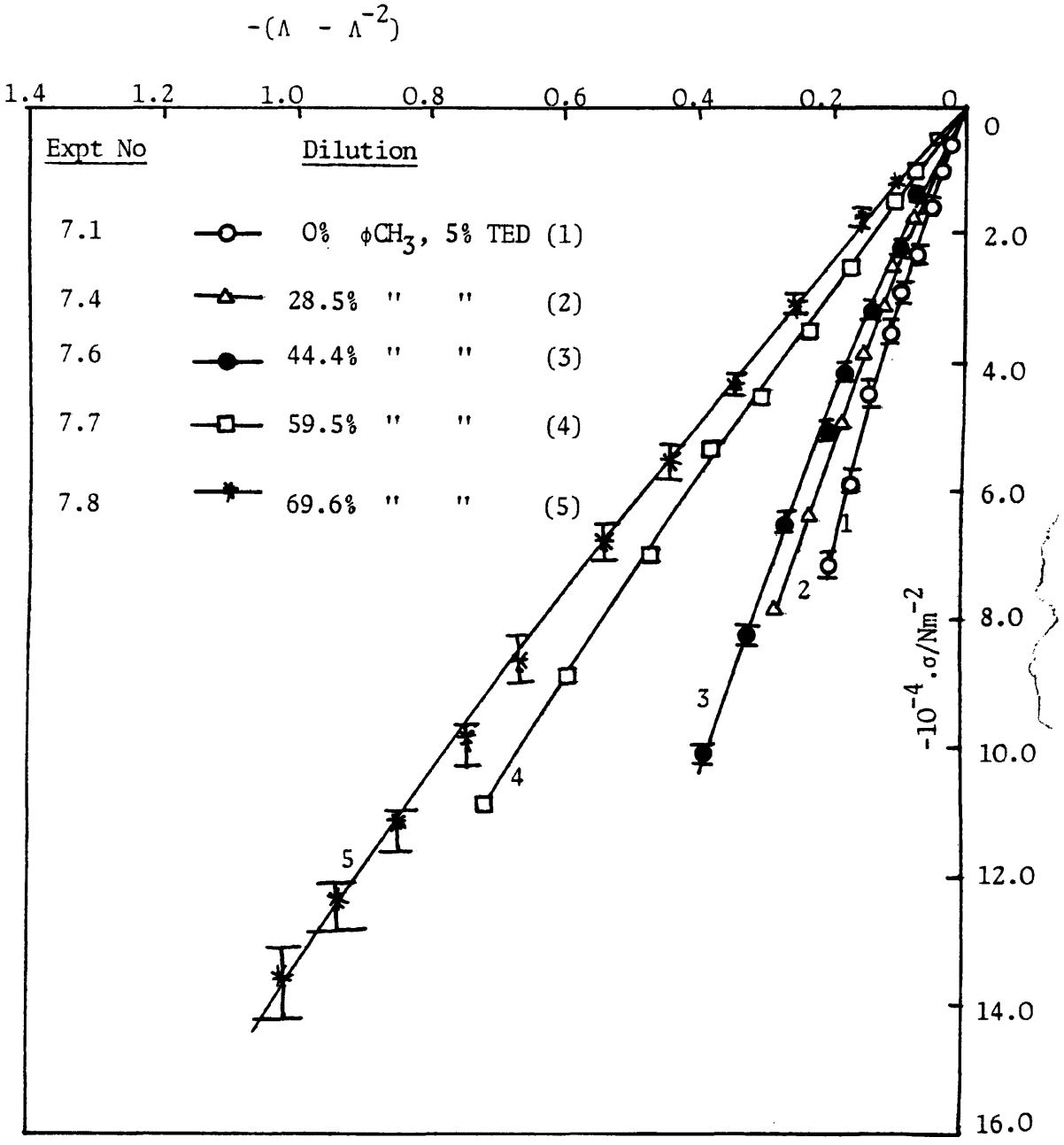

Fig. 7.4 Gaussian stress-strain plots of catalysed, swollen networks (Experimental system - 7)

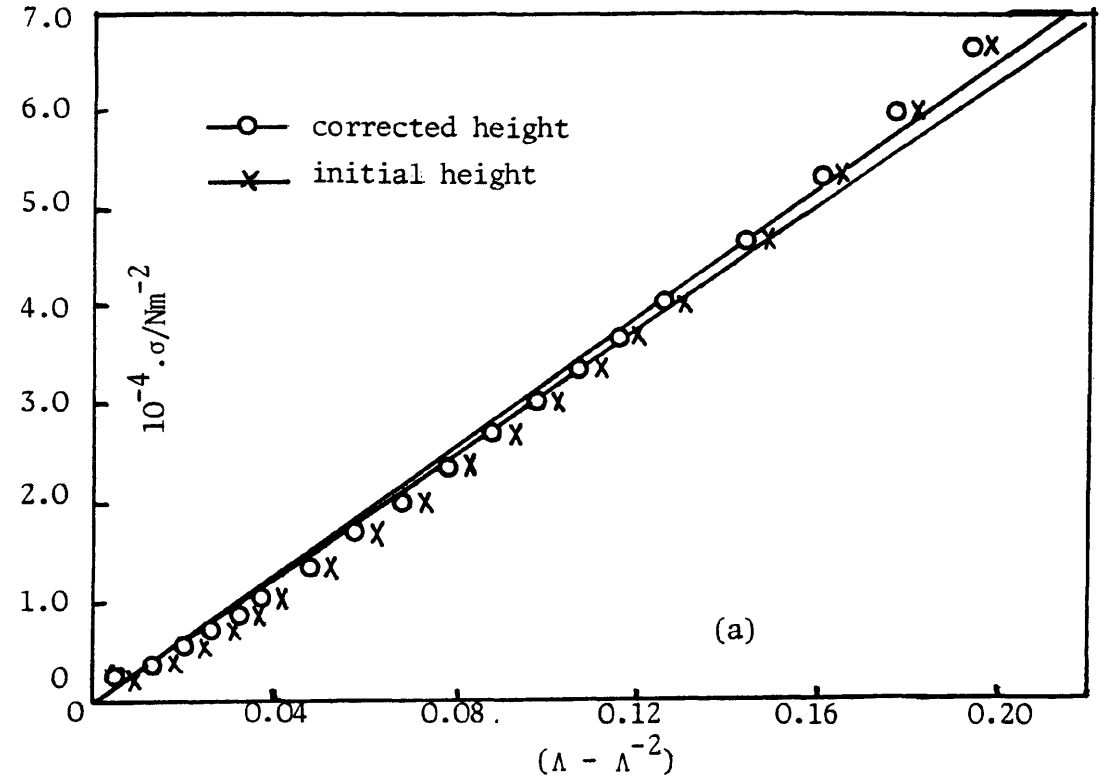

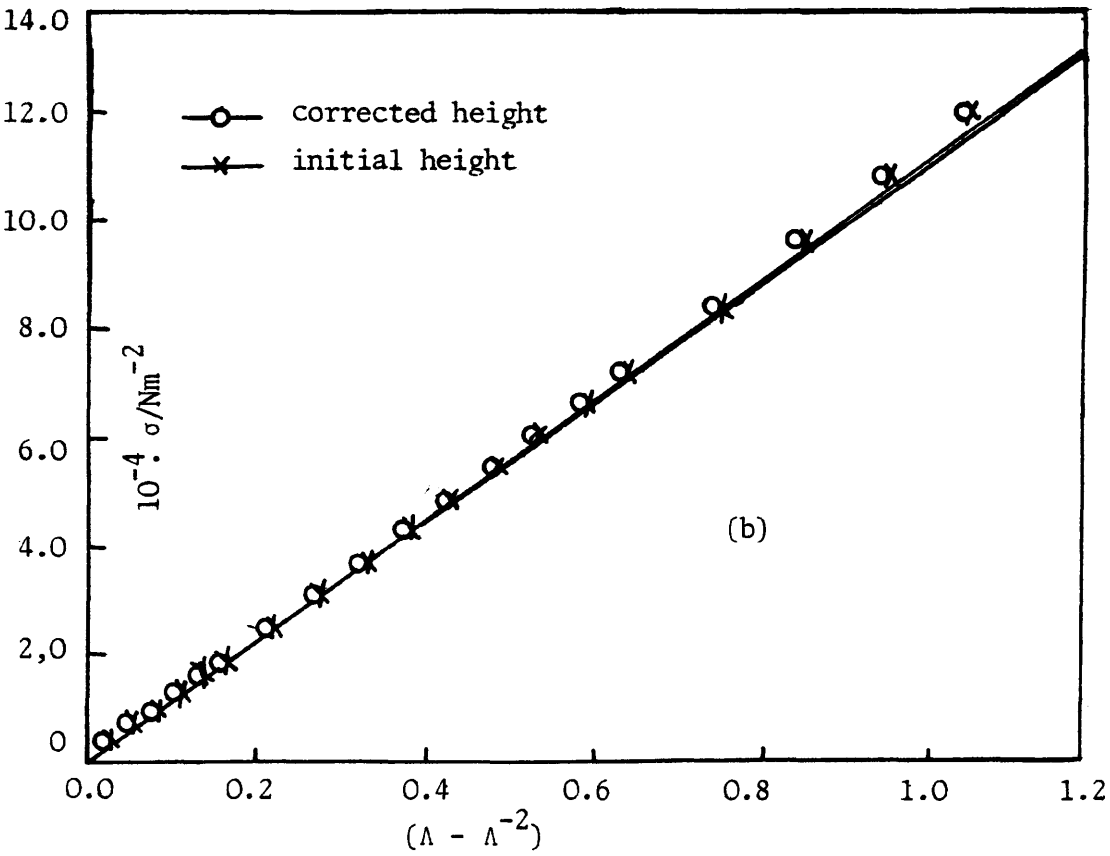

Fig. 7.5 σ versus $(\Lambda - \Lambda^{-2})$ plots for equilibrium swollen networks synthesised from (a) 0% ϕCH_3, 5% DABCO and (b) 69.5% ϕCH_3, 5% DABCO, showing the effect of dilution on deviation from Gaussian behaviour

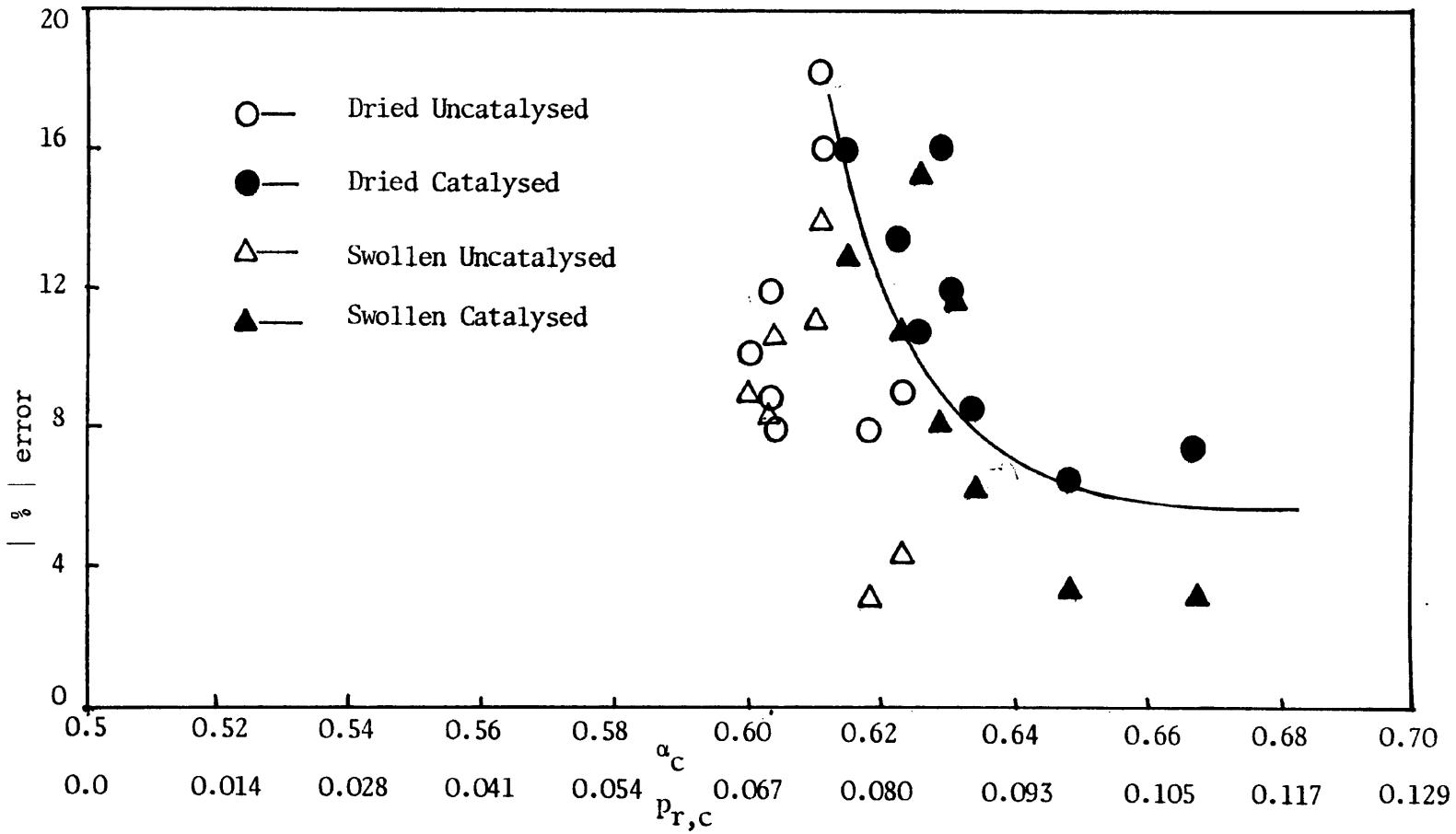

Fig. 7.6 |% error| versus $\alpha_c/p_{r,c}$ plots for polyurethane networks

was generally found to decrease as the dilution of the reaction mixture increased, independent of whether compression was measured in the dry or the swollen state. This trend is illustrated in figures 7.5(a) and 7.5(b), showing the Gaussian stress-strain plots for swollen (catalysed) networks prepared using 0% and 69.6% solvent, respectively, in the reaction mixtures. Marked deviations from Gaussian behaviour are observed with the former system. A similar trend in deviations is also shown in figure 7.6, with |% error| plotted against α_c (and $p^*_{r,c}$). Thus in general |% error| decreases with increase in dilution (ie α_c and $p_{r,c}$) and the networks show more Gaussian behaviour the higher is the dilution of preparation. The present networks are essentially Gaussian above $\alpha_c \simeq 0.66$ corresponding to $M_c \simeq 5000$ g mol^{-1} assuming A = 1 (see Tables 7.1 and 7.2).

A similar trend has also been observed in recent works on trifunctional[74,138] and tetrafunctional[73] polyurethane and trifunctional polyester[109] networks, although it is often stated[84] that Gaussian theory is obeyed in compression. It may be mentioned that in earlier works[139,140] this curvature in Gaussian stress-strain plots had not been appreciated because of the uncertainty of measurement of strain near zero-strain level. Deviations from Gaussian behaviour in compression have also been observed by van der Kraats et al[141], but not commented upon. Fasina and Stepto[109] showed that this curvature is probably a manifestation of the non-Gaussian character of the network chains. The curvature can only be observed with the use of high precision instrument such as the unidirectional compression apparatus used in this study and also other previous studies[73,74,109,138].

$p^*_{r,c}$ (Extent of intramolecular reaction at gelation) = $\alpha_c^{\frac{1}{2}} - ((f-1)^{-1})^{\frac{1}{2}}$

Neglecting the curvature of the plots in figures 7.1 to 7.4, the slope, G, of a given plot was obtained from the linear least-squares lines through the origin of all the data points obtained from the experiment. Thus for each network from a particular reaction mixture, the value of G was calculated. The mean value of G was calculated from compression experiments conducted on three samples and thus the average modulus calculated. The average modulus was used to calculate M_c/A using equation (5-48) and hence M_c/AM_c^o. M_c/AM_c^o values for all the networks studied are presented in Tables 7.1 (dried networks) and 7.2 (swollen networks); M_c^o is the molar mass between the junction points in the perfect network and M_c is the effective molar mass between junction points in the real network. The tables show that M_c/AM_c^o range from 1.6 to 2.0 for dried networks and 1.7 to 2.3 for swollen networks (except experiments 6.2 and 6.3 which do not follow the general trend of variation of M_c/AM_c^o with α_c - see the bracketed points in figs 7.7 and 7.8).

Figures 7.7 and 7.8 show the plots of M_c/AM_c^o versus α_c, the critical branching coefficient (and $p_{r,c}$) for dried and swollen networks, respectively. These plots show that the effect of catalyst on M_c/AM_c^o values is less significant as compared with that on gel-point data. Lines through the experimental points have been tentatively extrapolated to $M_c/AM_c^o = 1$ at the ideal gel point ($\alpha_c = \frac{1}{2}$, $p_{r,c} = 0$) consistent with $A = 1$ (affine behaviour) and $M_c = M_c^o$.

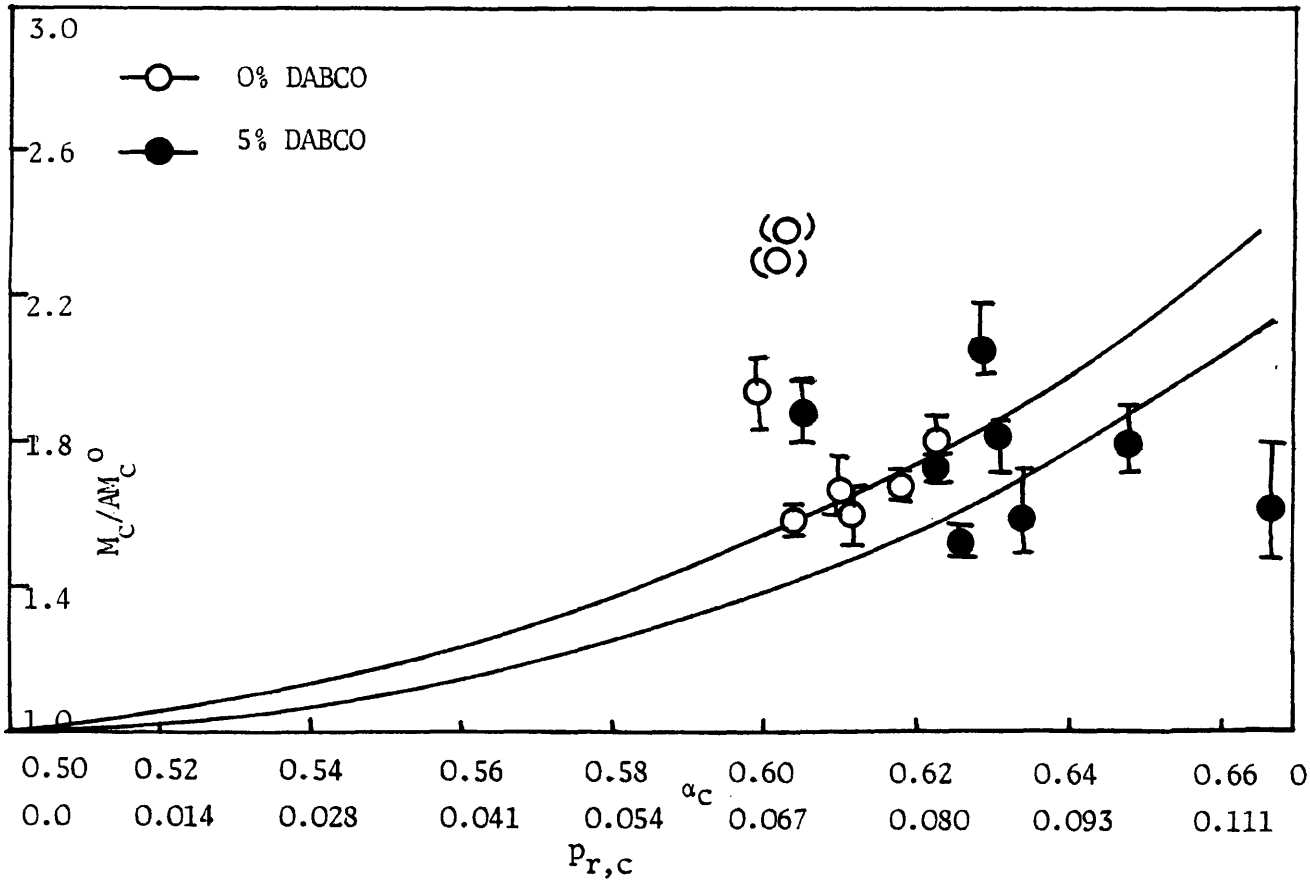

Fig. 7.7 M_c/AM_c^o versus α_c and $p_{r,c}$ for trifunctional dried polyurethane networks.

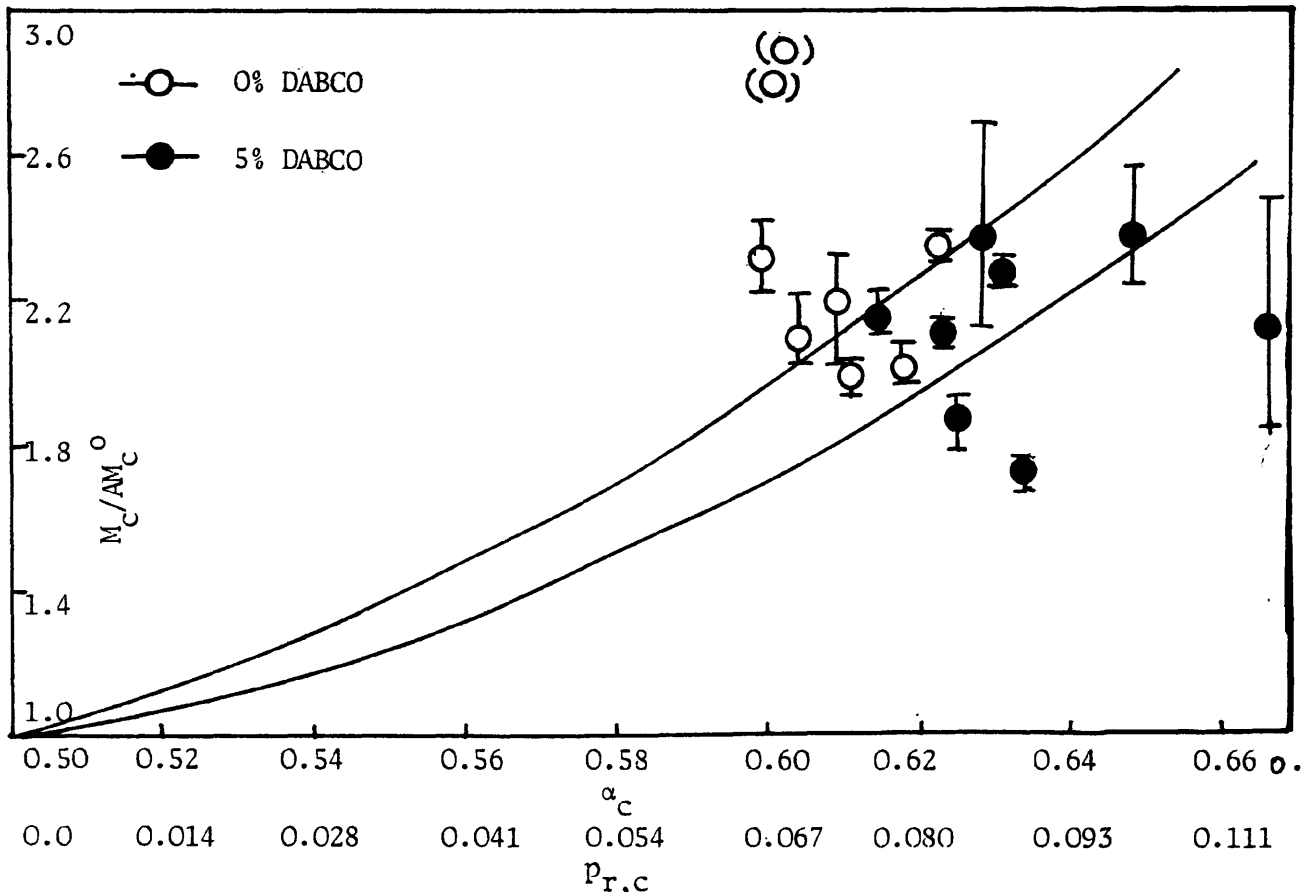

Fig. 7.8 M_c/AM_c^o versus α_c and $p_{r,c}$ for trifunctional swollen polyurethane networks.

TABLE 7.1 Results from uniaxial compression tests on dried samples ($\phi_2 = 1$)

Expt No	% toluene	α_c	$10^{-3}.\ \rho/kgm^{-3}$ ($\pm$ 0.001)	$10^6.V_D/m^3$	$10^6.V_f/m^3$	$10^{-5}.G/Nm^{-2}$	M_c/AM_c^o
6.1	0	0.600	1.031	0.999 $\pm$ .004	0.999 $\pm$ .002	6.14 $\pm$ .30	1.93 $\pm$ .10
6.2	9.1	0.603	1.031	0.994 $\pm$ .002	1.145 $\pm$ .020	4.71 $\pm$ .07	(2.30 $\pm$ .04)
6.3	20.0	0.603	1.034	0.867 $\pm$ .020	1.057 $\pm$ .012	4.39 $\pm$ .07	(2.38 $\pm$ .04)
6.4	28.6	0.604	1.032	0.766 $\pm$ .005	1.105 $\pm$ .005	5.90 $\pm$ .11	1.58 $\pm$ .04
6.5	37.5	0.610	1.034	0.617 $\pm$ .002	1.057 $\pm$ .025	5.00 $\pm$ .25	1.66 $\pm$ .06
6.6	44.4	0.611	1.033	0.579 $\pm$ .001	1.041 $\pm$ .020	5.04 $\pm$ .25	1.60 $\pm$ .08
6.7	59.6	0.618	1.031	0.403 $\pm$ .003	1.063 $\pm$ .030	3.70 $\pm$ .02	1.68 $\pm$ .01
6.8	69.5	0.623	1.037	0.300 $\pm$ .012	1.049 $\pm$ .040	2.88 $\pm$ .09	1.80 $\pm$ .06
7.1	0	0.615	1.032	1.102 $\pm$ .001	1.132 $\pm$ .016	6.33 $\pm$ .28	1.88 $\pm$ .08
7.2	9.1	0.623	1.034	0.984 $\pm$ .004	1.140 $\pm$ .020	6.24 $\pm$ .03	1.73 $\pm$ .01
7.3	20.0	0.626	1.031	0.853 $\pm$ .003	1.126 $\pm$ .006	6.51 $\pm$ .11	1.52 $\pm$ .03
7.4	28.6	0.629	1.034	0.847 $\pm$ .010	1.114 $\pm$ .002	4.82 $\pm$ .20	2.06 $\pm$ .07
7.5	37.5	0.631	1.037	0.610 $\pm$ .003	1.026 $\pm$ .013	4.67 $\pm$ .06	1.81 $\pm$ .06
7.6	44.4	0.634	1.031	0.564 $\pm$ .020	1.013 $\pm$ .010	5.04 $\pm$ .17	1.59 $\pm$ .12
7.7	59.5	0.648	1.032	0.412 $\pm$ .015	1.076 $\pm$ .030	3.49 $\pm$ .17	1.80 $\pm$ .10
7.8	69.6	0.667	1.032	0.301 $\pm$ .010	1.032 $\pm$ .035	3.23 $\pm$ .32	1.62 $\pm$ .15

TABLE 7.2 Results from unixial compression tests on swollen samples

Expt No	% toluene	α_c	$10^{-3}.\rho/kgm^{-3}$ ($\pm$ .001)	($\phi_2 \pm 0.002$)	$10^{6}.V_D/m^3$	$10^{6}.V_f/m^3$	$10^{-5}.G/Nm^{-2}$	M_c/AM_c^o
6.1	0	0.600	1.031	0.203	0.999 $\pm$ .004	0.999 $\pm$ .002	3.00 $\pm$ .13	2.33 $\pm$ .10
6.2	9.1	0.603	1.031	0.187	0.994 $\pm$ .002	1.145 $\pm$ .020	2.20 $\pm$ .10	(2.82 $\pm$ .15)
6.3	20.0	0.603	1.034	0.181	0.867 $\pm$ .030	1.057 $\pm$ .012	2.04 $\pm$ .15	(2.89 $\pm$ .20)
6.4	28.6	0.604	1.032	0.197	0.766 $\pm$ .005	1.105 $\pm$ .005	2.59 $\pm$ .12	2.09 $\pm$ .12
6.5	37.5	0.610	1.034	0.190	0.617 $\pm$ .002	1.057 $\pm$ .025	2.18 $\pm$ .15	2.19 $\pm$ .14
6.6	44.4	0.611	1.033	0.193	0.579 $\pm$ .001	1.041 $\pm$ .020	2.37 $\pm$ .03	1.96 $\pm$ .03
6.7	59.6	0.618	1.031	0.169	0.403 $\pm$ .003	1.063 $\pm$ .030	1.70 $\pm$ .04	2.03 $\pm$ .05
6.8	69.5	0.623	1.037	0.144	0.300 $\pm$ .012	1.049 $\pm$ .040	1.15 $\pm$ .01	2.36 $\pm$ .02
7.1	0	0.615	1.032	0.218	1.102 $\pm$ .001	1.132 $\pm$ .016	3.32 $\pm$ .08	2.15 $\pm$ .06
7.2	9.1	0.623	1.034	0.207	0.984 $\pm$ .004	1.140 $\pm$ .020	3.04 $\pm$ .04	2.10 $\pm$ .03
7.3	20.0	0.626	1.031	0.208	0.853 $\pm$ .003	1.126 $\pm$ .006	3.13 $\pm$ .12	1.86 $\pm$ .06
7.4	28.6	0.629	1.034	0.188	0.847 $\pm$ .010	1.114 $\pm$ .002	2.39 $\pm$ .28	2.38 $\pm$ .26
7.5	37.5	0.631	1.037	0.185	0.610 $\pm$ .003	1.026 $\pm$ .013	2.10 $\pm$ .03	2.29 $\pm$ .04
7.6	44.4	0.634	1.031	0.178	0.564 + .020	1.013 $\pm$ .010	2.63 $\pm$ .06	1.72 $\pm$ .04
7.7	59.5	0.648	1.032	0.158	0.412 $\pm$ .015	1.076 $\pm$ .030	1.42 $\pm$ .09	2.38 $\pm$ .16
7.8	69.6	0.667	1.032	0.154	0.301 $\pm$ .010	1.032 $\pm$ .035	1.32 $\pm$ .19	2.13 $\pm$ .30

Figure 7.9 represents the plot of M_c/AM_c^o, the average value obtained from dried and swollen networks, versus α_c (and $p_{r,c}$) for the polyurethane networks of the present work. The plot shows that the average values apparently have very large error bars possibly due to the effect of sol fraction not being removed or the assumption of V_f = reference state for both dry and swollen networks. A comparison of M_c/AM_c^o versus $p_{r,c}$ plots of the present trifunctional polyurethane networks with previously studied trifunctional[74] and tetrafunctional[73] polyurethane networks (see figure 7.10) show that the error bars on M_c/AM_c^o values of the present networks are comparable to (and sometimes smaller than) those of the previously studied networks[73].

The behaviour exemplified in figures 7.7 and 7.8 is typical of that shown by the other polyurethane systems[73,74] as shown in figure 7.10. However, the increase in M_c with α_c (or $p_{r,c}$) is not so significant as compared with other systems. M_c/AM_c^o is always greater than unity. In general, the results (figures 7.7, 7.8 and 7.10) indicate that in the limit of the ideal gel-point (Flory-Stockmayer gel-point ie, $\alpha_c = 1/_{(f-1)} = \frac{1}{2}$) a perfect, affine, rather than phantom network is formed. All the values of M_c/AM_c^o are greater than unity, and tend to 1 as $p_{r,c} \rightarrow 0$, and have a tendency to increase with $p_{r,c}$, indicating that pre-gel loops are an important factor in determining network defects and that entanglements are of apparently negligible importance. It is assumed that these pre-gel loops are elastically inactive in the networks at complete reaction.

The relative positions of the lines in figure 7.10 for the various systems can be related to M_c^o (or ν), f (functionality) and the chain structures of the reactants[24,60,73,109,128]. The slopes of the lines show that the effect of pre-gel intramolecular reaction or loops in reducing

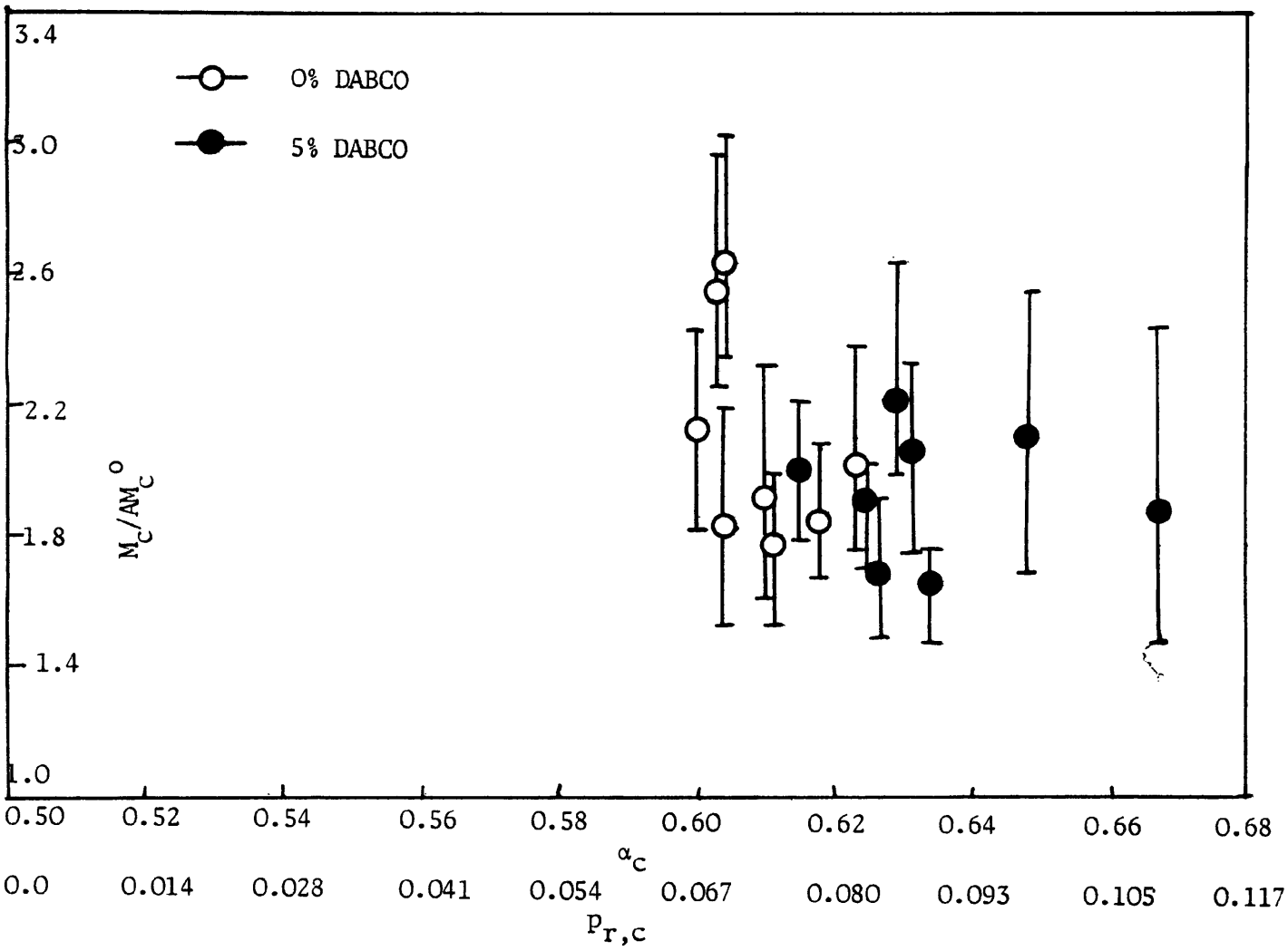

Fig. 7.9 M_c/AM_c^o (obtained averaging the M_c/AM_c^o values of both dried and swollen networks) versus $\alpha_c/p_{r,c}$ plots.

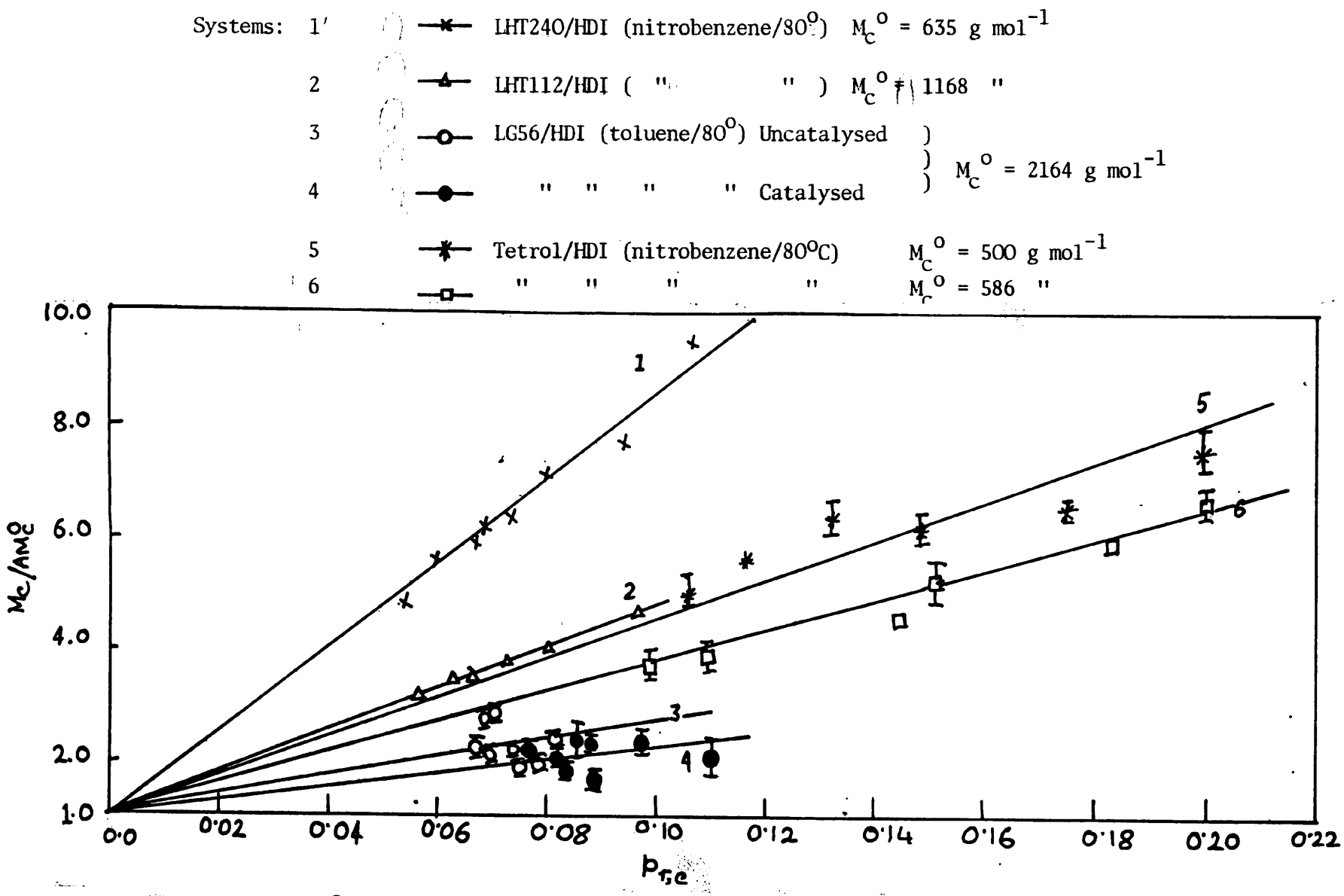

Fig. 7.10 M_c/AM_c^o versus $p_{r,c}$ for tri- and tetra-functional polyurethane network systems.

the modulus is generally larger for trifunctional (systems 1 and 2) compared with tetrafunctional networks (systems 5 and 6) for a given value of $p_{r,c}$. However, comparison of the slopes of the lines of trifunctional networks of high M_c^o ($\simeq$ 2164 g mol^{-1}) of the present work (systems 3 and 4) with those of tetrafunctional networks of low M_c^o (system 5 with M_c^o = 500 and system 6 with M_c^o = 580 g mol^{-1}) shows that this effect of pre-gel intramolecular reaction in reducing the modulus becomes less for these trifunctional compared with tetrafunctional networks; that is, the effect of pre-gel intramolecular reaction or loops may be less at a given $p_{r,c}$. In addition, for a given functionality, the reduction in modulus is larger for smaller values of M_c^o (compare systems 1 to 4 for trifunctional networks and systems 5 and 6 for tetrafunctional networks); that is, for a given amount of pre-gel intramolecular reaction (or for a given value of $p_{r,c}$) systems with smaller loops have larger proportions of those loops elastically ineffective.

Thus, the results of the present work and previous works (fig.7.10) shows that the higher the M_c^o (or ν) of the network, the lower is the effect of pre-gel intramolecular reaction on modulus and probably less are the network defects.

7.1.2 Analysis of Stress-Strain Data in Terms of Mooney-Rivlin Equation

Stress-strain data can be analysed in terms of the Mooney-Rivlin equation (chapter 5, section 5.2).

$$\sigma = (2C_1 + 2C_2 \Lambda^{-1})(\Lambda - \Lambda^{-2}) \quad .... \quad (5\text{-}49)$$

where $2C_1$ and $2C_2$ are constants independent of Λ. According to this

equation the value of modulus is $2C_1$ in the limit at large deformation ($\Lambda^{-1} \to 0$; $\Lambda \to \infty$) and $(2C_1 + 2C_2)$ in the limit at small deformation ($\Lambda^{-1} \to 1$; $\Lambda \to 1$). The plot of $\sigma/(\Lambda - \Lambda^{-2})$ versus Λ^{-1} should give an intercept of $(2C_1 + 2C_2)$ at $\Lambda^{-1} = 1$ (ie at small deformation) and $2C_1$ at $\Lambda^{-1} = 0$ (ie at large deformation) on $\sigma/(\Lambda - \Lambda^{-2})$ axis, respectively.

Some typical Mooney-Rivlin stress-strain plots are shown in figures 7.11 to 7.14 showing the intercepts at $\Lambda^{-1} = 1$ on $\sigma/(\Lambda - \Lambda^{-2})$ axis. Least-squares analysis was used to locate the best lines through the experimental points and to calculate the intercepts at $\Lambda^{-1} = 1$ and $\Lambda^{-1} = 0$ and also the slopes of the Mooney-Rivlin plots. The values of the intercepts at small and large deformations (3rd and 4th column respectively) and slopes (5th column) are presented in Table 7.3.

Figures 7.11 to 7.14 show that the Mooney-Rivlin plots for networks synthesized from higher reactant concentrations are not linear and hence the networks do not follow Mooney-Rivlin equation. These curved plots give negative intercepts at $\Lambda^{-1} = 0$ on $\sigma/(\Lambda - \Lambda^{-2})$ axis. However, networks formed in presence of higher solvent concentrations (eg $\simeq$ 60% and 70% solvent in the present network, 65% solvent in polyester network[72,109] and 69% solvent in tetrafunctional network[142]) give linear Mooney-Rivlin plots (see figs 7.11 to 7.14) and so apparently following Mooney-Rivlin equation. These linear plots give positive intercepts at $\Lambda^{-1} = 0$ on $\sigma/(\Lambda - \Lambda^{-2})$ axis. Figure 7.15 is a representative Mooney-Rivlin plot showing positive and negative intercept at $\Lambda^{-1} = 0$ for the present networks.

Assuming affine to phantom transition of the networks (discussed in section 5.2.3, chapter 5), the slope and intercept of the Mooney-Rivlin plots may be related as:

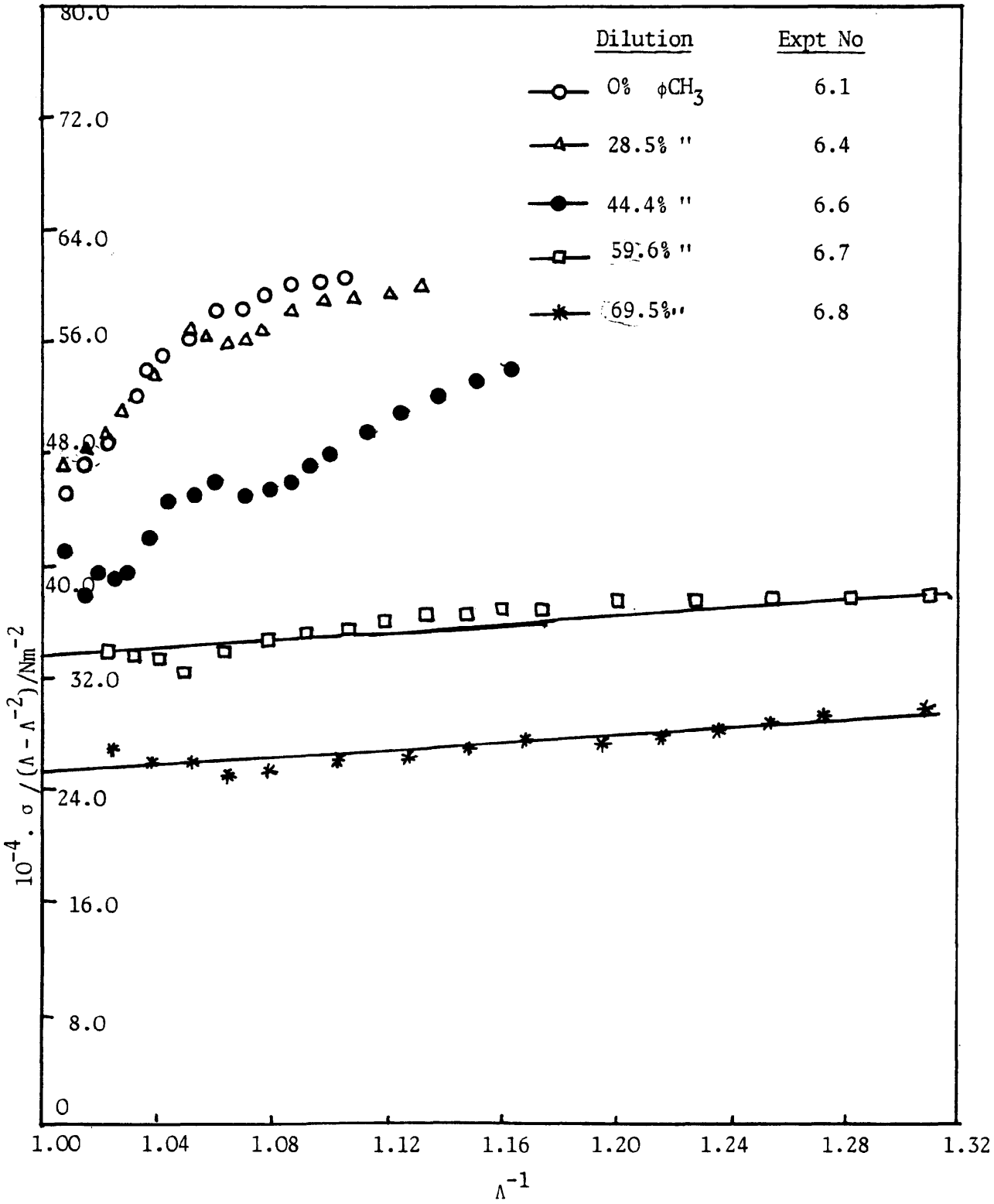

Fig. 7.11 Mooney-Rivlin plot for dried, uncatalysed polyurethane networks

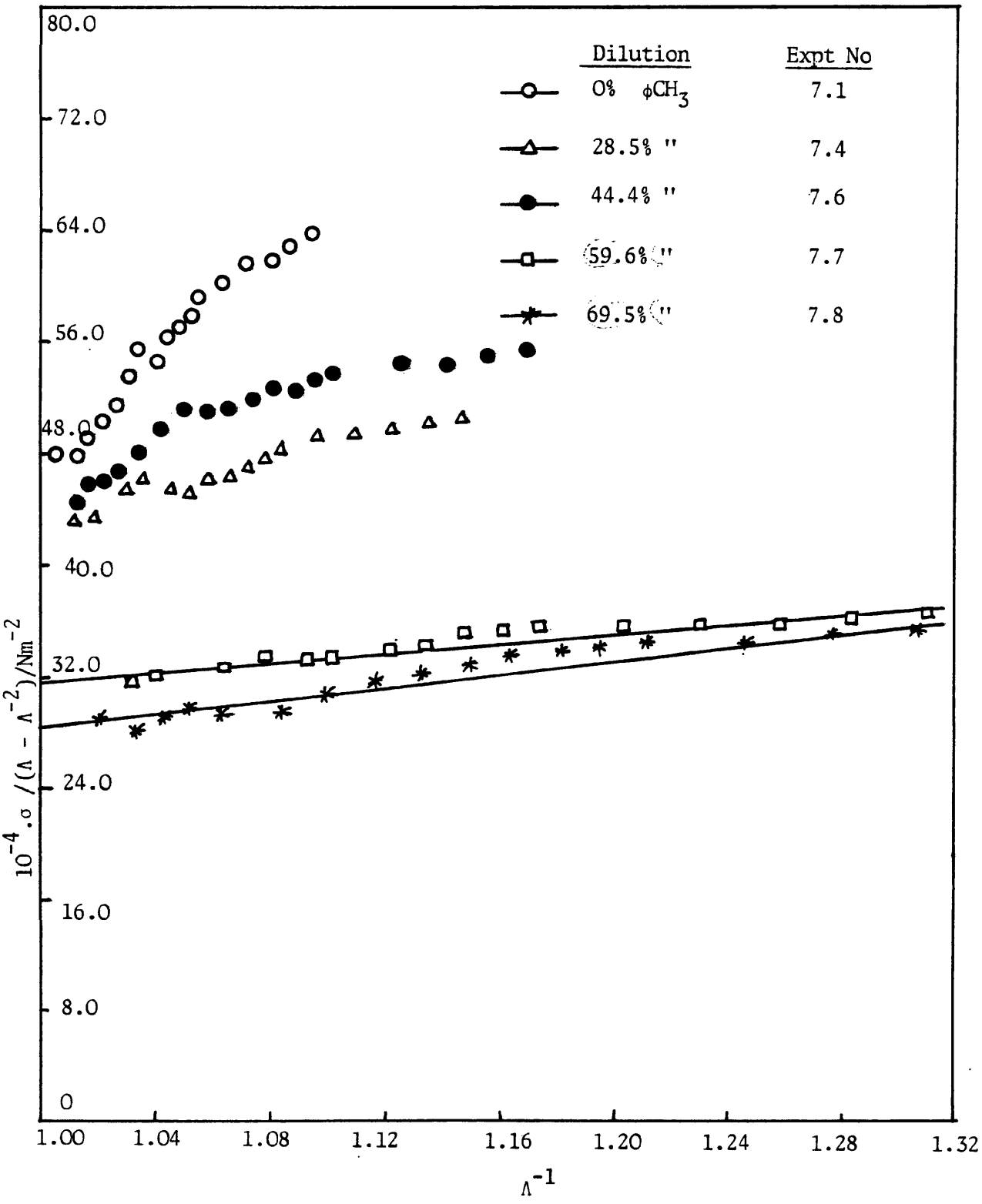

Fig. 7.12 Mooney-Rivlin plot for dried catalysed polyurethane networks.

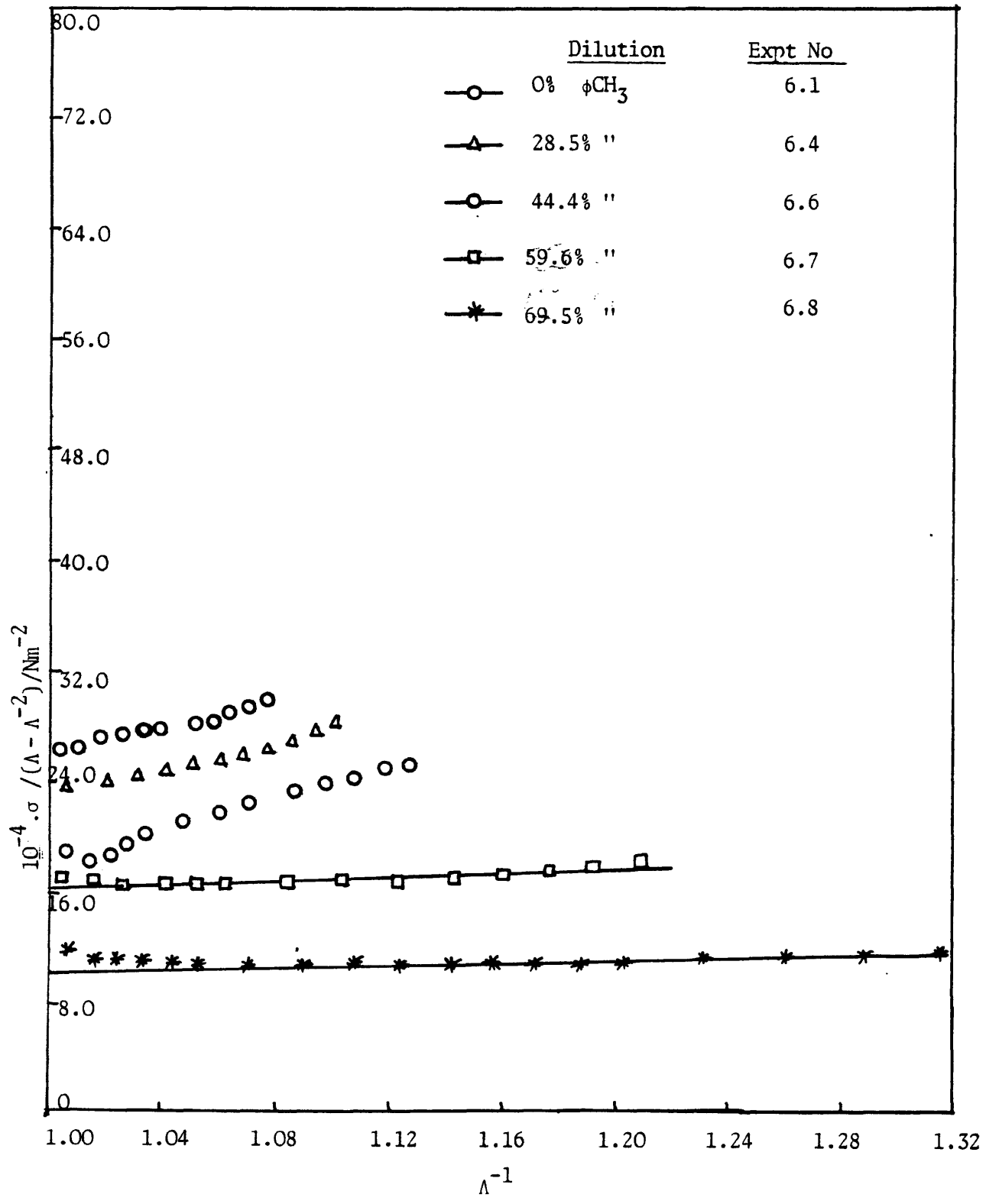

Fig. 7.13 Mooney-Rivlin plot for swollen, uncatalysed polyurethane networks.

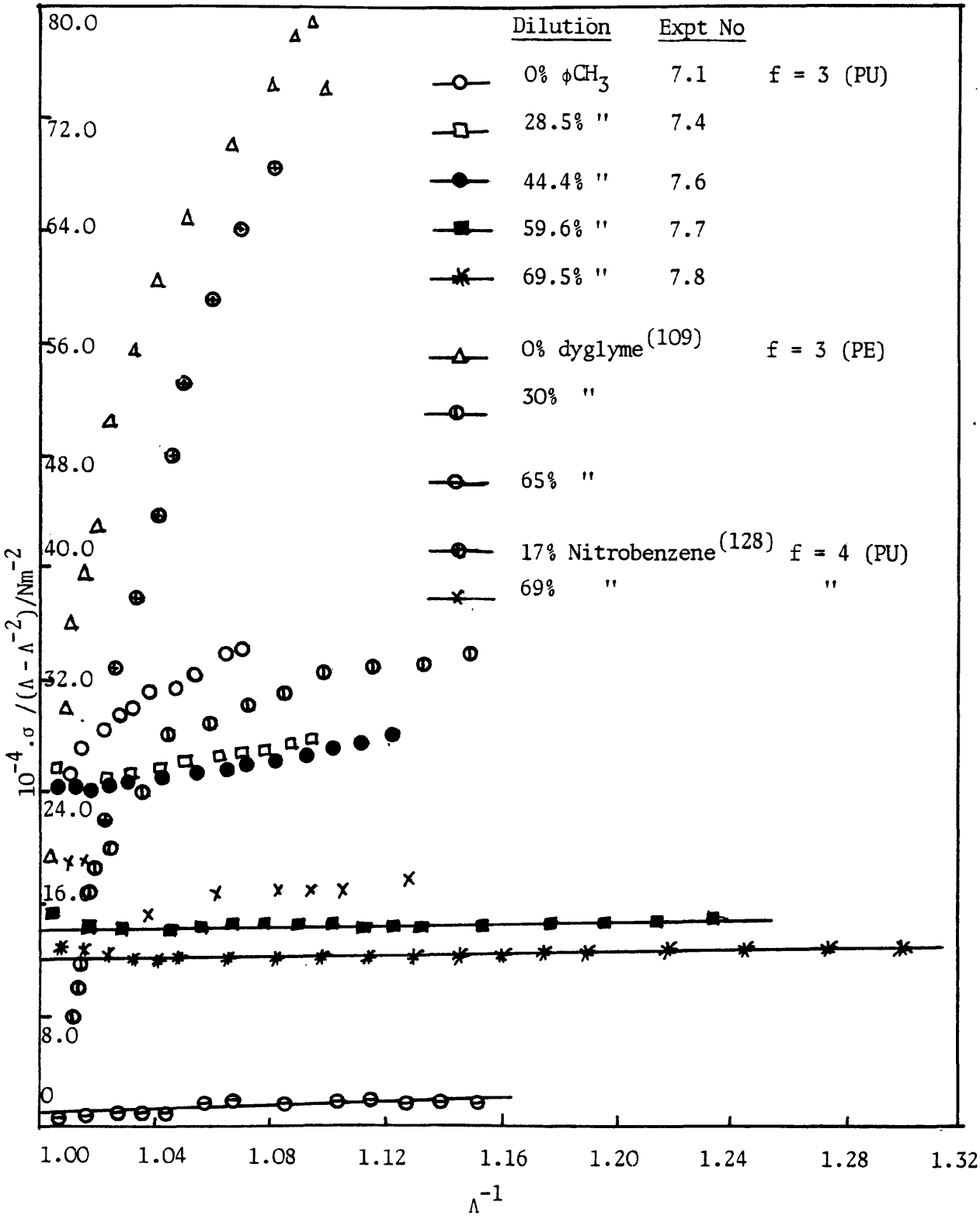

Fig. 7.14 Mooney-Rivlin plot for swollen, catalysed polyurethane(128) (PU) and polyester(109) (PE) networks.

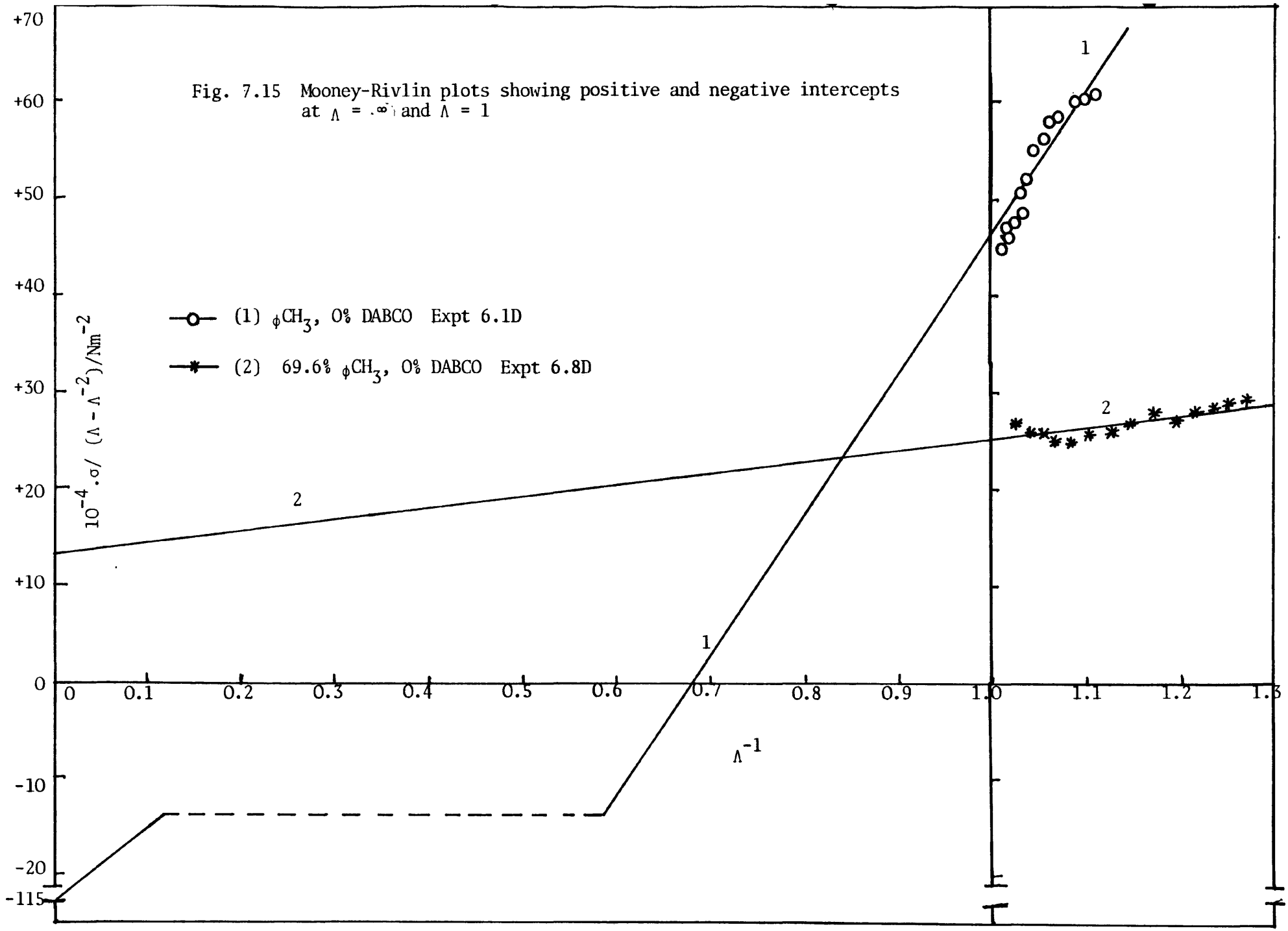

Fig. 7.15 Mooney-Rivlin plots showing positive and negative intercepts at $\Lambda = \infty$ and $\Lambda = 1$

TABLE 7.3 Mooney-Rivlin constants and structural characteristics of polyurethane networks

Expt No	% toluene	$10^{-5}.(2C_1+2C_2)$ /Nm^{-2}	$10^{-5}.2C_1/Nm^{-2}$	$10^{-5}.2C_2/Nm^{-2}$	$\frac{\text{Slope}}{\text{Intercept}}$
6.1D	0	4.75	- 11.49	16.21	3.41
6.4D	28.5	4.79	- 6.17	10.96	2.29
6.6D	44.4	3.82	- 7.64	11.47	3.00
6.7D	59.6	3.32	1.50	1.82	0.55
6.8D	69.5	2.55	1.44	1.11	0.43
7.1D	0	4.86	- 14.57	19.43	4.00
7.4D	28.5	4.28	- 1.52	5.80	1.35
7.6D	44.4	4.25	1.99	8.04	1.89
7.7D	59.5	3.19	1.48	1.71	0.54
7.8D	69.6	2.96	1.32	1.64	0.55
6.1S	0	2.63	- 2.24	4.88	1.85
6.4S	28.5	2.29	- 2.46	4.75	2.07
6.6S	44.4	1.86	- 3.79	5.65	3.04
6.7S	59.6	1.62	0.95	0.67	0.41
6.8S	69.5	1.04	0.61	0.43	0.41
7.1S	0	2.52	- 13.40	15.92	6.32
7.4S	28.5	2.43	- 1.30	3.72	1.53
7.6S	44.4	2.37	- 1.22	3.59	1.51
7.7S	59.5	1.45	1.14	0.30	0.21
7.8S	69.6	1.32	0.96	0.36	0.27

D → represents dried networks

S → represents swollen networks

$$\frac{2C_2}{2C_1+2C_2} = \frac{2}{f} = \frac{2}{3} \quad \ldots\ (5\text{-}53)$$

when f = 3.

The equation shows that the ratio of the slope to intercept (at $\Lambda = 1$) of the Mooney-Rivlin plots should be 2/f, which is 2/3 in the present networks, if the stress-strain data of the present networks follow Mooney-Rivlin equation. Table 7.3 shows that the ratios (6th column) are not 2/3. Thus, the assumption of affine (smaller deformation) to phantom (larger deformation) transition of the networks during deformation can not be interpreted by Mooney-Rivlin equation, although some of the networks at higher dilutions are apparently following the equation over the limited range of Λ studied.

7.2 RESULTS OF TORSION PENDULUM EXPERIMENTS

Dynamic properties of the dried, completely reacted polyurethane networks synthesized from experimental series 6 (dilution series-uncatalysed) and 7 (dilution series-catalysed) were measured using a torsion pendulum apparatus. Three types of data were obtained as a function of temperature: storage and loss moduli (G' and G'') and damping ($\tan\delta$). The glass transition temperatures (Tg) were estimated from the major peak observed in $\tan\delta$ versus T plots and are presented in Table 7.4. For comparative purposes, glass transition temperatures obtained from Differential Scanning Calorimetry (D.S.C.) data are also included in the table. The D.S.C. measurements were made on a Du Pont -900 model D.S.C. machine at a heating rate of $20^{o}C$ per minute.

All the experimental data obtained from the torsion pendulum apparatus are presented in Appendix E.

Since all the G′, G′′ and tanδ versus T plots are similar for all dilutions, only representative plots of G′, G′′ and tanδ versus T, for a completely reacted polyurethane network made from a reaction mixture containing 59.6% toluene and 0% DABCO, is shown in figure 7.16. The curves conform to those for typical amorphous polymers. The glassy modulus G′ ranges from 1.5 to 1.8 GNm^{-2} and decreases only slowly with increasing temperature until the transition region (around Tg) when G′ falls sharply to a value of about 0.6 to 0.8 MNm^{-2}, after which there is a clear increase in rubbery modulus. The tanδ and G′′ curves are similar in shape to each other both showing well-defined peaks defining the Tg at about -65°C, (α - peak) and a less intense and broader peak (β - peak) at about -140°C.

Previous workers[24,53] have observed more than two transitions in polyurethane systems. Cawse[24] observed γ- and δ- transitions in LHT240/MDI polyurethane (aromatic) systems. Wilson[53] observed a γ-transition in LHT240/HDI polyurethane (aliphatic) systems. No such low temperature transitions were observed in the present polyurethane systems.

Damping curves of different dilutions of the present system show mainly two transitions: α- and β- transitions. α- transitions correspond to glass-rubber transitions and are sharp, occurring in the range -58°C to -67°C. β- transitions (secondary transitions) were observed between -130°C to -140°C. This secondary transition may be associated with the oxypropylene unit and more specifically with the methyl side groups in this unit[24].

Table 7.4 shows that both the torsion pendulum and D.S.C. results indicate that Tg tends to decrease with increasing dilution of preparation both in catalysed and uncatalysed networks. This decrease in Tg may be correlated with the α_c-values (obtained from gel points) of the corresponding reaction systems, and is represented as a plot of Tg versus α_c in fig. 7.17.

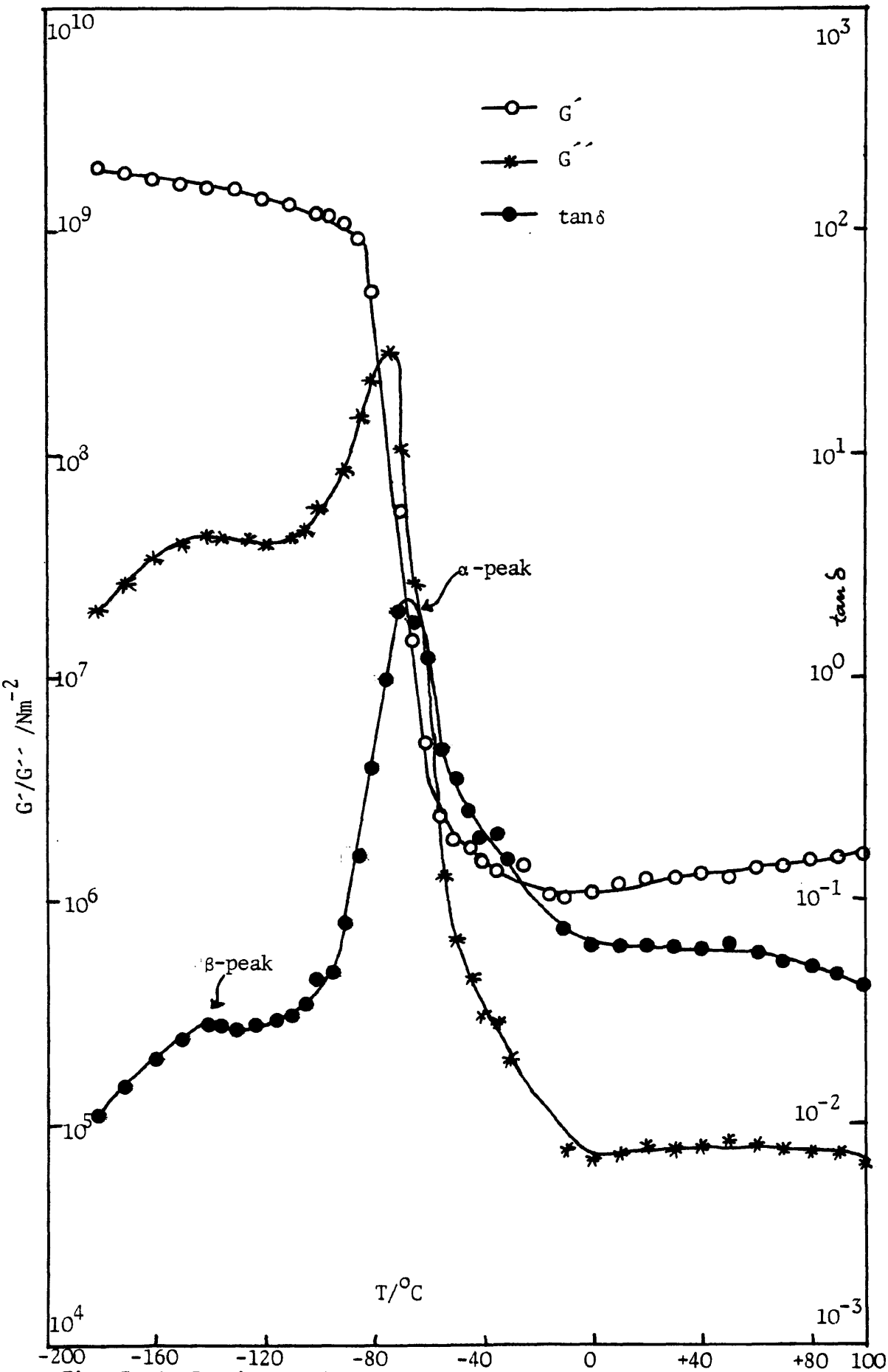

Fig. 7.16 Torsion pendulum data: G´, G´´ and tanδ versus T plots for network of composition 60% ϕCH_3, 0% DABCO.

Cawse[24] also observed a similar decrease with increase in α_c in LHT240/MDI (nitrobenzene as solvent) polyurethane system. Higher α_c values correspond to networks with lower junction point density and higher structural defects such as elastically inactive rings or loops formed by pre-gel intramolecular reactions.

TABLE 7.4 Effect of Dilution on Transitional Behaviour of Polyurethane Networks. (Experimental series: 6 - Uncatalysed and 7 - Catalysed)

Expt No	% Solvent	α_c	T_α+2/°C (T.P.)	T_α+0.5/°C (D.S.C.)	T_β+5/°C (T.P.)
6.1	0	0.600	-60	-57.0	-130
6.2	9.0	0.603	-58	-56.5	-135
6.3	20.0	0.603	-61	-57.5	-140
6.4	28.6	0.604	-60	-56.0	-130
6.5	37.5	0.610	-62	-57.0	-130
6.6	44.4	0.611	-64	-58.0	-130
6.7	59.6	0.618	-67	-59.0	-140
6.8	69.5	0.623	-	-60.0	-
7.1	0	0.615	-56	-56.0	-135
7.2	9.1	0.623	-60	-56.0	-135
7.3	20.0	0.626	-62	-55.0	-130
7.4	28.6	0.629	-64	-56.0	-130
7.5	37.5	0.631	-63	-56.0	-140
7.6	44.4	0.634	-65	-56.5	-135
7.7	59.5	0.648	-62	-59.0	-140
7.8	69.6	0.667	-62	-60.0	-140

T.P. → Torsion Pendulum

D.S.C. → Differential Scanning Calorimetry

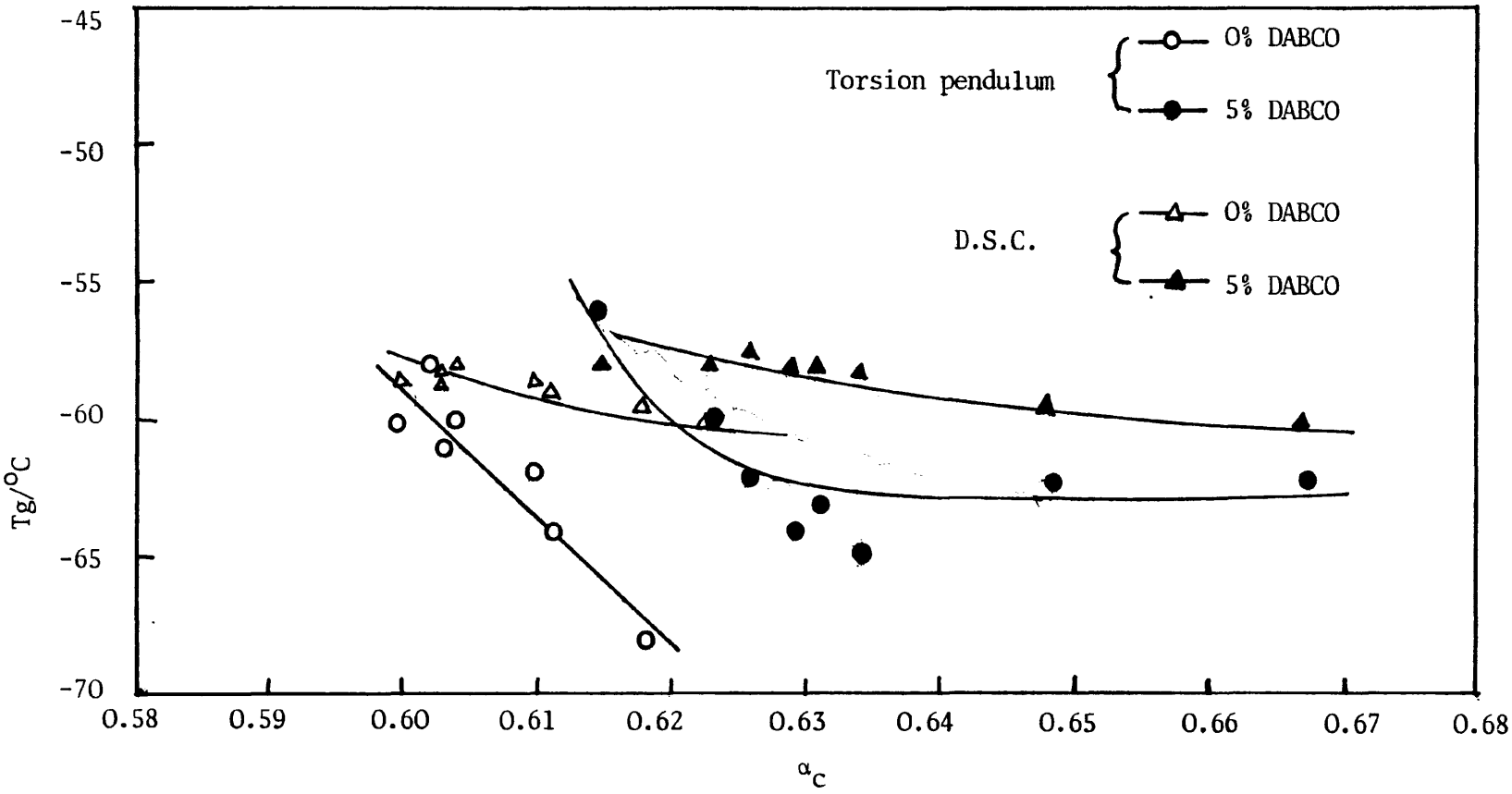

Fig. 7.17 Dependence of glass transition temperature (Tg) on gel point (α_c) for polyurethane networks

This defect increases the free volume and hence decreases[143] Tg. Table 7.4 shows that Tg values obtained from the damping curves, shown in figures 7.18 (uncatalysed) and 7.19 (catalysed), are always lower than those from D.S.C. The higher Tg values from the D.S.C. as compared with those from damping may be the result of different heating rates (in torsion pendulum 1^{o} per minute and in D.S.C. 20^{o} per minute) and frequency (1 Hz in torsion pendulum and D.S.C. is static).

It may also be mentioned that glass transition and other transitions depend on the molar mass of the triols, more specifically on M_c^{o} (the molar mass between two junction points). The transition temperatures also depend on the nature of diisocyanates - whether it is aliphatic or aromatic. Transition temperatures of the present aliphatic polyurethane systems and other aromatic and aliphatic polyurethane systems are presented in Table 7.5. The table shows that the more flexible chains

TABLE 7.5 Transition temperatures of different polyurethane systems (Bulk) obtained from torsion pendulum

System	Triol molar mass ($g\ mol^{-1}$)	M_c^{o} ($g\ mol^{-1}$)	$T_\alpha/^{o}C$	$T_\beta/^{o}C$	$T_\gamma/^{o}C$	$T_\delta/^{o}C$
1. Present work LG-56/HDI	3,000	2,164	-56	-135	-	-
2. LHT 112/HDI[60]	1,500	1,168	-45			-
3. LHT 240/HDI[53]	700	635	- 9	- 68	-119	-
4. LHT 112/MDI[138]	1,450	1,200	-14	-100	-135	-
5. LHT 240/MDI[24]	700	705	37	- 3	- 78	-128

Fig. 7.18 tanδ versus T plots for uncatalysed polyurethane networks.

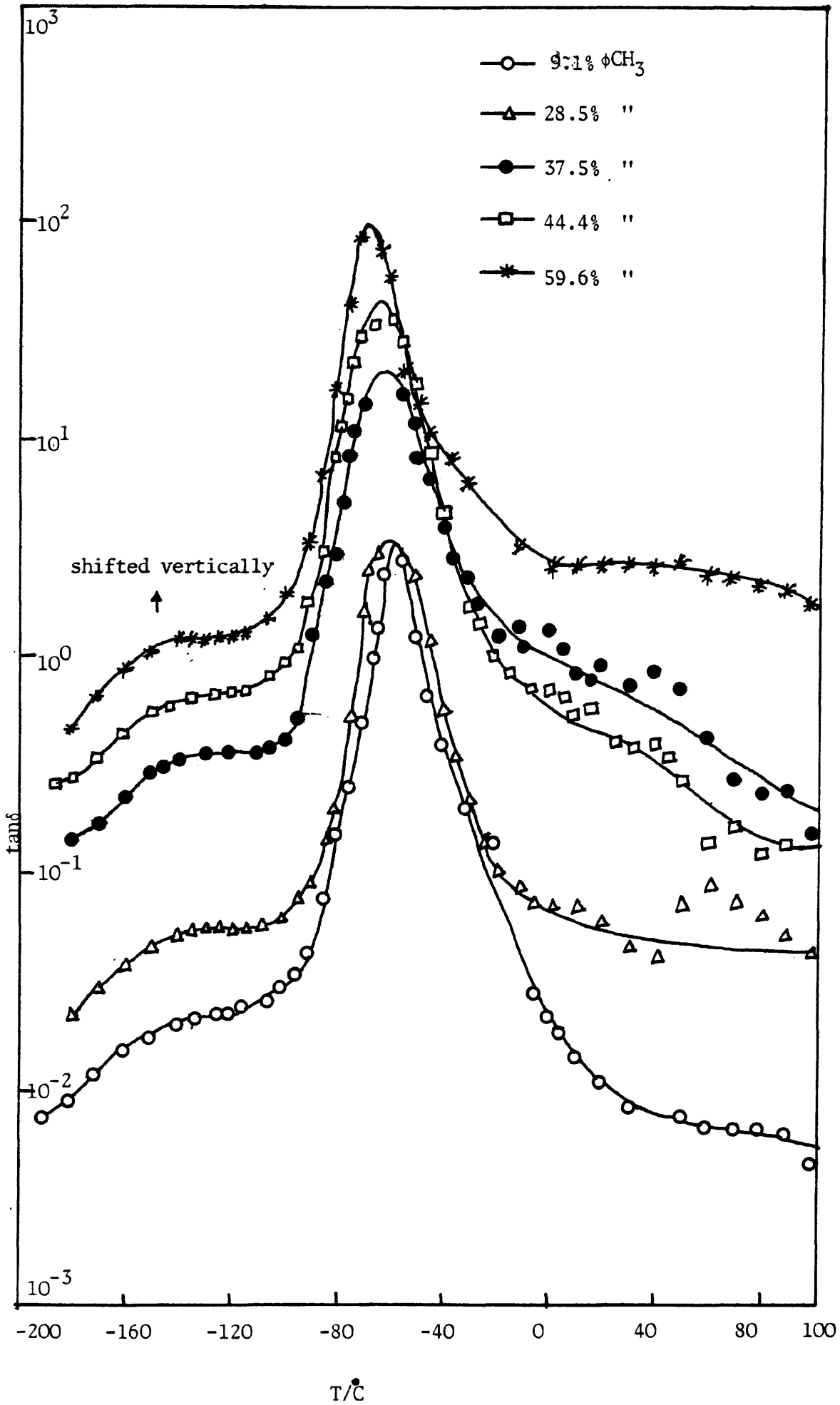

Fig. 7.19 tanδ versus T plots for catalysed polyurethane networks

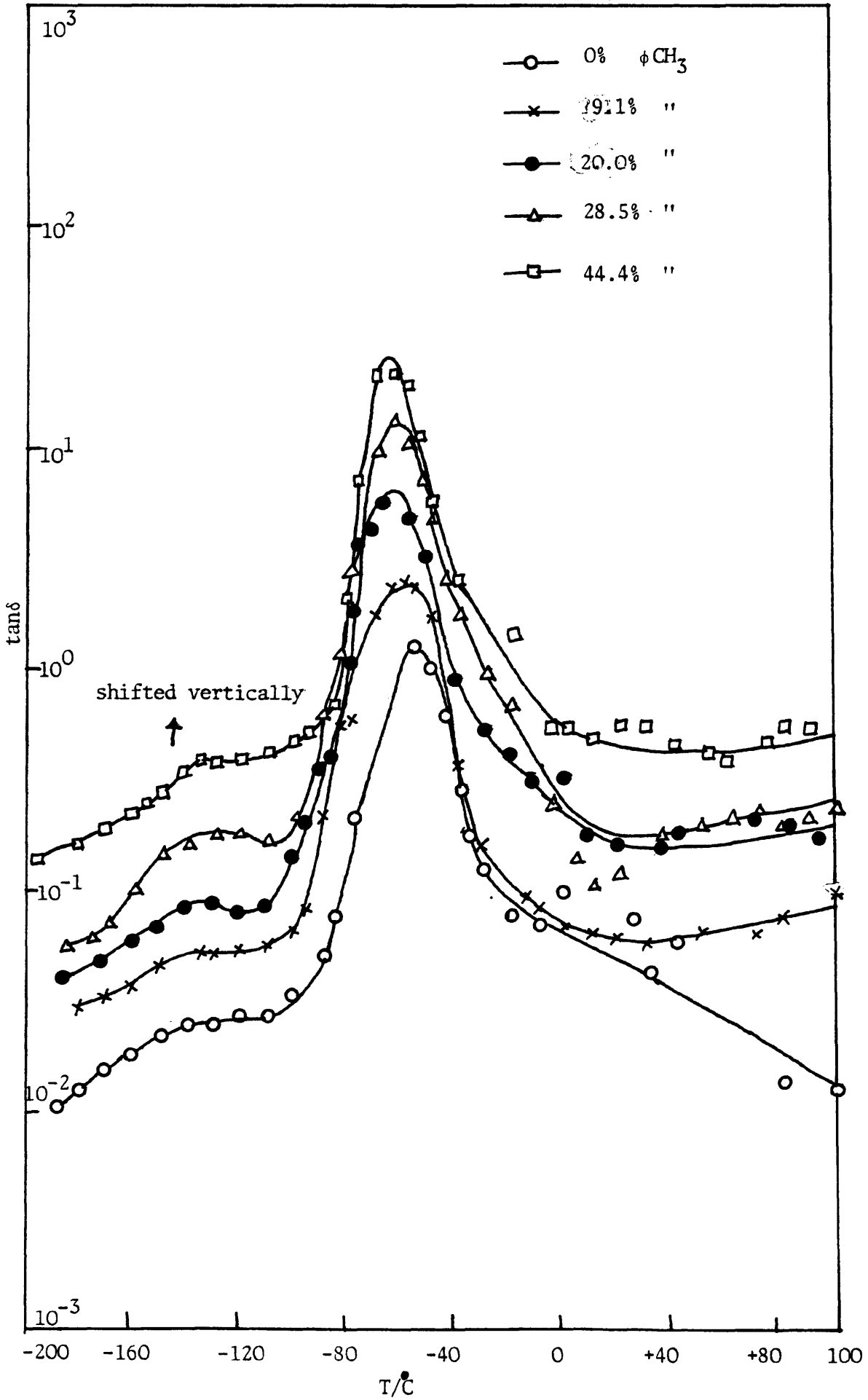

of the aliphatic systems (systems 1,2,3) give lower values of Tg, resulting in elastomers at room temperatures. On the other hand, the presence of a rigid aromatic ring in the network structure gives higher values of Tg, resulting in glassy materials at room temperature (specially with low molar mass polyols). The effect of M_c^o of the network on Tg and other transitions is significant. The higher is the M_c^o, the lower is the transition temperature (see Table 7.5), which is true for both aliphatic (systems 1,2,3) and aromatic (systems 4,5) polyurethanes. This is a reflection of the effect of junction point density on transition temperatures. The higher is the M_c^o, the lower is the junction point density (ie, more flexible is the chain) and also the more is the free volume and hence lower is the transition temperature. Thus the results of the present work follow the expected and previously observed trends in transition temperatures.

In most of the plots of G′ versus T, G′′ versus T and tanδ versus T, scatter in the experimental points is observed at temperatures above Tg. The very soft nature of the networks (ie, higher M_c^o) may be mainly responsible for the scatter. The rubbery modulus versus temperature plots are shown in figures 7.20 and 7.21. Least-squares analysis is used to calculate the slope of G′ versus T plots. From the slopes, M_c/A evaluated using equation (5-48) and hence M_c/AM_c^o. M_c/A and M_c/AM_c^o values are shown in Table 7.6. The table and fig. 7.22 show that M_c/AM_c^o values have decreasing trend with increasing dilution for both catalysed and uncatalysed networks; but it is difficult to draw any conclusion from these results and α_c (or $p_{r,c}$) versus M_c/AM_c^o plots (fig. 7.22) because of the uncertainties in the experimental points. Some of the M_c/AM_c^o values (experiments 6.7, 7.7 and 7.8), especially at higher dilutions are less than 1, which do not have any significance. An apparent increasing tendency of G′ with dilution in torsion pendulum is also observed which is not explainable.

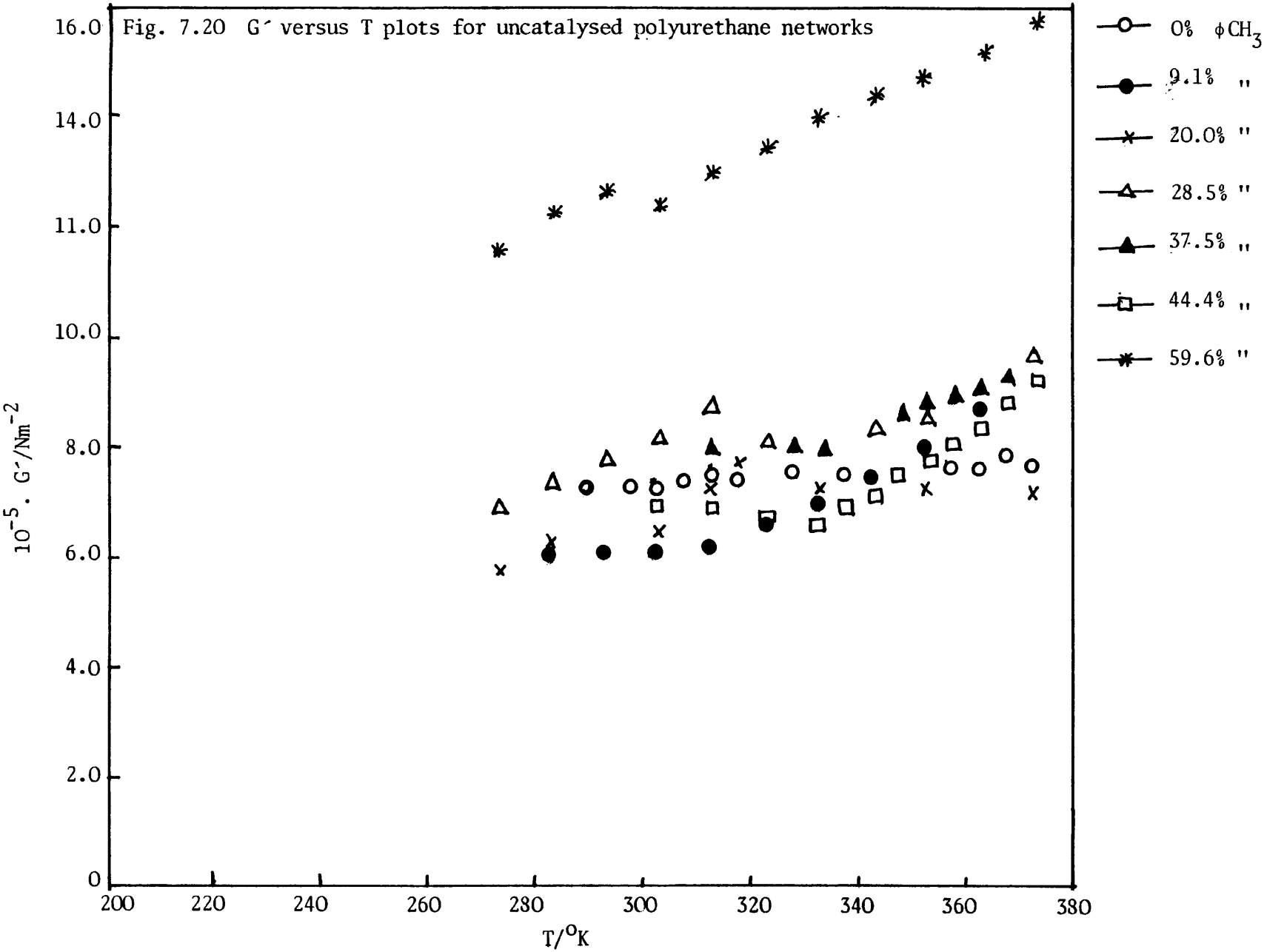
Fig. 7.20 G´ versus T plots for uncatalysed polyurethane networks
16.0
14.0
11.0
10.0
8.0
6.0
4.0
2.0
0
200
220
240
260
280
300
320
340
360
380
10^{-5}. G´/Nm^{-2}
T/°K
0% φCH3
9.1% "
20.0% "
28.5% "
37.5% "
44.4% "
59.6% "

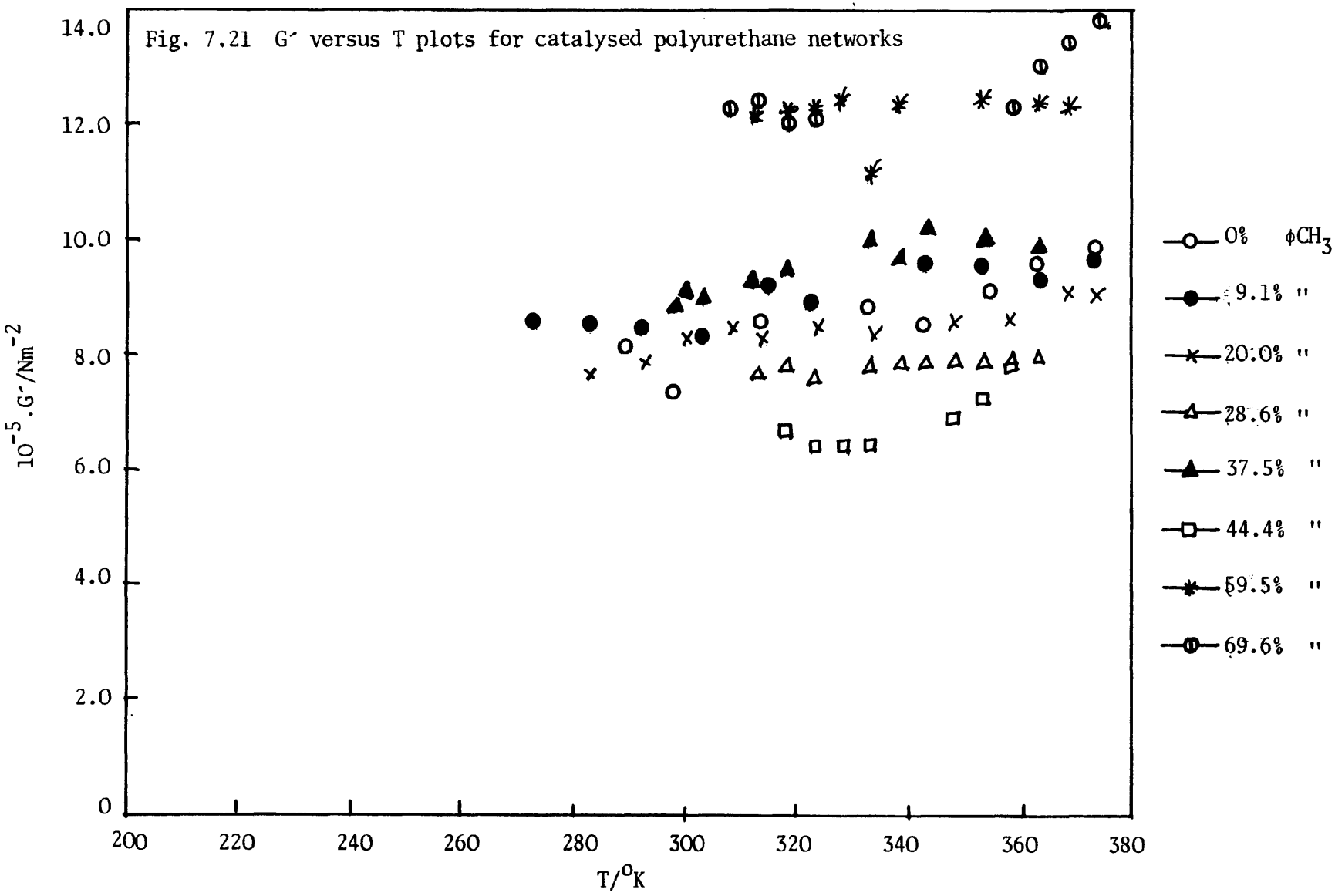
Fig. 7.21 G′ versus T plots for catalysed polyurethane networks
14.0
12.0
10.0
8.0
6.0
4.0
2.0
0
10^{-5}.G′/Nm^{-2}
200
220
240
260
280
300
320
340
360
380
T/°K
0% φCH3
9.1% "
20.0% "
28.6% "
37.5% "
44.4% "
59.5% "
69.6% "

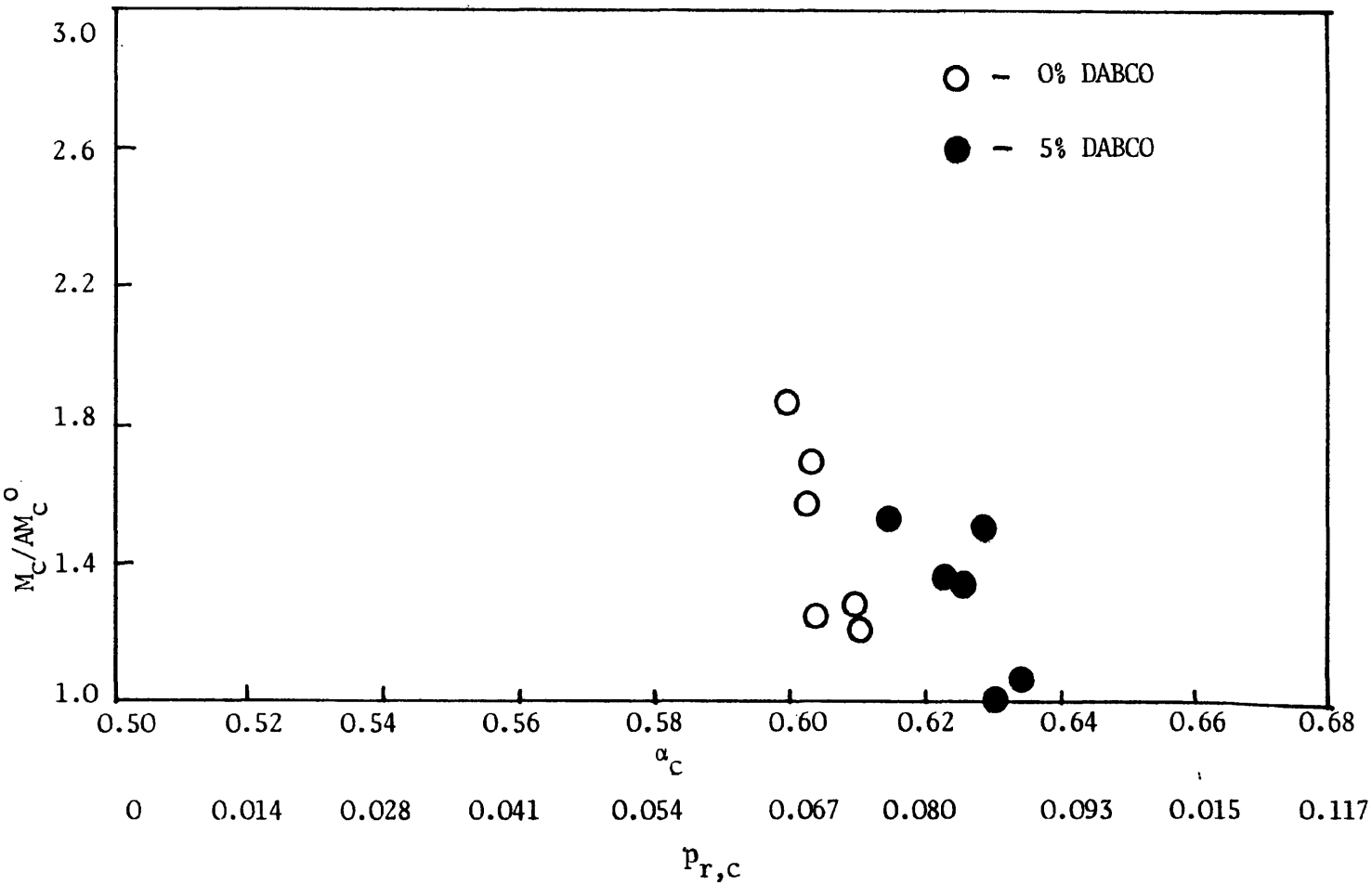

Fig. 7.22 M_c/AM_c^o (obtained from torsion pendulum data) versus α_c (and $p_{r,c}$) for dried polyurethane networks ($M_c/AM_c^o > 1$ values are only plotted)

TABLE 7.6 M_c/A and M_c/AM_c^o values obtained from Torsion Pendulum data on the dried networks

Expt No	% Solvent	α_c	$10^3.M_c/A(g\ mol^{-1})$	M_c/AM_c^o
6.1	0	0.600	4.03	1.86
6.2	9.0	0.603	3.40	1.57
6.3	20.0	0.603	3.63	1.68
6.4	28.6	0.604	2.68	1.24
6.5	37.5	0.610	2.73	1.26
6.6	44.4	0.611	2.63	1.21
6.7	59.6	0.618	1.07	0.49
6.8	69.5	0.623	-	-
7.1	0	0.615	3.34	1.54
7.2	9.1	0.623	2.95	1.36
7.3	20.0	0.626	2.92	1.35
7.4	28.6	0.629	3.28	1.51
7.5	37.5	0.631	2.12	0.98
7.6	44.4	0.634	2.32	1.07
7.7	59.5	0.648	1.33	0.61
7.8	69.6	0.667	1.14	0.52

The rubbery moduli obtained from torsion pendulum experiments (from the least-squares plots) at 27°C are compared with those obtained from uniaxial compression tests in Table 7.7 at the same temperature. The table shows that the rubbery modulus has a decreasing trend with dilution in case of uniaxial compression data, but such a trend is not observed in case of torsion pendulum data. However, the magnitude of the modulus value obtained from torsion pendulum measurement is always higher than that obtained from uniaxial compression tests at a given dilution. The difference in two methods of measurements such as frequency (frequency of

TABLE 7.7 Comparison of the rubbery modulus obtained from uniaxial compression and torsion pendulum experiments at 27°C

Expt No	% of Solvent	$10^{-5}.G_C/Nm^{-2}$	$10^{-5}.G_T/Nm^{-2}$
6.1	0	6.14	6.38
6.2	9.1	4.71	6.88
6.3	20.0	4.39	6.21
6.4	28.6	5.90	7.53
6.5	37.5	5.00	6.60
6.6	44.4	5.04	6.62
6.7	59.6	3.70	12.62
6.8	69.5	2.88	-
7.1	0	6.33	7.71
7.2	9.0	6.24	7.93
7.3	20.0	6.51	7.30
7.4	28.6	4.82	6.56
7.5	37.5	4.67	8.63
7.6	44.4	5.04	7.48
7.7	59.5	3.49	10.20
7.8	69.6	3.23	9.96

G_C → Rubbery modulus obtained from compression test (see Table 7.1)

G_T → Rubbery modulus obtained from the least-squares line of G′ versus T plots of torsion pendulum data

torsion pendulum experiment is ≃ 1 Hz whereas uniaxial compression is a static method) may be responsible for the difference.

Thus, the results of the torsion pendulum experiments show that Tg decreases as α_c increases, and thus reflect the effect of network structure on its transition properties. But it can not explain the effect of network structure on modulus, because it is difficult to get precise absolute moduli at temperatures above Tg because of the very soft nature of the networks.

CHAPTER - 8

GENERAL SUMMARY, CONCLUSIONS AND SUGGESTIONS FOR FUTURE WORK

The reactions between oxypropylated triol (LG-56) and hexamethylene diisocyanate (HDI) have been studied at 80°C in bulk, in toluene and in nitrobenzene as solvents, with or without added catalyst (DABCO). Kinetics and gelation of the reactions have been investigated. The gelation data have been interpreted in terms of approximate gelation theories and polyfunctional rate theory. The effect of pre-gel intramolecular reaction on gel points is discussed. The kinetics study shows that the kinetics of polyol/isocyanate reactions are affected by solvents and catalyst. In spontaneous reactions, the autocatalytic effect predominates giving positive deviations from second order kinetics. In catalysed reactions the autocatalytic effect is still present, as evident from slight positive deviations from second order kinetics of reactions in toluene and nitrobenzene solutions. The gel points are also affected by solvent and catalyst, the amount of pre-gel intramolecular reactions and other side reactions increasing, in nitrobenzene, with catalyst and dilution. Such effects are less in toluene as compared with nitrobenzene. b (the effective bond length) values are evaluated from the approximate gelation and rate theories, and are found to be higher for the uncatalysed than the catalysed systems due to more side reactions in the latter. b values of the present work are compared with previous values for polyurethane-forming systems and indicate that for chemically similar systems of a given functionality

the amount of pre-gel intramolecular reaction depends primarily on the size (ν) of the smallest ring structure with a secondary dependence of chain stiffness (b). b values are also observed to decrease with increase in ν. Thus it is clear that intramolecular reaction is an integral part of the random polymerisation process. In irreversible polymerisations the extent to which it occurs depends on dilution (C_{ext}^{-1}), reactant functionalities (f), molar mass (ν), chain flexibility (b) and reactant ratio (r).

Networks were synthesised by allowing aliquots from reaction mixtures to react to completion in moulds. The shear moduli of the dried networks and networks at equilibrium swelling in toluene were determined through uniaxial compression measurements. The results of the uniaxial compression measurements are discussed in terms of Gaussian theory and the Mooney-Rivlin equation of rubber elasticity. Deviations from Gaussian theory are observed both in dried and swollen networks. However, the deviations are observed to decrease with increase in dilution of preparation (ie, with increase in α_c and hence M_c). Similar deviations have also been observed with trifunctional polyester[109] and tetrafunctional polyurethane[73] networks. However, Gaussian behaviour for the present systems is observed for values of M_c greater than about 5000.

The shear moduli (G) obtained are interpreted according to Gaussian theory to give values of M_c/A (M_c - the effective molar mass between the junction points) and hence M_c/AM_c^o. In all cases, M_c/AM_c^o is greater than unity. The plots of M_c/AM_c^o versus α_c and $p_{r,c}$ show that only in the limit of the ideal gel point (ie, $\alpha_c = (f-1)^{-1} = 0.5$ and $p_{r,c} = 0$) can a perfect, affine, rather than phantom network be formed in the present system. Similar affine behaviour, in the limit of the ideal gel point, was also predicted with triol/HDI and tetrol/HDI systems.

Stress-strain data are also analysed in terms of Mooney-Rivlin equation in the limit of small and large deformations. In the limit of small deformation, positive intercepts ($2C_1 + 2C_2$) are observed throughout the dilution of the reaction mixtures. In the limit of large deformation, non-linear Mooney-Rivlin plots and negative intercepts ($2C_1$) (which do not have any significance) are observed at lower initial dilutions. However, at higher dilutions, linear Mooney-Rivlin plots and positive intercepts result. Stress-strain plots always give positive slopes ($2C_2$) both in the limit of small and large deformations with increase in dilution but never become zero. In the limit of small and large deformations, assuming the transition of affine (small strain) to phantom (large strain) behaviour during the deformation of the networks, the ratio of the slope to intercept (ie, $2C_2/(2C_1 + 2C_2)$) should be $2/f$ (= 2/3 in the present case). No such value of the slope to intercept ratio was observed, indicating that stress-strain data of the present networks cannot be interpreted using Mooney-Rivlin equation.

Dynamic-mechanical tests have been carried out on dried, completely reacted networks using a torsion pendulum apparatus to investigate the transition behaviour, such as the primary transition (the glass transition or α- transition) and a secondary transition (β- transition), of the networks. To supplement the transition data obtained from the torsion pendulum, differential scanning calorimetry (D.S.C.) has been performed on dried networks. The effect of gel point (α_c) and hence, the pre-gel intramolecular reaction on transition temperatures are discussed. Both the torsion pendulum and D.S.C. results show that glass transition temperatures decrease with increase in α_c and hence with increase in pre-gel intramolecular reaction or ring formation. A similar decreasing trend in Tg with α_c has also previously been observed in trifunctional aromatic polyurethane systems[24].

Thus the factors which influence pre-gel intramolecular reaction in random polymerisations are shown to influence strongly the moduli of the networks formed at complete reaction. For the polyurethane networks studied, the moduli are always lower than those expected for no pre-gel intramolecular reaction, indicating the importance of such reaction in determining the number of elastically ineffective loops in the networks. In the limit of the ideal gel point, perfect networks (affine) are predicted to be formed. Perfect networks are not realised with bulk reaction systems. At a given extent of pre-gel intramolecular reaction ($p_{r,c}$), the effect of inelastic loop is generally less on tetrols than triols; however, for triols of high M_c^o, the effect becomes less.

The reduction in moduli is also larger for reactants of lower molar mass, at a given extent of pre-gel intramolecular reaction ($p_{r,c}$), for a given functionality.

Deviations from Gaussian stress-strain behaviour in compression have been observed which relate to the M_c of the networks formed, rather than their degrees of swelling during compression measurements.

Intramolecular reactions in non-linear polymerisations and its effect on gel points and network properties are not well-characterised, although much theoretical work has been done in this area. So more data linking dilution (C_{ext}^{-1}), reactant ratio (r), reactant functionality (f), molar mass ($M_c^{\tilde{G}}$ or ν) and chain flexibility (b) on a variety of model systems are needed.

This project, based on triol of higher molar mass than those used before, now suggests that the higher the molar mass of the triol (or polyol) the less the loops formed and also less the effect of loops on modulus.

However, loops still exist, so preference may be given to study the kinetics, gelation and properties of more triol- and tetrol-based network-forming systems such as LG-56/MDI (diphenylmethane diisocyanate), LG-56/DDI (decamethylene diisocyanate), tetrols/MDI and some high molar mass tetrol/MDI or HDI or DDI. The solvent, temperature and catalyst should be chosen suitably with respect to particular system. These systems may provide appreciable amounts of data, which can be analysed with different approximate gelation theories and the rate theory as well, to give a better understanding and a firm basis for the examination of intramolecular reaction, with particular reference to ring or loop formation, in non-linear polymerisations.

For a better analysis of Gaussian theory and Mooney-Rivlin equation, more compression data from the previously mentioned systems and also some low molar mass triols (eg, LHT 240, LHT 112) and HDI or DDI should be obtained. Experiments should be performed both in the dry and swollen states. Analysis of the experimental data of these systems under smaller deformations (compression) and larger deformations (tension) should give information about the characteristic of the network structures.

Networks synthesised from previously mentioned systems can also be studied by Dynamic Mechanical Thermal Analysis (D.M.T.A.) and D.S.C. Both the methods will correlate the network structures with mechanical and transition properties of the networks.

REFERENCES

1. Carothers, W.H., J. Am. Chem. Soc., 1929, 51, 2548.

2. Flory, P.J., Principles of Polymer Chemistry, Cornel University Press, Ithaca, N.Y. (1953), p-38.

3. Stanford, J.L. and Stepto, R.F.T., J. Chem. Soc. Farady Trans. I., 1975, 71, 1292.

4. Carothers, W.H., Trans. Faraday Soc., 1936, 32, 39.

5. Reference - 2, p-318.

6. Jacobson, H. and Stockmayer, W.H., J. Chem. Phys., 1950, 18, 1600.

7. Reference - 2, Chapter - IX.

8. Stockmayer, W.H., J. Polym. Sci., 1952, 9, 69;
   1953, 11, 424.

9. Stockmayer, W.H. and Weil, L.L., Advancing Fronts in Chemistry, Reinhold, N.Y. (1945), Chapter-IV.

10. Price, F.P., Gibbs, J.H. and Zimm, B.H., J. Phys. Chem., 1958, 62, 972.

11. (a) Hopkins, W., Peters, R.H. and Stepto, R.F.T., Polymer, 1974, 15, 315.
    (b) Hopkins, W., Ph.D. Thesis, University of Manchester (1967).

12. Peters, R.H. and Stepto, R.F.T., Soc. of Chem. Industry, Monograph No-20, p-157 (1965).

13. Birley, G.I., M.Sc. Thesis, University of Manchester (1967).

14. (a) Smith, R.S. and Stepto, R.F.T., Makromol. Chem., 1974, 175, 2365.
    (b) Smith, R.S., M.Sc. Thesis, University of Manchester (1970).

15. Case, L.C., J. Polym. Sci., 1957, 26, 333.

16. Frisch, H.L., Paper presented to the 128th Meeting of Am. Chem. Soc., Polymer Division, Mineapolis (1955).

17. Kilb, R.W., J. Phys. Chem., 1958, 62, 969.

18. Stepto, R.F.T., Faraday Disc. Chem. Soc., 1974, 57, 69.

19. Stanford, J.L., Ph.D. Thesis, University of Manchester (1972).

20. (a) Gordon, M., Proc. Roy. Soc. (London), 1962, A-268, 240.
    (b) Gordon, M. and Temple, W.B., Makromol. Chem., 1972, 160, 263.
    (c) Gordon, M. and Scantlebury, G.R., Proc. Roy. Soc. (London), 1966 A-292, 380.

21. Temple, W.B., Makromol. Chem., 1972, 160, 277.

22. Shashoua, V.E., Sweeney, W. and Tietz, R.F., J. Am. Chem. Soc., 1960, 82, 866.

23. Saunders, J.H. and Frisch, K.C., 'Polyurethanes: Chemistry and Technology', Part-1 (Chemistry), Interscience, N.Y. (1962).

24. Cawse, J.L., Ph.D. Thesis, University of Manchester (1979).

25. Stepto, R.F.T. and Waywell, D.R., Makromol. Chem., 1972, 152, 247; 263.

26. Encyclopaedia of Chemical Technology, 1982, 18, 639.

27. Frisch, K.C., 'Fundamental Chemistry and Catalysis of Polyurethanes' in Polyurethane Technology, ed. P.F. Bruins, Interscience-Willey, N.Y. (1969).

28. Chriastianson, L.R., Dheming, M. and Ochoa, E.L., J. Cell. Plastics, p-111 (March/April, 1977).

29. Knodel, L.R., U.S. Patt., 3,865,806 (to Dow Chem. Co.), 1975.

30. Patton, J.I. and Schulz, J.F., U.S. Patt.; 3,346,557 (to Wyandoffe Chem. Corp.) 1967.

31. Wismer, M., Lebras, L.R., Peffer, J.R. and Foote, J.F., U.S. Patt., 3,222,357 (to Pittsburg Plate-Glass Co.) 1965.

32. Frisch, K.C. and Kresta, J.E., 'An Overview of Sugars in Urethanes' in 'Sucrochemistry', ed. J.L. Hickson (1977).

33. Moss, P.H. and Cascurida, M., U.S. Patt., 3,535,307 (to Jefferson Chem. Co.) 1970.

34. Lowe, A.J., Chandley, E.F., Leigh, H.W. and Molinario, L., J. Cell. Plast., 1965, p-121.

35. Twitchett, H.J., Chem. Soc. Reviews, 1974, 3, 209.

36. Davis, J.S. and Farnum, J.M., J. Am. Chem. Soc., 1934, 56, 883.

37. (a) Baker, J.W. and Holdsworth, J.B., J. Chem. Soc., 1947, p-713.
(b) Baker, J.W. and Gaunt, J., J. Chem. Soc., 1949, p-19&27.
(c) Baker, J.W., Davis, M.M. and Gaunt, J., J. Chem. Soc., 1949, p-24.

38. Borkent, G., Adv. Urethane Sci. & Tech., 1974, 3, 1.

39. (a) Sato, M., J. Am. Chem. Soc., 1960, 82, 3893.
(b) Sato, M., J. Org. Chem., 1962, 27, 819.

40. Okada, H. and Iwakura, Y., Makromol. Chem., 1963, 66, 91.

41. Ephraim, S., Woodward, A.E. and Mesrobian, R.B., J. Am. Chem. Soc., 1958, 80, 1326.

42. Robertson, W.G.P. and Stuchbury, J.E., J. Chem. Soc., 1964, p-4000.

43. Lyman, D.J., 'Stepgrowth Polymerisations', ed. D.H. Solomon, Marceb-Dekker, N.Y. (1972), Chapter-3.

44. Bailey, M.E., Kriss, V. and Spaunberg, R.G., Ind. Eng. Chem., 1956, 48, 794.

45. Ferstanding, L.L. and Scherrer, R.A., J. Am. Chem. Soc., 1959, 81, 4838.

46. Burkus, J. and Eckert, C.F., J. Am. Chem. Soc., 1958, 80, 5948.

47. Kogon, I.C., J. Org. Chem., 1959, 24, 438.

48. Iwakura, Y., Okada, H. and Yamashiro, S., Makromol. Chem., 1962, 58, 237.

49. Nufuri, A.D., Zubko, S.A. and Lipatova, T.E., C.A. 84 (1976), 57395.

50. Frisch, K.C., Reegan, S.L. and Thir, B., J. Polym. Sci., 1967, C-16, 2191.

51. Greenshield, J.N., Peters, R.H. and Stepto, R.F.T., J. Chem. Soc., 1964, p-5101.

52. Waywell, D.R., Ph.D. Thesis, University of Manchester (1968).

53. Wilson, J.D., Ph.D. Thesis, University of Manchester (1980).

54. Fogiel, A.W. and Stewart, C.W. Sr., J. Polym. Sci., 1969, Part A-2, 7, 1116.

55. Flory, P.J., Chem. Revs., 1946, 39, 137.

56. Truesdell, C.A., Ann. Math., 1945, 46, 144.

57. Ahmad, Z. and Stepto, R.F.T., Colloid and Polym. Sci., 1980, 258, 3209.

58. Ahmad, Z., Ph.D. Thesis, University of Manchester (1977).

59. Matejka, L. and Dusek, K., Polymer Bulletin, 1980, 3, 489.

60. Stanford, J.L. and Stepto, R.F.T., in 'Elastomers and Rubber Elasticity', Eds. Mark, J.E. and Lal, J.; ACS Symp. Series No.193, Am. Chem. Soc.: Washington D.C., 1982, Chapter-20.

61. Fogiel, A.W., Makromol. Chem., 1969, 2, 581.

62. Guise, G.B. and Zoch, C.G., J. Makromol. Sci., (Chem.), 1976, A-10, 1161.
J. Polym. Sci. Symp., 1976, No-55, 61.

63. Cawse, J.L., Stanford, J.L. and Stepto, R.F.T., Proc. IUPAC Intern. Symp. on Makromolecules, Mainz (1979), p-693.

64. Sorensen, W.R. and Campbell, T.W., 'Preparative Methods of Polymer Chemistry' - Interscience, N.Y. (1961), p-134.

65. Pearson, J.R.A. in 'Polymer Science', vol-1, Ed. Jenkins, A.D., North-Holland, London (1972), p-457.

66. Farkas, A. and Strohm, P.F., Ind. Eng. Chem. Fundamental, 1965, 4, 32.

67. Farkas, A. and Flynn, K.G., J. Am. Chem. Soc., 1960, 82, 642.

68. Farkas, A., Mills, G.A., Erner, W.E. and Maerker, J.B., Ind. Eng. Chem., 1959, 51, 1299.

69. Reegan, S.L. and Frisch, K.C., J. Polym. Sci., Part A-1, 1966, 4, 2321.

70. Lipatova, T.E., Bakalo, L.A., Sirolinskaya and Syntkina, O.P., C.A. 69 (1982), 19559k.

71. Table of Dielectric Constants of Pure Liquids, National Bureau of Standard, Circular-514, August, 1951.

72. Fasina, A.B., Ph.D. Thesis, University of Manchester (1975).

73. Hunt, N.G.K., Stepto, R.F.T. and Still, R.H., Proc. 26th IUPAC Int. Sypm. on Makromolecules, Mainz (1979), p-697.

74. Rose, S.V. and Stanford, J.L., Unpublished work.

75. Kurata, M., Tsunashina, Y., Iwama, M. and Kamada, K., in Polymer Handbook, ed. Brandrup, J. and Immergut, E.H., Interscience, London (1975), section-IV-I.

76. Flory, P.J., 'Statistical Mechanics of Chain Molecules', Interscience, London (1969), p-40.

77. Stanford, J.L. and Stepto, R.F.T., Br. Polym. J., 1977, 9, 124.

78. Askitopoulos, V., M.Sc. Thesis, University of Manchester (1981).

79. Stanford, J.L., Stepto, R.F.T. and Still, R.H., Presented in Part at Div. Org. Coating and Plastics Chem., 181st ACS National Meeting, Atlanta, 1981, p-164.

80. Treloar, L.R.G., 'Physics of Rubber Elasticity', Clarendon Press, 1958, p-11.

81. Krigbaum, W.R. and Roe, R.J., Rubber Chem. Tech., 1965, 38, 1039.
J. Polym. Sci., 1962, 61, 167.

82. Gee, G., Polymer, 1966, 7, 373.

83. Dusek, K. and Prins, W., Adv. Polym. Sci., 1969, 6, 1.

84. Treloar, L.R.G., Rep. Prog. Phys., 1973, 36, 755.

85. Wall, F.T. and Flory, P.J., J. Chem. Phys., 1950, 18, 108; 1951, 19, 1435.

86. Wall, F.T., ibid, 1943, 11, 527.

87. Reference-2, p-464.

88. Flory, P.J., J. Chem. Phys., 1950, 18, 108.

89. James, H.M. and Guth, E., ibid., 1943, 11, 455; 1947, 15, 651.

90. James, H.M. and Guth, E., ibid., 1953, 21, 1039.

91. Guth, E., J. Polym. Sci., 1966, C-12, 89

92. Hermans, J.J., Trans. Faraday Soc., 1947, 43, 591.

93. Hermans, J.J., J. Polym. Sci., 1962, 59, 191.

94. Reference-80, Chapter-4.

95. Graessley, W.W., Makromolecules, 1975, 8, 186, 865.

96. Mark, J.E. and Flory, P.J., J. Amer. Chem. Soc., 1964, 86, 138.

97. Flory, P.J., Crescenzi, V. and Mark, J.E., J. Amer. Chem., 1964, 86, 146.

98. Mark, J.E. and Flory, P.J., J. Appl. Phys., 1966, 37, 4635.

99. Vailles, E.M. and Macosco, C.W., Makromolecules, 1979, 12, 673; Rubber Chem. Technol., 1978, 49, 1232.

100. Andrady, A.L., Llorente, M.A., Sharab, M.A., Rahalkar, R.R., Mark, J.E., Sullivan, J.L., Yu, C.U. and Falender, J.R., J. Appl. Polym. Sci., 1981, 26, 1829.

101. Andrady, A.L., Llorente, M.A. and Mark, J.E., J. Chem. Phys., 1980, 72,2282.

102. Andrady, A.L., Llorente, M.A. and Mark, J.E., ibid., 1980, 73, 1439.

103. Falender, J.R., Yeh, G.S.Y. and Mark, J.E., Makromolecules, 1979, 12, 1207.

104. Falender, J.R., Yeh, G.S.Y. and Mark, J.E., J. Am. Chem. Soc., 1979, 101, 7353.

105. Flory, P.J., Proc. Roy. Soc., 1976, A-351, 351.

106. Stepto, R.F.T., Private communication.

107. Volkenstein, M.V., 'Configurational Statistics of Polymer Chains', N.Y. Interscience, 1963 (Translated from the Russian edition by S.N. Timasheff and M.J. Timasheff).

108. Eichinger, B., Makromolecules, 1972, 5, 496.

109. Fasina, A.B. and Stepto, R.F.T., Makromol. Chem., 1981, 182, 2479.

110. Mooney, M., J. Appl. Phys., 1940, 11, 582;
1948, 19, 434.

111. Grumbell, S.M., Mullins, L. and Rivlin, R.S., Trans. Faraday Soc., 1953, 49, 1495.

112. Ciferri, A. and Flory, P.J., J. Appl. Phys., 1959, 30, 1498.

113. Mullins, L., J. Appl. Polym. Sci., 1959, 2, 257.

114. Ciferri, A., J. Polym. Sci., 1961, 54, 149.

115. Green, A. and Ciferri, A., Kolloid. Z., 1962, 186, 1.

116. Smith Jr., K.J., Green, A. and Ciferri, A., ibid., 1964, 194, 49.

117. Krans, G. and Maczygemta, G.A., J. Polym. Sci., 1964, A-2, 277.

118. Booth, C., Gee, G., Holden, G. and Williamson, G.R., Polymer, 1964, 5, 343.

119. Rivlin, R.S., Phil. Trans. Roy. Soc., 1948, A-241, 379.

120. Mark, J.E., Rubber Chem. Technol., 1975, 48, 495.

121. Flory, P. J., Polymer, 1979, 20, 1317.

122. Lipatov, Y., Adv. Polym. Sci., 1978, 26, 64.

123. Doolittle, A.K. and Doolittle, D.B., J. Appl. Phys., 1957, 28, 901.

124. Ferry, J.D., 'Viscoelastic Properties of Polymers', Wiley, N.Y., 2nd edn., 1970, p-308.

125. Baykam, C., Ph.D. Thesis, University of Manchester (1983).

126. Shibayama, K., Progr. in Org. Coatings, 1975, 3, 245.

127. Stepto, R.F.T., Polymer, 1979, 20, 1324.

128. Stanford, J.L., Stepto, R.F.T. and Still, R.H., in 'Reaction Injection Moulding and Fast Polymerisation Reactions' - Kresta, J.E., ed., Plenum Publ. Co., N.Y., 1982, p-31.

129. Shibayama, K. and Suzuki, V., J. Polym. Sci., 1965, A-3, 2637.

130. Shibayama, K. and Kodama, M., J. Polym. Sci., 1966, A-1, 83.

131. Katz, D. and Zewi, I.G., J. Polym. Sci. (Chem.), 1978, 16, 597.

132. McCrum, N.G., Read, B.E. and Williams, G., 'Anelastic and Dielectric Effects in Polymeric Solids' - Wiley, N.Y. (1967).

133. Nielsen, L.E., 'Mechanical Properties of Polymers and Composites' - Mercel-Dekker Inc., N.Y. (1974).

134. Bates, R.F., Ph.D. Thesis, University of Manchester (1965).

135. Geary, A., Lowry, H.V. and Hayden, H.A., 'Advanced Mathematics for Technical Students' - Part-I, Longmans Green and Co., London, 1952, p-337.

136. Heijboer, J., Dekking, P. and Staverman, A.J. in Harrison, V.G.W. (ed.), Proc. 2nd Intern. Congr. Rheology, Adademic, N.Y., p-123 (1953)

137. Read, B.E. and Dean, G.D., 'The Determination of Dynamic Properties of Polymers and Composites' - Hilger, Bristol, 1978.

138. Soto-Alvarez, R.A., Ph.D. Thesis, University of Manchester (1983).

139. Treloar, L.R.G., Trans. Faraday Soc., 1944, 40, 59.

140. Cluff, E.F., Gladding, E.K. and Pariser, R., J. Polym. Sci., 1960, 45, 341.

141. Van der Kraats, E.J., Potters, J.J.M., Winkeler, M.A.M. and Prins, W., Rec. Trav. Chim., 1969, 88, 449.

142. Stanford, J.L., Stepto, R.F.T. and Still, R.H., ACS Symp. Series 243, 'Characterisation of Highly Cross-linked Polymers' - eds. Dickie, P.A. and Labana, S.S., Am. Chem. Soc., Washington D.C., 1984, p-1.

143. Chompff, A.J. in 'Polymer Networks: Structure and Mechanical Properties' - Plenum, N.Y. (1971), p-145.

APPENDIX-A

The densities of the materials were calculated from their values at 25°C from the following equation:

$$d_t = d_{25} - \alpha(t - 25)$$

where α is the coefficient of cubical expansion

Material	d_{25} (gcm^{-3})	d_{80}(gcm^{-3})	α($gcm^{-3}deg^{-1}$)
LG 56	1.0072*	0.9797	$0.5x10^{-3}$***
HDI	1.0341*	0.9791	$1.0x10^{-3}$***
Toluene	0.8623**	0.8128	$0.9x10^{-3}$**

* Manufacturers' data

** International Critical Tables of Numerical Data: Physics Chemistry and Technology, vol. 3 (1928)

*** Ahmad, Z., Ph.D. thesis, University of Manchester (1977)

APPENDIX-B

Kinetics and Gelation Data

Symbols

a = Initial isocyanate concentration, $(NCO)_o$

b = Initial hydroxyl concentration $(OH)_o$

a-x = Isocyanate concentration at time t, (NCO)

b-x = Hydroxyl concentration at time t, (OH)

x = Polyurethane concentration at time t,

t_c = Gel time

Expt. 1.1 (Bulk, uncatalysed)

a = 0.9248 equiv.kg^{-1}
b = 0.9222 "

Time (mins)	x (equiv.kg^{-1})	x/a(a-x) (kg equiv^{-1})
240	0.1169	0.1565
1140	0.3559	0.6764
1440	0.4139	0.8760
1680	0.4581	0.0613
2580	0.5860	1.8705
2880	0.6146	2.1423
3120	0.6157	2.1536
3360	0.6504	2.5629
3720	0.6770	2.9708
4020	0.6951	3.2722
4140	0.7025	3.4171

t_c = 4410 mins

Expt. 1.2 (Bulk, 5% DABCO)

a = 0.9188 equiv.kg^{-1}
b = 0.9176 "

Time (mins)	x (equiv.kg^{-1})	x/a(a-x) (kg equiv^{-1})
30	0.2230	0.3489
80	0.4012	0.8435
120	0.4910	1.2490
160	0.5517	1.6359
200	0.6017	2.0654
240	0.6336	2.4176
270	0.6544	2.6934
300	0.6748	3.0109
335	0.6939	3.3575
365	0.7060	3.6104

t_c = 388 mins

Expt. 1.3 (Bulk, 10% DABCO)

a = 0.9193 equiv.kg^{-1}
b = 0.9170 "

Time (mins)	x (equiv.kg^{-1})	x/a(a-x) (kg equiv^{-1})
15	0.2083	0.3187
45	0.4120	0.8834
65	0.4980	1.2858
85	0.5573	1.6746
100	0.5969	2.0139
120	0.6323	2.3965
140	0.6649	2.8430
155	0.6818	3.1192
170	0.6960	3.3905
190	0.7191	3.9203

t_c = 206 mins

Expt. 1.4 (Bulk, 15% DABCO)

a = 0.9334 equiv.kg^{-1}
b = 0.9081 "

Time (mins)	x (equiv.kg^{-1})	$\frac{1}{a-b} \ln \frac{b}{a} \cdot \frac{(a-x)}{b-x}$ (kg equiv^{-1})
10	0.1964	0.2950
25	0.3702	0.7295
35	0.4491	1.0324
46	0.5051	1.3180
60	0.5687	1.7562
70	0.6034	2.0676
85	0.6452	2.5500
105	0.6575	2.7140
125	0.7100	3.6662

t_c = 144 mins

Expt. 1.5 (Bulk, 20% DABCO)

a = 0.9092 equiv.kg^{-1}
b = 0.9077 "

Time (mins)	x (equiv.kg^{-1})	x/a(a-x) (kg equiv^{-1})
5	0.1493	0.2162
15	0.3210	0.6001
25	0.4324	0.9975
35	0.5071	1.3874
45	0.5593	1.7580
55	0.6029	2.1655
65	0.6375	2.5804
75	0.6635	2.9699
87	0.6868	3.3968
99	0.7116	3.9616

t_c = 106 mins

Expt. 2.1 (16.7% ϕ NO_2, uncatalysed)

a = 0.7734 equiv.kg^{-1}
b = 0.7722 "

Time (mins)	x (equiv.kg^{-1})	x/a(a-x) (kg equiv^{-1})
210	0.0569	0.1028
1050	0.1948	0.4352
1350	0.2409	0.5848
1650	0.2876	0.7653
2460	0.3865	1.2918
2760	0.4183	1.5234
3060	0.4537	1.8346
3900	0.5106	2.5123
4500	0.5490	3.1629
4950	0.5720	3.6722
5790	0.6015	4.5233

t_c = 6000 mins

Expt. 2.2 (16.7% ϕ NO_2, 5% DABCO)

a = 0.7696 equiv.kg^{-1}
b = 0.7677 "

Time (mins)	x (equiv.kg^{-1})	x/a(a-x) (kg equiv^{-1})
20	0.0945	0.1819
50	0.2047	0.4708
90	0.3023	0.8406
140	0.3879	1.3205
200	0.4538	1.8672
260	0.4978	2.3798
320	0.5416	3.0866
390	0.5710	3.7359
450	0.5934	4.3760
495	0.6056	4.8011

t_c = 515 mins

Expt. 2.3 (16.7% ϕ NO_2, 10% DABCO)

a = 0.7616 equiv.kg^{-1}
b = 0.7622 "

Time (mins)	x (equiv.kg^{-1})	x/a(a-x) (kg equiv^{-1})
15	0.1321	0.2755
40	0.2761	0.7467
70	0.3983	1.4395
110	0.4634	2.0404
155	0.5266	2.9423
190	0.5555	3.5390
210	0.5739	4.0146
225	0.5846	4.3367
240	0.5965	4.7439
250	0.5971	4.7689

t_c = 270 mins

Expt. 2.4 (16.7% ϕ NO_2, 20% DABCO)

a = 0.7562 equiv.kg^{-1}
b = 0.7536 "

Time (mins)	x (equiv.kg^{-1})	x/a(a-x) ($_{-1}$) (kg equiv^{-1})
10	0.1629	0.3631
20	0.2699	0.7339
35	0.3703	1.2689
50	0.4386	0.8268
65	0.4876	2.4006
80	0.5209	2.9275
95	0.5491	3.5062
110	0.5683	3.9996
125	0.5881	4.6264
140	0.6062	5.3442

t_c = 150 mins

Expt. 3.1 (37.5% ϕ NO_2, uncatalysed)

a = 0.5785 equiv.kg^{-1}
b = 0.5789 "

Time (mins)	x (equiv.kg^{-1})	x/a(a-x) ($_{-1}$) (kg equiv^{-1})
300	0.0266	0.0834
1260	0.0903	0.3198
1740	0.1301	0.5015
2760	0.1955	0.8825
4140	0.2842	1.6701
4980	0.3222	2.1732
6000	0.3595	2.8385
7440	0.4031	3.9725
8940	0.4400	5.4911
9600	0.4566	6.4722
9840	0.4618	6.8412

t_c = 10,020 mins

Expt. 3.2 (37.5% ϕ NO_2, 10% DABCO)

a = equiv.kg^{-1}
b = "

Time (mins)	x (equiv.kg^{-1})	x/a(a-x) ($_{-1}$) (kg equiv^{-1})
30	0.1275	0.4965
65	0.2115	1.0144
100	0.2746	1.5943
140	0.3244	2.2577
180	0.3575	2.8690
220	0.3858	3.5588
260	0.4082	4.2726
300	0.4247	4.9349
340	0.4382	5.5961
380	0.4500	6.2965
420	0.4604	7.0236

t_c = 440 mins

Expt. 3.3 (37.5% ϕ NO_2, 15% DABCO)

a = equiv.kg^{-1}
b = "

Time (mins)	x (equiv.kg^{-1})	x/a(a-x) ($_{-1}$) (kg equiv^{-1})
20	0.1224	0.4737
45	0.2132	1.0332
75	0.2814	1.6830
110	0.3387	2.5198
145	0.3739	3.2730
180	0.4052	4.2078
210	0.4206	4.8085
240	0.4391	5.7125
270	0.5432	6.5887
310	0.4654	7.5318

t_c = 316 mins

Expt. 3.4 (37.5% ϕNO_2, 20% DABCO)

a = 0.5656 equiv.kg^{-1}
b = 0.5671 "

Time (mins)	x (equiv.kg^{-1})	x/a(a-x)$_{-1}$ (kg equiv^{-1})
30	0.1974	0.9479
60	0.2909	1.8723
105	0.3672	3.2723
165	0.4218	5.1861
226	0.4567	7.4147
240	0.4617	7.8566

t_c = 244 mins

Expt. 4.1 (16.7% ϕCH_3, uncatalysed)

a = 0.7822 equiv.kg^{-1}
b = 0.7816 "

Time (mins)	x (equiv.kg^{-1})	x/a(a-x)$_{-1}$ (kg equiv^{-1})
300	0.0581	0.1026
1200	0.2003	0.4402
1680	0.2766	0.6995
2700	0.4052	1.3738
3120	0.4443	1.6807
4140	0.5171	2.4942
4620	0.5402	2.8536
5100	0.5723	3.4865
5400	0.5873	3.8537
5580	0.5968	4.1151

t_c = 5,850 mins

Expt. 4.2 (16.7% ϕCH_3, 5% DABCO)

a = 0.7664 equiv.kg^{-1}
b = 0.7680 "

Time (mins)	x (equiv.kg^{-1})	x/a(a-x)$_{-1}$ (kg equiv^{-1})
30	0.1603	0.3451
60	0.2129	0.5019
120	0.3360	0.0188
180	0.4150	1.5409
240	0.4696	2.0645
300	0.5118	2.6229
360	0.5418	3.1475
420	0.5678	3.7304
480	0.5871	4.2724
540	0.6058	4.9218

t_c = 561 mins

Expt. 4.3 (16.7% ϕCH_3, 10% DABCO)

a = 0.7678 equiv.kg^{-1}
b = 0.7640 "

Time (mins)	x (equiv.kg^{-1})	x/a(a-x)$_{-1}$ (kg equiv^{-1})
25	0.1829	0.4073
60	0.3328	0.9964
91	0.4140	1.5245
120	0.4659	2.0099
150	0.5047	2.4994
180	0.5353	2.9986
205	0.5575	3.4527
225	0.5696	3.7430
250	0.5828	4.1921
280	0.6032	4.7729

t_c = 297 mins

Expt. 4.4 (16.7% ϕCH_3, 20% DABCO)

a = 0.7609 equiv.kg^{-1}
b = 0.7562 "

Time (mins)	x (equiv.kg^{-1})	x/a(a-x) (kg equiv^{-1})
20	0.2640	0.6982
45	0.4046	1.4924
60	0.4552	1.9569
75	0.4938	2.4306
90	0.5231	2.8920
105	0.5487	3.3983
120	0.5697	3.9159
135	0.5850	4.3708
150	0.5981	4.8283
160	0.6089	5.2647

t_c = 162 mins

Expt. 5.1 (37.5% ϕCH_3, uncatalysed)

a = 0.5768 equiv.kg^{-1}
b = 0.5765 "

Time (mins)	x (equiv.kg^{-1})	x/a(a-x) (kg equiv^{-1})
360	0.0307	0.0975
1320	0.0956	0.3443
1800	0.1261	0.4850
3000	0.1995	0.9164
4200	0.2645	1.4688
5700	0.3244	2.2282
6600	0.3481	2.6384
7740	0.3774	3.2810
9180	0.4102	4.2687
10620	0.4258	4.8893
11400	0.4422	5.6967

t_c = 11,880 mins

Expt. 5.2 (37.5% ϕCH_3, 5% DABCO)

a = 0.5735 equiv.kg^{-1}
b = 0.5736 "

Time (mins)	x (equiv.kg^{-1})	x/a(a-x) (kg equiv^{-1})
90	0.1210	0.4665
180	0.1987	0.9245
300	0.2677	1.5265
420	0.3153	2.1300
540	0.3490	2.7110
660	0.3805	3.4391
780	0.4017	4.0778
900	0.4222	4.8663
1020	0.4319	5.3187
1080	0.4400	5.7449
1200	0.4482	6.2400

t_c = 1290 mins

Expt. 5.3 (37.5% ϕCH_3, 10% DABCO)

a = 0.5752 equiv.kg^{-1}
b = 0.5730 "

Time (mins)	x (equiv.kg^{-1})	x/a(a-x) (kg equiv^{-1})
30	0.0927	0.3340
60	0.1597	0.6682
120	0.2485	1.3224
180	0.3062	1.9789
240	0.3478	2.6602
300	0.3793	3.3661
360	0.3999	3.9660
420	0.4206	4.7298
480	0.4331	5.2988
540	0.4482	6.1403
600	0.4602	6.9571

t_c = 625 mins

Expt. 5.4 (37.5% ϕ CH_3, 20% DABCO)

a = 0.5709 equiv.kg^{-1}
b = 0.5669 "

Time (mins)	x (equiv.kg^{-1})	x/a(a-x) ($kg\ equiv^{-1}$)
15	0.0916	0.3347
35	0.1736	0.7654
65	0.2513	1.3773
90	0.2973	1.9033
120	0.3362	2.5091
180	0.3875	3.6950
210	0.4093	4.4365
240	0.4251	5.1071
280	0.4386	5.8069
330	0.4590	7.1849

t_c = 340 mins

Expt. 6.1 (Bulk, uncatalysed)

a = 0.9248 equiv.kg^{-1}
b = 0.9222 "

Time (mins)	x (equiv.kg^{-1})	x/a(a-x) ($kg\ equiv^{-1}$)
240	0.1169	0.1565
1140	0.3559	0.6764
1440	0.4139	0.8760
1680	0.4581	1.0613
2580	0.5860	1.8705
2880	0.6146	2.1423
3120	0.6157	2.1536
3360	0.6504	2.5629
3720	0.6780	2.9708
4020	0.6951	3.2722
4140	0.7025	3.4171

t_c = 4,410 mins

Expt. 6.2 (9.1% ϕ CH_3, uncatalysed)

a = 0.8378 equiv.kg^{-1}
b = 0.8387 "

Time (mins)	x (equiv.kg^{-1})	x/a(a-x) ($kg\ equiv^{-1}$)
240	0.0737	0.1151
1140	0.2628	0.5456
1440	0.3095	0.6992
1800	0.3732	0.9586
2220	0.4271	1.2414
3060	0.5180	1.9334
3360	0.5392	2.1554
3660	0.5633	2.4498
4500	0.6150	3.2946
4920	0.6334	3.6979
5100	0.6429	3.9367

t_c = 5,370 mins

Expt. 6.3 (20% ϕ CH_3, uncatalysed)

Time (mins)	x (equiv.kg^{-1})	x/a(a-x) ($kg\ equiv^{-1}$)
240	0.0560	0.1113
1170	0.1790	0.4338
1680	0.2245	0.5924
2220	0.3066	0.9627
3180	0.3961	1.5689
3660	0.4287	1.8776
4560	0.4841	2.5831
5100	0.5073	2.9778
6060	0.5435	3.7838
6480	0.5560	4.1375
6720	0.5643	4.3993

t_c = 7,100 mins

Expt. 6.4 (28.6% ϕ CH_3, uncatalysed)

a = 0.6586 (equiv.kg^{-1})
b = 0.6588 "

Time (mins)	x (equiv.kg^{-1})	x/a(a-x) ($_{-1}$) (kg equiv^{-1})
300	0.0460	0.1139
1320	0.1445	0.4268
1800	0.1875	0.6041
2880	0.2791	1.1170
3360	0.3097	1.3479
4320	0.3692	1.9372
4740	0.3871	2.1654
6000	0.4393	3.0410
7200	0.4706	3.8016
7620	0.4795	4.0658
8640	0.5024	4.8847
8820	0.5083	5.1332

t_c = 9,000 mins

Expt. 6.5 (37.5% ϕ CH_3, uncatalysed)

a = 0.5768 equiv.kg^{-1}
b = 0.5765 "

Time (mins)	x (equiv.kg^{-1})	x/a(a-x) ($_{-1}$) (kg equiv^{-1})
360	0.0307	0.0975
1320	0.0956	0.3443
1800	0.1261	0.4850
3000	0.1995	0.9164
4200	0.2645	1.4688
5700	0.3244	2.2282
6600	0.3481	2.6384
7740	0.3774	3.2810
9180	0.4102	4.2687
11400	0.4422	5.6967

t_c = 11,880 mins

Expt. 6.6 (44.4% ϕ CH_3, uncatalysed)

a = 0.5153 equiv.kg^{-1}
b = 0.5123 "

Time (mins)	x (equiv.kg^{-1})	x/a(a-x) ($_{-1}$) (kg equiv^{-1})
360	0.0212	0.0833
1500	0.0737	0.3239
3000	0.1379	0.7091
4380	0.1937	1.1688
5760	0.2447	1.7555
7290	0.2862	2.4253
10080	0.3416	3.8164
11580	0.3634	4.6427
12960	0.3835	5.2886
13380	0.3886	5.5374
14400	0.3990	6.2211

t_c = 14,640 mins

Expt. 6.7 (59.6% ϕ CH_3, uncatalysed)

a = 0.3717 equiv.kg^{-1}
b = 0.3724 "

Time (mins)	x (equiv.kg^{-1})	x/a(a-x) ($_{-1}$) (kg equiv^{-1})
1500	0.0269	0.2101
3300	0.0580	0.4972
4680	0.0788	0.7244
6180	0.1057	1.0686
9960	0.1651	2.1495
11880	0.1808	2.5486
13320	0.2019	3.1984
14700	0.2158	3.7224
16200	0.2288	4.3090
17700	0.2398	4.8895
19140	0.2469	5.3231
21600	0.2623	6.4554
25440	0.2834	8.6374
26520	0.2873	9.1591
27360	0.2911	9.7113

t_c = 27,600 mins

Expt. 6.8 (69.5% ϕCH_3, uncatalysed)

a = 0.2816 equiv.kg^{-1}
b = 0.2810 "

Time (mins)	x (equiv.kg^{-1})	x/a(a-x) (kg equiv^{-1})
1500	0.0068	0.0886
2940	0.0169	0.2275
5820	0.0391	0.5722
11100	0.0819	1.4575
15900	0.1146	2.4369
20100	0.1430	3.6629
25680	0.1642	4.9639
31380	0.1864	6.9549
36060	0.2016	8.9437
40320	0.2091	10.2401
44400	0.2163	11.7646
46560	0.2189	12.3889
48000	0.2216	13.1386

t_c = 48,660 mins

Expt. 7.1 (Bulk, 5% DABCO)

a = 0.9188 equiv.kg^{-1}
b = 0.9176 "

Time (mins)	x (equiv.kg^{-1})	x/a(a-x) (kg equiv^{-1})
30	0.2230	0.3489
80	0.4012	0.8435
120	0.4910	1.2490
160	0.5517	1.6359
200	0.6017	2.0654
240	0.6336	2.4176
270	0.6544	2.6934
300	0.6748	3.0109
335	0.6939	3.3575
365	0.7060	3.6104

t_c = 388 mins

Expt. 7.2 (9.1% ϕCH_3, 5% DABCO)

a = 0.8335 equiv.kg^{-1}
b = 0.8341 "

Time (mins)	x (equiv.kg^{-1})	x/a(a-x) (kg equiv^{-1})
30	0.1645	0.2950
75	0.3116	0.7165
120	0.3963	1.0875
180	0.4791	1.6222
225	0.5207	1.9977
270	0.5568	2.4149
315	0.5858	2.8372
360	0.6065	3.2048
405	0.6257	3.6123
450	0.6420	4.0223
480	0.6513	4.2879

t_c = 507 mins

Expt. 7.3 (20% ϕCH_3, 5% DABCO)

a = 0.7344 equiv.kg^{-1}
b = 0.7341 "

Time (mins)	x (equiv.kg^{-1})	x/a(a-x) (kg equiv^{-1})
60	0.1847	0.4575
150	0.3262	1.0882
210	0.3854	1.5036
300	0.4496	2.1494
390	0.4924	2.7707
450	0.4970	2.8517
510	0.5435	3.8758
570	0.5599	4.3697
630	0.5703	4.7322

t_c = 690 mins

Expt. 7.4 (28.6% ϕ CH_3, 5% DABCO)

a = 0.6540 equiv.kg^{-1}
b = 0.6556 "

Time (mins)	x (equiv.kg^{-1})	x/a(a-x) ($_{-1}$) (kg equiv^{-1})
90	0.1571	0.4834
180	0.2755	1.1130
270	0.3409	1.6645
360	0.3851	2.1900
450	0.4295	2.9254
570	0.4649	3.7603
660	0.4816	4.2715
780	0.5020	5.0513
840	0.5090	5.3703

t_c = 930 mins

Expt. 7.5 (37.5% ϕ CH_3, 5% DABCO)

a = 0.5735 equiv.kg^{-1}
b = 0.5736 "

Time (mins)	x (equiv.kg^{-1})	x/a(a-x) ($_{-1}$) (kg equiv^{-1})
90	0.1210	0.4654
180	0.1987	0.9245
300	0.2677	1.5265
420	0.3153	2.1300
540	0.3490	2.7110
660	0.3805	3.4391
780	0.4017	4.0778
900	0.4222	4.8663
1020	0.4319	5.3187
1080	0.4400	5.7449
1200	0.4482	6.2400

t_c = 1,290 mins

Expt 7.6 (44.4% ϕ CH_3, 5% DABCO)

a = 0.5093 equiv.kg^{-1}
b = 0.5098 "

Time (mins)	x (equiv.kg^{-1})	x/a(a-x) ($_{-1}$) (kg equiv^{-1})
120	0.1115	0.5506
300	0.2025	1.2958
420	0.2445	1.8125
600	0.2948	2.6981
780	0.3235	3.4189
960	0.3433	4.0625
1140	0.3684	5.1319
1320	0.3809	5.8231
1500	0.3964	6.8957
1620	0.4007	7.2445

t_c = 1,710 mins

Expt. 7.7 (59.5% ϕ CH_3, 5% DABCO)

a = 0.3740 equiv.kg^{-1}
b = 0.3718 "

Time (mins)	x (equiv.kg^{-1})	x/a(a-x) ($_{-1}$) (kg equiv^{-1})
240	0.0774	0.6977
480	0.1283	1.3962
1380	0.2275	4.1521
1620	0.2424	4.9250
1860	0.2506	5.4299
2040	0.2629	6.3271
2280	0.2704	6.9787
2460	0.2746	7.3940
2640	0.2824	8.2432
2880	0.2850	8.5621
3120	0.2954	10.0616
3300	0.2964	10.2128
3540	0.3005	10.9316

t_c = 3,580 mins

Expt. 7.8 (69.6% ϕCH_3, 5% DABCO)

a = 0.2796 equiv.kg^{-1}
b = 0.2792 "

Time(mins)	x (equiv.kg^{-1})	x/a(a-x)$_1$ (kg equiv^{-1})
360	0.0488	0.7562
1380	0.1289	3.0606
1800	0.1453	3.8675
2880	0.1815	6.6155
3240	0.1860	7.1136
4260	0.2074	10.2832
4740	0.2101	10.8164
5700	0.2185	12.7845
6180	0.2218	13.7162
6720	0.2250	14.7385
7260	0.2281	15.8033

t_c = 7,350 mins

APPENDIX-C

Calculation of Total Reactant Concentration at Gel ie. $(C_{ac} + C_{bc})$

Let initial conc. of isocyanate groups = a = C_{ao}

" " " hydroxyl " = b = C_{bo}

$$r = C_{ao}/C_{bo} \quad \ldots\ldots \text{(a)}$$ and extent of reaction = p;

$$p_{bc} = r\, p_{ac} \quad \ldots\ldots \text{(b)}$$

At gel, the extent of reaction of isocyanate groups

$$= p_{ac} = 1 - \frac{C_{ac}}{C_{ao}} \quad \ldots\ldots \text{(c)}$$

Similarly, the extent of reaction of hydroxyl groups

$$= p_{bc} = 1 - \frac{C_{bc}}{C_{bo}} \quad \ldots\ldots \text{(d)}$$

$$= r p_{ac}$$

Concentration of the reactants at gel = $C_{ac} + C_{bc}$

From (c) and (d), gel concentration

$$C_{ac} + C_{bc} = C_{bo}(1 - p_{bc}) + C_{ao}(1 - p_{ac})$$

$$= C_{bo}(1 - r p_{ac}) + C_{ao}(1 - p_{ac})$$

Since, $C_{bo} = C_{ao}/r$, $= \frac{C_{ao}}{r}(1 - r\, p_{ac}) + C_{ao}(1 - p_{ac})$

$$C_{ac} + C_{bc} = C_{ao}\left(1 - 2\, p_{ac} + \frac{1}{r}\right)$$

APPENDIX D

Uniaxial Compression Data at 27°C

Symbols:

h_o - Initial height measured by cathetometer

h_c - corrected height

r - radius of the sample

σ - compressive stress

Λ - compression ratio

G - shear modulus

$\bar{G}$ - Average shear modulus

Uniaxial Compression Data:

Expt. 6.1 (Dried samples): Bulk (uncatalysed)

Sample No.	1		2		3	
h_o/mm	9.70		9.72		9.750	
h_c/mm	9.67		9.70		9.738	
r/mm	5.922		5.80		5.78	
	$10^{-4}.\sigma$ /Nm^{-2}	Λ	$10^{-4}.\sigma$ /Nm^{-2}	Λ	$10^{-4}.\sigma$ /Nm^{-2}	Λ
	0.44	0.9978	0.46	0.9977	0.47	0.9979
	0.89	0.9938	0.93	0.9939	0.93	0.9951
	1.33	0.9903	1.39	0.9904	1.40	0.9926
	1.78	0.9873	1.86	0.9874	1.87	0.9901
	2.22	0.9846	2.32	0.9842	2.34	0.9875
	2.67	0.9817	2.78	0.9819	2.80	0.9845
	3.56	0.9762	3.71	0.9772	3.74	0.9803
	4.45	0.9716	4.64	0.9727	4.67	0.9754
	5.34	0.9671	5.57	0.9682	5.61	0.9703
	6.23	0.9630	6.50	0.9633	6.54	0.9655
	7.12	0.9588	7.42	0.9592	7.48	0.9614
	8.01	0.9547	8.35	0.9553	8.41	0.9572
	8.90	0.9501	9.28	0.9518	9.35	0.9530
	9.79	0.9462	10.21	0.9460	10.28	0.9489
	10.68	0.9425	11.14	0.9421	11.22	0.9448
	12.46	0.9338	12.99	0.9334	13.08	0.9366
	14.24	0.9263	14.83	0.9258	14.95	0.9291
	16.02	0.9187	16.71	0.9181	16.82	0.9212
	17.80	0.9109	18.56	0.9103	18.69	0.9136
	19.58	0.9033	20.42	0.9027	20.56	0.9059
$10^{-5}.G/Nm^{-2}$	5.863		6.104		6.463	
$10^{-5}.\bar{G}/Nm^{-2}$	6.143 ± 0.300					

Uniaxial Compression Data:

Expt. 6.2 (Dried sample): 9.1% toluene (uncatalysed)

Sample No.	1		2		3	
h_o/mm	9.300		9.190		9.210	
h_c/mm	9.285		9.177		9.202	
r/mm	5.93		6.01		5.935	
	$10^{-4}.\sigma/Nm^{-2}$	Λ	$10^{-4}.\sigma/Nm^{-2}$	Λ	$10^{-4}.\sigma/Nm^{-2}$	Λ
	0.44	0.9973	0.43	0.9973	0.44	0.9971
	0.89	0.9929	0.86	0.9935	0.89	0.9926
	1.33	0.9891	1.30	0.9896	1.33	0.9881
	1.77	0.9855	1.73	0.9860	1.77	0.9841
	2.22	0.9819	2,16	0.9823	2.22	0.9805
	2.66	0.9789	2.59	0.9787	2.66	0.9779
	3.55	0.9734	3.46	0.9724	3.54	0.9715
	4.44	0.9676	4.32	0.9662	4.43	0.9645
	5.33	0.9624	5.19	0.9604	5.32	0.9586
	6.21	0.9565	6.05	0.9546	6.20	0.9538
	7.10	0.9513	6.92	0.9494	7.09	0.9485
	7.99	0.9445	7.78	0.9445	7.98	0.9423
	8.88	0.9386	8.64	0.9397	8.86	0.9378
	9.77	0.9336	9.51	0.9351	9.75	0.9329
	10.65	0.9289	10.37	0.9304	10.64	0.9281
	12.43	0.9194	12.10	0.9211	12.41	0.9191
	14.21	0.9100	13.83	0.9115	14.18	0.9099
	15.98	0.9022	15.56	0.9018	15.96	0.9007
	17.76	0.8940	17.29	0.8925	17.73	0.8923
	19.53	0.8856	19.02	0.8841	19.50	0.8845
$10^{-5}.G/Nm^{-2}$	4.788		4.653		4.685	
$10^{-5}.\bar{G}/Nm^{-2}$	4.709 ± 0.067					

Uniaxial Compression Data:

Expt. 6.3 (Dried samples): 20% toluene (uncatalysed)

Sample No.	1		3		5	
h_o/mm	9.210		8.430		9.330	
h_c/mm	9.201		8.395		9.305	
r/mm	5.597		5.67		5.622	
	$10^{-4}.\sigma$ /Nm^{-2}	Λ	$10^{-4}.\sigma$ /Nm^{-2}	Λ	$10^{-4}.\sigma$ /Nm^{-2}	Λ
	0.50	0.9962	0.49	0.9962	0.48	0.9968
	0.97	0.9899	0.99	0.9907	0.97	0.9922
	1.49	0.9849	1.48	0.9852	1.44	0.9878
	1.99	0.9805	1.97	0.9810	1.94	0.9833
	2.49	0.9762	2.47	0.9767	2.43	0.9796
	2.99	0.9722	2.96	0.9726	2.91	0.9756
	3.99	0.9650	3.95	0.9664	3.88	0.9690
	4.98	0.9580	4.94	0.9589	4.85	0.9611
	5.98	0.9516	5.93	0.9527	5.83	0.9552
	6.98	0.9436	6.91	0.9462	6.80	0.9485
	7.97	0.9371	7.90	0.9401	7.77	0.9420
	8.97	0.9309	8.89	0.9338	8.74	0.9359
	9.97	0.9254	9.88	0.9277	9.71	0.9302
	10.96	0.9196	10.96	0.9210	10.68	0.9245
	11.96	0.9142	11.85	0.9155	11.65	0.9190
	13.95	0.9022	13.83	0.9021	13.60	0.9074
	15.94	0.8917	15.80	0.8919	15.54	0.8973
	17.94	0.8814	17.78	0.8823	17.48	0.8869
	19.93	0.8716	19.76	0.8717	19.42	0.8772
	21.92	0.8622	21.73	0.8624	21.37	0.8676
$10^{-5}.G/Nm^{-2}$	4.468		4.386		4.321	
$10^{-5}.\bar{G}/Nm^{-2}$	4.392 ± 0.073					

Uniaxial Compression Data:

Expt. 6.4 (Dried) 28.6% toluene (uncatalysed)

Sample No.	1		2		3	
h_o/mm	8.910		8.820		8.92	
h_c/mm	8.895		8.801		8.90	
r/mm	5.347		5.355		5.317	
	$10^{-4}.\sigma$/Nm^{-2}	Λ	$10^{-4}.\sigma$/Nm^{-2}	Λ	$10^{-4}.\sigma$/Nm^{-2}	Λ
	0.54	0.9973	0.54	0.9972	0.55	0.9974
	1.09	0.9931	1.09	0.9924	1.10	0.9935
	1.64	0.9893	1.63	0.9887	1.66	0.9898
	2.18	0.9861	2.18	0.9852	2.21	0.9868
	2.73	0.9830	2.72	0.9814	2.76	0.9833
	3.27	0.9802	3.27	0.9782	3.31	0.9804
	4.37	0.9741	4.35	0.9725	4.42	0.9748
	5.46	0.9683	5.44	0.9664	5.52	0.9688
	6.55	0.9611	6.53	0.9612	6.63	0.9633
	7.64	0.9558	7.62	0.9560	7.73	0.9581
	8.73	0.9506	8.71	0.9510	8.83	0.9525
	9.83	0.9456	9.80	0.9454	9.94	0.9474
	10.92	0.9399	10.89	0.9390	11.04	0.9421
	12.01	0.9348	11.98	0.9339	12.15	0.9369
	13.10	0.9292	13.07	0.9289	13.25	0.9314
	15.29	0.9190	15.24	0.9200	15.46	0.9211
	17.47	0.9099	17.42	0.9107	17.67	0.9109
	19.65	0.9011	19.60	0.9013	19.88	0.9021
	21.84	0.8919	21.78	0.8917	22.09	0.8928
	24.02	0.8836	23.96	0.8831	24.29	0.8845
$10^{-5}.G$/Nm^{-2}	5.852		5.820		6.042	
$10^{-5}.\bar{G}$/Nm^{-2}	5.905 ± 0.111					

Uniaxial Compression Data:

Expt. 6.5 (Dried 37.5% toluene (uncatalysed)

Sample No.	1		3		6	
h_o/mm	8.110		7.910		8.190	
h_c/mm	8.075		7.882		8.167	
r/mm	5.257		5.21		5.152	
	$10^{-4}.\sigma/Nm^{-2}$	Λ	$10^{-4}.\sigma/Nm^{-2}$	Λ	$10^{-4}.\sigma/Nm^{-2}$	Λ
	0.56	0.9964	0.57	0.9963	0.59	0.9958
	1.13	0.9902	1.15	0.9900	1.18	0.9884
	1.69	0.9845	1.72	0.9841	1.76	0.9822
	2.26	0.9798	2.30	0.9790	2.35	0.9864
	2.82	0.9754	2.87	0.9746	2.94	0.9717
	3.39	0.9717	3.45	0.9709	3.53	0.9678
	4.52	0.9652	4.60	0.9646	4.70	0.9610
	5.65	0.9591	5.75	0.9584	5.88	0.9530
	6.78	0.9523	6.90	0.9524	7.06	0.9454
	7.91	0.9464	8.05	0.9459	8.23	0.9393
	9.04	0.9397	9.20	0.9399	9.41	0.9319
	10.17	0.9335	10.35	0.9338	10.58	0.9252
	11.30	0.9276	11.50	0.9281	11.76	0.9184
	12.43	0.9223	12.65	0.9218	12.94	0.9124
	13.56	0.9173	13.80	0.9155	14.11	0.9068
	15.81	0.9078	16.16	0.9054	16.47	0.8954
	18.07	0.8982	18.41	0.8960	18.82	0.8839
	20.33	0.8882	20.71	0.8864	21.17	0.8732
	22.59	0.8781	23.01	0.8772	23.52	0.8626
	24.85	0.8699	25.31	0.8682	25.88	0.8527
$10^{-5}.G/Nm^{-2}$	5.153		5.175		4.666	
$10^{-5}.\bar{G}/Nm^{-2}$	4.998 ± 0.254					

Uniaxial Compression Data:

Expt. 6.6 (dried) 44.4% toluene (uncatalysed)

Sample No.	1		2		7	
h_o/mm	7.680		7.580		7.8000	
h_c/mm	7.645		7.552		7.7768	
r/mm	5.225		5.065		5.08	
	$10^{-4}.\sigma/Nm^{-2}$	Λ	$10^{-4}.\sigma/Nm^{-2}$	Λ	$10^{-4}.\sigma/Nm^{-2}$	Λ
	0.57	0.9963	0.61	0.9962	0.60	0.9963
	1.14	0.9900	1.22	0.9902	1.21	0.9899
	1.71	0.9839	1.82	0.9844	1.81	0.9851
	2.29	0.9788	2.43	0.9800	2.42	0.9799
	2.86	0.9746	3.04	0.9748	3.02	0.9754
	3.43	0.9706	3.65	0.9702	3.63	0.9708
	4.57	0.9617	4.87	0.9630	4.84	0.9633
	5.72	0.9551	6.08	0.9566	6.05	0.9569
	6.86	0.9481	7.30	0.9489	7.26	0.9509
	8.01	0.9417	8.52	0.9421	8.47	0.9445
	9.15	0.9335	9.74	0.9331	9.68	0.9377
	10.29	0.9271	10.95	0.9256	10.89	0.9320
	11.44	0.9214	12.17	0.9193	12.10	0.9265
	12.58	0.9158	13.39	0.9138	13.31	0.9210
	13.72	0.9105	14.61	0.9085	14.52	0.9155
	16.01	0.8999	17.04	0.8979	16.94	0.9041
	18.30	0.8892	19.47	0.8879	19.36	0.8931
	20.59	0.8795	21.81	0.8781	21.78	0.8829
	22.87	0.8700	24.34	0.8687	24.20	0.8731
	25.16	0.8607	26.78	0.8594	26.62	0.8637
$10^{-5}.G/Nm^{-2}$	4.788		5.032		5.293	
$10^{-5}.\bar{G}/Nm^{-2}$	5.037 ± 0.252					

Uniaxial Compression Data:

Expt. 6.7 (Dried 59.6% toluene (uncatalysed)

Sample No.	1		2		4	
h_o/mm	7.13		7.230		6.68	
h_c/mm	7.10		7.211		6.64	
r/mm	4.375		4.455		4.407	
	$10^{-4}.\sigma/Nm^{-2}$	Λ	$10^{-4}.\sigma/Nm^{-2}$	Λ	$10^{-4}.\sigma/Nm^{-2}$	Λ
	0.81	0.9937	0.79	0.9937	0.80	0.9940
	1.63	0.9850	1.57	0.9847	1.61	0.9849
	2.45	0.9765	2.36	0.9750	2.41	0.9769
	3.26	0.9686	3.15	0.9680	3.21	0.9690
	4.08	0.9609	3.93	0.9612	4.02	0.9619
	4.89	0.9521	4.72	0.9551	4.82	0.9554
	6.52	0.9399	6.29	0.9426	6.43	0.9440
	8.16	0.9275	7.87	0.9304	8.04	0.9302
	9.79	0.9153	9.44	0.9185	9.64	0.9184
	11.42	0.9038	11.01	0.9059	11.25	0.9070
	13.05	0.8932	12.59	0.8958	12.86	0.8940
	14.68	0.8825	14.16	0.8858	14.47	0.8807
	16.31	0.8715	15.73	0.8752	16.07	0.8700
	17.94	0.8618	17.31	0.8652	17.68	0.8600
	19.58	0.8514	18.88	0.8555	19.29	0.8505
	22.84	0.8324	22.03	0.8362	22.50	0.8321
	26.10	0.8143	25.17	0.8183	25.72	0.8148
	29.36	0.7968	28.32	0.8012	28.93	0.7978
	32.63	0.7796	31.47	0.7846	32.15	0.7805
	35.89	0.7635	34.61	0.7688	35.36	0.7642
$10^{-5}.G/Nm^{-2}$	3.725		3.702		3.684	
$10^{-5}.\bar{G}/Nm^{-2}$	3.704 ± 0.020					

Uniaxial Compression Data:

Expt. 6.8 (Dried) 69.5% toluene (uncatalysed)

Sample No.	1		2		4	
h_o/mm	6.70		6.640		6.04	
h_c/mm	6.67		6.612		6.00	
r/mm	3.917		4.052		3.957	
	$10^{-4}.\sigma/Nm^{-2}$	Λ	$10^{-4}.\sigma/Nm^{-2}$	Λ	$10^{-4}.\sigma/Nm^{-2}$	Λ
	1.02	0.9903	0.95	0.9895	1.00	0.9897
	2.03	0.9757	1.90	0.9741	1.99	0.9752
	3.05	0.9625	2.85	0.9612	2.99	0.9631
	4.07	0.9504	3.80	0.9489	3.99	0.9513
	5.07	0.9369	4.75	0.9382	4.98	0.9392
	6.10	0.9269	5.70	0.9281	5.98	0.9283
	8.14	0.9068	7.60	0.9077	7.97	0.9101
	10.17	0.8869	9.51	0.8903	9.97	0.8894
	12.21	0.8707	11.41	0.8716	11.96	0.8745
	14.24	0.8557	13.31	0.8551	13.96	0.8591
	16.28	0.8365	15.21	0.8387	15.95	0.8435
	18.31	0.8223	17.11	0.8247	17.94	0.8288
	20.35	0.8097	19.01	0.8125	19.94	0.8158
	22.38	0.7977	20.9.	0.7989	21.93	0.8029
	24.42	0.7864	22.82	0.7867	23.92	0.7897
	28.48	0.7636	26.62	0.7634	27.91	0.7654
	32.55	0.7380	30.42	0.7402	31.9L	0.7408
	36.62	0.7180	34.22	0.7192	35.89	0.7191
	40.69	0.6985	38.03	0.6993	39.87	0.6983
	44.76	0.6794	41.83	0.6810	43.86	0.6783
$10^{-5}.G/Nm^{-2}$	2.943		2.771		2.921	
$10^{-5}.\bar{G}/Nm^{-2}$	2.878 ± 0.086					

Uniaxial Compression Data:

Expt. 7.1 (Dried Samples) Bulk (5% DABCO)

Sample No.	$\overline{1}$		$\overline{2}$		$\overline{3}$	
h_o/mm	10.0000		10.00		10.300	
h_c/mm	9.9875		9.98		10.282	
r/mm	6.11		6.047		6.032	
	$10^{-4}.\sigma/Nm^{-2}$	Λ	$10^{-4}.\sigma/Nm^{-2}$	Λ	$10^{-4}.\sigma/Nm^{-2}$	Λ
	0.42	0.9978	0.43	0.9981	0.43	0.9981
	0.84	0.9942	0.85	0.9950	0.86	0.9954
	1.25	0.9914	1.28	0.9918	1.29	0.9924
	1.67	0.9882	1.71	0.9889	1.72	0.9901
	2.09	0.9857	2.13	0.9864	2.14	0.9875
	2.51	0.9831	2.56	0.9842	2.57	0.9852
	3.34	0.9783	3.41	0.9793	3.43	0.9810
	4.18	0.9738	4.27	0.9752	4.29	0.9766
	5.02	0.9698	5.12	0.9708	5.15	0.9725
	5.85	0.9661	5.98	0.9670	6.01	0.9684
	6.69	0.9608	6.83	0.9635	6.86	0.9645
	7,53	0.9573.	7.68	0.9595	7.72	0.9610
	8.36	0.9535	8.54	0.9555	8.58	0.9575
	9.20	0.9499	9.39	0.9522	9.44	0.9540
	10.04	0.9466	10.25	0.9475	10.30	0.9502
	11.71	0.9395	11.95	0.9410	12.01	0.9425
	13.38	0.9327	13.66	0.9341	13.73	0.9355
	15.05	0.9252	15.37	0.9271	15.44	0.9290
	16.73	0.9188	17.08	0.9202	17.16	0.9225
	18.40	0.9124	18.78	0.9136	18.88	0.9158
$10^{-5}.G/Nm^{-2}$	6.038		6.349		6.607	
$10^{-5}.\bar{G}/Nm^{-2}$	6.331 ± 0.284					

Uniaxial Compression Data:

Expt. 7.2 (Dried Samples) 9.1% toluene (5% DABCO)

Sample No.	1		2		3	
h_o/mm	9.650		9.56		9.5100	
h_c/mm	9.633		9.56		9.4909	
r/mm	5.825		5.862		5.792	
	$10^{-4}.\sigma/Nm^{-2}$	Λ	$10^{-4}.\sigma/Nm^{-2}$	Λ	$10^{-4}.\sigma/Nm^{-2}$	Λ
	0.46	0.9976	0.45	0.9958	0.46	0.9979
	0.92	0.9936	0.91	0.9923	0.93	0.9939
	1.38	0.9901	1.36	0.9889	1.39	0.9878
	1.84	0.9872	1.82	0.9855	1.86	0.9863
	2.30	0.9839	2.27	0.9826	2.33	0.9834
	2.76	0.9813	2.72	0.9800	2.79	0.9808
	3.68	0.9765	3.63	0.9753	3.72	0.9761
	4.60	0.9719	4.54	0.9711	4.65	0.9712
	5.52	0.9681	5.45	0.9670	5.58	0.9672
	6.44	0.9637	6.36	0.9631	6.51	0.9630
	7.36	0.9596	7.27	0.9593	7.44	0.9576
	8.28	0.9553	8.18	0.9557	8.37	0.9536
	9.20	0.9512	9.08	0.9522	9.31	0.9499
	10.12	0.9476	9.99	0.9482	10.24	0.9460
	11.04	0.9435	10.90	0.9443	11.17	0.9422
	12.88	0.9361	12.72	0.9357	13.03	0.9344
	14.72	0.9280	14.54	0.9287	14.89	0.9270
	16.56	0.9207	16.35	0.9217	16.75	0.9204
	18.40	0.9138	18.17	0.9155	18.61	0.9134
	20.25	0.9074	19.99	0.9081	20.47	0.9069
$10^{-5}.G/Nm^{-2}$	6.247		6.260		6.208	
$10^{-5}.\bar{G}/Nm^{-2}$	6.239 ± 0.026					

Uniaxial Compression Data:

Expt. 7.3 (Dried Samples) 20.0% toluene (5% DABCO)

Sample No.	1		2		3	
h_o/mm	9.18		9.1300		9.230	
h_c/mm	9.16		9.1155		9.215	
r/mm	5.555		5.54		5.56	
	$10^{-4}.\sigma$/Nm^{-2}	Λ	$10^{-4}.\sigma$/Nm^{-2}	Λ	$10^{-4}.\sigma$/Nm^{-2}	Λ
	0.50	0.9979	0.51	0.9977	0.50	0.9976
	1.01	0.9941	1.02	0.9940	1.01	0.9943
	1.52	0.9913	1.53	0.9909	1.51	0.9908
	2.02	0.9879	2.03	0.9886	2.02	0.9876
	2.53	0.9853	2.54	0.9849	2.52	0.9844
	3.03	0.9829	3.05	0.9821	3.03	0.9817
	4.05	0.9780	4.07	0.9772	4.04	0.9768
	5.06	0.9732	5.09	0.9723	5.05	0.9721
	6.07	0.9675	6.10	0.9672	6.06	0.9676
	7.08	0.9631	7.12	0.9627	7.07	0.9634
	8.09	0.9636	8.14	0.9582	8.08	0.9589
	9.10	0.9535	9.16	0.9532	9.09	0.9545
	10.12	0.9493	10.17	0.9486	10.10	0.9504
	11.13	0.9450	11.19	0.9443	11.11	0.9464
	12.14	0.9405	12.21	0.9394	12.12	0.9423
	14.60	0.9316	14.24	0.9314	14.14	0.9338
	16.18	0.9228	16.28	0.9229	16.16	0.9255
	18.21	0.9149	18.31	0.9149	18.18	0.9178
	20.23	0.9068	20.35	0.9060	20.20	0.9104
	22.26	0.8993	22.38	0.8986	22.22	0.9034
$10^{-5}.G$/Nm^{-2}	6.459		6.425		6.638	
$10^{-5}.\bar{G}$/Nm^{-2}	6.507 ± 0.106					

Uniaxial Compression Data:

Expt. 7.4 (Dried Samples): 28.6% toluene (5% DABCO)

Sample No.	1		2		3	
h_o/mm	9.06		9.270		9.210	
h_c/mm	9.04		9.252		9.192	
r/mm	5.53		5.55		5.517	
	$10^{-4}.\sigma/Nm^{-2}$	Λ	$10^{-4}.\sigma/Nm^{-2}$	Λ	$10^{-4}.\sigma/Nm^{-2}$	Λ
	0.51	0.9972	0.51	0.9969	0.51	0.9965
	1.02	0.9925	1.01	0.9923	1.02	0.9919
	1.53	0.9884	1.52	0.9886	1.54	0.9871
	2.04	0.9844	2.03	0.9844	2.05	0.9816
	2.55	0.9809	2.53	0.9808	2.56	0.9774
	3.06	0.9769	3.04	0.9768	3.08	0.9739
	4.08	0.9710	4.05	0.9706	4.10	0.9667
	5.10	0.9648	5.07	0.9644	5.13	0.9601
	6.13	0.9570	6.08	0.9578	6.15	0.9535
	7.15	0.9501	7.01	0.9520	7.18	0.9480
	8.17	0.9444	8.11	0.9445	8.20	0.9417
	9.19	0.9380	9.12	0.9388	9.23	0.9344
	10.21	0.9325	10.14	0.9340	10.26	0.9286
	11.23	0.9275	11.15	0.9287	11.28	0.9231
	12.25	0.9224	12.16	0.9240	12.31	0.9176
	14.29	0.9123	14.19	0.9137	14.36	0.9028
	16.34	0.9010	16.22	0.9032	16.41	0.8929
	18.38	0.8909	18.25	0.8932	18.46	0.8829
	20.42	0.8813	20.27	0.8833	20.51	0.8735
	22.46	0.8721	22.30	0.8743	22.57	0.8642
$10^{-5}.G/Nm^{-2}$	4.937		4.968		4.560	
$10^{-5}.\bar{G}/Nm^{-2}$	4.821 ± 0.204					

Uniaxial Compression Data:

Expt. 7.5 (Dried Samples): 37.5% toluene (5% DABCO)

Sample No.	1		5		6	
h_o/mm	8.02		7.82		7.890	
h_c/mm	7.99		7.80		7.873	
r/mm	5.157		5.072		5.19	
	$10^{-4}.\sigma/Nm^{-2}$	Λ	$10^{-4}.\sigma/Nm^{-2}$	Λ	$10^{-4}.\sigma/Nm^{-2}$	Λ
	0.59	0.9957	0.61	0.9963	0.58	0.9960
	1.17	0.9901	1.21	0.9902	1.16	0.9902
	1.76	0.9850	1.82	0.9849	1.74	0.9841
	2.35	0.9792	2.43	0.9803	2.32	0.9789
	2.93	0.9757	3.03	0.9759	2.90	0.9749
	3.52	0.9705	3.64	0.9721	3.48	0.9705
	4.69	0.9622	4.85	0.9551	4.64	0.9630
	5.87	0.9552	6.07	0.9581	5.80	0.9559
	7.04	0.9466	7.28	0.9511	6.95	0.9492
	8.22	0.9384	8.49	0.9408	8.11	0.9420
	9.29	0.9310	9.71	0.9329	9.27	0.9336
	10.56	0.9244	10.92	0.9269	10.43	0.9286
	11.74	0.9180	12.13	0.9199	11.59	0.9195
	12.91	0.9118	13.35	0.9145	12.75	0.9131
	14.09	0.9053	14.56	0.9088	13.91	0.9063
	16.43	0.8921	16.99	0.8962	16.23	0.8930
	18.78	0.8784	19.42	0.8854	18.55	0.8810
	21.13	0.8674	21.85	0.8751	20.87	0.8698
	23.48	0.8567	24.27	0.8629	23.18	0.8594
	25.83	0.8463	26.70	0.8525	25.50	0.8492
$10^{-5}.G/Nm^{-2}$	4.539		4.910		4.561	
$10^{-5}.\bar{G}/Nm^{-2}$	4.670 ± 0.065					

Uniaxial Compression Data:

Expt. 7.6 (Dried Samples): 44.4% toluene (5% DABCO)

Sample No.	1		3		5	
h_o/mm	8.050		7.670		7.57	
h_c/mm	8.032		7.656		7.56	
r/mm	4.907		4.925		4.96	
	$10^{-4}.\sigma/Nm^{-2}$	Λ	$10^{-4}.\sigma/Nm^{-2}$	Λ	$10^{-4}.\sigma/Nm^{-2}$	Λ
	0.65	0.9963	0.64	0.9958	0.63	0.9958
	1.30	0.9909	1.29	0.9908	1.27	0.9895
	1.94	0.9858	1.93	0.9846	1.90	0.9844
	2.59	0.9816	2.57	0.9790	2.54	0.9790
	3.24	0.9771	3.22	0.9752	3.17	0.9737
	3.89	0.9727	3.86	0.9691	3.81	0.9693
	5.19	0.9653	5.15	0.9586	5.08	0.9627
	6.48	0.9585	6.44	0.9514	6.35	0.9549
	7.78	0.9520	7.72	0.9445	7.61	0.9399
	9.08	0.9442	9.01	0.9367	8.88	0.9399
	10.37	0.9368	10.30	0.9288	10.15	0.9330
	11.67	0.9304	11.59	0.9215	11.42	0.9266
	12.96	0.9244	12.87	0.9141	12.69	0.9205
	14.26	0.9173	14.16	0.9060	13.96	0.9150
	15.56	0.9117	15.45	0.8998	15.23	0.9082
	18.15	0.8993	18.02	0.8859	17.77	0.8969
	20.74	0.8883	20.60	0.8719	20.31	0.8839
	23.34	0.8755	23.17	0.8600	22.85	0.8731
	25.93	0.8650	25.75	0.8484	25.38	0.8622
	28.52	0.8549	28.32	0.8374	27.92	0.8527
$10^{-5}.G/Nm^{-2}$	5.395		4.654		5.086	
$10^{-5}.\bar{G}/Nm^{-2}$	5.044 ± 0.174					

Uniaxial Compression Data:

Expt. 7.7 (Dried Samples): 59.5% toluene (5% DABCO)

Sample No.	1		2		5	
h_o/mm	7.360		7.39		6.72	
h_c/mm	7.346		7.38		6.70	
r/mm	4.46		4.432		4.502	
	$10^{-4}.\sigma$/Nm^{-2}	Λ	$10^{-4}.\sigma$/Nm^{-2}	Λ	$10^{-4}.\sigma$/Nm^{-2}	Λ
	0.78	0.9938	0.79	0.9933	0.77	0.9929
	1.57	0.9848	1.59	0.9848	1.54	0.9847
	23.5	0.9751	2.38	0.9771	2.31	0.9766
	3.14	0.9780	3.18	0.9689	3.08	0.9683
	3.92	0.9610	3.97	0.9621	3.85	0.9608
	4.71	0.9517	4.77	0.9541	4.62	0.8534
	6.28	0.9397	6.36	0.9415	6.16	0.9415
	7.85	0.9276	7.95	0.9291	7.70	0.9258
	9.42	0.9137	9.54	0.9166	9.24	0.9114
	10.99	0.9011	11.12	0.9058	10.78	0.8981
	12.56	0.8909	12.71	0.8944	12.32	0.8838
	14.13	0.8815	14.30	0.8836	13.86	0.8708
	15.70	0.8715	15.89	0.8740	15.40	0.8611
	17.27	0.8615	17.48	0.8624	16.94	0.8514
	18.84	0.8520	19.08	0.8520	18.40	0.8413
	21.98	0.8313	22.25	0.8327	21.56	0.8223
	25.12	0.8130	25.43	0.8127	24.64	0.8041
	28.26	0.7948	28.61	0.7941	27.72	0.7864
	31.40	0.7793	31.79	0.7785	30.81	0.7676
	34.54	0.7641	34.96	0.7627	33.89	0.7509
$10^{-5}.G$/Nm^{-2}	3.566		3.624		3.273	
$10^{-5}.\bar{G}$/Nm^{-2}	3.488 ± 0.175					

Uniaxial Compression Data:

Expt. 7.8 (Dried Samples) 69.6% toluene (5% DABCO)

Sample No.	3		4		6	
h_o/mm	6.84		6.260		6.310	
h_c/mm	6.80		6.212		6.275	
r/mm	3.972		4.017		4.075	
	$10^{-4}.\sigma/Nm^{-2}$	Λ	$10^{-4}.\sigma/Nm^{-2}$	Λ	$10^{-4}.\sigma/Nm^{-2}$	Λ
	0.94	0.9915	0.99	0.9910	0.94	0.9903
	1.88	0.9789	1.98	0.9800	1.88	0.9785
	2.82	0.9676	2.97	0.9682	2.82	0.9640
	3.76	0.9587	3.96	0.9595	3.76	0.9524
	4.70	0.9504	4.95	0.9488	4.70	0.9434
	5.64	0.9399	5.94	0.9392	5.64	0.9331
	7.52	0.9216	7.91	0.9221	7.52	0.9157
	9.40	0.9080	9.89	0.9071	9.40	0.8999
	11.28	0.8954	11.87	0.8923	11.28	0.8819
	13.16	0.8824	13.85	0.8752	13.16	0.8649
	15.04	0.8692	15.83	0.8600	15.04	0.8495
	16.92	0.8581	17.18	0.8450	16.92	0.8359
	18.80	0.8463	19.79	0.8317	18.80	0.8225
	20.68	0.8365	21.77	0.8204	20.68	0.8098
	22.56	0.8243	23.74	0.8088	22.56	0.7977
	26.33	0.8012	27.70	0.7862	26.33	0.7729
	30.09	0.7830	31.66	0.7640	30.09	0.7491
	33.85	0.7649	35.62	0.7429	33.85	0.7260
	37.61	0.7483	39.57	0.7231	37.61	0.7041
	41.37	0.7319	43.53	0.7036	41.37	0.6831
$10^{-5}.G/Nm^{-2}$	3.298		3.517		2.866	
$10^{-5}.\bar{G}/Nm^{-2}$	3.227 $\pm$ 0.325					

Uniaxial Compression Data:

Expt. 6.1 (Swollen Samples): Bulk (Uncatalysed)

Sample No.	1		2		3	
h_o/mm	16.060		16.290		16.00	
h_c/mm	16.056		16.275		15.99	
r/mm	9.82		9.46		9.665	
	$10^{-4}.\sigma/Nm^{-2}$	Λ	$10^{-4}\sigma$ /Nm^{-2}	Λ	$10^{-4}.\sigma/Nm^{-2}$	Λ
	0.16	0.9983	0.17	0.9984	0.17	0.9985
	0.32	0.9963	0.35	0.9961	0.33	0.9961
	0.48	0.9940	0.52	0.9941	0.50	0.9939
	0.65	0.9920	0.70	0.9921	0.67	0.9917
	0.81	0.9901	0.87	0.9901	0.83	0.9899
	0.97	0.9880	1.05	0.9880	1.00	0.9877
	1.29	0.9844	1.39	0.9843	1.34	0.9840
	1.62	0.9806	1.74	0.9807	1.67	0.9803
	1.94	0.9769	2.09	0.9772	2.00	0.9766
	2.27	0.9733	2.44	0.9738	2.34	0.9730
	2.59	0.9698	2.79	0.9702	2.67	0.9694
	2.91	0.9662	3.14	0.9669	3.01	0.9661
	3.24	0.9628	3.49	0.9635	3.34	0.9626
	3.56	0.9592	3.84	0.9601	3.68	0.9594
	3.88	0.9557	4.19	0.9566	4.01	0.9559
	4.53	0.9490	4.88	0.9499	4.68	0.9491
	5.18	0.9430	5.58	0.9438	5.35	0.9430
	5.83	0.9376	6.28	0.9382	6.02	0.9375
	6.48	0.9322	6.98	0.9392	6.68	0.9322
	7.12	0.9271	7.68	0.9276	7.35	0.9271
$10^{-5}.G/Nm^{-2}$	2.882		3.148		2.971	
$10^{-5}.\bar{G}/Nm^{-2}$	3.000 ± 0.133					

Uniaxial Compression Data:

Expt. 6.2 (Swollen Samples) 9.1% toluene (Uncatalysed)

Sample No.	1		2		3	
h_o/mm	15.620		15.770		15.670	
h_c/mm	15.618		15.759		15.658	
r/mm	10.525		10.31		10.395	
	$10^{-4}.\sigma/Nm^{-2}$	Λ	$10^{-4}.\sigma/Nm^{-2}$	Λ	$10^{-4}.\sigma/Nm^{-2}$	Λ
	0.14	0.9979	0.15	0.9978	0.14	0.9981
	0.28	0.9953	0.29	0.9953	0.29	0.9955
	0.42	0.9931	0.44	0.9923	0.43	0.9930
	0.56	0.9909	0.59	0.9896	0.58	0.9906
	0.70	0.9886	0.73	0.9896	0.72	0.9883
	0.84	0.9864	0.88	0.9845	0.87	0.9861
	1.13	0.9812	1.17	0.9803	1.15	0.9820
	1.41	0.9798	1.47	0.9749	1.44	0.9776
	1.69	0.9765	1.76	0.9703	1.73	0.9735
	1.97	0.9722	2.06	0.9658	2.02	0.9695
	2.25	0.9680	2.35	0.9615	2.31	0.9657
	2.54	0.9635	2.64	0.9571	2.60	0.9617
	2.82	0.9596	2.94	0.9527	2.89	0.9578
	3.10	0.9557	3.23	0.9489	3.18	0.9545
	3.38	0.9517	3.52	0.9447	3.47	0.9507
	3.95	0.9439	4.11	0.9367	4.04	0.9429
	4.51	0.9364	4.70	0.9296	4.62	0.9366
	5.07	0.9292	5.29	0.9232	5.20	0.9306
	5.64	0.9225	5.87	0.9171	5.78	0.9247
	6.20	0.9165	6.46	0.9111	6.36	0.9191
$10^{-5}.G/Nm^{-2}$	2.231		2.078		2.84	
$10^{-5}.\bar{G}/Nm^{-2}$	2.198 ± 0.103					

Uniaxial Compression Data:

Expt. 6.3 (Swollen Samples) 20% toluene (uncatalysed)

Sample No.	1		3		5	
h_o/mm	16.160		16.000		14.590	
h_c/mm	16.155		15.979		14.555	
r/mm	9.645		9.81		9.72	
	$10^{-4}.\sigma$ /Nm^{-2}	Λ	$10^{-4}.\sigma$/Nm^{-2}	Λ	$10^{-4}\sigma$ /Nm^{-2}	Λ
	0.17	0.9978	0.16	0.9977	0.16	0.9974
	0.33	0.9949	0.32	0.9943	0.33	0.9936
	0.50	0.9922	0.49	0.9913	0.49	0.9901
	0.67	0.9896	0.65	0.9883	0.66	0.9870
	0.84	0.9867	0.81	0.9856	0.83	0.9836
	1.01	0.9839	0.97	0.9827	0.99	0.9805
	1.34	0.9789	1.30	0.9772	1.32	0.9745
	1.68	0.9738	1.62	0.9718	1.65	0.9691
	2.01	0.9686	1.95	0.9665	1.98	0.9636
	2.35	0.9641	2.27	0.9613	2.31	0.9584
	2.68	0.9592	2.60	0.9562	2.64	0.9529
	3.02	0.9547	2.92	0.9513	2.97	0.9479
	3.36	0.9503	3.24	0.9462	3.30	0.9430
	3.69	0.9456	3.57	0.9417	3.63	0.9384
	4.03	0.9412	3.89	0.9371	3.97	0.9333
	4.70	0.9329	4.54	0.9284	4.63	0.9243
	5.37	0.9247	5.19	0.9196	5.29	0.9167
	6.04	0.9179	5.84	0.9120	5.95	0.9082
	6.71	0.9112	6.49	0.9049	6.61	0.9008
	7.38	0.9046	7.14	0.8978	7.27	0.8939
$10^{-5}.G/Nm^{-2}$	2.217		1.989		1.919	
$10^{-5}.\bar{G}/Nm^{-2}$	2.042 ± 0.149					

Uniaxial Compression Data:

Expt. 6.4 (Swollen Samples) 28.6% toluene (uncatalysed)

Sample No.	1		2		3	
h_o/mm	15.20		14.8300		14.910	
h_c/mm	15.18		14.8215		14.905	
r/mm	8.94		9.005		8.955	
	$10^{-4}.\sigma$/Nm^{-2}	Λ	$10^{-4}.\sigma$/Nm^{-2}	Λ	$10^{-4}.\sigma$/Nm^{-2}	Λ
	0.19	0.9979	0.19	0.9976	0.19	0.9975
	0.39	0.9947	0.38	0.9953	0.39	0.9946
	0.59	0.9918	0.58	0.9924	0.58	0.9914
	0.78	0.9890	0.77	0.9898	0.78	0.9884
	0.98	0.9864	0.96	0.9874	0.97	0.9854
	1.17	0.9837	1.15	0.9850	1.17	0.9827
	1.56	0.9788	1.54	0.9798	1.56	0.9773
	1.95	0.9741	1.92	0.9752	1.95	0.9723
	2.34	0.9692	2.31	0.9706	2.33	0.9668
	2.73	0.9643	2.69	0.9661	2.72	0.9618
	3.12	0.9598	3.08	0.9616	3.11	0.9567
	3.52	0.9552	3.46	0.9570	3.50	0.9518
	3.91	0.9510	3.85	0.9528	3.89	0.9471
	4.30	0.9467	4.23	0.9488	4.28	0.9426
	4.69	0.9427	4.62	0.9447	4.67	0.9381
	5.47	0.9343	5.39	0.9364	5.45	0.9291
	6.25	0.9273	6.16	0.9282	6.23	0.9216
	7.03	0.9205	6.93	0.9211	7.01	0.9141
	7.81	0.9141	7.70	0.9144	7.79	0.9071
	8.59	0.9080	8.47	0.9079	8.57	0.9006
$10^{-5}.G$/Nm^{-2}	2.657		2.674		2.440	
$10^{-5}.\bar{G}$/Nm^{-2}	2.590 ± 0.117					

Uniaxial Compression Data:

Expt. 6.5 (Swollen samples) 37.5% toluene (Uncatalysed)

Sample No.	1		2		6	
h_o/mm	13.430		13.44		14.320	
h_c/mm	13.411		13.41		14.272	
r/mm	9.06		8.69		8.75	
	$10^{-4}.\sigma/Nm^{-2}$	Λ	$10^{-4}.\sigma/Nm^{-2}$	Λ	$10^{-4}.\sigma/Nm^{-2}$	Λ
	0.19	0.9974	0.21	0.9975	0.20	0.9967
	0.38	0.9938	0.41	0.9940	0.41	0.9906
	0.57	0.9902	0.62	0.9907	0.61	0.9859
	0.76	0.9865	0.83	0.9875	0.81	0.9817
	0.95	0.9832	1.03	0.9842	1.02	0.9779
	1.14	0.9799	1.24	0.9809	1.22	0.9745
	1.52	0.9736	1.65	0.9752	1.63	0.9681
	1.90	0.9680	2.07	0.9695	2.04	0.9619
	2.28	0.9620	2.48	0.9637	2.45	0.9555
	2.66	0.9567	2.89	0.9584	2.85	0.9501
	3.04	0.9511	3.31	0.9828	3.26	0.9443
	3.42	0.9460	3.72	0.9476	3.67	0.9392
	3.80	0.9412	4.13	0.9424	4.08	0.9343
	4.18	0.9361	4.55	0.9375	4.49	0.9295
	4.56	0.9306	4.96	0.9327	4.89	0.9244
	5.32	0.9216	5.79	0.9235	5.71	0.9140
	6.09	0.9135	6.62	0.9145	6.52	0.9057
	6.85	0.9050	7.44	0.9061	7.34	0.8971
	7.61	0.8978	8.27	0.8986	8.16	0.8895
	8.37	0.8910	9.10	0,8919	8.97	0.8824
$10^{-5}.G/Nm^{-2}$	2.128		2.361		2.052	
$10^{-5}.\bar{G}/Nm^{-2}$	2.180 $\pm$ 0.154					

Uniaxial Compression Data:

Expt. 6.6 (Swollen samples) 44.4% toluene (Uncatalysed)

Sample No.	1		2		7	
h_o/mm	13.360		13.020		13.080	
h_c/mm	13.297		12.975		13.046	
r/mm	8.51		8.35		8.51	
	$10^{-4}.\sigma/Nm^{-2}$	Λ	$10^{-4}.\sigma/Nm^{-2}$	Λ	$10^{-4}.\sigma/Nm^{-2}$	Λ
	0.21	0.9970	0.22	0.9971	0.21	0.9972
	0.43	0.9917	0.45	0.9921	0.43	0.9928
	0.65	0.9875	0.67	0.9878	0.65	0.9890
	0.86	0.9838	0.89	0.9839	0.86	0.9855
	1.08	0.9805	1.12	0.9800	1.08	0.9825
	1.29	0.9771	1.34	0.9768	1.29	0.9793
	1.72	0.9712	1.79	0.9704	1,72	0.9737
	2.15	0.9653	2.24	0.9647	2.15	0.9679
	2.59	0.9595	2.69	0.9589	2.59	0.9622
	3.02	0.9538	3.13	0.9535	3.02	0.9567
	3.45	0.9484	3.58	0.9478	3.45	0.9511
	3.88	0.9434	4.03	0.9424	3.88	0.9461
	4.31	0.9384	4.48	0.9374	4.31	0.9409
	4.74	0.9332	4-92	0.9327	4.74	0.9357
	5.17	0.9282	5.37	0.9280	5.17	0.9312
	6.04	0.9207	6.27	0.9187	6.04	0.9217
	6.90	0.9121	7.16	0.9101	6.90	0.9126
	7.76	0.9039	8.06	0.9015	7.76	0.9042
	8.62	0.8965	8.96	0.8939	8.62	0.8965
	9.48	0.8894	9.85	0.8865	9.48	0.8893
$10^{-5}.G/Nm^{-2}$	2.340		2.378		2.393	
$10^{-5}.\bar{G}/Nm^{-2}$	2.370 ± 0.026					

Uniaxial Compression Data:

Expt. 6.7 (Swollen samples) 59.6% toluene (Uncatalysed)

Sample No.	1		2		4	
h_o/mm	12.95		13.0800		11.980	
h_c/mm	12.95		13.0455		11.980	
r/mm	7.715		7.77		7.73	
	$10^{-4}.\sigma/Nm^{-2}$	Λ	$10^{-4}.\sigma/Nm^{-2}$	Λ	$10^{-4}.\sigma/Nm^{-2}$	Λ
	0.26	0.9950	0.26	0.9957	0.26	0.9950
	0.52	0.9900	0.52	0.9897	0.52	0.9895
	0.79	0.9846	0.77	0.9843	0.78	0.9841
	1.05	0.9799	1.03	0.9789	1.04	0.9786
	1.31	0.9743	1.29	0.9736	1.31	0.9732
	1.57	0.9698	1.55	0.9684	1.57	0.9679
	2.10	0.9597	2.07	0.9583	2.09	0.9580
	2.62	0.9501	2.59	0.9488	2.61	0.9477
	3.15	0.9410	3.10	0.9391	3.13	0.9378
	3.67	0.9312	3.62	0.9303	3.66	0.9283
	4.20	0.9219	4.14	0.9219	4.18	0.9187
	4.72	0.9135	4.65	0.9135	4.70	0.9093
	5.25	0.9057	5.17	0.9050	5.22	0.9003
	5.77	0.8975	5.69	0.8973	5.75	0.8922
	6.29	0.8897	6.21	0.8888	6.27	0.8840
	7.34	0.8745	7.24	0.8744	7.32	0.8693
	8.39	0.8610	8.27	0.8605	8.36	0.8554
	9.44	0.8496	9.31	0.8484	9.41	0.8427
	10.49	0.8380	10.34	0.8370	10.45	0.8317
	11.54	0.8269	11.38	0.8263	11.50	0.8212
$10^{-5}.G/Nm^{-2}$	1.738		1.702		1.649	
$10^{-5}.\bar{G}/Nm^{-2}$	1.696 ± 0.044					

Uniaxial Compression Data:

Expt. 6.8 (Swollen samples) 69.5% toluene (Uncatalysed)

Sample No.	2		3		4	
h_o/mm	12.290		12.290		11.3400	
h_c/mm	12.285		12.280		11.3305	
r/mm	7.30		7.345		7.265	
	$10^{-4}.\sigma/Nm^{-2}$	Λ	$10^{-4}.\sigma/Nm^{-2}$	Λ	$10^{-4}.\sigma/Nm^{-2}$	Λ
	0.29	0.9919	029	0.9922	0.29	0.9920
	0.58	0.9835	0.58	0.9835	0.59	0.9830
	0.88	0.9748	0.87	0.9751	0.89	0.9741
	1.17	0.9664	1.16	0.9671	1.18	0.9650
	1.46	0.9581	1.45	0.9582	1.48	0.9568
	1.75	0.9493	1.74	0.9496	1.77	0.9479
	2.34	0.9327	2.31	0.9332	2.37	0.9314
	2.93	0.9177	2.89	0.9176	2.96	0.9155
	3.51	0.9029	3.47	0.9026	3.55	0.9006
	4.10	0.8886	4.05	0.8891	4.14	0.8867
	4.69	0.8752	4.63	0.8758	4.73	0.8720
	5.27	0.8632	5.21	0.8635	5.32	0.8588
	5.86	0.8510	5.79	0.8529	5.92	0.8469
	6.44	0.8389	6.37	0.8407	6.51	0.8343
	7.03	0.8283	6.94	0.8307	7.10	0.8238
	8.20	0.8100	8.10	0.8120	8.28	0.8034
	9.37	0.7928	9.26	0.7928	9.47	0.7866
	10.55	0.7751	10.42	0.7755	10.65	0.7711
	11.72	0.7587	11.58	0.7600	11.83	0.7557
	12.89	0.7440	12.73	0.7448	13.01	0.7416
$10^{-5}.G/Nm^{-2}$	1.162		1.156		1.143	
$10^{-5}.\bar{G}/Nm^{-2}$	1.153 ± 0.009					

Uniaxial Compression Data:

Expt. 7.1 (Swollen samples) Bulk (5% DABCO)

Sample No.	1		2		3	
h_o/mm	16.300		16.160		16.53	
h_c/mm	16.278		16.155		16.52	
r/mm	9.745		9.785		9.805	
	$10^{-4}.\sigma/Nm^{-2}$	Λ	$10^{-4}.\sigma/Nm^{-2}$	Λ	$10^{-4}.\sigma/Nm^{-2}$	Λ
	0.16	0.9984	0.16	0.9984	0.16	0.9984
	0.33	0.9956	0.33	0.9971	0.32	0.9958
	0.49	0.9933	0.49	0.9952	0.49	0.9939
	0.66	0.9913	0.65	0.9931	0.65	0.9921
	0.82	0.9893	0.82	0.9913	0.81	0.9903
	0.97	0.9876	0.98	0.9896	0.97	0.9885
	1.31	0.9843	1.30	0.9861	1.30	0.9851
	1.64	0.9809	1.63	0.9830	1.62	0.9821
	1.97	0.9776	1.96	0.9795	1.95	0.9788
	2.30	0.9744	2.28	0.9763	2.27	0.9756
	2.63	0.9713	2.61	0.9731	2.60	0.9727
	2.96	0.9683	2.93	0.9701	2.93	0.9697
	3.29	0.9653	3.26	0.9675	3.25	0.9670
	3.62	0.9628	3.59	0.9646	3.57	0.9641
	3.94	0.9596	3.92	0.9615	3.90	0.9618
	4.60	0.9540	4.56	0.9561	4.55	0.9572
	5.26	0.9491	5.22	0.9509	5,20	0.9517
	5.92	0.9442	5.87	0.9459	5.85	0.9469
	6.58	0.9393	6.52	0.9409	6.50	0.9428
	7.23	0.9343	7.17	0.9362	7.14	0.9386
$10^{-5}.G/Nm^{-2}$	3.229		3.359		3.385	
$10^{-5}.\bar{G}/Nm^{-2}$	3.324 ± 0.078					

Uniaxial Compression Data:

Expt. 7.2 (Swollen samples) 9.1% toluene (5% DABCO)

Sample No.	1		2		3	
h_o/mm	16.140		16.490		16.1200	
h_c/mm	16.134		16.481		16.1025	
r/mm	9.605		9.675		9.625	
	$10^{-4}.\sigma/Nm^{-2}$	Λ	$10^{-4}.\sigma/Nm^{-2}$	Λ	$10^{-4}.\sigma/Nm^{-2}$	Λ
	0.17	0.9984	0.17	0.9985	0.17	0.9984
	0.34	0.9962	0.33	0.9964	0.34	0.9961
	0.51	0.9940	0.50	0.9942	0.50	0.9937
	0.68	0.9918	0.67	0.9920	0.67	0.9916
	0.85	0.9897	0.83	0.9900	0.84	0.9894
	1.01	0.9876	1.00	0.9879	1.01	0.9874
	1.35	0.9839	1.33	0.9842	1.35	0.9833
	1.69	0.9801	1.67	0.9806	1.68	0.9797
	2.03	0.9762	2.00	0.9770	2.02	0.9759
	2.37	0.9731	2.33	0.9734	2.36	0.9723
	2.71	0.9695	2.67	0.9698	2.70	0.9690
	3.05	0.9657	3.00	0.9667	3.03	0.9655
	3.38	0.9625	3.33	0.9633	3.37	0.9623
	3.72	0.9594	3.67	0.9604	3.71	0.9588
	4.06	0.9561	4.00	0.9574	4.04	0.9558
	4.74	0.9501	4.67	0.9514	4.72	0.9499
	5.41	0.9440	5.34	0.9462	5.39	0.9434
	6.09	0.9385	6.00	0.9401	6.08	0.9381
	6.77	0.9330	6.67	0.9249	6.74	0.9326
	7.45	0.9283	7.34	0.9298	7.41	0.9276
$10^{-5}.G/Nm^{-2}$	3.041		3.084		2.999	
$10^{-5}.\bar{G}/Nm^{-2}$	3.041 $\pm$ 0.042					

Uniaxial Compression Data:

Expt. 7.3 (Swollen samples) 20.0% toluene (5% DABCO)

Sample No.	1		2		3	
h_o/mm	15.40		15.300		15.050	
h_c/mm	15.37		15.267		15.041	
r/mm	9.08		9.32		9.05	
	$10^{-4}.\sigma/Nm^{-2}$	Λ	$10^{-4}.\sigma/Nm^{-2}$	Λ	$10^{-4}.\sigma/Nm^{-2}$	Λ
	0.19	0.9980	0.18	0.9983	0.19	0.9984
	0.38	0.9947	0.36	0.9959	0.38	0.9960
	0.57	0.9924	0.54	0.9931	0.57	0.9938
	0.76	0.9902	0.72	0.9907	0.76	0.9917
	0.95	0.9879	0.90	0.9886	0.95	0.9896
	1.14	0.9857	1.08	0.9866	1.14	0.9877
	1.51	0.9815	1.44	0.9827	1.52	0.9834
	1.89	0.9773	1.80	0.9787	1.91	0.9794
	2.27	0.9735	2.16	0.9747	2.29	0.9753
	2.65	0.9697	2.52	0.9711	2.67	0.9713
	3.03	0.9657	2.87	0.9673	3.05	0.9676
	3.41	0.9623	3.23	0.9637	3.43	0.9644
	3.79	0.9589	3.59	0.9600	3.81	0.9605
	4.17	0.9553	3.95	0.9565	4.20	0.9571
	4.54	0.9521	4.31	0.9535	4.57	0.8540
	5.30	0.9453	5.03	0.9472	5.34	0.9474
	6.06	0.9397	5.75	0.9411	6.10	0.9413
	6.82	0.9332	6.47	0.9348	6.86	0.9357
	7.57	0.9274	7.19	0.9293	7.62	0.9303
	8.33	0.9220	7.91	0.9240	8.39	0.9262
$10^{-5}.G/Nm^{-2}$	3.095		3.035		3.273	
$10^{-5}.\bar{G}/Nm^{-2}$	3.134 ± 0.119					

Uniaxial Compression Data:

Expt. 7.4 (Swollen samples) 28.6% toluene (5% DABCO)

Sample No.	1		2		3	
h_o/mm	15.95		16.170		16.170	
h_c/mm	15.94		16.130		16.155	
r/mm	9.33		9.375		9.465	
	$10^{-4}.\sigma/Nm^{-2}$	Λ	$10^{-4}.\sigma/Nm^{-2}$	Λ	$10^{-4}.\sigma/Nm^{-2}$	Λ
	0.18	0.9976	0.18	0.9980	0.17	0.9977
	0.36	0.9946	0.35	0.9956	0.35	0.9942
	0.54	0.9918	0.53	0.9932	0.52	0.9909
	0.72	0.9888	0.71	0.9907	0.70	0.9878
	0.90	0.9859	0.89	0.9882	0.87	0.9848
	1.08	0.9832	1.06	0.9858	1.04	0.9820
	1.43	0.9781	L.42	0.9810	1.39	0.9764
	1.79	0.9729	1.78	0.9766	1.74	0.9711
	2.15	0.9682	2.13	0.9730	2.09	0.9659
	2.51	0.9632	2.49	0.9685	2.44	0.9607
	2.87	0.9586	2.84	0.9643	2.79	0.9555
	3.23	0.9541	3.20	0.9602	3.14	0.9507
	3.59	0.9498	3.55	0.9563	3.48	0.9459
	3.94	0.9455	3.91	0.9526	4.18	0.9367
	4.30	0.9408	4.27	0.4989	3.83	0.9409
	5.02	0.9332	4.97	0.9419	4.88	0.9282
	5.74	0.9259	5.68	0.9343	5.58	0.9200
	6.46	0.9184	6.39	0.9273	6.27	0.9123
	7.17	0.9108	7.10	0.9207	6.97	0.9047
	0.789	0.9041	7.82	0.9143	7.67	0.8975
$10^{-5}.G/Nm^{-2}$	2.363		2.684		2.162	
$10^{-5}.\bar{G}/Nm^{-2}$	2.391 $\pm$ 0.279					

Uniaxial Compression Data:

Expt. 7.5 (Swollen samples) 37.5% toluene (5% DABCO)

Sample No.	1		5		6	
h_o/mm	14.06		13.650		13.7700	
h_c/mm	14.04		13.635		13.7675	
r/mm	8.845		8.83		8.93	
	$10^{-4}.\sigma$/Nm^{-2}	Λ	$10^{-4}.\sigma$/Nm^{-2}	Λ	$10^{-4}.\sigma$/Nm^{-2}	Λ
	0.20	0.9969	0.20	0.9972	0.19	0.9970
	0.40	0.9935	0.40	0.9932	0.39	0.9938
	0.60	0.9902	0.60	0.9893	0.59	0.9905
	0.80	0.9867	0.80	0.9862	0.78	0.9870
	1.00	0.9838	1.00	0.9829	0.98	0.9837
	1.20	0.9800	1.20	0.9801	1.17	0.9804
	1.60	0.9738	1.60	0.9738	1.57	0.9741
	1.99	0.9677	2.00	0.9678	1.96	0.9680
	2.39	0.9614	2.40	0.9616	2.35	0.9622
	2.79	0.9557	2.80	0.9560	2.74	0.9560
	3.19	0.9498	3.20	0.9497	3.13	0.9501
	3.59	0.9446	3.60	0.9443	3.52	0.9443
	3.99	0.9394	4.00	0.9388	3.91	0.9394
	4.39	0.9336	4.40	0.9336	4.31	0.9339
	4.79	0.9287	4.80	0.9288	4.70	0.9291
	5.59	0.9190	5.61	0.9187	5.48	0.9190
	6.39	0.9085	6.41	0.9091	6.26	0.9091
	7.18	0.8957	7.21	0.9005	7.05	0.9006
	7.98	0.8878	8.01	0.8919	7.83	0.8925
	8.78	0.8797	8.81	0.8843	8.61	0.8848
$10^{-5}.G$/Nm^{-2}	2.081		2.136		2.099	
$10^{-5}.\bar{G}$/Nm^{-2}	2.105 ± 0.027					

Uniaxial Compression Data:

Expt. 7.6 (Swollen samples) 44.4% toluene (5% DABCO)

Sample No.	1		3		5	
h_o/mm	13.95		13.050		12.9900	
h_c/mm	13.95		13.028		12.9725	
r/mm	8.165		8.43		8.225	
	$10^{-4}.\sigma/Nm^{-2}$	Λ	$10^{-4}.\sigma/Nm^{-2}$	Λ	$10^{-4}.\sigma/Nm^{-2}$	Λ
	0.23	0.9974			0.23	0.9975
	0.47	0.9936			0.46	0.9940
	0.70	0.9904			0.69	0.9907
	0.94	0.9873			0.92	0.9875
	1.17	0.9841	Cracked		1.15	0.9844
	1.40	0.9810			1.38	0.9812
	1.87	0.9752			1.85	0.9753
	2.34	0.9695			2.31	0.9692
	2.81	0.9639			2.77	0.9634
	3.28	0.9584			3.23	0.9576
	3.75	0.9533			3.69	0.9519
	4.21	0.9477			4.15	0.9465
	4.68	0.9427			4.61	0.9411
	5.15	0.9378			5.08	0.9359
	5.62	0.9334			5.54	0.9309
	6.56	0.9244			6.46	0.9214
	7.59	0.9154			7.38	0.9122
	8.43	0.9070			8.31	0.9035
	9.37	0.8993			9.23	0.8962
	10.30	0.8920			10.15	0.8889
$10^{-5}.G/Nm^{-2}$	2.693				2.566	
$10^{-5}.\bar{G}/Nm^{-2}$			2.629 ± 0.063			

Uniaxial Compression Data:

Expt. 7.7 (Swollen samples) 59.5% toluene (5% DABCO)

Sample No.	1		2		5	
h_o/mm	13.26		13.42		12.26	
h_c/mm	13.25		13.41		12.27	
r/mm	7.855		7.935		7.96	
	$10^{-4}.\sigma/Nm^{-2}$	Λ	$10^{-4}.\sigma/Nm^{-2}$	Λ	$10^{-4}.\sigma/Nm^{-2}$	Λ
	0.25	0.9945	0.25	0.9947	0.25	0.9937
	0.51	0.9885	0.49	0.9890	0.49	0.9883
	0.76	0.9828	0.74	0.9835	0.74	0.9821
	1.01	0.9767	0.99	0.9776	0.98	0.9756
	1.26	0.9711	1.24	0.9722	1.23	0.9693
	1.52	0.9657	1.49	0.9668	1.48	0.9634
	2.02	0.9546	1.98	0.9563	1.97	0.9520
	2.53	0.9437	2.48	0.9465	2.46	0.9402
	3.04	0.9329	2.97	0.9380	2.96	0.9284
	3.54	0.9226	3.47	0.9283	3.45	0.9173
	4.05	0.9123	3.97	0.9186	3.94	0.9065
	4.55	0.9025	4.46	0.9093	4.43	0.8958
	5.06	0.8929	4.96	0.8996	4.93	0.8860
	5.57	0.9935	5.45	0.8909	5.42	0.8762
	6.07	0.8745	5.95	0.8818	5.91	0.8673
	7.08	0.8588	6.94	0.8658	6.90	0.8505
	8.10	0.8436	7.93	0.8505	7.88	0.8343
	9.11	0.8295	8.93	0.8358	8.87	0.8184
	10.12	0.8163	9.92	0.8232	9.86	0.8047
	11.13	0.8041	10.91.	0.8114	10.84	0.7921
$10^{-5}.G/Nm^{-2}$	1.449		1.504		1.315	
$10^{-5}.\bar{G}/Nm^{-2}$	1.422 ± 0.094					

Uniaxial Compression Data:

Expt. 7.8 (Swollen samples) 69.6% toluene (5% DABCO)

Sample No.	3		4		6	
h_o/mm	12.16		11.070		11.190	
h_c/mm	12.15		11.065		11.175	
r/mm	7.125		6.95		7.235	
	$10^{-4}.\sigma/Nm^{-2}$	Λ	$10^{-4}.\sigma/Nm^{-2}$	Λ	$10^{-4}.\sigma/Nm^{-2}$	Λ
	0.31	0.9922	0.32	0.9936	0.30	0.9917
	0.61	0.9846	0.65	0.9860	0.60	0.9826
	0.92	0.9769	0.97	0.9786	0.89	0.9739
	1.23	0.9681	1.29	0.9716	1.19	0.9649
	1.53	0.9606	1.62	0.9645	1.49	0.9566
	1.84	0.9532	1.94	0.9575	1.79	0.9495
	2.46	0.9387	2.58	0.9437	2.39	0.9326
	3.07	0.9243	3.23	0.9307	2.98	0.9168
	3.69	0.9103	3.88	0.9183	3.58	0.9018
	4.30	0.8977	4.52	0.9069	4.17	0.8879
	4.92	0.8851	5.17	0.8949	4.77	0.8752
	5.53	0.8734	5.82	0.8842	5.37	0.8615
	6.15	0.8618	6.46	0.8739	5.96	0.8504
	6.77	0.8509	7.11	0.8631	6.56	0.8379
	7.38	0.8402	7.76	0.8531	7.16	0.8270
	8.61	0.8207	9.05	0.8339	8.35	0.8035
	9.84	0.8029	10.34	0.8158	9.54	0.7835
	11.07	0.7852	11.64	0.8003	10.74	0.7649
	12.30	0.7681	12.93	0.7859	11.93	0.7474
	13.53	0.7522	14.22	0.7718	13.12	0.7303
$10^{-5}.G/Nm^{-2}$	1.306		1.519		1.131	
$10^{-5}.\bar{G}/Nm^{-2}$	1.319 ± 0.194					

APPENDIX E

TORSION PENDULUM DATA OF DRIED NETWORKS

Expt. 6.1: Bulk (0% TED)				Expt. 6.2: 9.1% toluene (0% TED)			
Temp°C	logG'/Nm^{-2}	logG''/Nm^{-2}	tan δ	Temp°C	logG'/Nm^{-2}	logG''/Nm^{-2}	tan δ
-188	9.230	7.247	1.038×10^{-2}	-190	9.241	7.117	7.512×10^{-3}
-165	9.186	7.341	1.428	-180	9.227	7.186	9.086
-160	9.180	7.364	1.525	-170	9.217	7.302	1.216×10^{-2}
-150	9.169	7.429	1.818	-160	9.199	7.383	1.528
-145	9.171	7.469	1.989	-150	9.184	7.431	1.765
-140	9.163	7.475	2.050	-145	9.176	7.465	1.947
-135	9.153	7.485	2.149	-140	9.170	7.481	2.047
-130	9.143	7.484	2.192	-135	9.159	7.491	2.150
-125	9.133	7.484	2.243	-130	9.151	7.496	2.217
-120	9.119	7.463	2.206	-125	9.140	7.500	2.291
-115	9.103	7.447	2.209	-120	9.129	7.493	2.309
-110	9.086	7.450	2.312	-110	9.110	7.495	2.427
-105	9.074	7.480	2.551	-100	9.083	7.560	3.000
-100	9.056	7.572	3.276	-95	9.066	7.597	3.399
-95	9.040	7.660	4.169	-90	9.037	7.685	4.442
-90	9.014	7.896	7.613	-85	8.977	7.865	7.724
-85	8.963	8.206	1.749×10^{-1}	-80	8.919	8.106	1.573×10^{-1}
-80	8.856	8.491	4.316	-76	8.897	8.309	2.578
-76	8.475	8.335	7.255	-70	8.510	8.208	4.980
-70	7.940	8.176	1.719×10^{0}	-66	8.373	8.393	1.048×10^{0}
-66	7.675	7.829	1.425x	-60	7.415	7.735	2.092
-60	7.201	7.338	1.370x	-55	6.737	7.181	2.783
-55	6.712	6.914	1.592x	-50	6.445	6.557	1.295
-50	6.235	6.263	1.066	-40	6.096	5.695	3.970×10^{-1}
-45	5.952	5.763	6.460×10^{-1}	-30	5.941	5.249	2.022
-40	5.813	5.425	4.089	-20	5.897	5.031	1.362
-30	5.670	5.027	2.274	-10	5.870	4.871	1.001
-25	5.667	5.230	3.663	0	5.787	4.136	2.232×10^{-2}
-10	5.574	4.332	5.724×10^{-2}	10	5.779	3.951	1.485
0	5.562	4.158	3.944	20	5.786	3.828	1.102
10	5.556	4.585	1.069×10^{-1}	27	5.787	3.816	1.067
20	5.867	3.745	1.102×10^{-2}	30	5.787	3.713	8.426×10^{-3}
27	5.862	3.624	1.067	40	5.792	3.474	4.808
30	5.862	3.604	8.426×10^{-3}	50	5.823	3.712	7.742
40	5.876	3.592	4.808	60	5.842	3.673	6.772
50	5.867	3.498	7.742	70	5.872	3.707	6.833
60	5.872	3.466	6.772	80	5.907	3.731	6.678
70	5.874	3.412	6.833	90	5.938	3.735	6.261
80	5.865	3.407	6.678	100	5.967	3.636	4.669
90	5.881	3.390	6.261				
100	5.889	3.363	4.669				

Expt. 6.3 20% toluene (0% TED)				Expt. 6.4: 28.6% toluene (0% TED)			
Temp^{o}C	log G'/Nm^{-2}	log G''/Nm^{-2}	tan δ	Temp^{o}C	log G'/Nm^{-2}	log G''/Nm^{-2}	tan δ
-185	9.268	7.338	1.175×10^{-2}	-185	9.235	7.271	1.085×10^{-2}
-180	9.260	7.288	1.066	-170	9.224	7.363	1.376
-170	9.243	7.390	1.404	-160	9.212	7.463	1.783
-160	9.225	7.488	1.829	-150	9.196	7.534	2.179
-145	9.278	7.636	2.463	-145	9.186	7.551	2.314
-140	9.188	7.618	2.696	-140	9.177	7.577	2.512
-135	9.174	7.617	2.772	-135	9.172	7.606	2.713
-130	9.172	7.585	2.587	-130	9.127	7.567	2.754
-125	9.165	7.586	2.634	-125	9.152	7.596	2.781
-120	9.148	7.595	2.793	-120	9.140	7.588	2.806
-115	9.135	7.769	4.295	-115	9.132	7.582	2.816
-110	9.128	7.595	2.934	-110	9.124	7.582	2.866
-105	9.119	7.614	3.122	-105	9.118	7.590	2.970
-100	9.115	7.625	3.240	-100	9.119	7.620	3.165
-95	9.117	7.705	3.868	-95	9.099	7.684	3.837
-90	9.087	7.878	6.170	-90	9.095	7.739	4.408
-85	9.047	8.123	1.191×10^{-1}	-85	9.063	7.925	7.281
-80	8.988	8.359	2.348	-80	9.035	8.038	1.007×10^{-1}
-76	8.921	8.473	3.566	-75	8.990	8.417	2.675
-70	8.360	8.454	1.241×10^{o}	-70	8.541	8.448	8.073
-66	7.669	7.959	1.942	-66	7.914	8.077	1.456×10^{o}
-60	6.945	7.291	2.218	-60	7.393	7.492	1.256
-56	6.649	6.893	1.752	-54	6.872	6.859	1.077
-50	6.169	6.068	7.921×10^{-1}	-50	6.331	6.401	1.173
-40	6.003	5.470	2.928	-40	5.971	5.445	2.980×10^{-1}
-30	5.895	5.068	1.487	-30	5.863	4.899	1.087
-25	5.878	4.948	1.173	-20	5.837	4.544	5.088×10^{-2}
-15	5.736	4.283	3.521×10^{-2}	-10	5.828	4.476	4.446
-10	5.732	4.190	2.867	0	5.843	4.400	3.611
0	5.761	4.030	1.857	10	5.866	4.434	3.697
10	5.800	3.868	1.169	20	5.893	4.371	3.006
20	5.853	3.888	1.082	27	5.911	4.373	2.898
27	5.890	3.877	9.712×10^{-3}	30	5.918	4.269	2.245
30	5.814	3.554	5.484	40	5.939	4.241	2.003
40	5.867	3.604	5.465	50	5.909	4.471	3.647
50	5.923	3.614	4.909	60	5.905	4.576	4.678
60	5.860	3.413	3.572	70	5.921	4.503	3.820
70	5.854	3.436	3.816	80	5.932	4.457	3.349
80	5.860	3.489	4.255	90	5.957	4.383	2.662
90	5.854	3.483	4,256	100	5.987	4.298	2.046
100	5.854	3.504	4.469				

Expt. 6.5: 37.5% ϕ CH_3 (0% TED)				Expt. 6.6: 44.4% ϕ CH_3 (0% TED)			
Temp°C	$\log G'/Nm^{-2}$	$\log G''/Nm^{-2}$	$\tan\delta$	Temp°C	$\log G'/Nm^{-2}$	$\log G''/Nm^{-2}$	$\tan\delta$
-180	9.194	7.233	1.093×10^{-2}	-185	9.211	7.236	1.058×10^{-2}
-170	9.171	7.295	1.331	-180	9.202	7.252	1.121
-160	9.154	7.404	1.779	-170	9.191	7.335	1.394
-150	9.137	7.458	2.227	-160	9.184	7.441	1.806
-145	9.129	7.511	2.406	-150	9.170	7.527	2.274
-140	9.121	9.535	2.596	-145	9.175	7.549	2.365
-135	9.115	7.553	2.737	-140	9.164	7.565	2.520
-130	9.095	7.544	2.809	-135	9.148	7.538	2.726
-125	9.085	7.534	2.812	-130	9.148	7.595	2.801
-120	9.075	7.531	2.862	-125	9.136	7.585	2.810
-115	9.065	7.525	2.881	-120	9.128	7.586	2.866
-110	9.046	7.501	2.848	-115	9.118	7.576	2.866
-105	9.036	7.520	3.050	-110	9.112	7.609	3.138
-100	9.034	7.550	3.276	-105	9.113	7.656	3.488
-95	9.035	7.656	4.173	-100	9.108	7.703	3.933
-90	8.937	7.911	9.417	-95	9.099	7.768	4.665
-85	8.881	8.127	1.761×10^{-1}	-90	9.070	7.956	7.691
-80	8.663	8.031	2.332	-85	9.010	8.113	1.268×10^{-1}
-76	8.469	8.290	6.619	-80	8.950	8.479	3.383
-70	7.981	8.031	1.123×10^{0}	-76	8.679	8.488	6.440
-66	7.663	7.681	1.043	-70	7.996	8.108	1.294×10^{0}
-60	7.222	7.231	1.019	-66	7.597	7.685	1.223
-55	6.743	6.843	1.256	-60	7.031	7.217	1.536
-50	6.344	6.305	9.149×10^{-1}	-55	6.450	6.522	1.180
-40	6.052	5.540	3.070	-50	6.129	5.933	6.365×10^{-1}
-30	5.985	5.255	1.863	-40	5.822	5.098	1.886
-20	5.942	4.940	9.946×10^{-2}	-30	5.763	4.631	7.379×10^{-2}
-10	5.981	4.936	9.012	-20	5.894	4.518	4.211
0	5.960	4.983	1.053×10^{-1}	-10	5.883	4.385	3.177
10	5.932	4.748	6.549×10^{-2}	0	5.909	4.387	3.005
20	5.921	4.773	7.105	10	5.866	4.216	2.240
27	5.921	4.710	6.147	20	5.878	4.264	2.433
30	5.925	4.694	5.880	27	5.857	4.033	1.497
40	5.903	4.716	6.513	30	5.849	4.074	1.676
50	5.916	4.654	5.468	40	5.839	4.084	1.759
60	5.899	4.407	3.219	50	5.829	3.907	1.195
70	5.888	4.225	2.172	60	5.820	3.571	5.630×10^{-3}
80	5.891	4.161	1.859	70	5.856	3.706	7.091
90	5.913	4.185	1.871	80	5.892	3.617	5.306
100	5.911	3.776	7.324×10^{-3}	90	5.932	3.715	6.062
				100	5.967	3.804	6.868

Expt. 6.7: 59.6% ϕCH_3 (0% TED)

Temp°C	LogG'/Nm^{-2}	logG''/Nm^{-2}	tan δ
-180	9.276	7.308	1.074×10^{-2}
-170	9.260	7.435	1.498
-160	9.237	7.531	1.968
-150	9.217	7.605	2.444
-140	9.194	7.640	2.789
-135	9.181	7.633	2.829
-130	9.173	7.610	2.735
-125	9.168	7.621	2.838
-120	9.147	7.605	2.869
-115	9.136	7.606	2.952
-110	9.121	7.627	3.204
-105	9.106	7.650	3.492
-100	9.088	7.758	4.667
-95	9.064	7.759	4.956
-90	9.036	7.945	8.112
-85	8.958	8.170	1.632×10^{-1}
-80	8.717	8.325	4.059
-75	8.444	8.444	9.987
-70	7.741	8.029	1.942×10^{0}
-65	7.171	7.414	1.751
-60	6.708	7.064	2.272
-55	6.391	6.080	4.885×10^{-1}
-50	6.276	5.826	3.555
-40	6.187	5.499	2.051
-30	6.145	5.317	1.487
-15	6.024	4.874	7.086×10^{-2}
-10	6.013	4.890	7.536
0	6.036	4.849	6.117
10	6.092	4.877	6.091
20	6.105	4.907	6.335
27	6.111	4.870	5.742
30	6.095	4.889	6.231
40	6.114	4.897	6.069
50	6.127	4.935	6.426
60	6.149	4.908	5.729
70	6.160	4.886	5.327
80	6.171	4.880	5.112
90	6.183	4.866	4.111
100	6.200	4.814	4.111

Expt. 7.1: Bulk (5% TED)				Expt. 7.2: 9.1% ϕCH_3 (5% TED)			
Temp°C	logG'/Nm^{-2}	logG''/Nm^{-2}	tan δ	Temp°C	logG'/Nm^{-2}	logG''/Nm^{-2}	tan δ
-187	9.276	7.285	1.021×10^{-2}	-180	9.109	7.276	1.469×10^{-2}
-180	9.277	7.358	1.205	-170	9.099	7.338	1.732
-170	9.263	7.742	1.524	-160	9.091	7.367	1.887
-160	9.249	7.497	1.772	-150	9.074	7.443	2.336
-150	9.229	7.551	2.095	-135	9.065	7.478	2.587
-140	9.204	7.584	2.398	-130	9.053	7.476	2.644
-130	9.187	7.562	2.372	-120	9.037	7.463	2.666
-125	9.178	7.552	2.370	-110	9.020	7.465	2.791
-120	9.167	7.621	2.839	-100	8.981	7.503	3.327
-110	9.149	7.564	2.601	-90	8.872	7.928	1.136×10^{-1}
-100	9.142	7.664	3.327	-84	8.647	8.118	2.957
-90	9.143	7.846	5.045	-80	8.555	8.026	2.952
-85	9100	7.972	7.453	-75	8.558	7.970	2.583
-80	9.014	8.359	2.213×10^{-1}	-70	7.948	7.899	8.933
-56	6.797	6.927	1.349×10^{0}	-65	7.503	7.581	1.196×10^{0}
-50	6.411	6.440	1.069	-60	7.039	7.177	1.212
-45	6.146	5.927	6.035×10^{-1}	-56	6.655	6.722	1.166
-40	6.018	5.451	2.712	-50	6.404	6.331	8.466×10^{-1}
-35	6.003	5.241	1.731	-45	6.089	5.788	4.997
-30	5.956	5.028	1.181	-40	5.950	5.241	1.956
-25	5.940	4.963	1.054	-30	5.945	4.871	8.434×10^{-2}
-20	5.943	4.829	7.693×10^{-2}	-15	5.928	4.600	4.700
-15	5.943	4.801	7.199	-10	5.924	4.458	4.214
-10	5.933	4.777	6.969	0	5.933	4.463	3.389
0	5.950	4.950	9.989	10	5.933	4.458	3.351
10	5.957	5.205	1.768×10^{-1}	20	5.928	4.419	3.097
17	5.911	4.727	6.549×10^{-2}	27	5.919	4.402	3.035
25	5.866	4.730	7.302	30	5.920	4.381	2.889
29	5.957	4.569	4.090	40	5.969	4.603	4.304
41	5.933	4.691	5.719	50	5.951	4.470	3.305
50	5.969	4.879	8.138	60	5.952	4.612	4.570
60	5.947	5.274	2.127×10^{-1}	70	5.982	4.487	3.199
70	5.932	5.081	1.409	80	5.982	4.551	3.713
80	5.960	4.074	1.300×10^{-2}	90	5.970	4.246	1.887
90	5.981	4.412	2.693	100	5.986	4.704	5.231
100	5.994	4.089	1.244				

Expt. 7.3: 20% ϕ CH_3 (5% TED)				Expt. 7.4: 28.6% ϕ CH_3 (5% TED)			
Temp°C	logG'/Nm^{-2}	logG''/Nm^{-2}	tan δ	Temp°C	logG'/Nm^{-2}	logG''/Nm^{-2}	tan δ
-185	9.175	7.211	1.084×10^{-2}	-185	9.244	7.183	8.705×10^{-3}
-180	9.155	7.234	1.200	-175	9.245	7.218	9.387
-170	9.145	7.275	1.348	-170	9.234	7.293	1.44×10^{-2}
-160	9.138	7.351	1.634	-160	9.215	7.410	1.566
-150	9.133	7.422	1.946	-150	9.190	7.549	2.283
-140	9.132	7.499	2.328	-145	9.180	7.589	2.554
-130	9.112	7.497	2.422	-140	9.169	7.575	2.544
-120	9.098	7.447	2.238	-130	9.143	7.591	2.804
-110	9.068	7.440	2.355	-125	9.137	7.575	2.873
-100	8.988	7.583	3.938	-120	9.128	7.585	2.862
-90	8.930	7.929	9.986	-110	9.276	7.685	2.567
-85	8.925	7.980	1.135×10^{-1}	-100	9.247	7.764	3.288
-80	8.751	8.232	3.025	-90	9.199	8.173	9.414
-76	8.349	8.371	1.053×10^{0}	-85	9.220	8.242	1.050×10^{-1}
-70	8.241	8.312	1.175	-80	9.062	8.692	4.265
-66	7.724	7.931	1.612	-76	9.046	8.680	4.134
-60	7.266	7.392	1.336	-70	8.290	8.461	1.479×10^{0}
-56	6.838	6.920	1.233	-66	7.869	8.102	1.709
-50	6.274	6.220	8.819×10^{-1}	-60	7.164	7.358	1.562
-40	6.098	5.501	2.528	-56	6.642	6.738	1.248
-30	5.987	5.141	1.426	-50	6.833	6.701	7.381×10^{-1}
-20	5.967	5.037	1.174	-40	6.035	5.466	2.696
-10	5.919	4.860	8.723×10^{-2}	-30	5.980	5.145	1.462
0	5.911	4.847	8.646	-20	5.943	4.973	1.071
10	5.887	4.579	4.925	-5	5.899	4.487	3.878×10^{-2}
20	5.900	4.545	4.414	0	5.879	4.242	2.214
27	5.919	4.696	5.982	10	5.894	4.135	1.744
40	5.919	4.637	5.221	25	5.897	4.084	1.539
50	5.931	4.373	2.768	40	5.886	4.338	2.836
60	5.926	4.769	6.963	50	5.884	4.371	3.069
70	5.925	4.691	5.833	60	5.895	4.408	3.260
85	5.934	4.661	5.333	70	5.899	4.449	3.551
95	5.958	4.641	4.816	80	5.899	4.382	3.044
100	5.958	4.748	6.165	90	5.902	4.430	3.372
				100	5.893	4.465	3.731

Expt. 7.5: 37.5% ϕCH_3 (5% TED)				Expt. 7.6: 44.6% ϕ CH_3 (5% TED)			
Temp°C	logG'/Nm^{-2}	logG''/Nm^{-2}	tan δ	Temp°C	logG'/Nm^{-2}	logG''/Nm^{-2}	tan δ
-180	9.130	7.280	1.412×10^{-2}	-190	9.362	7.323	9.147×10^{-3}
-170	9.117	7.361	1.754	-180	9.341	7.400	1.144×10^{-2}
-160	9.116	7.447	2.146	-170	9.322	7.426	1.272
-150	9.103	7.495	2.462	-160	9.311	7.495	1.529
-145	9.085	7.502	2.616	-155	9.300	7.524	1.675
-140	9.083	7.509	2.666	-150	2.296	7.580	1.921
-135	9.085	7.522	2.740	-145	9.288	7.631	2.203
-130	9.078	7.528	2.817	-140	9.272	7.637	2.316
-125	9.080	7.541	2.892	-135	9.260	7.682	2.644
-120	9.078	7.547	2.943	-130	9.256	7.669	2.588
-110	9.046	7.564	3.299	-120	9.233	7.664	2.697
-100	9.004	7.648	4.408	-110	9.215	7.679	2.910
-90	8.986	7.823	6.866	-100	9.194	7.700	3.205
-80	8.882	8.379	3.637×10^{-1}	-90	9.169	7.754	3.854
-76	8.714	8.395	4.794	-86	9.156	7.834	4.757
-70	8.249	8.152	7.998	-80	9.098	8.231	1.360×10^{-1}
-66	7.825	7.989	1.460×10^{0}	-76	8.919	8.594	4.733
-60	7.321	7.427	1.275	-70	8.141	8.275	1.362×10^{0}
-55	6.707	6.829	1.323	-66	7.672	7.834	1.451
-50	6.253	6.199	8.826×10^{-1}	-60	6.858	7.007	1.410
-38	5.978	5.364	2.428	-55	6.203	6.090	7.706×10^{-1}
-25	5.920	4.866	8.811×10^{-2}	-40	5.888	5.110	1.667
-20	5.921	4.736	6.537	-30	6.296	5.739	2.953
-10	5.925	4.788	7.294	-20	5.773	4.776	1.005
+10	6.039	5.061	1.052×10^{-1}	-5	5.894	4.461	3.689×10^{-2}
+20	5.959	4.552	3.919×10^{-2}	0	5.939	4.515	3.768
27	5.960	4.607	4.435	10	5.838	4.355	3.283
30	5.955	4.527	3.729	20	5.892	4.418	3.885
40	5.968	4.503	3.423	30	5.810	4.388	3.784
50	6.002	4.492	3.085	40	5.810	4.308	3.152
60	6.001	4.469	2.937	50	5.919	4.364	2.790
70	6.012	4.365	2.253	60	5.864	4.273	2.367
80	6.001	4.382	2.406	70	5.950	4.324	2.367
90	5.995	4.398	2.527	80	6.026	4.624	3.963
100	5.984	4.381	2.492	90	5.965	4.610	4.424
				100	5.970	4.539	3.706

Expt. 7.7 : 59.5% ϕCH_3 (5% TED)				Expt. 7.8 : 69.6% ϕCH_3 (5% TED)			
Temp°C	logG'/Nm^{-2}	logG''/Nm^{-2}	tan δ	Temp°C	logG'/Nm^{-2}	log G''/Nm^{-2}	tan δ
-180	9.287	7.306	1.045×10^{-2}	-150	9.041	7.303	1.827×10^{-2}
-170	9.270	7.432	1.450	-145	9.043	7.305	1.828
-160	9.248	7.510	1.828	-140	9.046	7.349	2.005
-150	9.227	7.573	2.218	-135	9.033	7.328	o.972
-145	9.220	7.609	2.446	-130	9.054	7.384	2.138
-140	9.209	7.604	2.480	-125	9.001	7.345	2.205
-135	9.193	7.610	2.609	-120	9.075	7.440	2.318
-130	9.196	7.614	2.615	-115	9.015	7.391	2.380
-125	9.180	7.611	2.697	-110	8.995	7.408	2.588
-120	9.167	7.602	2.722	-100	8.962	7.456	3.117
-110	9.147	7.670	3.333	-90	8.903	7.747	6.987
-100	9.118	7.752	4.307	-85	8.866	7.889	1.053×10^{-1}
-90	9.014	8.109	1.243×10^{-1}	-80	8.701	8.146	2.790
-80	8.806	8.282	2.991	-75	8.629	8.153	3.340
-75	8.537	8.319	6.051	-70	8.343	8.328	9.666
-70	8.244	8.435	1.554×10^{0}	-65	7.824	7.891	1.166×10^{0}
-65	7.641	7.835	1.562	-60	7.168	7.208	1.096
-60	7.240	7.605	2.319	-55	6.952	1.184	1.184
-55	6.633	6.856	1.671	-50	6.411	6.399	9.730×10^{-1}
-50	6.386	6.377	9.797×10^{-1}	-40	6.278	5.556	1.897
-40	6.218	5.563	2.211	-30	6.457	5.615	1.436
-30	6.178	5.268	1.229	-20	6.234	5.278	1.106
-20	6.147	5.120	9.383×10^{-2}	-10	6.165	5.472	2.023
-10	6.102	4.963	7.266	+5	6.373	5.549	1.500
0	6.117	4.854	5.453	10	6.236	5.532	1.977
10	6.088	4.864	5.970	20	6.091	5.271	1.516
20	6.100	4.814	5.184	27	6.121	5.064	8.761×10^{-2}
27	6.092	4.802	5.126	30	6.114	5.375	1.826×10^{-2}
30	6.100	4.820	5.247	40	6.092	4.877	6.090×10^{-2}
40	6.097	4.800	5.045	50	6.083	4.949	7.357
50	6.091	4.810	5.239	55	6.061	4.927	7.351
60	6.051	5.287	1.720×10^{-1}	70	6.024	4.091	1.165
70	6.093	4.777	4.830×10^{-2}	75	6.052	4.185	1.353
80	6.098	4.725	4.232	80	6.053	4.059	1.014
90	6.093	4.754	4.577	90	6.117	4.663	3.514
100	6.093	4.789	4.959	100	6.142	4.680	3.450